Visco-elastic finite element analysis of subduction zones

Woodward, D. J.

VISCO-ELASTIC FINITE ELEMENT ANALYSIS OF SUBDUCTION ZONES

by

D.J. WOODWARD

A thesis submitted for the degree of
Doctor of Philosophy in the University of Durham

Graduate Society

May, 1976.

ABSTRACT

A new visco-elastic finite element method is developed and applied to some of the processes in subduction zones. The effects of phase changes are simulated by deriving an equation of state for the mantle under mineralogical equilibrium. Using the elastic parameters determined from this equation, the stresses due to the contraction of the descending slab as it changes phase at the olivine-spinel transition are shown to be about 8×10^8 N/m^2.

The phase changes are also shown to play an important role in the flexure and bending of the lithosphere from the earth's surface to plunge at 45 - 60^o into the asthenosphere. The phase changes effectively reduce the bulk modulus and so the lithosphere bends more easily. The major bending is at 30 - 60 km depth where the stresses due to bending extend the area of phase transitions so that it extends throughout the thickness of the descending slab. Phase changes and fracture combine to reduce the flexural parameters of the lithosphere to that estimated from the shape of the outer-rise. Thin plate theory, however, is shown to be inapplicable to this region.

Tensional stresses aligned parallel to the dip of the descending slab are shown to be necessary to maintain the large negative gravity anomaly associated with subduction

zones. This applies in all subduction zones, and local stresses must be responsible for the earthquakes indicating down dip compression in the upper part of the descending slab.

The shear zone between two converging plates can be adequately modelled in visco-elastic finite element analysis by a row of elements whose viscosity is 2-3 orders of magnitude lower than the surrounding rocks.

ACKNOWLEDGEMENTS

I wish to thank Professor M.H.P. Bott for supervision during this research and many helpful suggestions and discussions. I also had many interesting discussions of the finite element method and its application with N.J. Kusznir.

Appreciation is expressed to the Department of Geological Sciences and the Computing Unit of the University of Durham for providing facilities for the carrying out of this research.

This research was carried out while I was on leave from the New Zealand Department of Scientific and Industrial Research and while I was financially supported by a post-graduate Fellowship of the New Zealand National Research Advisory Council. I thank both these organisations for the opportunity to work in Durham during the last three years.

Finally, I wish to thank Mrs. Hilda Winn who has ably and patiently typed this thesis.

CONTENTS

FIGURES

TABLES

CHAPTER 1

INTRODUCTION

The basic concept of plate tectonics (McKenzie and Parker, 1967; Morgan, 1968; Le Pichon *et al.*,1973) is that the lithosphere can be subdivided into a series of plates which do not suffer major internal deformation. The major tectonic activity in the earth occurs along the boundaries of the plates. There are three main types of plate boundary. Lithospheric plates are continuously being created at active oceanic ridges which are referred to as accretion boundaries, and, by lateral movement give rise to the magnetic anomalies observed over the oceans (Vine and Matthews, 1963). The plates slide past each other along large transform faults (Wilson, 1965) which are referred to as conservative boundaries, because lithosphere is neither created nor destroyed along them. The lithospheric plates are destroyed along consuming plate boundaries (Isacks *et al.*, 1968; Le Pichon *et al.*, 1973). Subduction zones are the most common form of consuming boundary (McKenzie and Parker, 1967; Isacks *et al.*, 1968) at which a plate of oceanic lithosphere is recycled into the mantle and is over ridden by another plate which may be oceanic (island arcs) or continental (active continental margins).

1.1 Morphology of subduction zones

The overridden or consumed plate sinks into the asthenosphere as a relatively cold rigid body and it is progressively heated until it loses its identity (Isacks and Molnar, 1969, 1970; McKenzie and Parker, 1968; McKenzie, 1969). Most subduction zones now occur along the circum-Pacific belt or in South East Asia, (Morgan, 1968; Le Pichon, 1968). The morphology and some of the manifestations of a typical subduction zone are shown in fig. 1.1.

The topography of the plate being consumed is similar for most subduction zones. The outer rise (fig. 1.1) is about 300 km wide and reaches about 700 m above the expected "non-deformed" level of the ocean floor (Le Pichon et al., 1973; Watts and Talwani, 1974). The depth of the trench varies but around the Pacific is typically 3 km below the sea floor (Hayes and Ewing, 1970). Most trenches have only thin sediments on their floor but some trenches are nearly filled with sediments (eg. South Chile, Ewing et al., 1969). The topography of the overriding plate is more variable. Sometimes there are several ridges parallel to the trench (Karig, 1970; Karig and Sharman, 1975) and sometimes a single volcanic arc occurs with a marginal sea behind. In New Zealand, Chile and the eastern end of the Aleutian trench the overriding plate has continental crust. The front

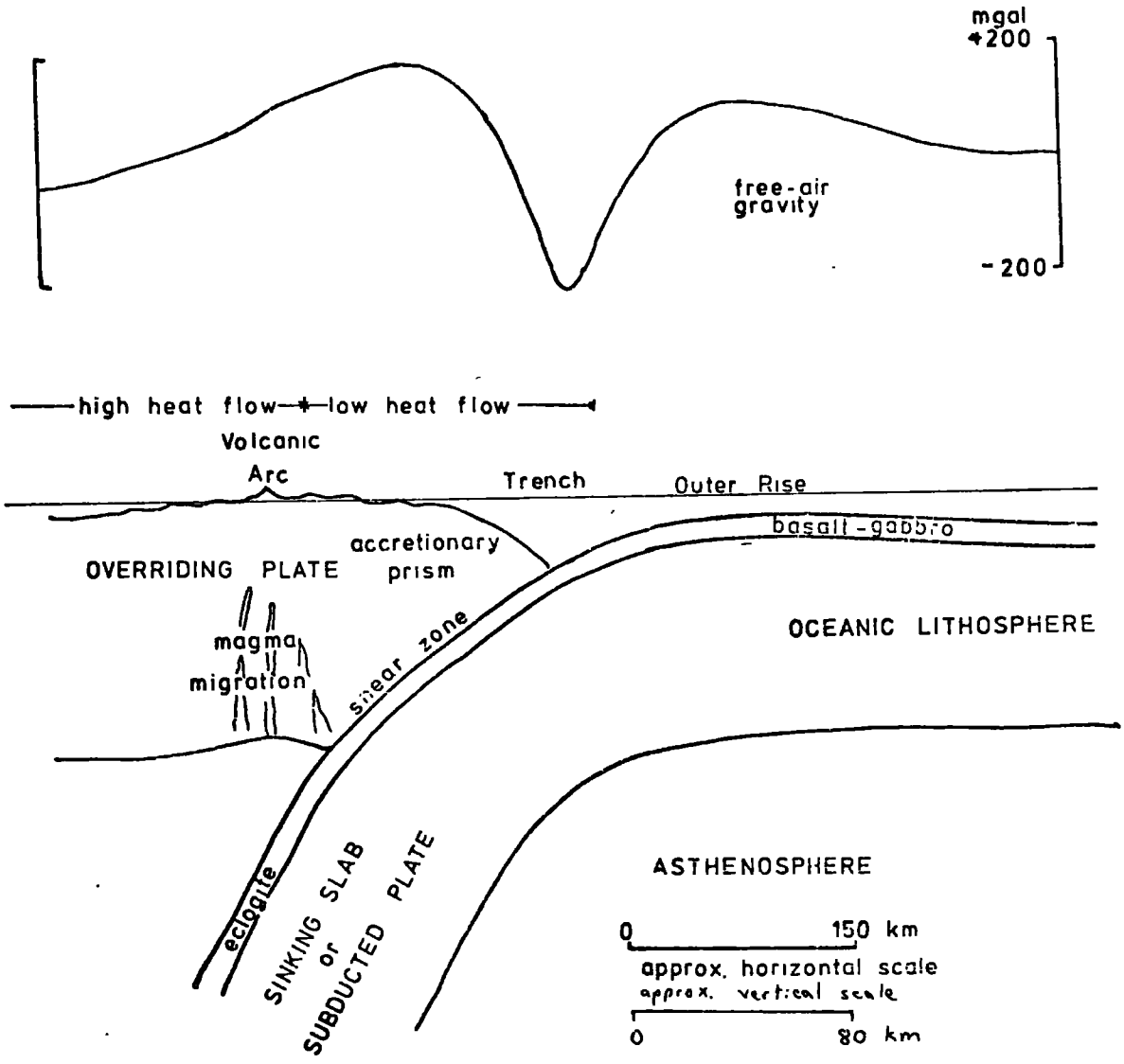

Fig. 1.1 Schematic diagram of processes in a subduction zone.

of the overriding plate is commonly extended by the accretion of igneous rocks and sediment derived from the consumed plate (Karig and Sharman, 1975). This forms an accretionary prism (fig. 1.1).

The most direct evidence for the shape of the cool sinking slab is the seismicity (Sykes, 1966; Isacks et al., 1968). Nearly all intermediate and deep earthquakes (depths > 60 km) are found near consuming plate boundaries. They occur in a thin belt dipping at about 45^{o} from below the inside of the trench, under the overriding plate. This belt of focii, the Benioff zone, (Gutenberg and Ritcher, 1954; Benioff, 1955) is only 20 to 40 km thick (Sykes, 1966; Hamilton and Gale, 1968) and the shape of it may be mapped with some accuracy (Stauder, 1973, 1975).

Earthquake mechanism studies based on earthquakes with focii deeper than 60 km in the vicinity of subduction zones (eg. Isacks and Molnar, 1971; Stauder, 1975) have shown that the principal stresses in the sinking lithospheric slab are usually aligned parallel and perpendicular to the Benioff zone, with either the compressional or tensional axes pointing downdip. Whether the downdip principal axis is compressional or tensional is dependent upon the configuration of the subduction zone. Isacks and Molnar (1969, 1971) showed (fig. 1.2) that if the slab is "suspended"

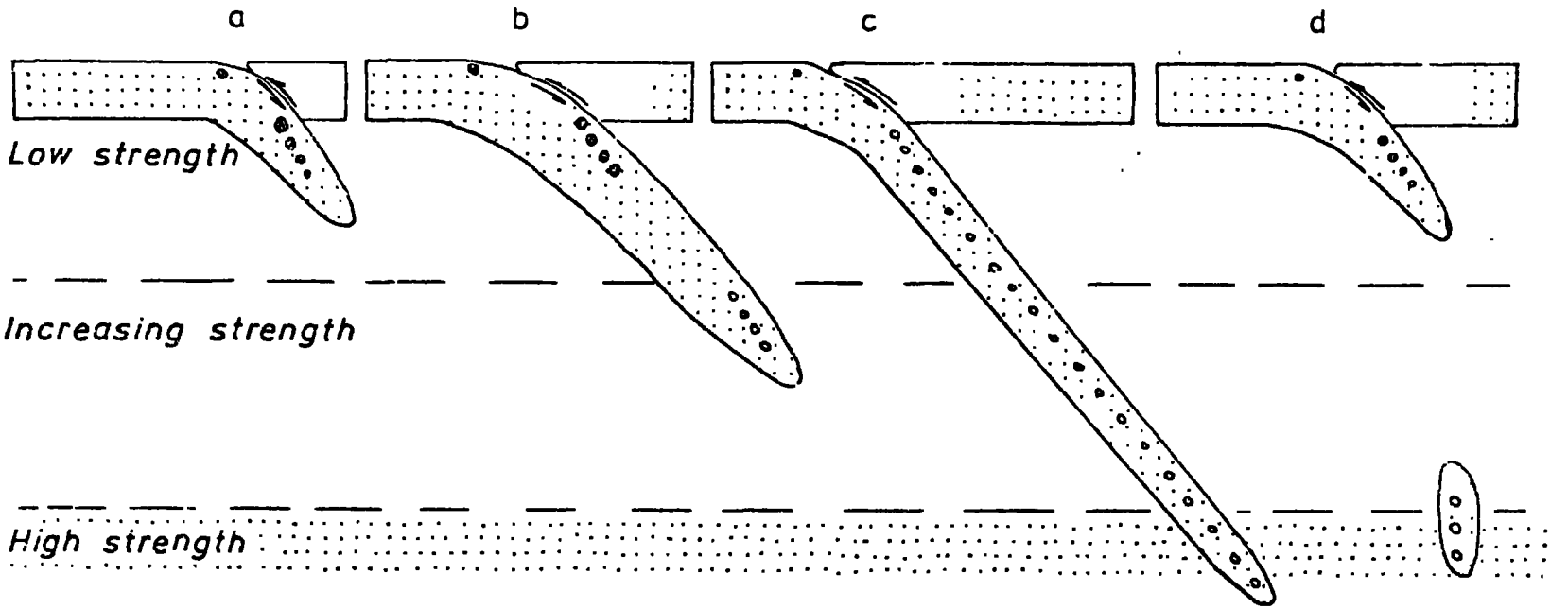

Fig. 1.2 Schematic diagram showing the distribution of stresses causing earthquakes in the descending lithosphere. Solid circles represent stresses with the least compressive stress down-dip and open circles the greatest compressive stress down-dip. Shaded areas have low seismic attenuation and unshaded high attenuation. (Partly after Isacks and Molnar, 1969)

in the asthenosphere tensional stresses predominate, otherwise the forces are compressional because of the resistance to sinking of the slab within the mesosphere. Earthquakes shallower than 60 km, between the ocean trenches and island arcs, indicate thrust faulting at angles of 5^{o} near the base of the trench, increasing to 20^{o} or 30^{o} at depths of about 60 km (Stauder 1968, 1973, 1975; Le Pichon et al., 1973). In many, but not all, trench regions the fault plane solution for earthquakes with focii under the trench and outer ridge indicate a horizontal tensional stress resulting in normal faulting (eg. Abe, 1972; Fitch, 1970; Stauder, 1968, 1975). Other evidence for the tensional character of the stress regime on the consumed plate is the normal faulting in the seabed on the outside edge of the trenches and up onto the outer rises (eg. Ludwig et al.,1966).

That the dipping slab is cool is also suggested by analyses of the distribution of seismic velocities and the seismic wave absorption in these regions (Oliver and Isacks, 1967). The slab has been shown to have higher velocity and lower absorption (figs. 1.2) than the surrounding asthenosphere, suggesting a cooler more rigid body (Davies and McKenzie, 1969). The region above the Benioff zone has an anomalously high seismic absorption suggesting a region of high temperatures and possible partial melt (Fedotov, 1968; Oliver and Isacks, 1967).

The gravity anomalies in the region of the outer rise are positive and in agreement with the topographical high being due to the flexure of the lithosphere as it is bent to be subducted (Watts and Talwani, 1974). There is a large negative Bouguer and isostatic gravity anomaly (about -100 mgal) commonly beyond the trench (fig. 1.1) but always where the projection of the Benioff zone at about 60 km meets the earth's surface (Hatherton, 1969). This anomaly has commonly been associated with the trench but in some areas it is displaced by 200 to 300 km from the trench axis over the overriding plate (eg. New Zealand).

Because of the lack of information from the subduction zones themselves, the relative motion between the two plates concerned nearly always has to be obtained indirectly from the motion of each of the plates with respect to other plates (Le Pichon, 1968; Morgan, 1968).1972). This gives the rate of convergence of the two plates. The rate of frontal accretion (Karig and Sharman, 1975) and formation of marginal seas (fig. 1.3) needs to be added to the convergence rate to give the rate of subduction. The difference in the convergence rate and subduction rate is usually small, but if some small plates are neglected in the analysis the difference may be substantial. The rate of convergence varies from 2.3 cm/yr for the Mariana Trench to 9.5 cm/yr in Philippine Trench (Le Pichon et al.,1973). The

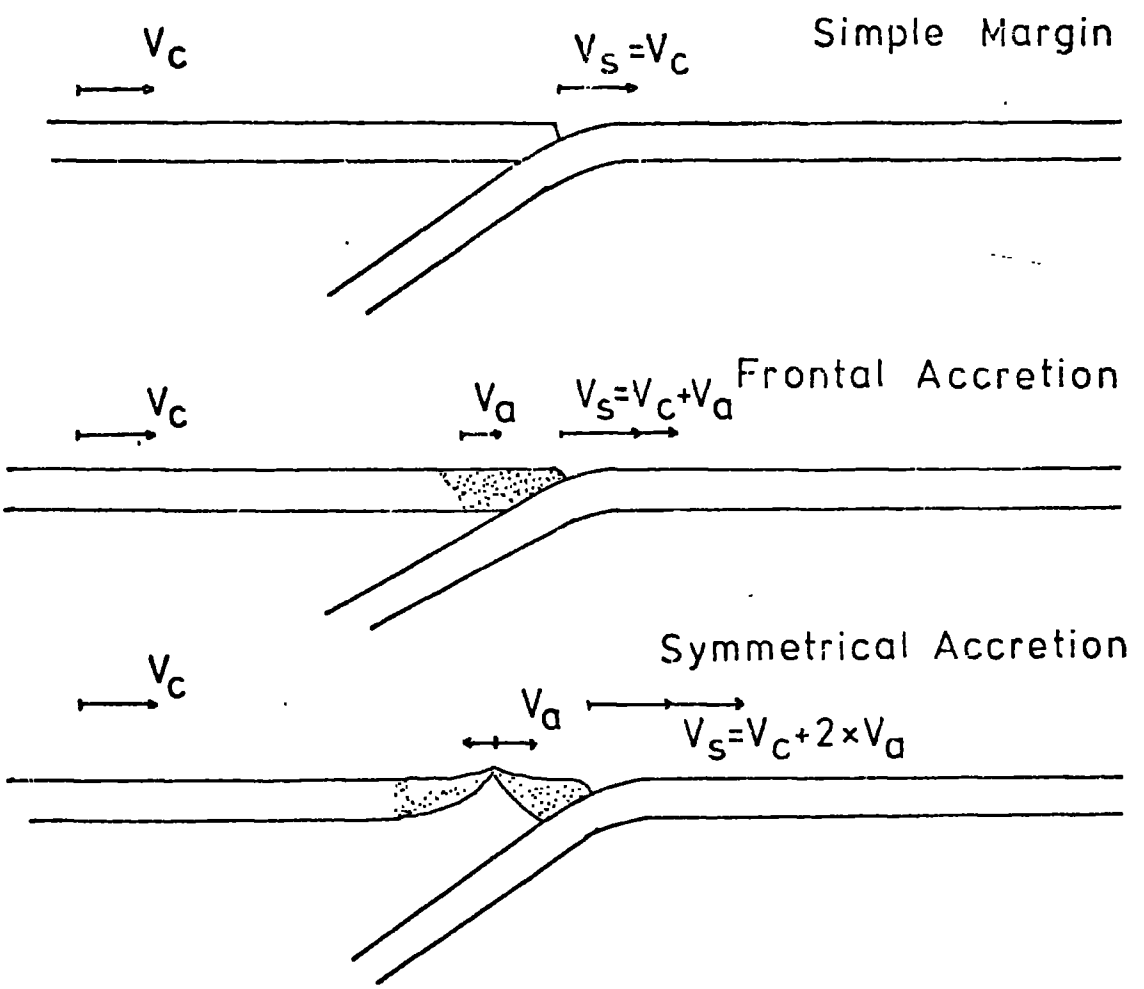

Fig. 1.3 Diagram showing the relationship of convergence rate (V_c) and subduction rate (V_s) when there is accretion and marginal sea opening on the overriding plate.

direction of motion between the two plates is generally not normal to the plate boundary but in our two dimensional models this will of necessity be assumed.

1.2 Thermal evolution of subduction zones

The thermal structure in the vicinity of subduction zones must be consistent with both the surface heat flow measurements and the relative motions of the two converging lithospheric plates. Heat flow measurements (eg. Uyeda and Vacquier (1968) and McKenzie and Sclater (1968)) show that the two most striking thermal manifestation of the subduction process are a decrease of surface heat flow from the trench towards the volcanic arc and a high heat flow on the overriding plate within and behind the volcanic arc (fig. 1.1). The low heat flow near the trench is caused by the cooling of the overlying rocks by the cold sinking slab. This may be accentuated by the cool wet sediments in the accretionary prism on the consumed plate being thrust down the upper part of the shear zone. The high surface heat flow beyond the arc is typically more than twice normal heat flow and occurs over a region almost 300 km wide. The excess heat probably originates by release of shear strain energy at the top of the sinking slab but it cannot rise to the surface by normal thermal conduction

alone (Hasebe et al., 1970). The presence of andesitic volcanism suggests that some of the heat is carried upwards by magma flow. Hasebe et al.,(1970) have modelled this fluid transport of heat by increasing the assumed thermal conductivity of the rocks above the subduction zone by an order of magnitude.

The temperature distribution in the downgoing lithospheric plate has been studied by McKenzie (1969, 1970); Minear and Toksöz (1970a, 1970b); Griggs (1972); Toksöz, Minear and Julian (1971); Toksöz, Sleep and Smith (1973) with progressive improvement in the approximation.

These papers have treated the sinking lithosphere as a rigid plate moving at a constant speed and dip into a stationary asthenosphere. McKenzie (1969, 1970) solved the steady state temperature distribution analytically by assuming that the asthenosphere remained at a constant temperature. He showed that the low temperatures in the oceanic lithosphere persist to great depths in the sinking slab for subduction rates of 8 - 10 cm/yr. and that in the Tonga-Kermadec Trench area a temperature of about 680^{o}C is reached at the depth of the deepest earthquakes in spite of the varying subduction rate along the boundary.

Minear and Toksöz (1970a) solved the problem of the temperature distribution by a finite difference numerical scheme. They included radioactive, adiabatic compression,

phase changes, and shear strain heating in their analysis. The inclusion of shear strain heating resulted in the temperature distribution being asymmetric with the temperatures in the upper surface of the slab being greater than the surrounding asthenosphere in some of their models. Two major criticisms of this paper resulted from doubts as to the numerical accuracy of their calculations because of the coarseness of their finite difference grid and time interval and that the amount of heat produced by shear strain heating is unknown and had to be assumed (Hanks and Whitcomb, 1971; Luyendyk, 1971; McKenzie, 1971; Minear and Toksöz, 1971a,b). They did show, however, that gravity and heat flow measurements cannot be used to choose between thermal models of the subducted slab because these fields are less sensitive to variations in the model than to various other sources. They indicated, however, that seismic delay times may be sensitive to the temperature distribution within the slab.

Griggs (1972) approximated the thermal analysis by a one dimensional finite difference scheme and showed that thermal models of slabs sinking at appropriate angles and velocities result in density distributions which give gravity anomalies remarkably similar to those measured across the Tonga Trench by Talwani et al. (1961).

Toksöz et al. (1971) and Toksöz et al. (1973) followed the approach of Minear and Toksöz (1970a) but they used a finer finite difference grid and smaller time steps, and assumed less shear strain heating. Toksöz et al. (1971) treat in detail the effect of the temperature distribution on the seismic delay times. Toksöz et al. (1973) used the temperature field to determine the density and then a finite element analysis to compute the stresses associated with the cooler slab assuming visco-elastic steady state flow.

These studies show that the temperature in the descending slab is lower than in the surrounding asthenosphere but reaches thermal equilibrium after sinking for about 10 Myr. The temperature distribution within the slab is dependent on the amount and distribution of shear-strain heating which is difficult to estimate. No allowance was made in any of the analyses for possible flow of the asthenosphere due either to induced density inhomogeneities as it is cooled, or to viscous drag near the descending slab. This flow will tend to increase the time required for a given thermal state to be reached.

1.3 Stresses in subduction zones

The stresses and strains associated with the lithosphere bending and sinking into the asthenosphere at a

subduction zone have been studied previously by several distinct methods. The study of the direction of the first arrivals and seismic moments of earthquakes has placed limits on the order of the stress drop in the source region and the directions of the principal stresses (fig. 1.2).

The tensional stresses (fig. 1.2) causing shallow earthquakes in the vicinity of and outside the trench have variously been ascribed to the pull of the heavy slab as it sinks in the asthenosphere (eg. Abe, 1972) or to deformation stress due to the bending of the lithosphere before it is subducted (eg. Stauder, 1968; Hanks, 1971; Watts and Talwani, 1974). Sykes (1971) has pointed out that all the large earthquakes outside trenches, which give normal fault solutions have been preceded within 10 years by large earthquakes resulting from thrusting in the shear zone (fig. 1.1). This may indicate that the stresses are caused by the pulling mechanism. Both mechanisms are likely to cause high tensional stresses in the upper layers of the lithosphere and to contribute to the earthquakes (Stauder, 1975). They are probably complementary; the "pulling" almost certainly contributing to the stresses which are "bending" the plate.

The absence of normal fault mechanisms outside some subduction zones has been explained by Hanks (1971) by a

superimposed large (several kilobar) compressional horizontal stress.

The stress drop calculated for earthquakes near subduction zones varies widely from a few bars to about one kilobar (eg. Abe, 1972; Hanks, 1971; Linde and Sacks, 1972; Wyss, 1970). The differences are often ascribed to the various assumptions as to the proportion of released elastic energy which is dissipated by seismic waves. It is unlikely, however, that the stress drop would be more than 2.0×10^8 N/m^2 (2 kbar) for most earthquakes.

Computation of the elastic bending of the lithosphere has been successful in simulating the surface shape of the plate being consumed. In these analyses the lithosphere is approximated by a thin plate with non-viscous fluid above and below (Walcott, 1970; Le Pichon et al., 1973; Watts and Talwani, 1974). The elasticity is assumed constant throughout the thickness of the plate. The effective thickness of the lithosphere determined from these calculations is 25 to 50 km which is much smaller than the determinations by other methods. Walcott (1970) suggested the use of visco-elastic parameters in the analysis but considered that the constraints are too poorly known to determine the parameters relevant to these flexures. Even with thicknesses of only 25 to 50 km the stresses due to the bending of an elastic lithosphere through 35^o are several kilobars. These are

tensional at the top surface of the plate and compressional at the bottom. The strength of the rocks is much less than this, invalidating the simple elastic analysis. Also, as the plate is progressively subducted the bend migrates backwards along it so that the stresses released by failure or creep will tend to be replaced by stresses of opposite sign as the bent part of the slab is re-straightened.

The thin plate analysis of the slab being subducted also gives an estimate of the horizontal stress at the boundary between the two lithospheric plates. By comparing the topography outside ocean trenches with the deflections computed for a thin plate Watts and Talwani (1974) showed that these stresses may be as large as 13 kbar for some arcs but negligible for others.

Other estimates of the horizontal stress between the two plates may be made from the formation of magma at depths of 100 - 120 km by shear strain heating at the junction of the two plates. This magma results in the andesitic volcanicity which is characteristic of these areas of the earth (fig. 1.1). The values thus estimated for the shear stress in the plane of the slip between the plates is a few kilobars (eg. Hasebe et al., 1970; Toksöz et al., 1973).

It has been suggested that the pull of the cool sinking slab on the lithosphere before it is subducted contributes

a large part of the driving force of plate tectonics (McKenzie, 1969; Elsasser, 1971; Harper, 1975; Forsyth and Uyeda, 1975). The stress estimated simply from the negative buoyancy is of the order of several kilobars (McKenzie, 1969; Turcotte and Schubert, 1971).

The method employed for computing the stresses within and near the descending slab depends on estimating the density distribution from the computed temperature distributions. Smith and Toksöz (1972) used the temperature distributions of Toksöz et al., (1971) and then applied an electrostatic analog of the elastic stress problem. They used temperature dependent elastic properties. Toksöz et al., (1973), and Neugebaur and Breitmayer (1975) used similar temperature distributions and visco-elastic finite element analyses to calculate the stresses due to the negative buoyancy of the sinking slab. Sleep (1975) used a viscous finite difference analysis to model the subduction below the Aleutian Arc. The direction of principal stresses given in these papers are consistent with earthquake mechanism studies. The calculated deviatoric stresses are about 0.5 kbar. The flow rates and directions predicted (especially by Neugebaur and Breitmayer) are not consistent with those assumed in the temperature analysis and so some doubt is placed on the validity of the results. These analyses have only accounted for the stresses induced in

the slab by the negative buoyancy of the cold lithospheric slab.

Despite the limitations of these analyses it is evident that the viscosity of the asthenosphere plays an important role in supporting the cold slab. If the viscosity is too low the asthenosphere does not support the slab sufficiently so that the slab tends to bend and distortional stresses become great. To get agreement between his models and the topography in the Aleutian area Sleep (1975) had to introduce a low viscosity wedge in the vicinity of the accretionary prism (fig. 1.1). Neugebaur and Breitmayer (1975) showed that it is necessary to use a stress-dependent viscosity to adequately model the asthenosphere and sinking slab. They suggest a power law in which the viscosity is inversely proportional to the square of the shear stress.

1.4 Sources of stress in the earth

There are several sources of stress within the earth which need to be considered. They may be classified according to the origin of the forces or displacements which induce the stresses in the model. The stress distribution must also depend on the variations of the physical properties throughout the model.

The main subdivision of the forces acting on a model are the body forces and boundary forces. Body forces act throughout the model and are a result of the physical properties and state of the body. The main body forces are:

(a) Gravitational body forces due to the density distribution throughout the model.

(b) Initial stresses (Jaeger and Cook (1969) call them residual stresses) are related to the previous history of the rocks, and include stresses present prior to the analysis. These stresses are usually poorly known but may alter the computed stresses and flow to a considerable extent. In longer term visco-elastic analyses the effect of stresses generated at any one time decrease with increasing time. Thus the significance of the initial stresses decreases with time and depending on the flow laws may be neglected.

(c) Stresses due to volume changes may be sub-classified according to the cause of the volumetric change. These can be due to changes in temperature, phase changes or loss of mass by fluid extraction. In elastic analyses, these stresses are treated as initial stresses or strains (Zienkiewicz, 1971).

Boundary forces can be either implied by the specification of displacements or added as explicit pressures on the boundaries. Restrictions on the motion of any part

of a model imply the addition of forces to impose the restrictions. It is usual, but not essential, that the added forces are normal to the direction of motion. One type of boundary where this is not so is when it is desired to impose some frictional forces to a boundary.

The most common explicit pressures applied to models are those due to the sea and other hydrostatic stresses. If only the lithosphere is considered in the model the force due to the asthenosphere on the base of the model may be included as an explicit hydrostatic pressure.

To compute the stresses and strains in a model of part of the earth several "tools" are required. These are developed in Chapters 2 and 3. Mathematical expressions suitable for use in computers for the physical properties of the earth required for the models are developed in Chapter 2. In Chapter 3 finite element methods for computing the stresses and strains in visco-elastic models are developed and a method of computing the variation of temperature with time described.

CHAPTER 2

PHYSICAL PROPERTIES OF THE CRUST AND UPPER MANTLE

For this study the bulk physical properties, under slowly varying conditions, of the oceanic crust and upper mantle are required. These properties depend on temperature and stress.

It is possible to estimate the elastic properties and density as a function of depth from seismic wave velocities and the mass and moment of inertia of the earth (Birch, 1952; Bullen, 1963; Clark and Ringwood, 1964). These estimates, which are averages over large areas of the earth, are useful for studying the response to small stresses and strains when the rocks are close to their normal conditions. However, these average properties do not show how the properties vary as the rock is subjected to substantial changes in temperature and pressure, as for example when oceanic crust and upper mantle move downward in a subduction zone. In addition the seismic wave velocities only indicate the response of the rocks to high frequency elastic waves, and so estimates of elastic parameters from them may not be applicable to the response of rocks to slowly varying conditions. For example, if the rocks are within $\alpha\lambda$ phase transition, a change in pressure will cause a much larger change in volume than that suggested by the seismic velocities.

Many measurements have been made over the last century of the properties of rocks and minerals (Clark, 1966) but only recently have experimental temperatures and pressures reached those existing in the lower crust and upper mantle. Furthermore, many of the measurements have been made on individual minerals rather than rocks. It will normally be assumed that a bulk property of the rock is the weighted mean of the properties of the constituent minerals. For a nearly monominerallic rock it will be assumed equal to that of the mineral.

The major units which will be considered are the mantle and the oceanic crust. These are assumed to be compositional divisions and their physical properties depend on the pressure and temperature. In this chapter functions, for each of the properties, are developed which are suitable for use in a digital computer.

Another useful subdivision of the outer layers of the earth is that of lithosphere, asthenosphere and mesosphere. The lithosphere (0 to about 80 km in the oceans and 110 km under the continents (Walcott, 1970)) is not significantly susceptible to creep, having an apparent Newtonian viscosity of 1.0×10^{23} Ns/m^2 (Walcott, 1970) or 1.0×10^{25} Ns/m^2 (Watts and Cochran, 1974). Below the lithosphere, the asthenosphere has a much lower viscosity. This has been estimated as about 1.0×10^{21} Ns/m^2 (Haskell, 1935, 1937;

McConnell, 1968). At a depth of about 350 km there is a phase change in the rocks composing the mantle and this probably causes an increase in the viscosity (Stoker and Ashby, 1973). The mantle below this phase transition is termed the mesosphere. The viscosities mentioned here should be treated as approximate. It will be shown later in the chapter that they are dependent not only on the ambient pressure and temperature but also on the shear stress.

The pyrolite model for the mantle proposed by Ringwood (1962a,b, 1966a,b), Green and Ringwood (1967) and Ringwood (1969a) has now largely been accepted (Harris et al., 1972). This model gives the chemical composition of the mantle as being equivalent to 3 parts of dunite to 1 part of basalt. The mineralogical composition depends on the pressure and temperature (fig. 2.1). At low pressures the mantle is plagioclase peridotite (A in fig. 2.1). At about 15-20 km the plagioclase reacts to form spinel and pyroxene, to give spinel peridotite (B in fig. 2.1). This in turn changes to garnet peridotite at about 70 km. (Ringwood, 1969a). All these rocks consist largely of olivine with the minor constituents changing phase. At the start of the transition zone (350-400 km) the olivine itself changes to a more dense spinel crystal structure. At about 600-700 km the minerals progressively change to more dense crystal structures in the post-spinel phase.

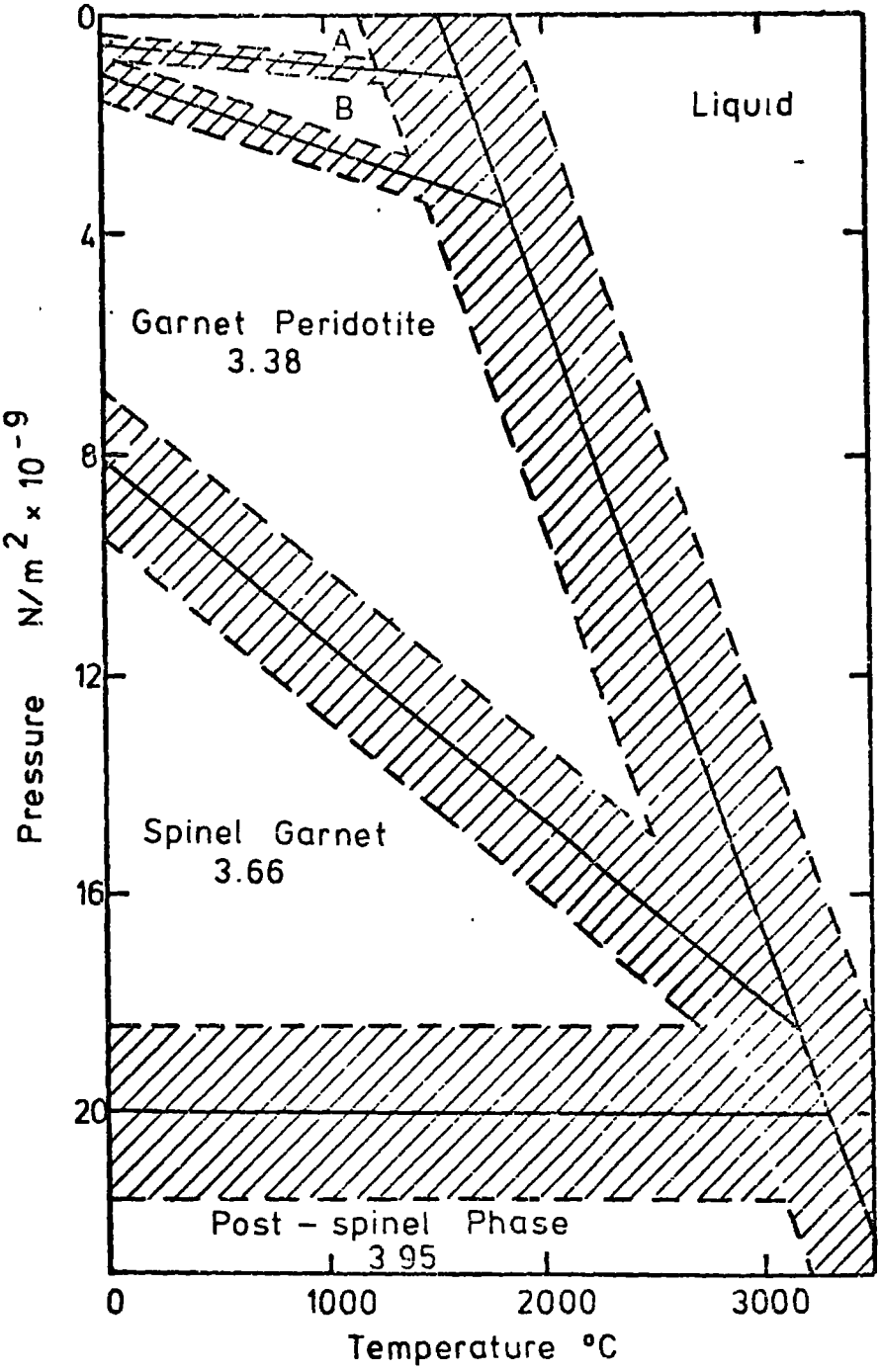

Fig. 2.1 Phase diagram for a pyrolitic mantle. Areas of phase transition are shaded. A = plagioclase peridotite (ρ = 3.24 Mg/m^3); B = spinel peridotite (ρ = 3.32 Mg/m^3). Numbers are room condition densities of the phases.

The olivine in this model has a composition of 85 - 95% forsterite and 5 - 15% fayalite. Because of the widely assumed predominance of olivine in the mantle there has been, in the past decade, a great emphasis in experimental work on determining the high temperature, high pressure properties of olivine (Chung, 1971; Schaltz and Simmons, 1972) and the olivine-rich rocks - dunite and peridotite (eg. Carter and Ave' Lallemant, 1970).

The oceanic crust is often divided into three layers (eg. Shor et al., 1971). Layer 1 consists of sediments typically less than 0.5 km thick but sometimes much thicker near continental margins. Layer 2 consists of basalt about 1.5 km thick (Shor et al., 1971). The composition of layer 3 is uncertain, possibilities being gabbro, amphibolite or serpentinite; Cann (1974) favours gabbro with a thin zone of amphibolite near the layer 2-layer 3 boundary. It is here assumed, for the purposes of ascribing physical properties, that layer 2 is basalt and layer 3 is gabbro.

2.1 Mechanical properties

In the analysis of tectonic processes the rheology of parts of the crust and upper mantle have been described variously as elastic (Watts and Cochran, 1974; Watts and Talwani, 1974), having Newtonian viscosity, (Haskel, 1935,

1937; Turcotte and Oxburgh, 1969; Sleep, 1975) or as a Maxwell substance (Walcott, 1970; Tosköz et al., 1973· Neugebauer and Breitmayer, 1975). In laboratory experiments on rock deformation a strongly time dependent primary creep is observed (eg. Murrell and Chakravarty, 1973) but this becomes negligible after a few months and can be ignored in modelling tectonic processes.

The combination of changes in density during phase transitions and instantaneous elastic effects may be rheologically modelled (fig. 2.2) by a Maxwell and a Kelvin element in series, which is a Bergers substance (Jaeger and Cook, 1969). The Maxwell elastic element, L_m, represents an instantaneous response to an applied stress, σ , and the corresponding viscous element, V_m, represents the steady state creep. The Kelvin element applies to a region of phase transition; the elastic response, L_k, describing the volumetric change and the viscous member, V_k, the rate of reaction. At temperatures above 300^{o}C the phase changes we are concerned with are fast enough to be studied in the laboratory and so the delay caused by V_k can be ignored in the analysis of tectonic processes; however, the apparent elastic parameters will differ from those estimated from seismic velocities, which depend only on L_m.

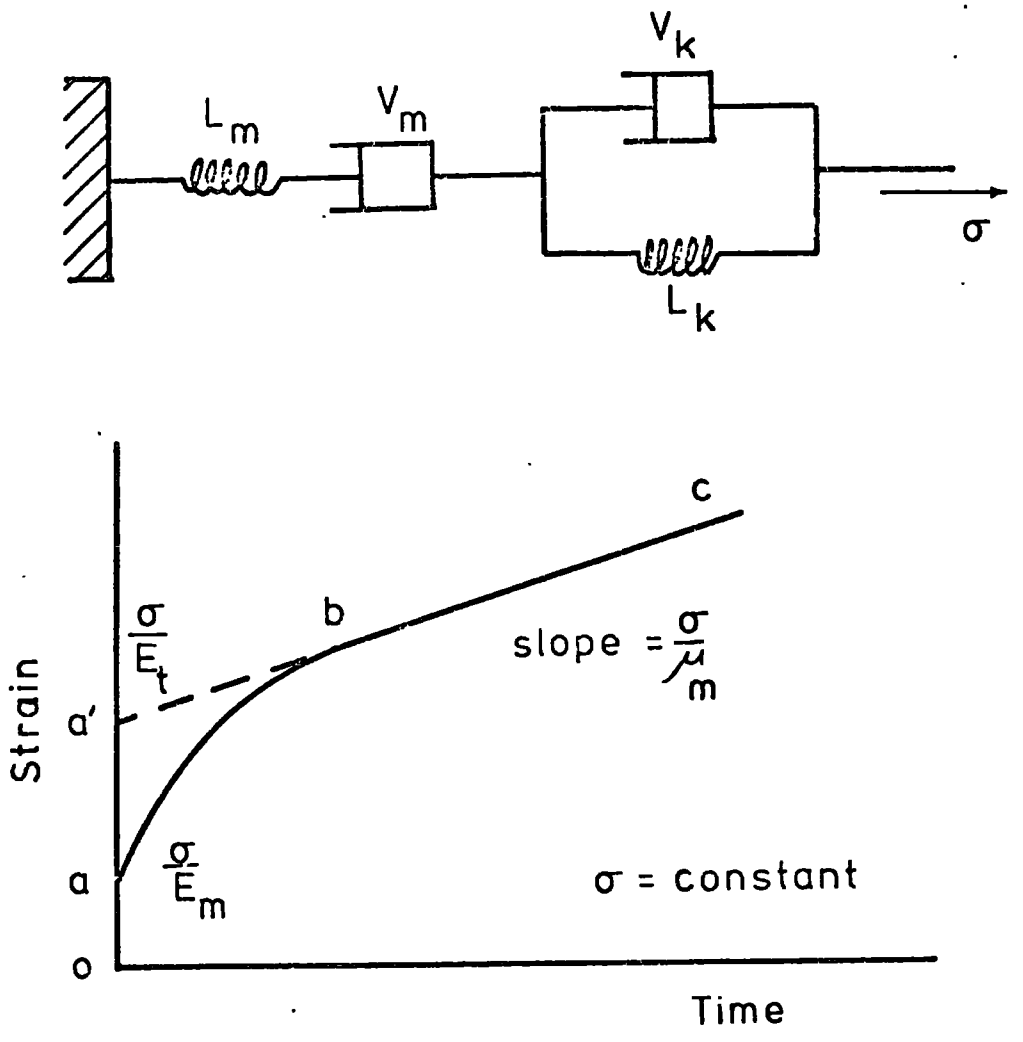

Fig. 2.2 Rheological model for rocks. The Maxwell element (L_m, V_m) applies throughout the pressure temperature range, but the Kelvin element (L_k, V_k) applies only in areas of phase transition.

2.1.1 Equation of state for a two phase system

The equation of state for rocks has commonly been determined by compressional experiments or by seismic velocity determinations on single crystals or monominerallic samples (Clark, 1966; Chung 1971, 1972; Anderson, 1972; Ahrens, 1975). These have often been expressed in terms of the Birch equation (Birch, 1952; Chung, Wang, and Simmons, 1970):

$$p = (3K_o/2)(y^7 - y^5)[1 + 0.75(m-4)(y^2-1)] \qquad 2.1$$

where p is the pressure and $y = (\rho/\rho_o)$. K_o, m and ρ_o are dependent upon temperature alone (Birch, 1952) and correspond to the bulk modulus, first pressure derivative of the bulk modulus and density, all at zero pressure.

This equation gives an excellent method of extrapolating experimental data to the high pressures encountered in the earth, provided that the same phases are present under both sets of conditions (Chung, 1972). Its application to the present problem has two major difficulties. Firstly, it only applies where there are no phase changes, and secondly, the derivatives of density with respect to temperature and pressure are complicated expressions involving the cube roots of the density. Further, to find the standard density at a given temperature and pressure,

it is necessary to evaluate K_o, m and ρ_o for that temperature and then to solve a 7th order polynomial for y.

The density of a phase within its stability field may be approximated by a polynomial, F(P,T) such that

$$\rho = \rho_o F(P,T) \qquad 2.2$$

where ρ_o is the density at room conditions. Normally a second or third order expression for F is required to give sufficient accuracy.

The density function of a single component system is discontinuous at a phase boundary (Ricci, 1951). Rocks are usually multicomponent systems and the change from one phase to another takes place over a transition zone within which both phases exist. The actual variation of density within the zone depends on the density and proportion of each phase. The composition, density and proportion of each phase continuously change throughout the zone.

Many changes considered as phase boundaries in geophysics are in fact a combination of two or more mineralogical phase boundaries (eg. Ringwood, 1969a,b) and hence the density changes in the transition zone may be complex. As a simplification it will be assumed that the density function is continuous and has a simple analytical form in the vicinity of the phase boundary. It will be

shown (Section 4.1) that in the study of reasonably large scale tectonic processes the actual function used does not alter the computed stresses and strains significantly.

If the proportion of each phase is assumed to be dependent only on the distance from the centre of the transition zone then we may define a variable, d, by

$$d = k(a + bT + cP) \qquad 2.3$$

where d = 0 describes the centre of the transition zone in P , T space, a, b, c being constants and k a scaling factor. B(d) is a function defined to describe the relative proportions of each phase such that:

$$B(d) = 1 \text{ for } d \ll 0,$$
$$B(d) = 0 \text{ for } d \gg 0, \qquad 2.4$$
$$\text{and } B(-d) = 1 - B(d).$$

For two phases, the density function may be expressed as

$$\rho = \rho_1 F_1 B(-d) + \rho_2 F_2 B(d) \qquad 2.5$$

where ρ_1 , ρ_2 are the densities of the two phases at room conditions. F_1 and F_2 are functions describing how the density of the individual phases change with pressure and temperature.

If the proportion of the phases varies linearly across

the transition zone then

$$B(d) = \begin{cases} 0 & d > 1 \\ 0.5(1-d) & -1 < d < 1 \\ 1 & d < -1 \end{cases} \qquad 2.6$$

and k in equation 2.3 is chosen so that d varies from -1 to +1 across the transition zone.

An alternative continuous function suitable for B(d) is

$$B(d) = 0.5 - \frac{1}{\pi}\tan^{-1}(d) \qquad 2.7$$

This has the advantage that not only the density but also the compressibility and thermal expansion are continuous functions and so some numerical methods of stress analysis which require iteration to a solution will be more stable. The value of k will of course be different from that for the linear function. The disadvantages of this function are that it deviates a little from 0 or 1 outside the transition zone and that the derivatives in the centre of the transition zone are about twice those for the linear function.

2.1.2 Equation of state for the mantle

The phase diagram for a pyrolite mantle is shown in fig. 2.1. Most of the phase boundaries are fairly well established from experimental work and have been taken from

Wyllie (1971). However, the boundary between the spinel garnet phase and the post-spinel phase is in dispute and it is not certain whether the reaction is exothermic or endothermic (Ringwood, 1972; Liu, 1975). The boundary is at about 2.0×10^{10} N/m^2 and the change in phase increases the density by about 8% (Anderson, 1967; Ringwood, 1969b). I assume that this boundary has no slope in the phase diagram, which implies that there is no heat of reaction and that the boundary will be at a nearly constant depth of 600 km.

The density function for fig. 2.1 may be written:

$$\rho(P,T) = \{[\rho_0 + (\rho_1 - \rho_0)\,B(d_1) + (\rho_2 - \rho_1)\,B(d_2)]\,B(-d_3)\,F_0(P,T) + \rho_3\,B(d_3)\,F_3(P,T)\}\,\{1 + 0.08\,B(d_5)\}\,\{1 - 0.09\,B(d_4)\} \qquad 2.8$$

The five phase boundary functions, d_1 - d_5, are:

$d_1 = k_1 \times (1800 + T - 3.0 \times 10^{-6} \times P)$ for the plagioclase peridotite-spinel peridotite transition

$d_2 = k_2 \times (964 + T - 8.03 \times 10^{-7} \times P)$ for the spinel peridotite-garnet peridotite transition

$d_3 = k_3 \times (2400 + T - 3.0 \times 10^{-7} \times P)$ for the garnet peridotite-spinel garnet transition

$d_4 = k_4 \times (1500 - T + 9.0 \times 10^{-8} \times P)$ for the dry solidus and

$d_5 = k_5 \times (200.0 - 1.0 \times 10^{-8} \times P)$ for the spinel garnet-post spinel transition. T is in ^{o}C and P in N/m^2.

The densities at room conditions of the plagioclase peridotite, spinel peridotite, garnet peridotite and spinel garnet phases ($\rho_0 - \rho_3$) have been evaluated from their mineralogical composition as 3.24, 3.32, 3.38 and 3.66 Mg/m^3 respectively (Green and Ringwood, 1963; Ringwood, 1969a,b). The term $\{1 + 0.08\,\beta(d_s)\}$ allows for an increase of 8% in the density at the spinel garnet - post spinel transition (Ringwood, 1969b) while the final term, $\{1 - 0.09\beta(d_u)\}$, allows for a 9% reduction in the density on melting. The effect on density of the compositional variations of the minerals within a phase is generally small in comparison with the compressibility of the minerals and so is neglected (Ahrens, 1973).

The peridotite phases all contain more than 55% olivine (Green and Ringwood, 1963) so the variation of their densities with pressure and temperature will be similar to that for olivine. Hence $F_o(P,T)$ is taken to represent the compressibility and thermal expansion effects for all three peridotite phases. The bulk modulus , K_o , and its derivative with respect to pressure, m, of olivine ($Fa_{90}\ Fo_{10}$) at zero pressure are

$$K_o = 1.274 \times 10^{11} - 0.177 \times 10^{8}\ T$$

$$m = 5.16 \quad \text{(Chung, 1971).}$$

Using these and the coefficients of thermal expansion at

zero pressure given in section 2.2.1, the fractional change in density, $(\rho - \rho_o)/\rho_o$, was determined at points on a grid in P and T over the stability field of the phases by using the Birch equation (equation 2.1). A cubic polynomial, Fo, was then fitted to the points. Similarly using Chung's (1972) estimate for the values of K_o and m for the spinel phase, a quadratic polynomial, F_s, was determined. The coefficients for both polynomials are given in Table 2.1.

When a linear function for the density variation across the phase transitions is used (equation 2.6), k_1 to k_5 are 0.001, 0.0025, 0.0011, 0.0014 and 0.0313 respectively. If equation 2.7 is used then values of k_1 to k_5 of 0.011, 0.0411, 0.0157, 0.0094 and 0.05 cause the functions $B(d_n)$ to change from 0.1 to 0.9 over the estimated ranges of the transitions.

2.1.3 Equation of state for the oceanic crust

Assuming the oceanic crust to be chemically equivalent to an alkali-poor olivine tholeiite, its phase diagram is shown in fig. 2.3 (from Ringwood and Green, 1966). The dry melting for basalts is taken from Cohen, Ito and Kennedy (1967) and the densities of the solid phases are given by Ringwood and Green. The value of 3.10 Mg/m^3 may be too high for the gabbroic oceanic crust but if allowance is made for about 5% pore space this would be reduced to a reasonable

Table 2.1 EQUATION FOR THE DENSITY OF VARIOUS PHASES AS A FUNCTION OF PRESSURE AND TEMPERATURE

The equation for the density of the phases (without regard to phase changes) is given by

$$\rho = \rho_o \left(1 + \sum_{i=1}^{N} a_i P^{k_i} T^{l_i} 10^{-m_i}\right)$$

i	k	l	m	olivine	spinel	gabbro	eclogite
1	1	0	11	0.7983	0.5407	1.15	0.7695
2	0	1	5	-2.9793	-2.6793	-1.4	-4.1965
3	2	0	22	-1.4796	-0.4188	-	0.7063
4	1	1	16	8.3380	3.5937	-	7.7171
5	0	2	9	-3.9511	1.0101	8.0	4.7881
6	3	0	33	3.2213	-	-	-
7	2	1	25	-3.0169	-	-	-
8	1	2	18	1.6102	-	-	-
9	0	3	12	6.2758	-	-	-

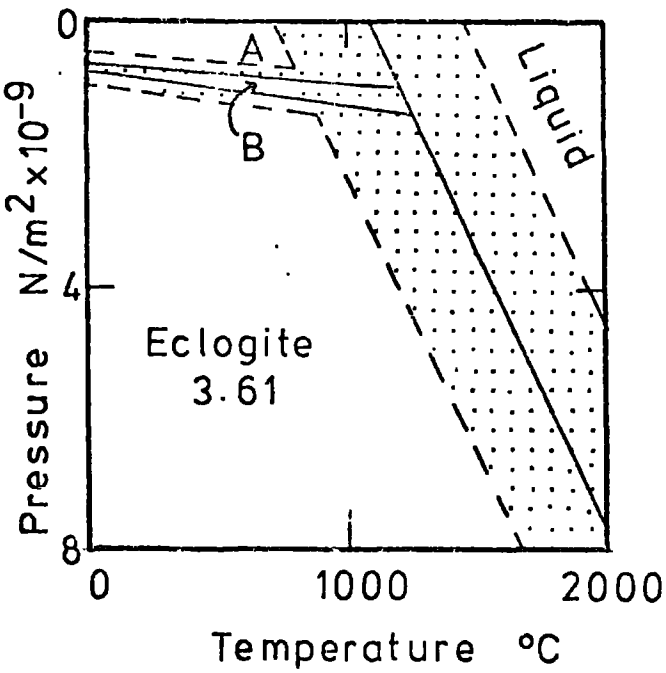

Fig. 2.3 Phase diagram for oceanic crust. Phase transitions are shaded. A = gabbro-basalt B = garnet granulite.

2.90 Mg/m^3. The density changes across the solid phase boundaries have been discussed by Wyllie (1971) and may occur as two or three distinct steps. However, for simplicity, it will be assumed that the density changes gradually from 2.90 Mg/m^3 for the low pressures assemblage to the density of eclogite of 3.40 Mg/m^3. The phase boundary will be taken as the mean of the gabbro-garnet granulite and garnet granulite-eclogite boundaries.

Thus the density function for the oceanic crust becomes

$$\rho = [\rho_0 F_g B(-d_1) + \rho_1 F_e B(d_1)][1 - 0.09 B(d_2)] \qquad 2.11$$

where $\rho_0 = 2900$

$\rho_1 = 3400$

$d_1 = k_1 \times (1500 - 2.3 \times 10^{-6} \times P + T)$ refers to the gabbro-eclogite phase transition and 2.12

$d_2 = k_2 \times (1080 - T + 1.2 \times 10^{-7} \times P)$ refers to the solidus. F_g and F_e are functions describing the change of the density of the low pressure assemblage and eclogite respectively with pressure and temperature.

For the linear variation of density across the phase boundary, k_1 and k_2 are 0.00067 and 0.002 respectively. If equation 2.7 is used, k_1 and k_2 are 0.013 and 0.011.

Since the stability zone for gabbro is small, the compressibility and coefficient of thermal expansion will

not vary much over its field and so F_g may be approximated by

$$F_g = 1.0 + 1.15 \times 10^{-11}P - (1.4 \times 10^{-5}T + 8.0 \times 10^{-9}T^2) \qquad 2.13$$

The pressure term is the mean compressibility for gabbro given by Birch (1966). The temperature terms are determined in section 2.2.1.

The effect of pressure and temperature on the density of eclogite is more difficult to estimate. Green and Ringwood (1967) indicate that as the pressure is increased at a given temperature so the ratio of garnet to pyroxene is increased. If the mineral proportions remain constant, the density function may be estimated from measurements on the individual minerals. When the mineralogy varies with P and T there is an additional cause for the change in volume. However, the lack of measurements on eclogites forces this effect to be neglected even though it may be substantial. The bulk modulus and its first pressure derivative at zero pressure were determined to be 1.38×10^{11} and 5.0 respectively by averaging the values for pyroxenes and garnets (Birch, 1966). The variation of K with temperature at zero pressure is unknown but for nearly all substances it decreases as the temperature increases Birch (1952). It was assumed that

$$K_o = 1.38 \times 10^{11} - 0.2 \times 10^{8} \times T \qquad 2.14$$

These values were used in the Birch equation of state, in a similar manner as the equivalent properties for the mantle, to determine Fe as a quadratic polynomial in pressure and temperature. The coefficients are given in table 2.1.

2.1.4 Elastic properties

Isothermal elastic properties are required but these are usually only a few percent different from the adiabatic properties (Birch, 1952). Unless otherwise stated I assume that these are equal.

The isothermal compressibility β_T, is defined as

$$\beta_T = \frac{1}{\rho}\left(\frac{\partial \rho}{\partial P}\right)_T \qquad 2.15$$

Assuming the density functions established in the previous sections (2.1.2 and 2.1.3) for the mantle and the oceanic crust the compressibility and bulk modulus can be directly determined.

In the analysis of elastic or visco-elastic processes two elastic parameters are required. Equation 2.15 gives β_T. The other parameter cannot be determined from the equation of state. Since the equation of state given here describes the density in a state of mineralogical equilibrium it incorporates the elastic constants relevant to both the

instantaneous response, L_m, and phase change, L_k, of fig.2.2. The two elastic parameters associated with L_m may be determined from a study of seismic velocities. Compressional velocity, V_p (Birch, 1961) and shear velocity V_s (Christensen, 1968) of rocks have been shown to be nearly linear with density for a given mean atomic weight. For the same chemical composition this linearity should hold to a good approximation.

The mean atomic weight of the mantle and basalt are about 21 and 22 respectively (Chung, 1971; Christensen, 1968). These give

$$V_p = 3.16\,\rho - 2206.0$$
$$V_s = 1.63\,\rho - 880.0$$

for the mantle and

$$V_p = 3.16\,\rho - 3000.0$$
$$V_s = 1.63\,\rho - 1280.0 \qquad 2.16$$

for the oceanic crust.

From these the instantaneous Young's modulus, E_m, and Poisson's ratio, ν_m, may be determined as

$$\nu_m = \tfrac{1}{2}\,(R-2)/(R-1), \text{ where } R = (V_p/V_s)^2,$$

and $$E_m = 2\,V_s^2\,(1+\nu_m).$$

For two sources of elasticity acting in series it may be shown that

$$\frac{1}{E_T} = \frac{1}{E_M} + \frac{1}{E_K}$$

and

$$\frac{\nu_T}{E_T} = \frac{\nu_m}{E_M} + \frac{\nu_K}{E_K}$$

Eliminating E_K and substituting $\beta_T = 3(1 - 2\nu_T)/E_T$ gives

$$\nu_T = \frac{3(\nu_m - \nu_K) + \nu_K E_m \beta_T}{E_m \beta_T + 6(\nu_m - \nu_K)} \qquad 2.17$$

The value of ν_K will depend on the type of phase change represented by the Kelvin element in the rheological model. If it is simply a change in the crystal lattice, the change in volume may be by equal strain in all directions indicating ν_K equal to -1. If recrystallization takes place then the new crystals are likely to grow preferentially in the direction of the least compressive stress and ν_K may take any value between -1.0 and 0.5. It will be shown in section 4.1 that ν has a much smaller effect than β on the stresses produced in a model and it is usually sufficient to take $\nu_T = \nu_m$.

2.1.5 Viscosity

Haskell (1935, 1937) showed that a uniform kinematic viscosity of 2.6×10^{21} Stokes is required to account for the rate of isostatic adjustment of Fennoscannia. This is equivalent to a dynamic viscosity of about 1.0×10^{21} Ns/m^2.

Since then viscosities of the upper mantle between 1.0×10^{19} and 1.0×10^{21} Ns/m^2 have been used successfully in modelling some processes which occur in the earth (Knopoff, 1964; Christoffel and Calhaem, 1973; Harper, 1975).

The main difficulties in measuring the creep behaviour of rocks in the laboratory are (1) different creep mechanisms predominate under different conditions and (2) natural strains are very slow in comparison with laboratory rates. If, however, the fabric and the dislocation patterns in the samples deformed at higher rates are similar to those in naturally deformed rocks, then it is likely that the creep mechanism is the same (Ave' Lallemant and Carter, 1970). Stocker and Ashby (1973) summarized seven steady state creep mechanisms of which five could be important in rocks for conditions thought to prevail at depth. The flow law for all these can be approximated by the empirical relationship employed by Weertman (1970):

$$\dot{\epsilon} = A f(\tau) D_o \exp(-Q/RT) . \qquad 2.18$$

$f(\tau)$ is a function of the shear stress, τ, usually expressed as a power:

$$f(\tau) = \tau^n \qquad n \geq 1.0 \qquad 2.19$$

D_o is a diffusion constant which is dependent upon the elastic modulii and temperature. This will vary slightly with conditions but the uncertainty in the other parameters makes the variations unimportant and they will be neglected. Q is an activation energy which is pressure dependent. However, its variation is closely linked to the variation of the melting temperature with pressure (Carter and Ave' Lallemant, 1970) so that if we replace the exponential term by $\exp(-q T_M/T)$ the new variable, q, may be taken as constant under a wide range of pressures.

a) Viscosity of the mantle

For olivines and olivine rich rocks deformed dry most determinations of Q are in the range 100-130 Kcal/mole (Table 2.2).

Some confusion has been evident in the use of $T_{M\lambda}$ the melting temperature. In most papers dealing with the experimental results, the value of the dry melting temperature of pure olivine given by Davis and England (1964) is used. However, the mantle is probably pyrolite and not pure olivine; Neugebauer and Breitmayer (1975), for instance, have used the dry melting temperature of pyrolite but have failed to

Table 2.2 CREEP LAWS FOR POSSIBLE MANTLE MATERIAL

DRY ROCKS

AUTHOR	$\bar{Q}$	$\bar{q}$	$\bar{T}_M$	P	n	T_M	q	SAMPLE
A	120	28.7	2100	15	4.8	1410	42.8	a
B	106	26.4	2100	15	5.0	1410	39.3	ab
C	96	23.0	2170	0	3.0	1316	37.9	c
D	111	-	-	15	3.3	1410	39.6	a

WET ROCKS

AUTHOR	$\bar{Q}$	$\bar{q}$	$\bar{T}_M$	P	n	T_M	q	SAMPLE
A	80	-	-	15	2.3	1010	39.8	b
A	80	-	-	15	2.4	1010	39.8	a
D	54	-	-	15	2.1	1010	26.8	a

AUTHOR
A Carter and Ave' Lallemant (1970)
B Raleigh and Kirby (1970)
C Kirby and Raleigh (1973)
D Carter (1975)

$\bar{Q}$ Activation energy given by above authors

$\bar{q}$ factor to be used with the melting temperature $\bar{T}_M$

P experimental pressure (K_b)

n power law for shear stress

T_M melting point of pyrolite at conditions of experiment

q factor to be used with T_M ($q = \bar{q}\ T_M/\bar{T}_M$)

Samples

a Dunite

b Lhertzolite

c Empirical relation

correct q accordingly.

I use the melting temperature of pyrolite but correct q so that the experimental creep rates are predicted by the expressions - that is

$$q = \bar{q}\ \bar{T}_M/T_M \qquad 2.20$$

where the bar represents the published values and the unbarred variables those used in this paper. $\bar{T}_M$ and T_M are evaluated at the pressure of the experiments. The results are shown in table 2.2. This indicates that, in spite of the difficulties in applying a theory derived for pure substances to complex rocks, the values of q calculated from various results are about the same. I assume a value of 40.0 for dry mantle.

n is dependent upon the flow mechanisms contributing to the creep and the crystal structure, particularly if dislocation creep mechanisms are important. Kohlstedt and Goetze (1974) have shown that $f(\sigma)$ is not a simple power law for olivine but Neugebauer and Breitmayer (1975), using the same data, have shown that it may be approximated by power laws of n = 3 and n = 5 depending on the shear stress, σ. Also using the same creep data, q = 40.0 and T_M = 1316°K (the melting temperature of pyrolite at atmospheric pressure) the following creep laws may be obtained:

$$\dot{\epsilon} = 1.6 \times 10^{-15} \exp(-40.0\, T_M/T)\, \sigma^3 \qquad \sigma \leq 1.0 \times 10^8$$

and

$$\dot{\epsilon} = 3.2 \times 10^{-32} \exp(-40.0\, T_M/T)\, \sigma^5 \qquad \sigma > 1.0 \times 10^8$$

There may be a range of conditions in which flow is linearly dependent on the shear stress, (n = 1), but this would be at very low shear stresses and so the flow would be very small and may be neglected. The transition stress has been estimated as 1.5×10^5 N/m^2 by Weertman (1970) and 0.7×10^5 N/m^2 by Stocker and Ashby (1973).

At pressures above about 30.0×10^8 N/m^2, the hydrous minerals are no longer stable (Green, 1973) and it is thus likely that there is a small amount of free water in the mantle. This would have a marked effect on the creep so that the laws determined from the experiments on "wet" dunite (Carter and Ave' Lallemant, 1970; Carter, 1975) may be more appropriate. Correcting for the melting point of "wet" pyrolite (Section 2.2.5) the revised expression of Carter (1975) becomes

$$\dot{\epsilon} = 1.3 \times 10^{-14} \exp(-26.8\, T_M/T)\, \sigma^{2.1} \qquad 2.21$$

At hydrostatic pressures so great that the olivine is changed to spinel structures, these flow relations are invalidated because of the change in the crystal parameters (Stocker and Ashby, 1973). Because of the closer packing of the atoms, the creep strength is likely to be increased considerably. An arbitrary increase of 3 orders of magnitude in the viscosity will be applied at the phase boundary.

The apparent viscosity is defined as

$$\mu = \frac{\sigma}{3\dot{\epsilon}} \quad .$$

For the above creep laws the viscosity, μ, in Ns/m^2 is

$$\left.\begin{aligned} \mu &= 2.1\times10^{14}\exp(40.0T_M/T)\,\sigma^{-2} \quad P<3.0\times10^9 \quad \sigma\leq 1.0\times10^8 \\ \mu &= 1.0\times10^{31}\exp(40.0T_M/T)\,\sigma^{-4} \quad P<3.0\times10^9 \quad \sigma>1.0\times10^8 \\ \mu &= 1.0\times10^{13}\exp(26.8T_M/T)\,\sigma^{-1.1}\,10^{3B(d_3)} \quad P\geq 3.0\times10^9 \end{aligned}\right\} \quad 2.22$$

where $B(d_3)$ is the function giving the proportion of spinel phase present (Section 2.1.2). P and σ are in N/m^2 and T in ^oK.

b) Viscosity of the oceanic crust

Murrell and Chakravarty (1973) measured transient creep in granodiorite and dolerite. If their assumption of Andrade creep is correct, their measurements suggest a viscosity of

$$\left.\begin{aligned} \mu &= 1.5\exp(53T_M/T)\,\sigma^{-1.5} \\ \text{and} \quad \mu &= 6.0\exp(42T_M/T)\,\sigma^{-1.5} \end{aligned}\right\} \quad 2.23$$

for dolerite and granodiorite respectively. These are not well determined but in the absence of any better measurements the first of these estimates will be applied to oceanic crust.

Because of computational difficulties the viscosities of all rocks will be limited to the range

$$10^{18} < \mu < 10^{45} \quad Ns/m^2 .$$

The lower limit reduces the chances of instabilities propagating in the model. If the viscosity is as great at 10^{45} Ns/m^2 no significant viscous flow can occur over periods much larger than those for which the models are studied.

2.1.6 Fracture and failure criteria

The Griffith's theory of brittle fracture (Murrell, 1964, 1965; Jaeger and Cook, 1969; Edmond and Murrell, 1973) has been applied to rocks. The initial theory has been extended to include the effects of high confining pressures (McClintock and Walsh, 1962; Murrell, 1964, 1965). I define a dimensionless variable, F, which indicates how close the stress in a rock is to causing brittle fracture. F becomes less negative as failure is approached and is positive if failure is predicted for a given state of stress. Pore fluid pressure has been neglected but is important in the failure of rocks. Its neglect gives an overestimate of the stress required for failure to occur. Following Service and Douglas (1973) three stress regimes exist.

a) If $3P + R \geqslant 0$ where P and R are the maximum and minimum principal stresses respectively (tension positive)

$$F = P/T - 1$$

where T is the tensile strength equal to about 0.5×10^8 N/m^2 for igneous rocks (Brace, 1961).

b) If $3P + R < 0$ and the compressive stress across the shear direction is not great enough to close any microcracks then

$$F = (P-R)^2/T^2 + 8\,(P+R)/T$$

c) If the microcracks are closed then

$$F = (P+R)/T + \alpha\,(P-R)/T - \beta/T$$

where $\alpha \doteq 1.356$ and $\beta = 0.02T$ are determined from values of 1.09 and -4.19T for the coefficient of friction and the compressive stress required to close the microcracks respectively (Murrell, 1965).

Whether these equations can be applied at great depths in the earth is not clear but they do give an indication of the relative likelihood of failure.

The Griffiths theory also gives the direction of failure but we will generally ignore this and simply lower the viscosity of any failed finite element thus treating the failure point more as a yield point than as brittle failure. This is purely a computational convenience.

2.2 Thermal properties

2.2.1 Coefficient of thermal expansion

A plot (fig. 2.4) of experimental measurements of the thermal expansion of minerals (Skinner, 1966) indicates

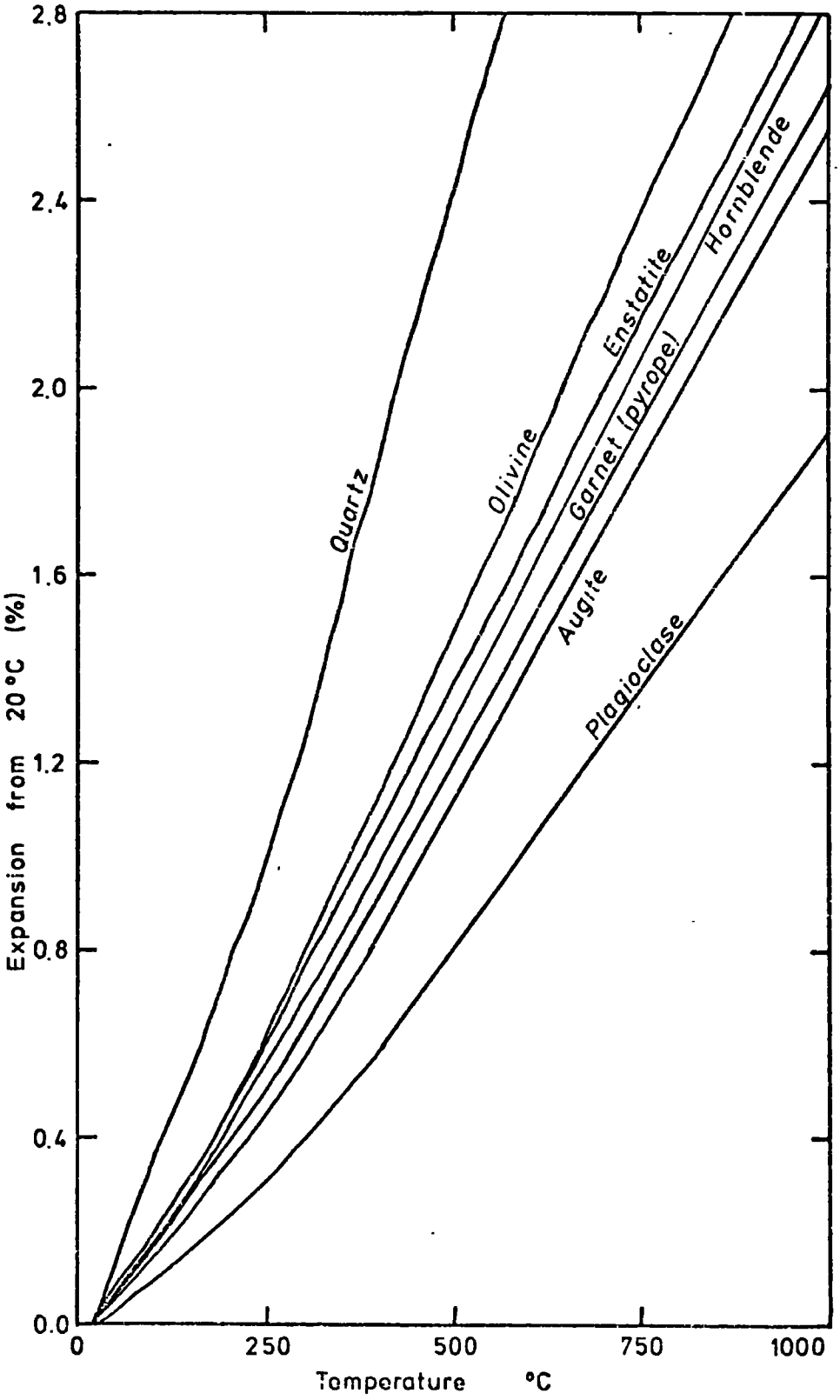

Fig. 2.4 Percent volume expansion of several minerals on heating from 20°C. (extracted from Skinner, 1966).

that above 400°C their volume increases linearly with temperature but below 400°C they expand as T^2. The expansion of rocks, at zero pressure, were estimated by averaging the values of their constituent minerals (Tables 2.3 and 2.4). These values were used to determine the density, at zero pressure, for use in the Birch equation (Sections 2.1.2 and 2.1.3) and thus in establishing expressions for the density as a function of pressure and temperature.

Once the density functions were established (Section 2.1) they were in turn used to determine the coefficients of thermal expansion as a function of pressure and temperature. By definition

$$\alpha = -\frac{1}{\rho}\left(\frac{\partial \rho}{\partial T}\right)_P \quad .$$

Using equations 2.8 and 2.11 for the density of the mantle and oceanic crust respectively gives thermal expansion coefficients which allow for the additional expansion during a phase change.

2.2.2 Thermal capacity

According to Debye the heat capacity at constant volume, C_v, of a crystalline solid at temperature T°K is given by

$$C_v = \frac{9R}{x_0^3}\int_0^{x_0} \frac{x^4 e^x}{(1-e^x)^2}\, dx \qquad 2.24$$

Table 2.3 THERMAL EXPANSION COEFFICIENTS FOR MINERALS AND ROCKS

Mineral	a x 10^5	b x 10^8	c x 10^5
Olivine ($Fa_{10}Fo_{90}$)	2.15	3.65	3.66
Amphibole	1.99	2.68	3.13
Pyroxene	1.70	2.28	3.07
Plagioclase	1.20	1.20	1.98
Garnet (Pyrope)	1.64	3.06	2.77

Rock	a x 10^5	b x 10^8	c x 10^5
Basalt	1.38	1.61	2.37
Gabbro	1.40	1.65	2.37
Amphibolite	1.77	2.27	2.81
Eclogite	1.67	2.73	2.90

The coefficient of thermal expansion α is given by

$$\alpha = a + b\,T \qquad T \leqslant 400^{\circ}C$$

$$\alpha = c \qquad T > 400^{\circ}C$$

where T is the temperature in $^{\circ}C$.

Table 2.4 MINERALOGICAL COMPOSITION OF VARIOUS ROCKS*

	basalt	gabbro	amphibolite	eclogite
Olivine	3	7	-	-
Amphibole	-	3	71	-
Pyroxene	29	20	-	45
Plagioclase	62	65	27	-
Garnet	-	-	-	55

* Extracted from Barth (1952)

where R is the gas constant, x_o is T/θ_D and θ_D is the Debye Temperature. For olivines of molecular weight 21.00 Chung (1971) gives $\theta_D = 727^oK$.

The specific heat at constant pressure, C_p, is related to C_v by

$$C_p = C_v + K\alpha^2 T/\rho \qquad 2.25$$

where K is the bulk modulus, α is the coefficient of thermal expansion, T is the temperature in ^oK and ρ is the density. Kelley (1960) has published tables of specific heat at constant pressure and expresses the variation with T by empirical equations of the form

$$C_p = a + bT + c/T^2 \quad .$$

Values of a, b, and c for several minerals are given in Table 2.5. Combining those for forsterite and fayalite (assuming zero excess heat capacity of mixing) gives

$$C_p = 1033.84 + 0.19434T - 0.2419 \times 10^8/T^2 \qquad 2.26$$

for $Fa_{10}\ Fo_{90}$. The value given by 2.26 is compared with theoretical values obtained by numerical integration of 2.24 and 2.25 using observed values of K, α and ρ for olivine at zero pressure is shown in fig. 2.5B.

At high temperatures, the gradients of the experimental and theoretical curves differ by a factor of 3.6. This implies that there must be an error of this order in either

Table 2.5 SPECIFIC HEAT AT CONSTANT PRESSURE FOR MINERALS AND ROCKS

	a	b	c x 10^{-8}
Mineral			
Fayalite*	750.08	0.19230	-0.13765
Forsterite*	1065.37	0.19457	-0.25348
Olivine ($Fa_{10}Fo_{90}$)	1033.84	0.19434	-0.24190
Amphibole (Magnesian)*	1023.24	0.22683	-0.24476
Pyroxenes			
Diopside*	1022.05	0.15156	-0.30428
Clinoenstatite*	1023.66	0.19764	-0.26186
Mean	1022.85	0.17460	-0.28307
Plagioclase			
Albite*	985.07	0.22192	-0.23968
Anorthite*	969.43	0.20617	-0.25417
Orthoclase*	960.10	0.19403	-0.25656
Mean	971.53	0.20737	-0.25014
Quartz*	781.76	0.57134	-0.18812
Rocks			
Basalt	989.35	0.19684	-0.26004
Gabbro	988.56	0.20013	-0.25630
Amphibolite	1008.99	0.22147	-0.24642

$$C_p = a + bT + c/T$$

where T is the temperature in ^{o}K.

* These values taken from Kelley (1960) and the others calculated from them.

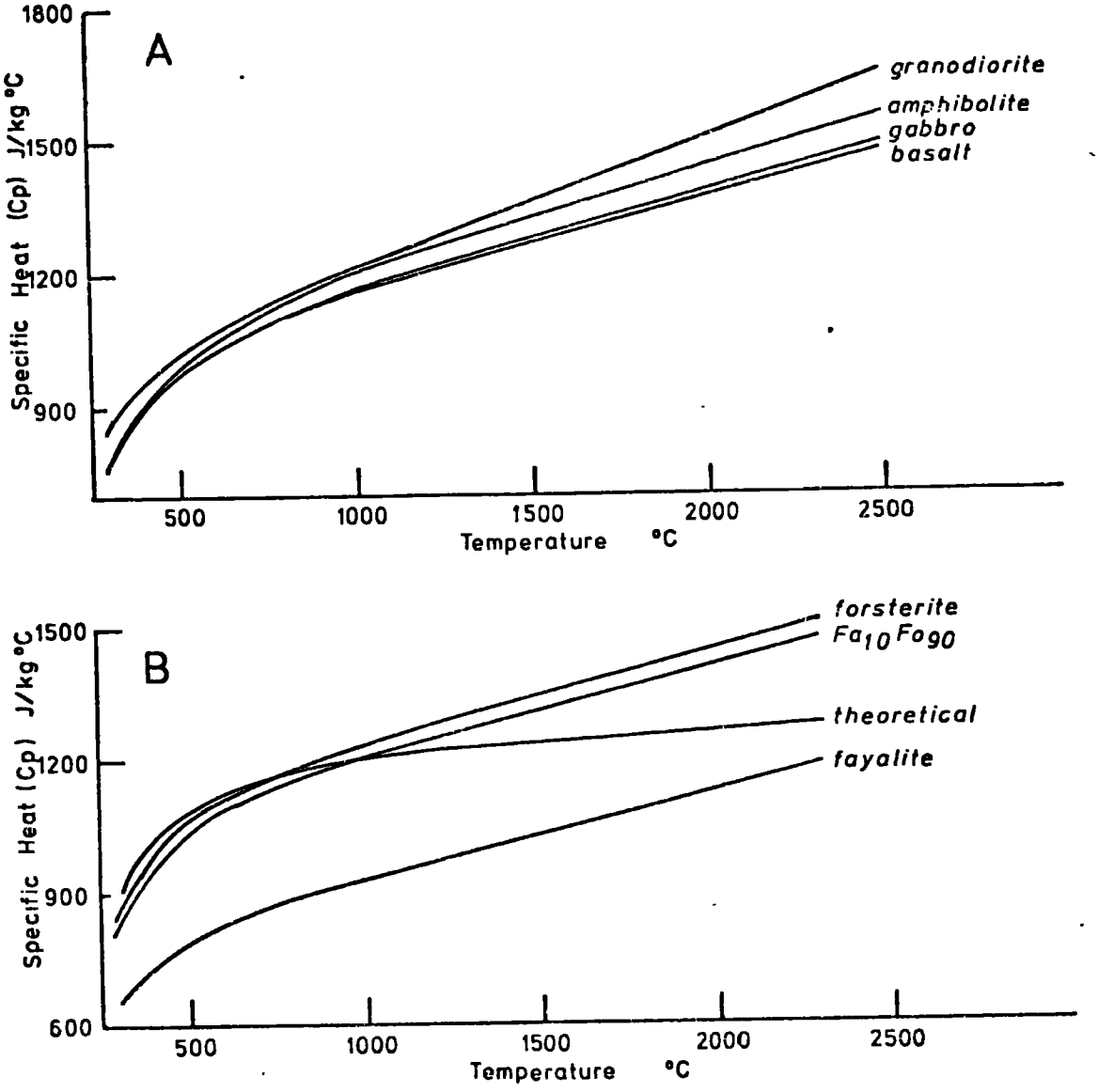

Fig. 2.5 Specific heats at constant pressure as a function of temperature.

the thermal expansion coefficient, bulk modulus, density or C_v. The Debye theory, however, is formulated for pure substances of relatively simple structure so that it may not be directly applicable to olivine solid solutions. Hence the experimentally determined value (equation 2.26) is used for the computations.

The heat capacity, C_p, for other relevant rocks were obtained from the values for their constituent minerals (fig. 2.5). Because these are all within about 5% of each other, the value for gabbro is used for the whole oceanic crust.

The effect of pressure on C_p has not been determined for rocks but for most substances it is very small (Birch, 1952). Hence C_p will be assumed to be invariant with pressure.

2.2.3 Latent heat of phase changes

The Clausius-Clapeyron equation for the latent heat of a phase change is

$$L = \Delta V . T . \frac{dP}{dT} \qquad 2.27$$

where ΔV is the change in specific volume due to the phase change, T the temperature and $\frac{dP}{dT}$ the gradient of the phase boundary. This equation applies to a sharp phase boundary. Where the phase changes take place over a range of temperatures (for a given pressure) the validity of the

expression is less certain.

It is assumed that at constant pressure: (1) the total latent heat in going from one phase to the other is that calculated for a sharp boundary; (2) the latent heat involved in part of the phase transition is proportional to the change in density, and (3) the latent heat can be simulated as an apparent increase in the specific heat $\Delta C_p'$ such that

$$\Delta C_p' = \left(\frac{\partial H}{\partial T}\right)_p$$

where H is the enthalpy.

With these assumptions the apparent increase in the thermal capacity at constant pressure ($\Delta C_p'$) is given by

$$\Delta C_p' = \left(\frac{\partial B(d)}{\partial T}\right)_p \left[\Delta V . T . \frac{\partial P}{\partial T}\right] \qquad 2.28$$

B(d) describes the proportion of the phases (Section 2.1.1). ΔV should be the change in volume at the conditions of the phase change (expressed as a sharp boundary) but as $\left(\frac{\partial B(d)}{\partial T}\right)_P$ is zero outside the transition zone, the error in taking the slowly changing ΔV at the conditions of P and T existing in the rock may be neglected.

If the densities of the phases are $\rho_0 F_0(P,T)$, $\rho_1 F_1(P,T)$ and the centre of the phase transition is $aP + bT + c = 0$

then

$$\Delta C_p' = - \frac{\rho_1 F_1 - \rho_0 F_0}{\rho_1 \rho_0 F_1 F_0} \left(P + \frac{c}{a}\right)\left(\frac{\partial B(d)}{\partial T}\right)_p \qquad 2.29$$

2.2.4 Thermal conductivity

Schaltz and Simmons (1972) measured the thermal conductivity (k_C) of olivines and gave the following expressions (converted to S.I. units) which they consider applicable to the upper mantle. If

$$k_C = k_L + k_R \qquad 2.30$$

and k_L is the conduction due to lattice vibrations and k_R is the conduction due to radiant energy propagated through the crystal, then

$$k_L = \text{maximum of } \begin{cases} 1.29 \times 10^{-6} V_p \rho^{2/3} \\ (0.0741 + 5.01 \times 10^{-4} T)^{-1} \end{cases} \qquad 2.31$$

$$k_R = \begin{cases} 0 & T \leq 500 \\ 2.3 \times 10^{-3} (T - 500) & T > 500 \end{cases} \qquad 2.32$$

T is the temperature in ^{o}K. These are used for the mantle.

The values of the conductivity of three samples of diabase at temperatures up to 400^{o}C tabulated by Clark (1966) are all within the range 2.09 - 2.34 J/m s ^{o}C. The mean and standard deviations are 2.14 $\pm$ .08 J/m s ^{o}C but the trend with respect to temperature is different for each of the three samples. Based on these determinations, a constant lattice conductivity of 2.1 J/m s ^{o}C is assumed for the oceanic crust. By a similar argument to that

presented by Schaltz and Simmons (1972), a minimum lattice conductivity for these crystalline rocks can be related to their compressional velocity and density by:

$$K_L = 1.29 \times 10^{-6} \; V_p \rho^{2/3}$$

The radiative conductivity for these rocks is unknown but will only become significant as the crust is heated in the descending subduction zone. The expression given for olivine by Schaltz and Simmons (equation 3.32) is used where needed.

Hence the thermal conductivities used for oceanic crust are

$$k_c = k_L + k_R$$

where:

$$k_L = \text{maximum of} \begin{cases} 2.1 \\ 1.29 \times 10^{-6} \; V_p \rho^{2/3} \end{cases} \qquad 2.33$$

$$k_R = \begin{cases} 0 & T \leq 500 \\ 2.3 \times 10^{-3} \, (T - 500) & T > 500 \end{cases} \qquad 2.34$$

2.2.5 Melting temperature

The melting temperature of a rock is dependent on the amount of water present. Melting curves for dry and hydrous conditions for materials which may constitute the upper mantle are shown in fig. 2.6. The melting of basic rocks with less than about 1.0% H_2O depends upon the

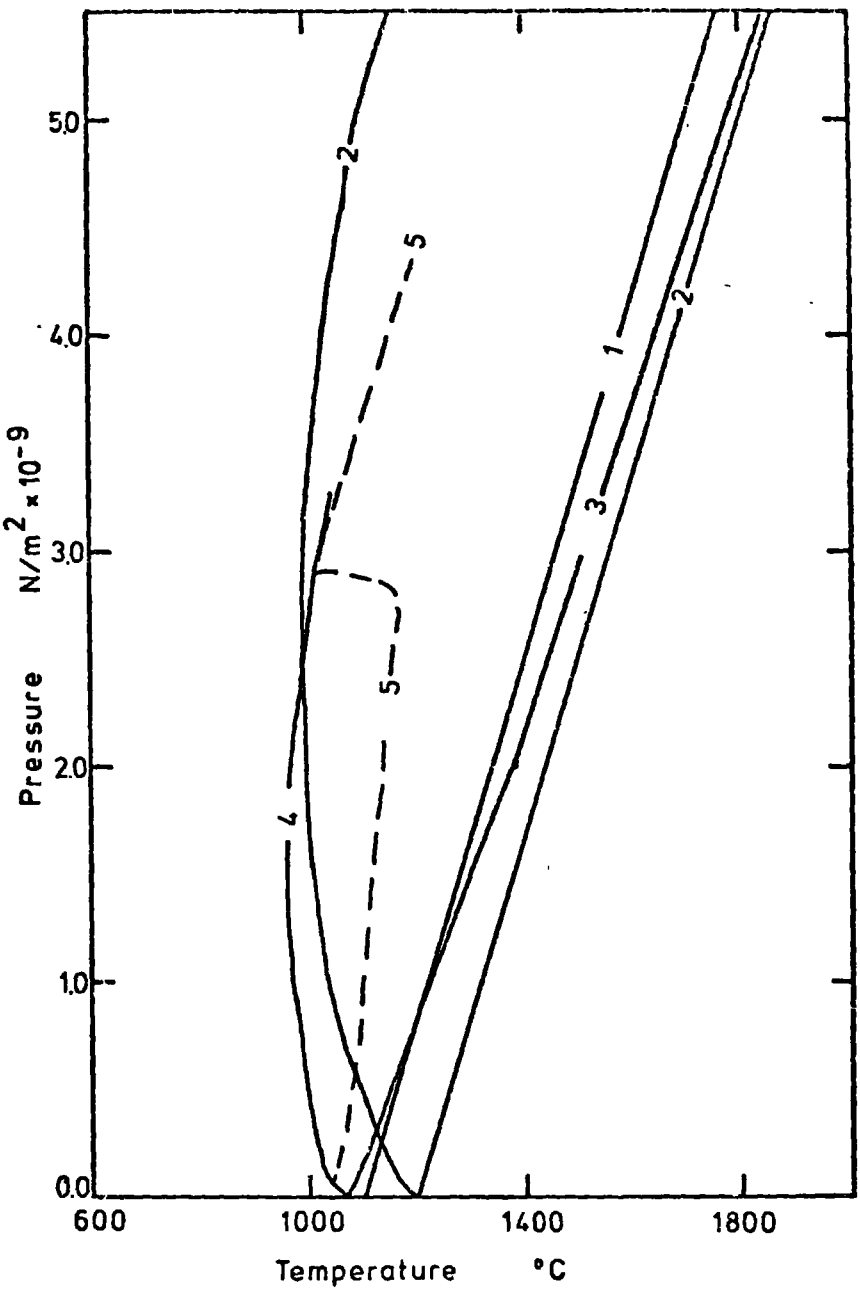

Fig. 2.6 Wet and dry melting temperatures for possible mantle materials.

(1) Peridotite (Ito and Kennedy, 1967)

(2) Lherzolite nodule (Kushiro et al.,1968)

(3) Pyrolite III (Green and Ringwood, 1970)

(4) Pyrolite - 40% olivine 6% H_2O (Green,1973)

(5) Pyrolite - 40% olivine 2% H_2O (Green,1973)

stability of the amphibole phases (Green, 1973). If these hydrous minerals are stable then the water may be used in converting pyroxene to amphibole so that $P_{H_2O} \ll P_{Total}$. If, However, the amphiboles are unstable then the water is in the fluid phases with $P_{H_2O} = P_{Total}$. Hence in curve 5 in fig. 3.6 the solidus below about 3.0×10^9 N/m^2 follows the stability field of amphiboles.

Adopting the melting temperature of pyrolite with 0.2% water (curve 5 - fig. 3.6) gives

$$T_M = 1316.0 + 8.703 \times 10^{-8} P - 1.657 \times 10^{-17} P^2 \qquad P < 2.9 \times 10^9 \qquad 2.35$$
$$T_M = 920.0 + 1.26 \times 10^{-7} P \qquad P \geq 2.9 \times 10^9$$

for mantle material. T_M is in ^oK and P in N/m^2.

The melting temperature probably increases rapidly across the olivine-spinel and spinel-post spinel phase transitions (e.g. Uffen, 1952). However, the other properties which are related to the melting temperature - in particular the viscosity - will also vary suddenly at these discontinuities. Consequently the complexity in trying to allow for these changes is not warranted.

For the oceanic crust, the melting curves given in fig. 2.7 for basalt and eclogite apply. The curve for $P_{H_2O} \leqslant 3.0 \times 10^8$ N/m^2 gives

$$T_M = 1315.0 - 8.5 \times 10^{-7} P + 5.0 \times 10^{-16} P^2 \qquad P < 3.0 \times 10^8$$
$$T_M = 1067.0 + 1.2 \times 10^{-7} P \qquad P \geqslant 3.0 \times 10^8 \qquad 2.36$$

where T is in ^oK and P in N/m^2.

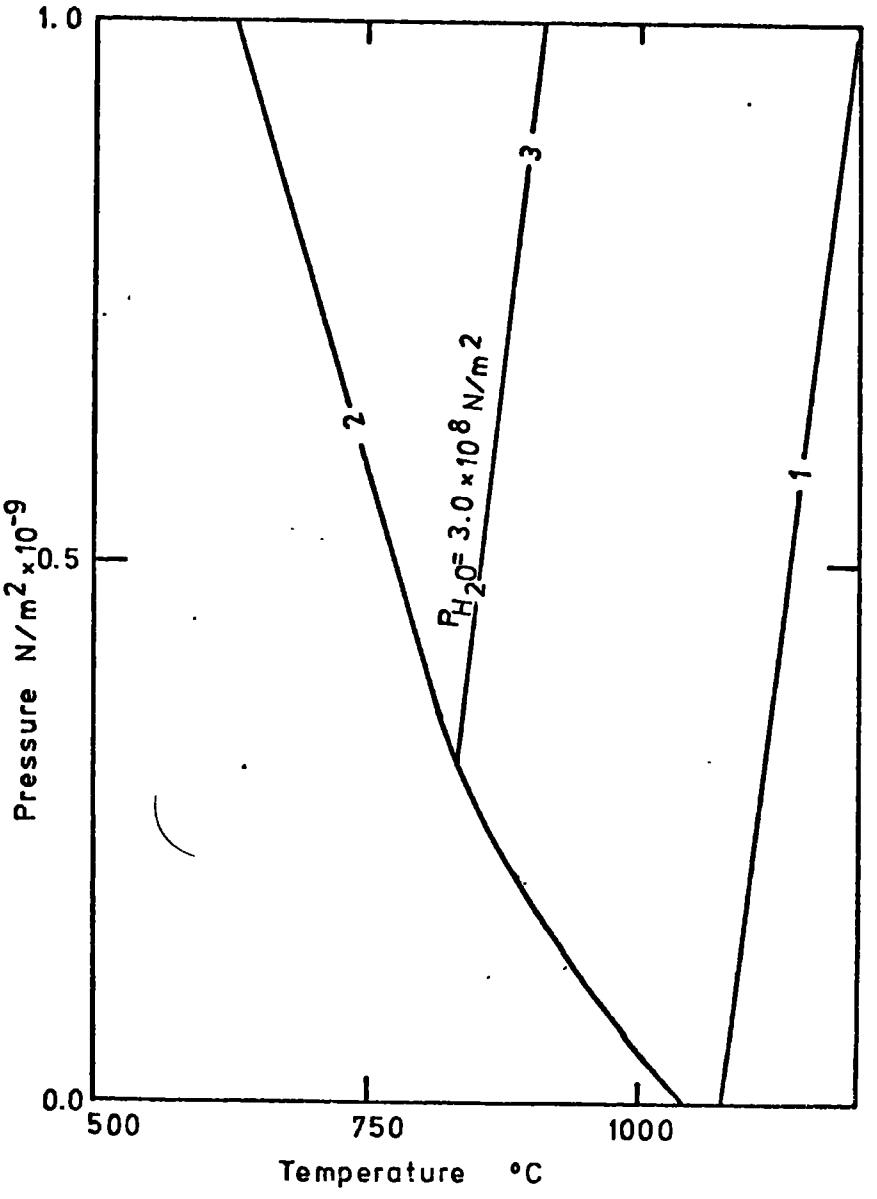

Fig. 2.7 Wet and dry melting curves for basalt

(1) Dry basalt (Cohen et al., 1967)
(2) Wet basalt (Yoder and Tilley, 1962)
(3) Used in this thesis

2.2.6 Heat production

The heat generated by radioactive decay is one of the most difficult parameters to estimate. Macdonald (1965) gave an average value for several rock types (Table 2.6). Generally the more acidic the rock, the higher the heat production, and so granites and granodiorites produce more radiogenic heat than basalts and peridotites.

One useful check on the heat production in a model earth is the computation of the temperature profile in steady state conditions. This fixes limits on the radiogenic heat production.

Other heat sources within the earth's outer layers are mechanical and chemical changes. The most important of these is latent heat of fusion and the free energy of some phase changes (Section 2.2.3). Heating of the rocks due to viscous flow (Section 3.1) has generally been ignored but may also be important.

2.3 Variation of temperature with depth

Because of the continual movement of the crust and mantle dictated by the theory of plate tectonics steady state thermal conduction conditions seldom exist in the earth. In the old ocean basins these conditions may be approximated in the lithosphere which is older than about

Table 2.6 AVERAGE RADIOGENIC HEAT PRODUCTION FOR VARIOUS ROCKS*

	$\times 10^{-8}$ cal/g yr	$\times 10^{-12}$ J/kg s
Granite	810	1080
Intermediate	340	480
Basalt	119	160
Eclogite		
Low Uranium	8.1	10.8
High Uranium	34.0	45.0
Peridotite	0.91	1.21
Dunite	0.19	.25
Chondritic Meteors	3.94	5.25

* From Macdonald (1965)

100 M. yr. (Sclater and Francheteau, 1970). There is probably some convection in the asthenosphere and so the thermal gradients below the base of the lithosphere will be lower than those for a conduction model.

Fig. 2.8 shows a steady state conduction geotherm compared with some previously published estimates of the variation of temperature with depth under ocean basins. This geotherm was constructed assuming that the heat lost at the surface is 0.046 W/m^2 (1.1 $\mu cal/cm^2 s$, Sclater and Francheteau, 1970), and that the thickness of the lithosphere is stabilized by the instability of the amphibole phases with pressure at 93 km and about 1000°C. These constraints and the use of the conductivities given in section 2.2.4 place limits on the heat sources within the lithosphere. Assuming 1.6×10^{-10} W/kg for oceanic crust and a constant value for the lithospheric mantle of 0.65×10^{-10} W/kg meets the previously assumed conditions. This heat generation density is compared with that used by Clark and Ringwood (1964) and Sclater and Francheteau (1970) in fig.2.9. The radiogenic heat sources are consistent with the pyrolite composition of the lithosphere.

The lithosphere is formed from the asthenosphere at the spreading ridges suggesting that their bulk composition should be similar. If, however, the density of radiogenic heat sources estimated here for the lithosphere continue

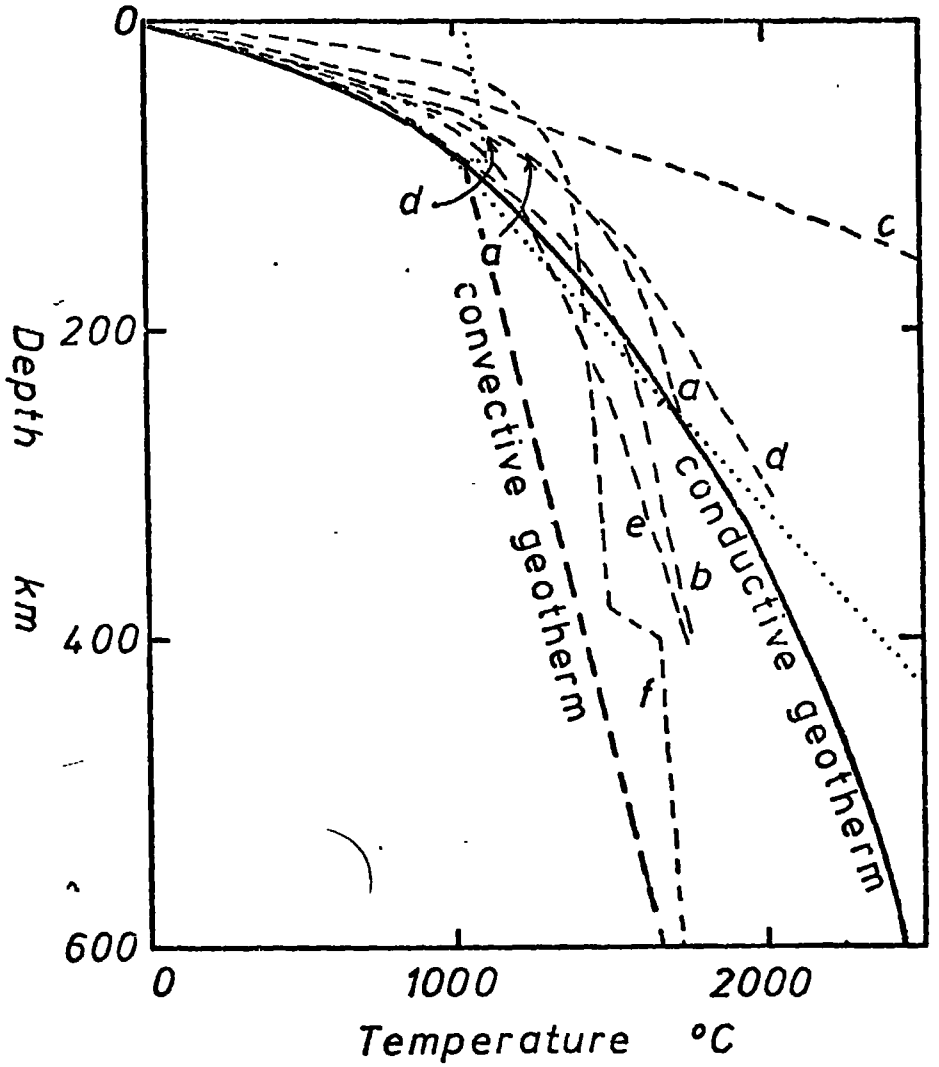

Fig. 2.8 Geotherms for a stable oceanic basin. Previously published curves are

(a) Ringwood (1969a)
(b-d) MacDonald (1965)
(e) Clark and Ringwood (1964)
(f) Turcotte and Oxburgh (1969)

Solid line is a conductive geotherm calculated using the properties in this chapter and radiogenic heat sources as in fig. 2.9. The convective geotherm is arbitrary but causes the olivine spinel transition to start at 325 km.

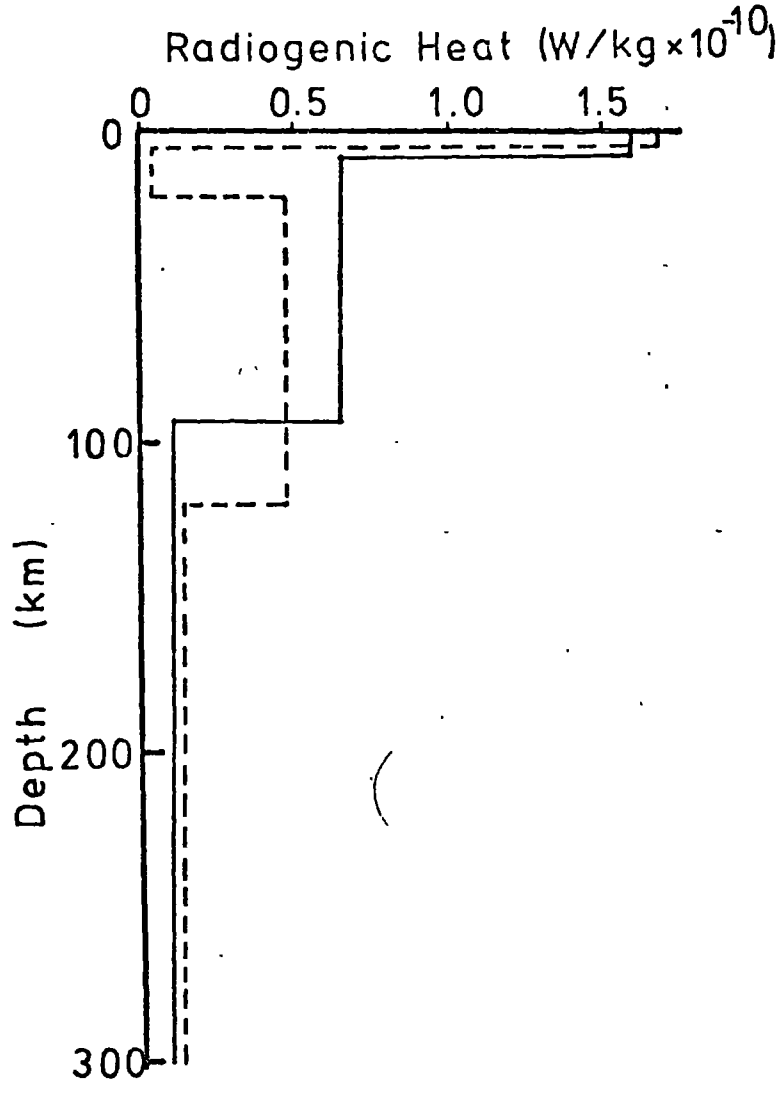

Fig. 2.9 Solid line shows the radiogenic heat sources assumed for computing the conductive geotherm in fig. 2.8. Dashed line is the distribution used by Clark and Ringwood (1964) and Sclater and Francheteau (1970).

through the asthenosphere all the heat lost at the surface of the earth would be generated in the upper 250 km. This is independent of the method of heat transfer - conduction or convection.

For the purpose of the conduction model the radiogenic heat was reduced to 0.1×10^{-10} W/kg for the asthenosphere and mesosphere. The temperatures on the conduction geotherm (fig. 2.8) are probably too high at depths greater than 200 km. In this model the start of the olivine-spinel transition is at about 410 km. This is in the lower part of the range estimated from seismic velocities (Toksöz et al., 1967; Julian and Anderson, 1968).

An alternative geotherm was constructed by assuming a linear variation of temperature with depth from the base of the lithosphere to intersect the beginning of the olivine-spinel transition at 325 km. This is an upper limit for the transition. This geotherm is arbitrary but the gradient of 1.4°/km is within a reasonable range for heat transfer by convection to be important in the asthenosphere.

2.4 Variation of physical properties with depth

The variation of various physical properties of the earth as a function of depth using the expressions in this

chapter and these temperature profiles are shown in figs. 2.10 and 2.11. The solid lines refer to temperatures given by the conductive geotherm and the dashed to the convective geotherm.

The density profiles (fig. 2.10) are within about 1% of that of Clark and Ringwood (1964). The velocities plotted are simply related to the density by a linear function (equations 2.16) and so the effect of partial melt in reducing the velocities in the low velocity zone is ignored. They are, however, in general agreement with seismically determined velocities (e.g. Tosköz et al., 1967 Julian and Anderson, 1968). The large increase in thermal conductivity with depth is due both to the radiative conduction increasing with temperature and to the lattice conduction increasing with density and compressional wave velocity (equation 2.31). The effect of the olivine to spinel phase change on the conductivity is uncertain, however, and may reduce the radiative heat transfer, thus altering the curve below 400 km substantially.

In fig. 2.11 the specific heats contain the effects of the latent heat of phase change (section 2.2.3). This has a much larger effect on C_p than C_v. At constant volume the temperature change tends to take place along the phase boundary (causing much larger changes in pressure) whereas at constant pressure, the phase change has to run. The

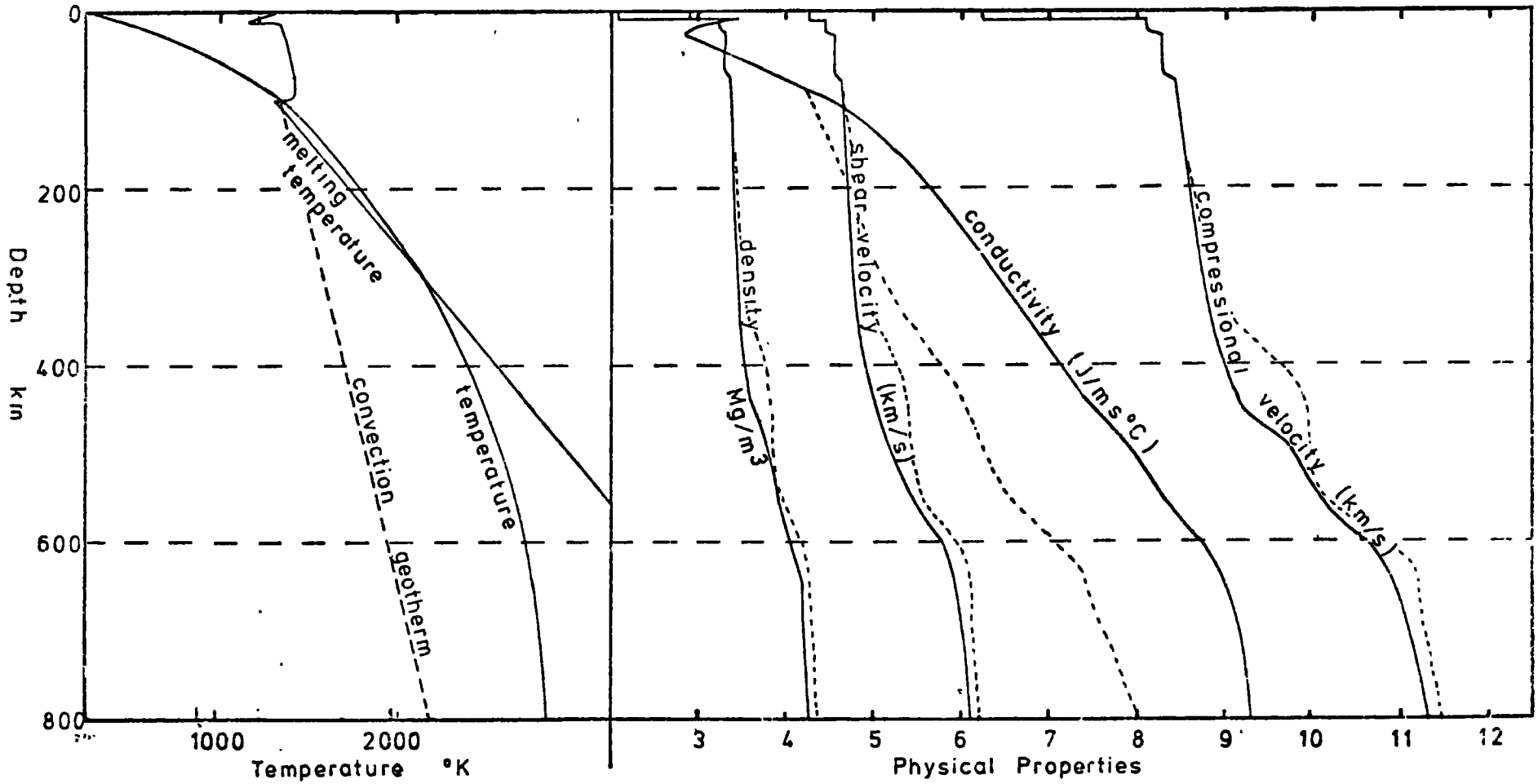

Fig. 2.10 Variation of physical properties with depth as computed from the expressions in this chapter and the geotherms in fig. 2.8. Solid lines for conductive geotherm dashed lines for convective geotherm .

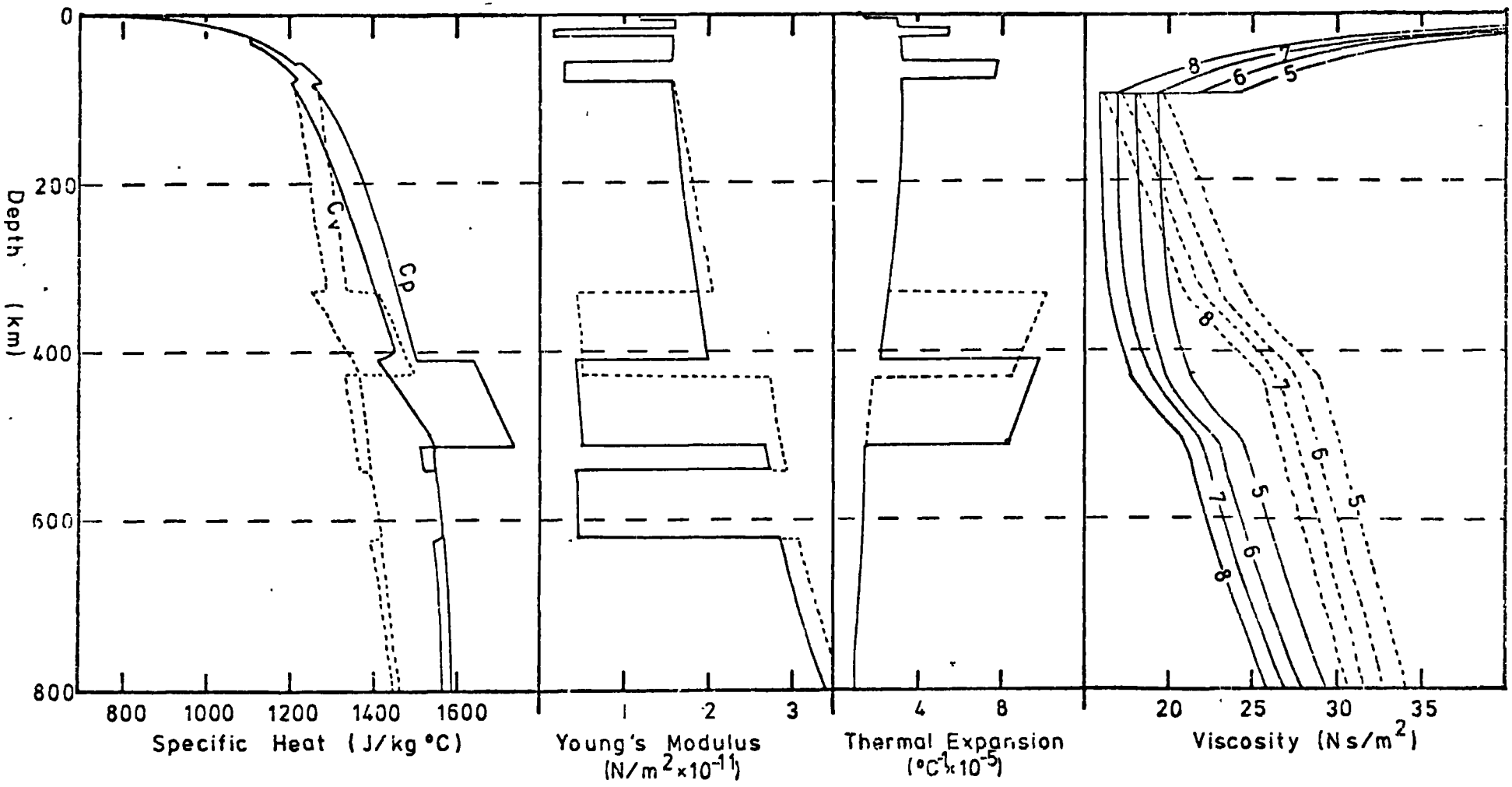

Fig. 2.11 Variation of further physical properties with depth as computed from the expressions in this chapter and the geotherms of fig. 2.9. The effect of the phase transitions are clearly evident. (note $C_v \leqslant C_p$). Solid lines for conductive geotherm dashed line for convective geotherm. Viscosity curves are for shear stresses of 10^n N/m^2 where n is the number labelling the curve.

The curves for Young's modulus and the coefficient of thermal expansion also show the effects of the phase changes. The linear variation of the proportion of phases within the phase transition were used (equation 2.6). In the vicinity of the phase change the effective Young's modulus is decreased by nearly an order of magnitude and the coefficient of thermal expansion increased by a factor of 3.

The viscosity is plotted for four different shear stresses, ranging from 1.0×10^5 N/m^2 (1 bar) to 1.0×10^8 N/m^2. The decrease in viscosity at the base of the lithosphere increases as the shear stress decreases. The effect of the arbitrary increase of viscosity by 10^3 on crossing the olivine-spinel transition is also evident.

The initial conditions for the models of processes in subduction zones are assumed to be given by these temperature profiles, the stresses being assumed hydrostatic and equal to the weight of the overlying rocks.

2.5 Summary

In this chapter expressions for the evaluation of the physical properties of mantle and oceanic crust by computer have been developed. Most of the properties are dependent upon pressure and temperature. Figure 2.12 shows the

Fig. 2.12 Properties of the pyrolitic model of the mantle is a function of pressure and temperature.

(A) Density in Mg/m^3 contour interval 0.05 Mg/m^3.

(B) -Log (coefficient of thermal expansion in $^oC^{-1}$) contour interval 0.2.

(C) -Log (compressibility in m^2/N) contour interval 0.2

(D) Log (Young's modulus in N/m^2) contour interval 0.2

(E) Specific heat at constant volume. Contour interval 100 J/kg^oC.

(F) Specific heat at constant pressure. Contour interval 100J/kg^oC.

(G) Log (viscosity in Ns/m^2) shear stress = 1.0×10^8 N/m^2 contour interval 1.0.

(H) Poisson's ratio (the Poisson's ratio corresponding to the phase transition ν_k was assumed to be -1.0). The contours were too close to draw in the hatched area. Contour interval 0.1.

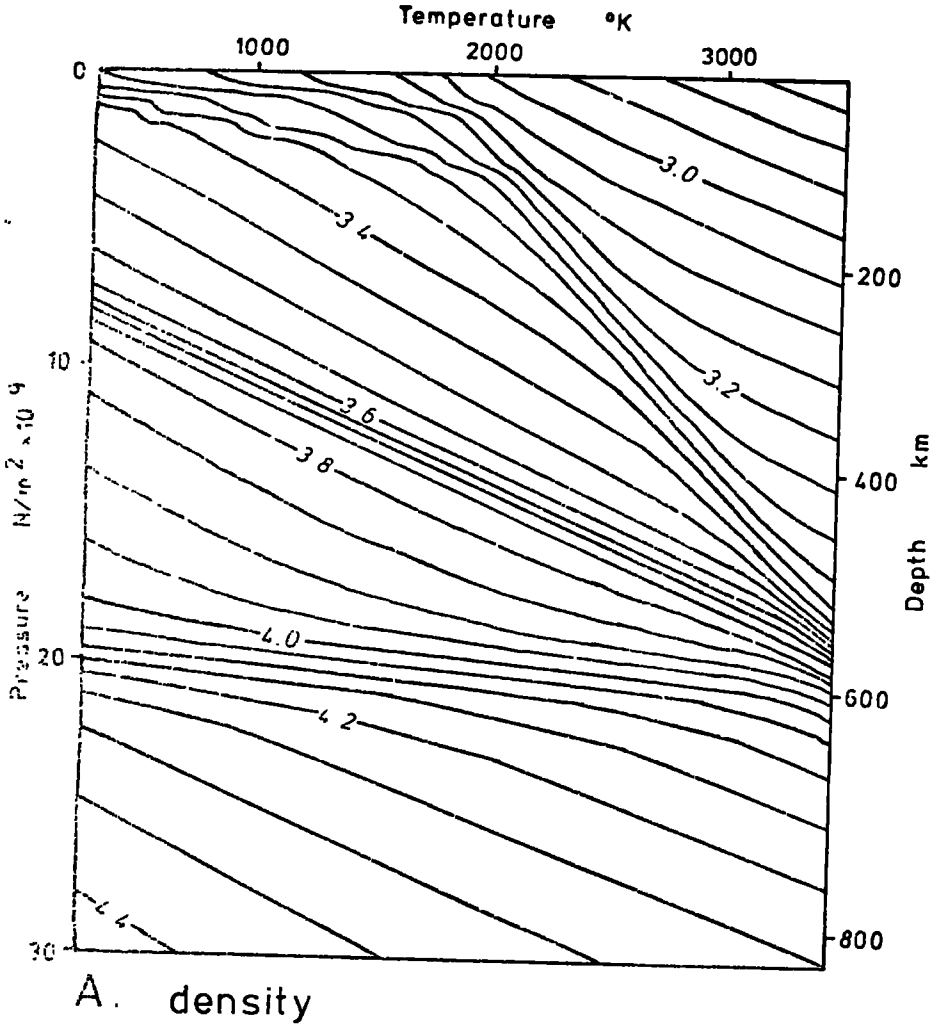

A. density

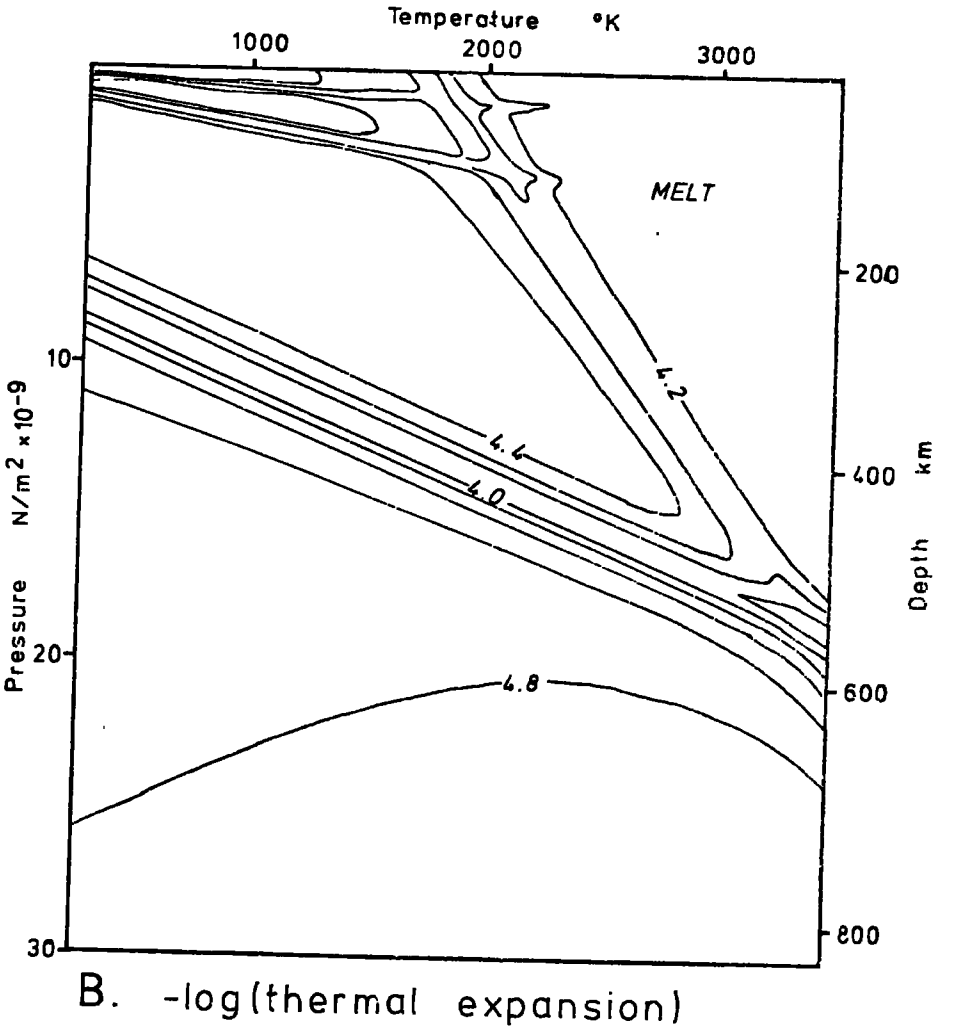

B. -log(thermal expansion)

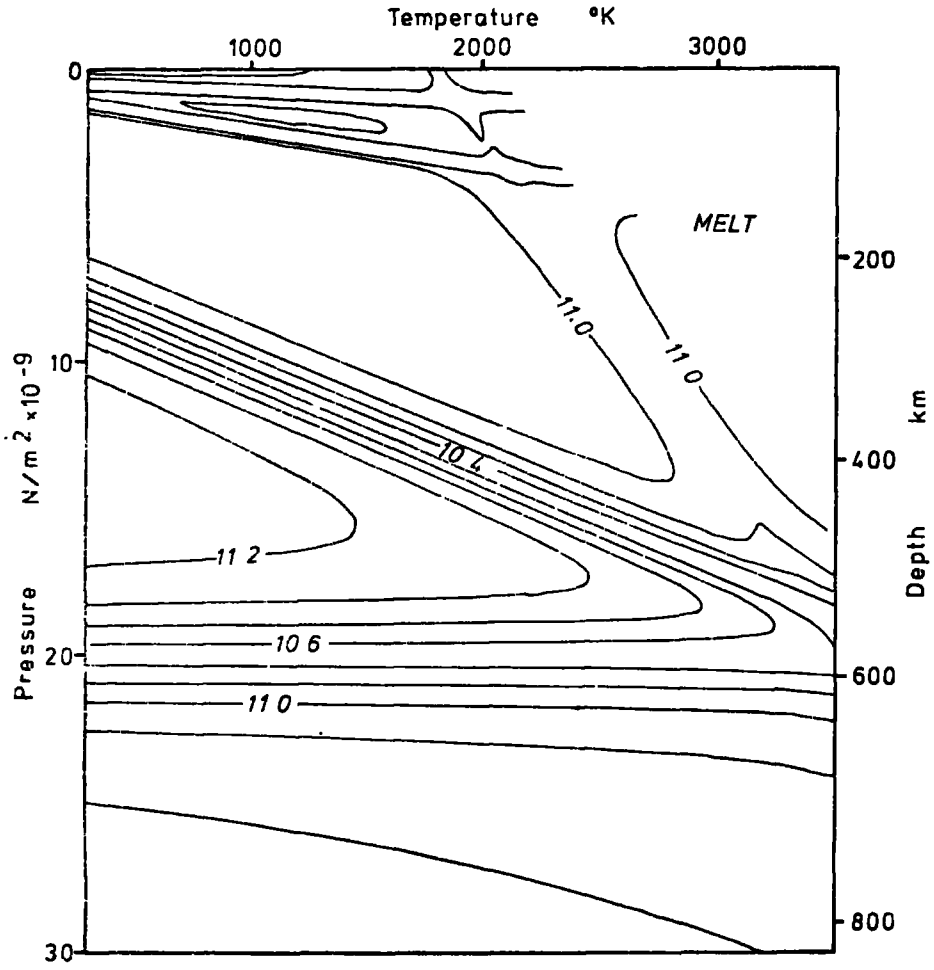

C. log(bulk modulus)

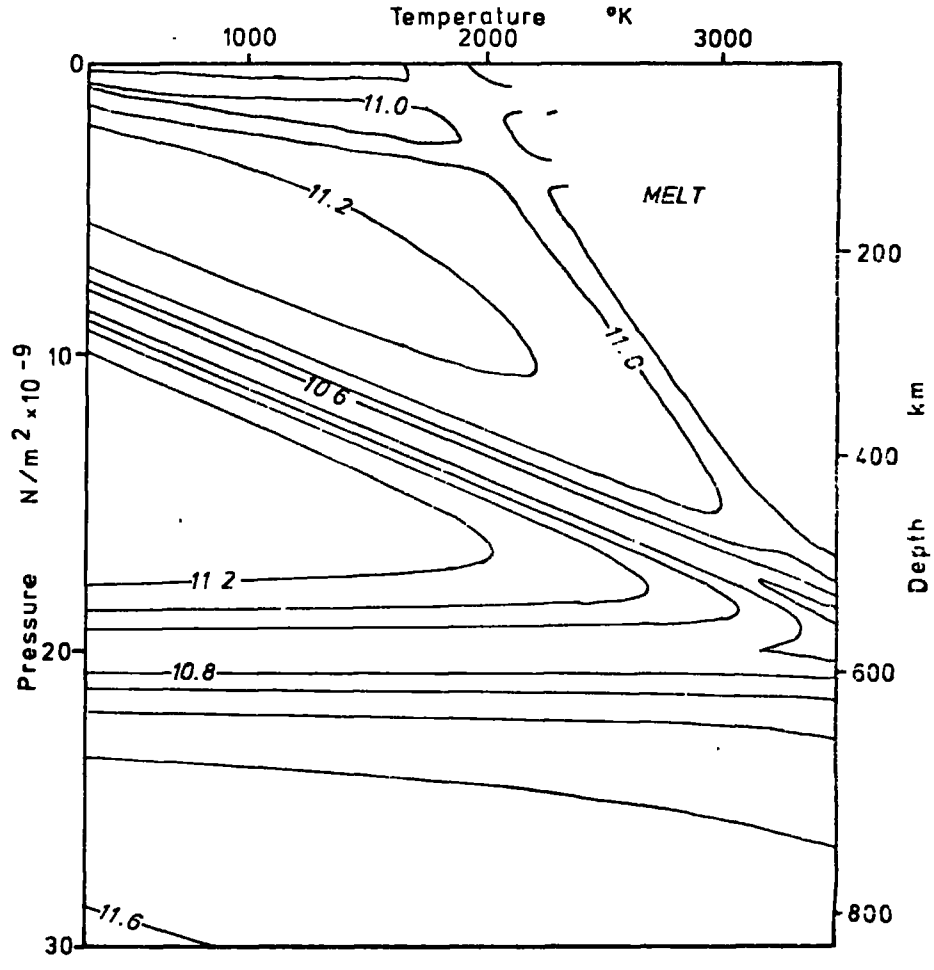

D. log(Young's modulus)

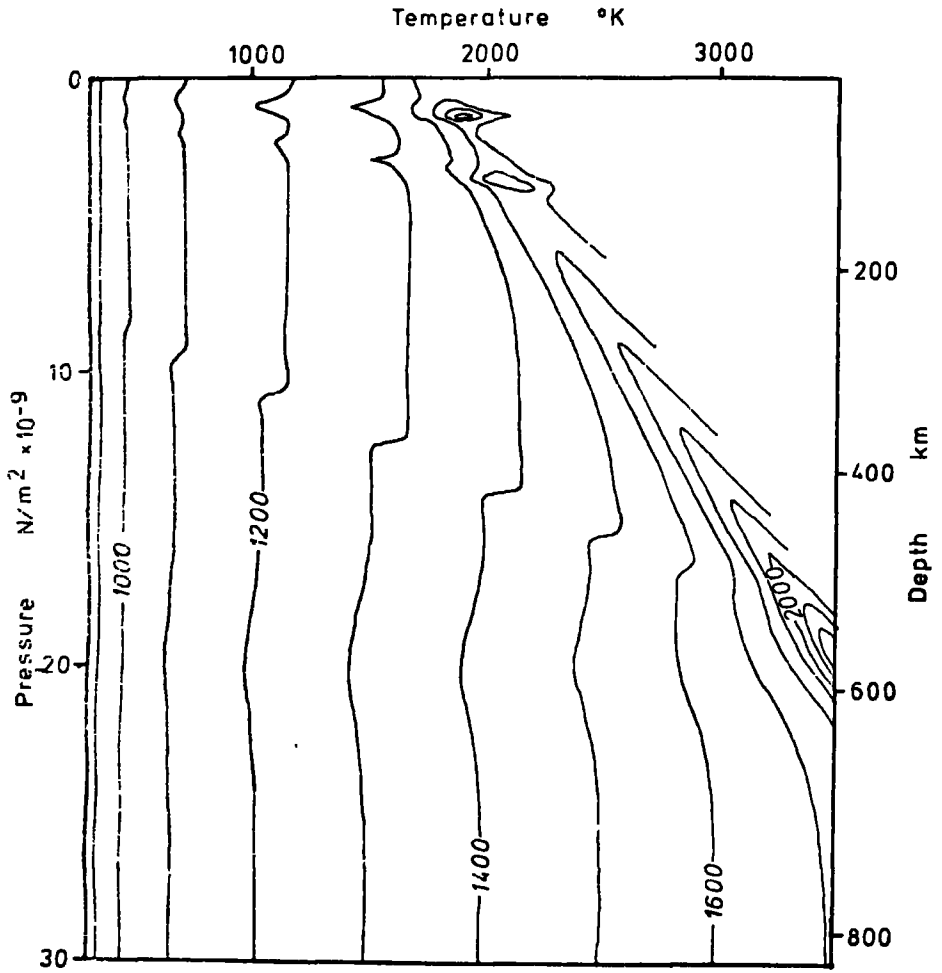

E. thermal capacity at constant volume

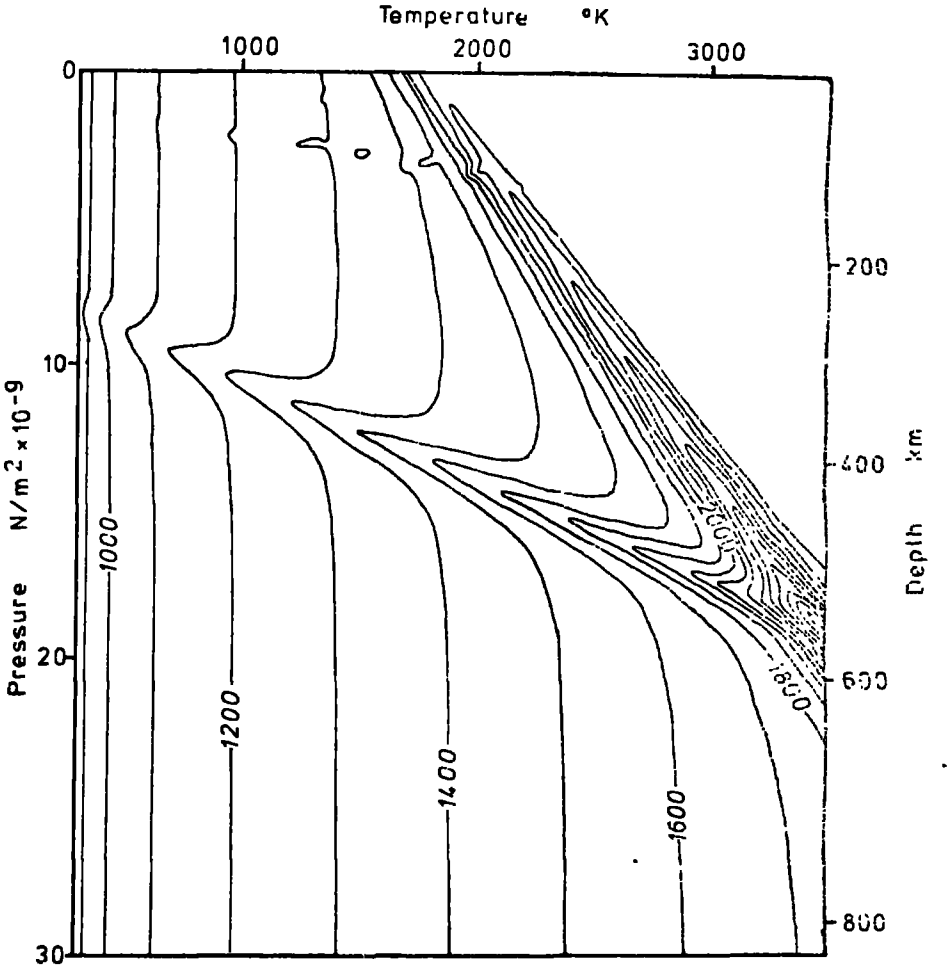

F. thermal capacity at constant pressure

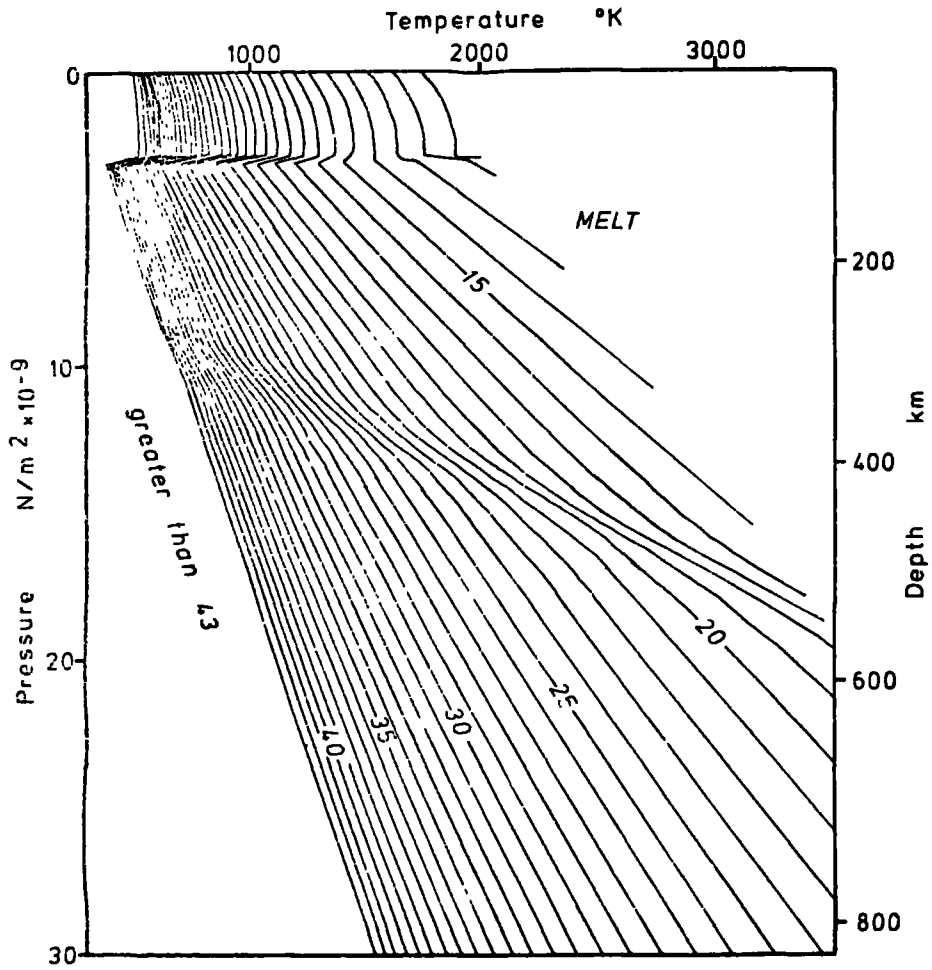

G. log(viscosity)

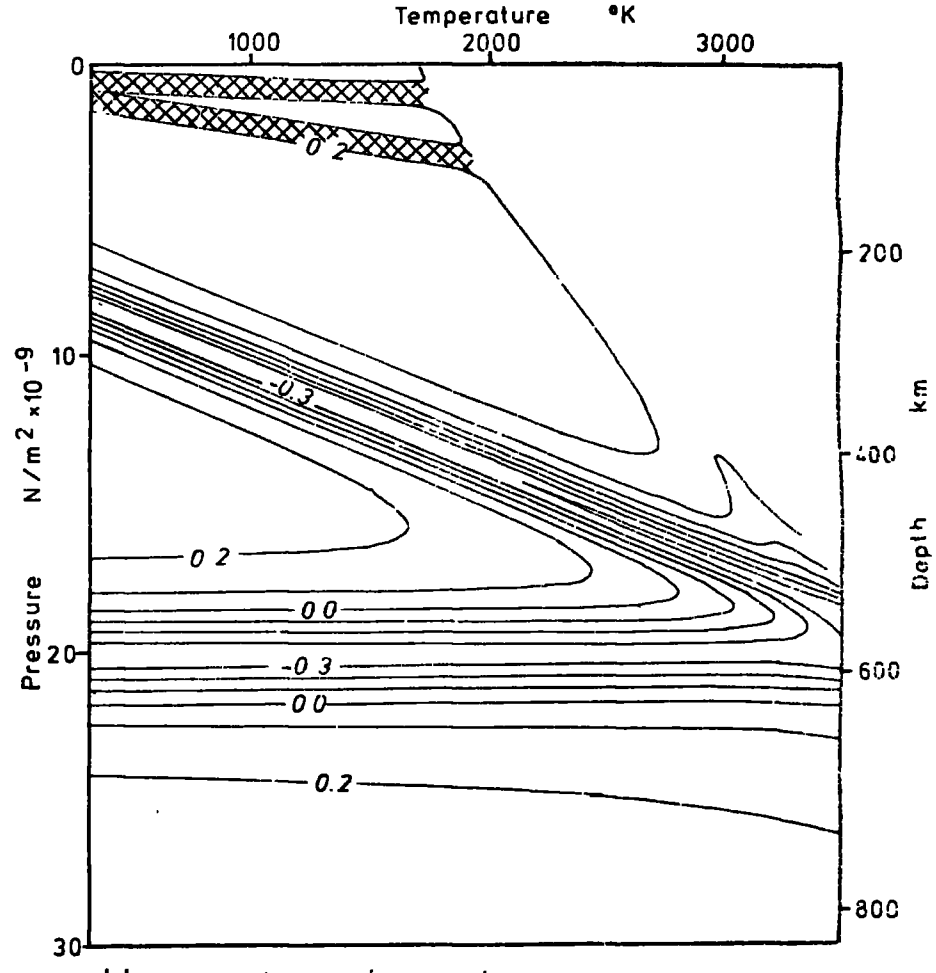

H. Poisson's ratio

resulting properties of mantle for temperatures between $300^{o}K$ and $3500^{o}K$ and pressures up to 3.0×10^{10} N/m^2 equivalent to a depth of about 800 km.

All the properties show the effect of phase changes. Equation 2.7, which gives a non-linear variation of phases across the transition, was used in compiling the diagrams.

The phase boundaries increase the coefficient of thermal expansion by a factor of 3 (fig. 2.12B)and decrease the bulk modulus and Young's modulus by an order of magnitude (figs. 2.12C and D). The specific heat at constant volume is less affected by the phase changes than that at constant pressure (figs. 2.12E and 2.12F). Heating the rock at constant volume within a transition zone causes little change in the proportions of the phases. At constant pressure the phase changes must run and the specific heat is increased by about 100 $J/kg^{o}C$.

The viscosity (fig. 2.12G) is plotted for a shear stress of 1.0×10^{6} N/m^2. The shape of the contours remain similar for higher stresses but their positions change.

The Poisson ratio contours (fig. 2.12H) were determined using a value of the Poisson ratio associated with the phase changes, ν_k, of -1.0. This assumes that the changes of volume associated with the phase transitions are caused by equal linear variations in all directions. This is an

extreme case. For other values of ν_K , the contours are of a similar shape but the extremes of the values within the transition zones are not as great. The hatched areas on this diagram are regions where the contours were too close to draw. The minimum values approach that of ν_K .

The expressions in this chapter are incorporated into the FORTRAN subroutine PROPS (page 170).

CHAPTER 3

FINITE ELEMENT ANALYSIS

Finite element analysis is a method of solving partial differential equations with complicated boundary conditions. It is allied to finite difference analysis but is more versatile because each small part of the field over which the equations are to be solved can be given a separate shape function so that more complicated problems may be evaluated. A comprehensive description of the method is given by Zienkiewicz (1971).

The method has been used largely to solve engineering problems but has also been applied to geological studies. It has been used in elastic analysis by Bott and Dean (1972), Service and Douglas (1973), Bridwell (1974) and Bridwell and Swolfs (1974). The solution of viscous problems in earth sciences using finite element techniques has mainly centred upon studies of folding in contrasting layers (e.g. Stephansson and Berner, 1971). The interpretation of steady state heat flow data near Lake Geneva has been modelled using finite element techniques by Lee and Henyey (1974). A visco-elastic analysis of stresses in a subduction zone has been made by Neugebauer and Breitmayer (1975).

3.1 Visco-elastic finite element analysis

In finite element analysis the model is subdivided into a finite number of small parts called elements. These are interconnected through common points called nodes. The analysis is based on defining the value of a variable throughout each element in turn based only on its value at the nodes contained in the element.

In elastic or visco-elastic analysis the basic variable is displacement. It is required from the analysis to determine first the displacements of the nodes and from these the displacements, strains and stresses throughout each element. I will consider only two-dimensional analyses using triangular elements in which the displacements are assumed to vary linearly over the elements and are specified by the six components of displacement of the nodes at the corners (fig. 3.1). The displacements ($\underset{\sim}{\delta}$) at the nodes can be mapped into strains ($\underset{\sim}{\epsilon}$) within the element by

$$\underset{\sim}{\epsilon} = [B]\,\underset{\sim}{\delta} \quad .$$

For these simple elements

$$[B] = \frac{1}{2\Delta}\begin{bmatrix} b_i & 0 & b_j & 0 & b_m & 0 \\ 0 & c_i & 0 & c_j & 0 & c_m \\ c_i & b_i & c_j & b_j & c_m & b_m \end{bmatrix}, \qquad 3.1$$

$$\underset{\sim}{\epsilon}^t = \{ \epsilon_x, \epsilon_y, \epsilon_{xy} \} ,$$

and $$\delta^t = \{ \delta_x^i, \delta_y^i, \delta_x^j, \delta_y^j, \delta_x^m, \delta_y^m \} \quad .$$

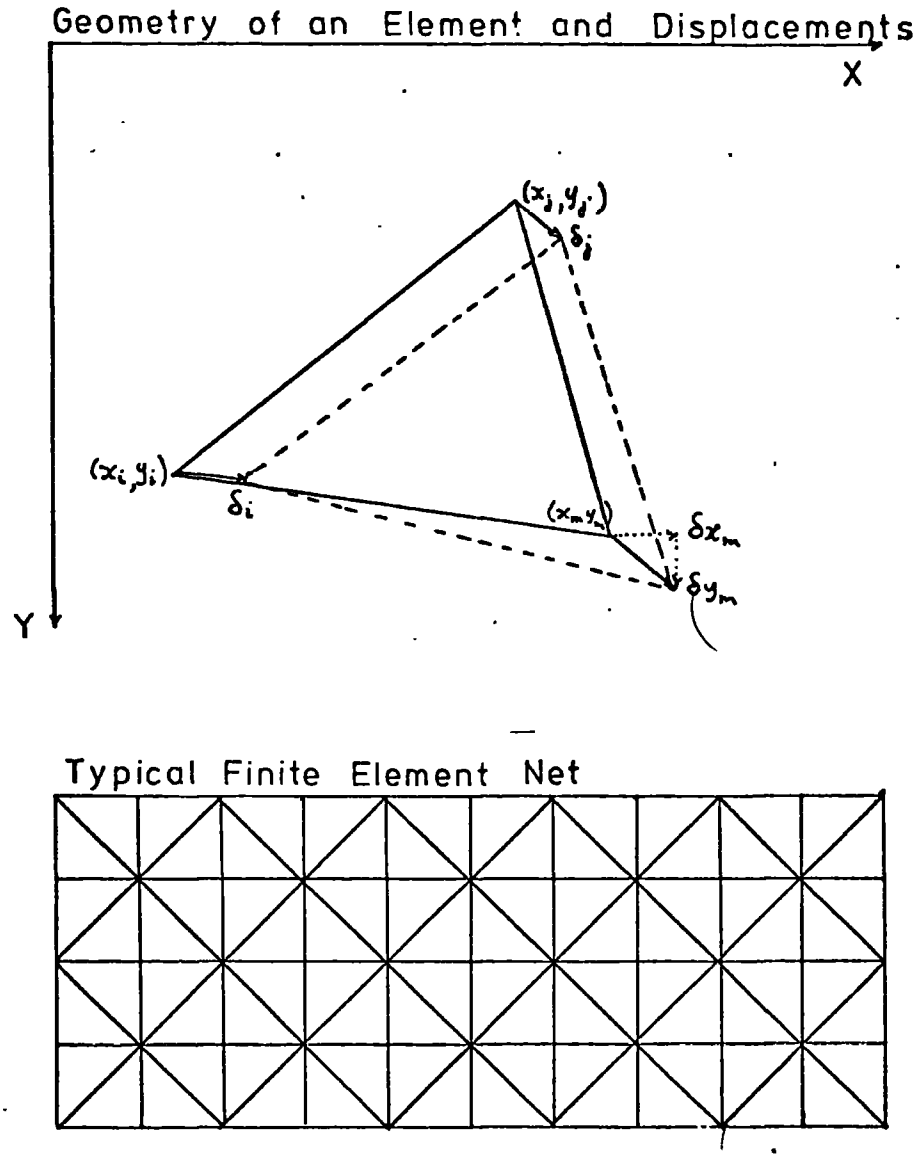

Fig. 3.1 The displacement of an element and a typical finite element net.

The superscript t denotes the transpose of the vector or matrix. The elements of $[B]$, b and c, are cyclic permutations of

$$b_i = y_j - y_m$$
$$c_i = x_m - x_j$$

x and y being the coordinates of the nodes and Δ is the area.

Since the displacements are assumed to vary linearly over the element the strains (being the derivative of displacement) are constant.

If the relationship between stress and strain is known, for the material of each element, the energy change within each element may be found as a function of the nodal displacements. By concentrating the body and boundary forces also onto the nodes the work done, over the whole system, may be determined as a function of the nodal displacements. This is minimized by differentiating with respect to each nodal displacement in turn. Together with the equilibrium equations for the body as a whole these form a set of simultaneous equations in the nodal displacements. Once the equations are solved the strain and stress within each element may be determined.

One method of solving visco-elastic problems by finite element analysis has been described by Zienkiewicz (1971). This method requires iteration for each time step to

determine initial strain conditions to be applied to the model. Carpenter (1972) has formulated a technique incorporating a Runga-Kutta method which allows the estimation of error and increases in the time step. This reduces the amount of computing required. These techniques are applicable to any rheological properties provided the deformations are small. If, however, the rheology is limited to a Maxwell substance then it is possible to solve directly for the displacements of the rocks and the stress after a given time interval. A new formulation along this line is given here.

Treating the solution of visco-elastic flow problems as an energy minimization problem, the energies to be minimized are those due to stress and strain and the movement of the applied forces.

The total energy, W, is

$$W = \int_{Vol} \left[\int_0^{\underset{\sim}{\eta}} \underset{\sim}{\sigma}^t \, d\underset{\sim}{\epsilon} + \int_0^{\underset{\sim}{\delta}} \underset{\sim}{f}^t \, d\underset{\sim}{\omega} \right] dv \qquad 3.2$$

where $\underset{\sim}{\sigma}$ is the stress vector at any point, $\{\sigma'_{xx}, \sigma'_{yy}, \sigma'_{zz}, \sigma'_{xy}, \sigma'_{yz}, \sigma'_{zx}\}^t$

$\underset{\sim}{\epsilon}$ is the strain vector at the point, $\{\epsilon_{xx}, \epsilon_{yy}, \epsilon_{zz}, \epsilon_{xy}, \epsilon_{yz}, \epsilon_{zx}\}^t$

$\underset{\sim}{\eta}$ is the final strain vector after a time interval,

$\underset{\sim}{\delta}$ is the displacement of the point,

and $\underset{\sim}{f}$ is the force acting at the point.

It is assumed that the rocks behave as a Maxwell substance in that on applying a constant stress ($\underset{\sim}{\sigma}'$) they instantaneously deform elastically and then flow at a constant rate (Jaeger and Cook, 1969). The viscous deformation, however, is assumed to conserve volume and hence only the deviatoric stresses cause flow. It is assumed, in keeping with the Maxwell substance, that the stress causing the viscous flow is equal to that causing the elastic deformation and that the total strain is the sum of that due to the two modes of deformation.

Hence the equation of flow is

$$\dot{\underset{\sim}{\varepsilon}} = [D]^{-1}\dot{\underset{\sim}{\sigma}}' + [Q]\underset{\sim}{\sigma}'$$

where $\dot{\underset{\sim}{\varepsilon}}$ is the rate of deformation, σ' is the instantaneous stress and $[D]$ and $[Q]$ are matrices, assumed constant, relating the deformation to the stresses.

If we assume that during a time step the rate of creep is constant, $\underset{\sim}{c}$, then

$$[D]^{-1}\dot{\underset{\sim}{\sigma}}' + [Q]\underset{\sim}{\sigma}' = \underset{\sim}{c} \quad . \tag{3.3}$$

The general solution of

$$\dot{\underset{\sim}{\sigma}}' = -[A]\underset{\sim}{\sigma}' \tag{3.4}$$

is $\underset{\sim}{\sigma}' = e^{-[A]t}\underset{\sim}{\sigma}'_0$ (Daniel and Moore, 1970)

where σ_0' is the stress at the start of the interval and the exponential term is defined by

$$e^{-[A]t} = [I] - t[A] + \tfrac{1}{2}t^2[A]^2 - \tfrac{1}{3!}t^3[A]^3 + \cdots ,$$

where $[I]$ is the unit matrix.

Now for an isotropic material with Young's modulus E, Poisson's ratio, ν , and viscosity, μ ,

$$\left.\begin{aligned} [Q] &= \frac{1}{\mu}\left\langle \tfrac{1}{3}, -\tfrac{1}{6}, 1 \right\rangle \\ [D] &= \frac{E}{2(1+\nu)}\left\langle \frac{2(1-\nu)}{1-2\nu}, \frac{2\nu}{1-2\nu}, 1 \right\rangle \end{aligned}\right\} \qquad 3.5$$

(Housner and Vreeland, 1966)

where the diamond brackets $\langle a,b,c \rangle$ define a matrix which is

$$\langle a,b,c \rangle \equiv \begin{bmatrix} a & b & b & 0 & 0 & 0 \\ b & a & b & 0 & 0 & 0 \\ b & b & a & 0 & 0 & 0 \\ 0 & 0 & 0 & c & 0 & 0 \\ 0 & 0 & 0 & 0 & c & 0 \\ 0 & 0 & 0 & 0 & 0 & c \end{bmatrix} .$$

Comparing 3.3 and 3.4

$$[A] = [D][Q] .$$

Substituting 3.5 gives

$$[A] = \frac{1}{\tau} \langle \tfrac{2}{3}, -\tfrac{1}{3}, 1 \rangle$$

where $\tau = \dfrac{2\mu(1+\nu)}{E}$.

It can easily be shown that

$$[A]^2 = \frac{1}{\tau^2} \langle \tfrac{2}{3}, -\tfrac{1}{3}, 1 \rangle$$

and $$[A]^n = \frac{1}{\tau^n} \langle \tfrac{2}{3}, -\tfrac{1}{3}, 1 \rangle$$

So that $$e^{-[A]t} = [I] - \tau \left\{ \frac{t}{\tau}[A] - \frac{1}{2}\left(\frac{t}{\tau}\right)^2 [A] + \cdots \right\}$$

$$= [I] - \tau\left(1 - e^{-\frac{t}{\tau}}\right)[A] \ .$$

The solution of 3.3 is

$$\underset{\sim}{\sigma} = \left\{[I] - \tau\left(1 - e^{-\frac{t}{\tau}}\right)[A]\right\} \underset{\sim}{\sigma}_0 + \tau\left(1 - e^{-\frac{t}{\tau}}\right)[D]\underset{\sim}{c} \qquad 3.6$$

The work per unit volume, ω , in the time interval $0 < t < T$ is given by

$$\omega = \int_0^T \underset{\sim}{\sigma}^t \dot{\underset{\sim}{\epsilon}}\, dt$$

$$= \int_0^T \underset{\sim}{c}^t \underset{\sim}{\sigma}\, dt$$

$$= c^t \left\{ T - T\tau[A] + \tau^2[A]\left(1 - e^{-\frac{T}{\tau}}\right)\right\} \sigma_0$$
$$+ c^t \left\{ T\tau[D] - \tau^2[D]\left(1 - e^{-\frac{T}{\tau}}\right)\right\} \underset{\sim}{c}$$

Putting $\underset{\sim}{\varepsilon} = \frac{1}{T}\underset{\sim}{\eta}$ where $\underset{\sim}{\eta}$ is the strain, after time T

$$\omega = \underset{\sim}{\eta}^t \left\{[I] - f\left[1 - \frac{f}{T}\left(1 - e^{-\frac{T}{f}}\right)\right][A]\right\}\underset{\sim}{\sigma}_0$$
$$+ \underset{\sim}{\eta}^t \frac{f}{T}\left\{1 - \frac{f}{T}\left(1 - e^{-\frac{T}{f}}\right)\right][D]\,\underset{\sim}{\eta} \quad .$$

ω is the work per unit volume done in the body during the time interval T. In the general 3-dimensional case the matrices ($[D]$ and $[A]$) are 6 x 6 and the vectors $\underset{\sim}{\sigma}_0$, $\underset{\sim}{\eta}$ and $\underset{\sim}{\sigma}$ have six elements.

Applying the assumption of plain strain, the elements in $\underset{\sim}{\eta}$ which indicate movement or shear into the third dimension (η_z , η_{xz} , η_{yz}) and the components of $\underset{\sim}{\sigma}$ which represent shear stresses into the third dimension (σ_{xz} , σ_{yz}) are all zero. Hence $\underset{\sim}{\sigma}$ and $\underset{\sim}{\eta}$ are reduced to 4 and 3 element vectors respectively. The corresponding rows and columns of the matrices may also be deleted.

If we further assume simple triangular elements with nodes only at the corners, the displacements are linear and the stresses and strains uniform throughout each element. If further the body forces (assumed constant) are considered to act at the nodes then the total work done, W , is

$$W = \sum \Delta_i \omega_i + \underset{\sim}{\delta}^t \underset{\sim}{F}$$

where $\sum$ denotes the summation over all the elements in the model, Δ_i is the area of the i^{th} element assumed to

be of unit thickness, $\underset{\sim}{\delta}$, is the displacement vector of all the nodes and $\underset{\sim}{F}$ is the vector containing the forces acting at the nodes.

Defining matrix $[B]$ to map the nodal displacements into strains (equation 3.1) gives

$$\underset{\sim}{\eta} = [B]\,\underset{\sim}{\delta}$$

and

$$W = \sum \Delta \underset{\sim}{\delta}^t [B]^t \left\{[I] - f\left[1 - \frac{f}{T}\left(1 - e^{-\frac{T}{f}}\right)\right][A]\right\} \underset{\sim}{\sigma_0} \qquad 3.7$$

$$+ \Delta \underset{\sim}{\delta}^t [B]^t \frac{f}{T}\left\{1 - \frac{f}{T}\left(1 - e^{-\frac{T}{f}}\right)\right\}[D][B]\,\underset{\sim}{\delta} + \underset{\sim}{\delta}^t F$$

To find the displacements, $\underset{\sim}{\delta}$, so as to minimize the energy we differentiate with respect to each element of $\underset{\sim}{\delta}$ in turn and equate to zero. This gives

$$\sum \Delta [B]^t \left\{[I] - f\left[1 - \frac{f}{T}\left(1 - e^{-\frac{T}{f}}\right)[A]\right\} \underset{\sim}{\sigma_0}$$

$$+ 2\Delta [B]^t \frac{f}{T}\left[1 - \frac{f}{T}\left(1 - e^{-\frac{T}{f}}\right)\right][D][B]\,\underset{\sim}{\delta} + \underset{\sim}{F} = 0 \qquad 3.8$$

The visco-elastic displacements for one step may be obtained by the simultaneous solution of the matrix equation 3.8 and the stress at the end of the interval (or start of the next interval) for each element is given by substitution in 3.6

$$\underset{\sim}{\sigma_f} = \left\{[I] - f\left(1 - e^{-\frac{T}{f}}\right)[A]\right\} \underset{\sim}{\sigma_0} + \frac{f}{T}\left(1 - e^{-\frac{T}{f}}\right)[D][B]\,\underset{\sim}{\delta} \qquad 3.9$$

It has been assumed that the elastic and viscous properties are constant throughout the time interval. They may, however, be changed between one interval and the next.

The heat generated by viscous flow is given by

$$H^V = \Delta \int_0^T \underset{\sim}{\sigma}^t \dot{\epsilon}_v \, dt$$

where $\dot{\epsilon}_v$ is the rate of the viscous component of the strain. From 3.3

$$\dot{\epsilon}_v = [Q] \underset{\sim}{\sigma}$$

and so $$H^V = \Delta \int_0^T \underset{\sim}{\sigma}^t [Q] \sigma \, dt .$$

Substituting 3.6 and integrating gives

$$H^V = \frac{\Delta}{6} \left\{ \frac{VT}{\mu} \left[(S_1 - S_2)^2 + (S_2 - S_3)^2 + (S_3 - S_1)^2 + 6 S_4^2 \right] \right.$$

$$+ 8 (1 - 2u + v) \left[\eta_1^2 - \eta_1 \eta_2 + \eta_2^2 + 1.5 \eta_3^2 \right] \mu / T$$

$$\left. + 4 (u - v) \left[S_1 (2\eta_1 - \eta_2) + S_2 (2\eta_2 - \eta_1) - S_3 (\eta_1 + \eta_2) + 3 \eta_3 S_4 \right] \right\} \qquad 3.10$$

where S_i is the i^{th} component of $\underset{\sim}{\sigma}_0$

η_i is the i^{th} component of the final strain

$u = f/T \, (1 - e^{-\frac{T}{f}})$

$v = f/2T \, (1 - e^{-2T/f})$

If the stresses are not changing much then an estimate of the heat generated by the viscous flow in one element is

$H^V \simeq \Delta . T . \underset{\sim}{\sigma}_m^t [Q] \underset{\sim}{\sigma}_m$ where $\underset{\sim}{\sigma}_m$ is a mean stress

during the interval.

From this

$$H^v = \frac{\Delta T}{6\mu}\left[(\sigma'_{m1} - \sigma'_{m2})^2 + (\sigma'_{m2} - \sigma'_{m3})^2 + (\sigma'_{m3} - \sigma'_{m1})^2 + 6\,\sigma'^2_{m4}\right]$$

For a viscosity of 1.0×10^{20} Ns/m^2 and a shear stress of about 1.0×10^{8} N/m^2 (1 kbar) the rate of viscous heating would be about 1.0×10^{-4} W/m^3 or 3.0×10^{-8} W/kg, about 60 times greater than the radiogenic heating of basalt (table 2.7). For a stress of 5.0×10^{6} N/m^2 (50 bar) the heat generated is about twice the average radiogenic heat supply per unit volume in the mantle.

The first test of the visco-elastic formulation is that for a zero time step the analysis becomes equivalent to an elastic analysis. With T = 0 equations 3.8 and 3.9 reduce to

$$\sum \left(\Delta B^t \underset{\sim}{\sigma}_0 + \Delta [B]^t [D][B] \underset{\sim}{\delta}\right) + F = 0$$

and $\underset{\sim}{\sigma}_f = \sigma_0 + [D][B]\,\underset{\sim}{\delta}$ respectively.

These are the equivalent elastic equations (Zienkiewicz, 1971).

Secondly, Zienkiewicz (1971) used the analytical analysis (Lee et al., 1959) of the stresses due to a suddenly applied internal pressure in an externally reinforced visco-elastic cylinder (fig. 3.2) to illustrate

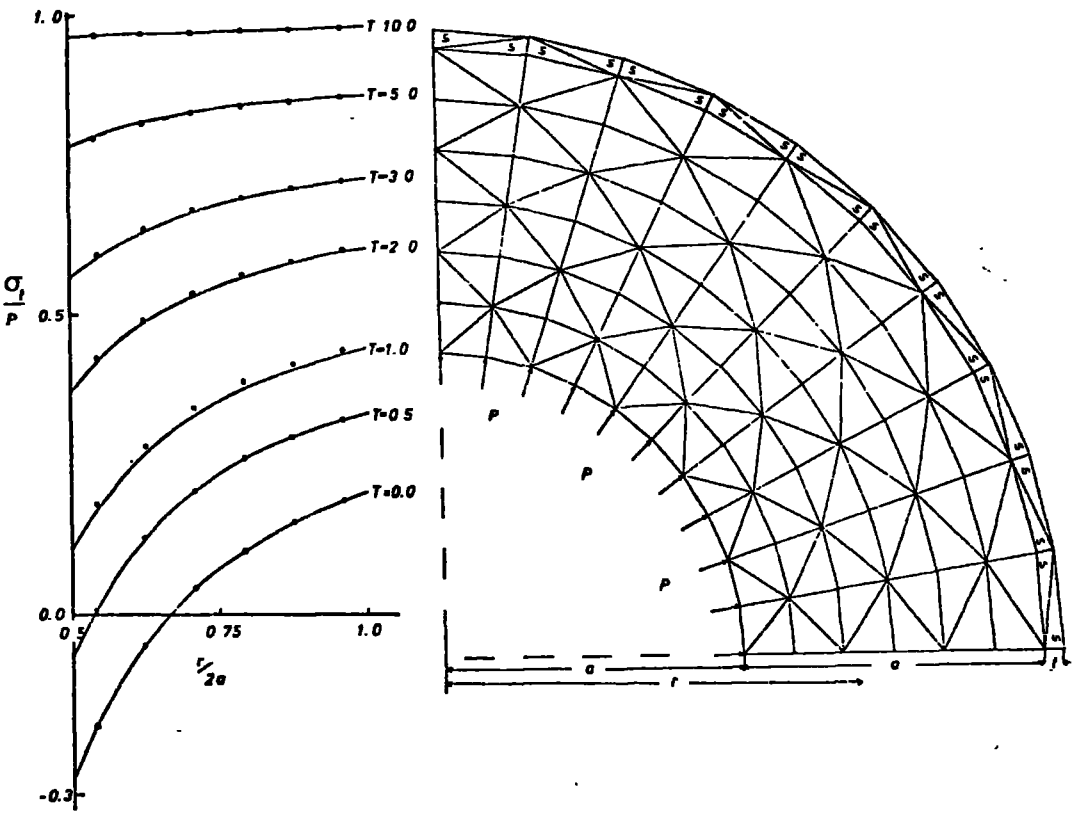

Fig. 3.2 Test of finite element visco-elastic program. A steel shell (elements marked with s) is lined with a visco-elastic material and an internal pressure, P, applied at zero time. The properties are

	visco-elastic material	steel
Young's modulus	10^5	3×10^7
Poisson's ratio	1/3	$1/\sqrt{11}$
Viscosity	$\frac{3}{8} \times 10^5$	∞

Dots show tangential stress computed by the finite element program and the lines the analytical solution of Lee et al. (1959)

the use of finite element analysis. This same analysis has been performed with the new formulation but with time steps 10 times greater than those used by Zienkiewicz (0.1 time units). Very good agreement between the analytical and finite element results was obtained (fig. 3.2).

3.2 Finite element analysis of transient heat flow problems

It is generally easier and quicker to solve heat flow problems using finite difference rather than finite element techniques, but when the heat flow problem is part of a larger integrated finite element problem it is convenient to use finite elements. This allows the use of the same nodes and elements as may be used in the visco-elastic solution.

Following Zienkiewicz (1971, p.335) the problem reduces to the solution of the differential equation,

$$[H]\underset{\sim}{\theta} + [C]\frac{\partial}{\partial t}\underset{\sim}{\theta} + Q = 0 \qquad 3.11$$

where $\underset{\sim}{\theta}$ is the temperature at the nodes,

$\underset{\sim}{Q}$ is the rate of heat input from mechanical and radiogenic sources,

$[C]$ is a function of the heat capacity and geometry,

and $[H]$ is a function of the geometry and conductivities of the materials.

When using triangular elements the temperature is approximated by a linear function over the element. From Zienkiewicz the values of $[C]$ and $[H]$ for such elements are:

$$[C] = \frac{\rho C_p \Delta}{3} \begin{bmatrix} \frac{1}{2} & \frac{1}{4} & \frac{1}{4} \\ \frac{1}{4} & \frac{1}{2} & \frac{1}{4} \\ \frac{1}{4} & \frac{1}{4} & \frac{1}{2} \end{bmatrix} \qquad 3.12$$

and

$$[H] = \frac{K}{4\Delta} \begin{bmatrix} b_i^2 + c_i^2 & b_i b_j + c_i c_j & b_m b_i + c_m c_i \\ b_i b_j + c_i c_j & b_j^2 + c_j^2 & b_j b_m + c_j c_m \\ b_i b_m + c_i c_m & b_j b_m + c_j c_m & b_m^2 + c_m^2 \end{bmatrix} \qquad 3.13$$

The b's and c's are obtained by cyclic permutations of

$$b_i = y_j - y_m$$
$$c_j = x_m - x_j$$

The subscripts referring to the vertices of the elements,

and Δ is the area

C_p is the specific heat

ρ is the density

and K is the thermal conductivity which is assumed to be isotropic.

If it is assumed that the temperature varies linearly with time during each time step then the change in temper-

ature $\Delta\underset{\sim}{\phi}$ during the interval Δt is given by

$$\left\{[H] + \frac{2}{\Delta t}[C]\right\}\Delta\underset{\sim}{\phi} = -2[H]\underset{\sim}{\phi}_0 + \frac{2}{\Delta t}\underset{\sim}{Q} \qquad 3.14$$

$\underset{\sim}{\phi}_0$ is the temperature at the nodes at the start of the interval.

The steady state heat flow problem can similarly be solved from

$$[H]\underset{\sim}{\phi}_S = \underset{\sim}{q} \qquad 3.15$$

where $\underset{\sim}{\phi}_S$ is the steady state temperature of the nodes and $\underset{\sim}{q}$ is the rate of heat generation associated with each node.

Alternatively the subroutine for transient heat flow may be used by setting $C_p = 0$ so that from 3.14

$$[H]\Delta\underset{\sim}{\phi} = -2[H]\underset{\sim}{\phi}_0 + 2\underset{\sim}{q}$$

but $$\underset{\sim}{q} = [H]\underset{\sim}{\phi}_S \qquad 3.16$$

so $$\underset{\sim}{\phi}_S = \underset{\sim}{\phi}_0 + \tfrac{1}{2}\Delta\underset{\sim}{\phi}$$

Hence the steady state temperature distribution may be found by incrementing the initial temperature distribution by half the computed increment when $[C] = 0$.

3.3 Boundary conditions

The two previous sections have presented methods of forming sets of simultaneous equations

$$[M]\underset{\sim}{S} = \underset{\sim}{b} \qquad 3.17$$

which may be solved for, $\underset{\sim}{S}$, the displacements in the case of visco-elastic analysis and the temperature increment for heat flow problems.

However, in both cases there are always constraints on some of the variables in $\underset{\sim}{S}$ and these need to be applied before the equations are solved. In general this requires the substitution of a new equation for one of those in the original set or else a modification to the original equation.

(a) Fixed Points

This is the most common type of boundary. If the variable S_i, must take a fixed value C_i (commonly zero) in the solution then it is a simple procedure to replace the i^{th} equation in 3.17 by

$$S_i = C_i$$

In visco-elastic solutions this allows points to be held on vertical or horizontal lines or to be forced to move at a fixed velocity. In the transient heat flow solution it allows for the fixing of some temperatures where there are "infinite" heat sinks or sources (e.g. on the top or bottom of the model).

(b) Constant heat flux boundary

The equations assembled as described in the previous sections contain the assumption that no heat flux crosses

the boundary. If, in fact, there is a heat flux across the boundary it may be allowed for by adding the heat per unit time crossing the boundary to the nearest node and so increment b_i by this amount. It is in fact an addition to the heat sources in equation 3.11.

(c) Boundaries with applied hydrostatic forces

If the boundary between two boundary nodes i, and j is not held on a vertical or horizontal line by undetermined forces but is constrained by a hydrostatic pressure then this is equivalent to applying additional forces at the two nodes.

If in fig. 3.3 the hydrostatic pressure on the boundary is assumed to vary linearly along the boundary between nodes i and j and if it is P_i and P_j at the nodes the equivalent forces on the nodes which allow for the hydrostatic pressure on this part of the boundary are

$$F_i^{ij} = L(P_i/3 + P_j/6)$$

$$F_j^{ij} = L(P_i/6 + P_j/3)$$

where L is the distance between the nodes i and j.

The x and y components of these forces are

$${}_xF_i^{ij} = \Delta y\,(P_i/3 + P_j/6)$$

and $${}_yF_i^{ij} = \Delta x\,(P_i/3 + P_j/6)$$

where Δx and Δy are the x and y components of L .

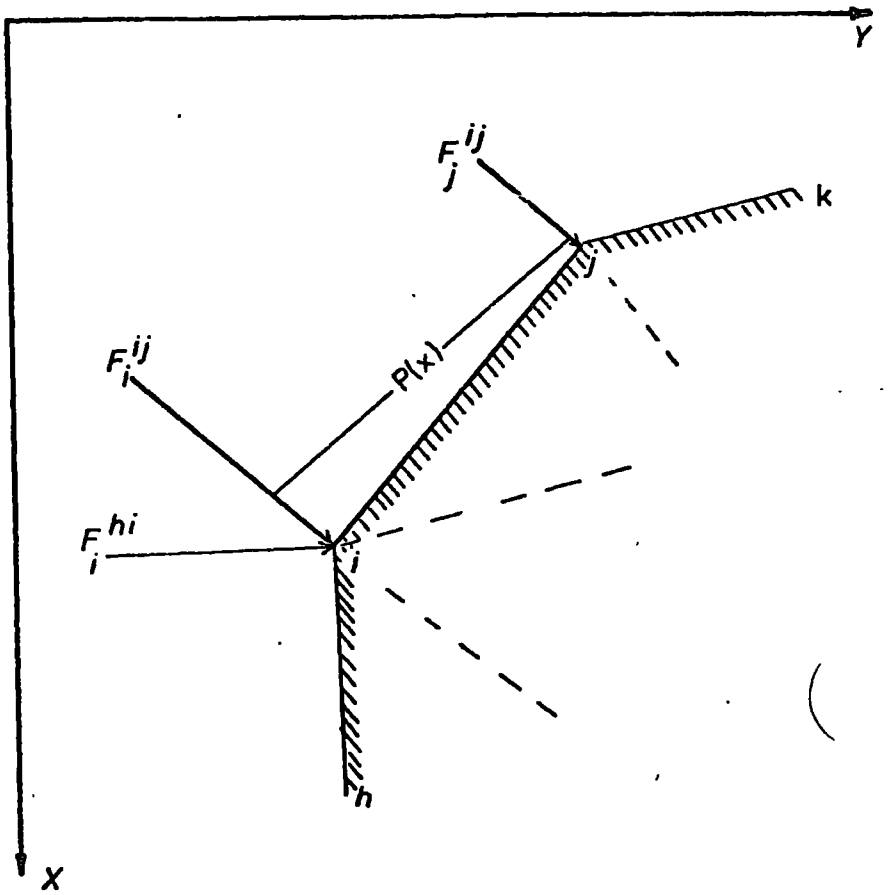

Fig. 3.3 A boundary under hydrostatic pressure. The shaded boundary (h,i,j,k) of the model is under hydrostatic pressure P(x). The equivalent nodal forces on node i, for the pressure on edge ij is F_i^{ij}.

These are to be added into the appropriate elements of the matrix $\underline{b}$ in 3.17.

However, if the pressure on the boundary varies during the interval because of the displacements of nodes i and j then matrix [M] in 3.17 should also be adjusted by the derivatives of each F with respect to the four appropriate displacements.

The four components of the forces are:

$$ {}_xF_i^{ij} = F_{x_i} = (y_j - y_i)(P_i/3 + P_j/6) $$

$$ {}_yF_i^{ij} = F_{y_i} = -(x_j - x_i)(P_i/3 + P_j/6) $$

$$ {}_xF_j^{ij} = F_{x_j} = (y_j - y_i)(P_i/6 + P_j/3) $$

and $$ {}_yF_j^{ij} = F_{y_j} = -(x_j - x_i)(P_i/6 + P_j/3) . $$

Assuming $\frac{\partial P_i}{\partial x_i} = \frac{\partial P_j}{\partial x_j} = g\rho_e = \frac{P_j - P_i}{x_j - x_i}$, where

g is the acceleration of gravity and ρ_e is an equivalent density, and the other derivatives of P_i and P_j are 0, then the derivatives of the components of the forces are

$$ \left.\begin{aligned}
&\frac{\partial F_{x_i}}{\partial x_i} = \frac{\partial F_{x_j}}{\partial x_j} = \frac{1}{3} g\rho_e (y_j - y_i) \\
&\frac{\partial F_{y_i}}{\partial y_i} = \frac{\partial F_{y_j}}{\partial y_j} = \frac{1}{2}\left(\frac{\partial F_{y_i}}{\partial y_j} + \frac{\partial F_{y_j}}{\partial y_i}\right) = 0 \\
&\frac{1}{2}\left(\frac{\partial F_{x_i}}{\partial x_j} + \frac{\partial F_{x_j}}{\partial x_i}\right) = \frac{1}{2}\left(\frac{\partial F_{x_j}}{\partial y_j} + \frac{\partial F_{y_j}}{\partial x_j}\right) = -\frac{1}{3}(x_j - x_i) g\rho_e \\
&\frac{1}{2}\left(\frac{\partial F_{x_i}}{\partial x_j} + \frac{\partial F_{x_j}}{\partial x_i}\right) = \frac{g\rho_e}{6}(y_j - y_i) \\
&\frac{1}{2}\left(\frac{\partial F_{x_i}}{\partial y_j} + \frac{\partial F_{y_j}}{\partial x_i}\right) = P_i/3 + P_j/6 \\
\text{and}\quad &\frac{1}{2}\left(\frac{\partial F_{y_i}}{\partial x_j} + \frac{\partial F_{x_j}}{\partial y_i}\right) = -\left(\frac{P_i}{6} + \frac{P_j}{3}\right)
\end{aligned}\right\} \quad 3.18 $$

The components of the forces are added to vector $\underset{\sim}{b}$ and the 16 elements in the matrix $[M]$ corresponding to the appropriate displacements are adjusted by the derivatives in 3.18.

(d) Nodes forced to move in a given direction not parallel to an axis

The constraint of a node, I, to move at a given angle, θ , to the x-axis (fig. 3.4) implies the addition of an unknown force, $\underset{\sim}{G}$, acting on the node. If this force is assumed to act normal to the imposed movement then its components in the direction of the axes are

$$G_x = G \sin\theta$$

$$\text{and} \quad G_y = G \cos\theta \quad .$$

The components of the displacement of the node are related by

$$\delta_y = \delta_x \tan\theta \quad . \qquad 3.19$$

If δ_x and δ_y are the i^{th} and j^{th} unknowns in vector $\underset{\sim}{\delta}$ of equation 3.17 the i^{th} and j^{th} equations of the matrix set are

$$\sum_{k=1}^{N} M_{ik}\,\delta_k = b_i + G_x \qquad 3.20$$

$$\text{and} \quad \sum_{k=1}^{N} M_{jk}\,\delta_k = b_j + G_y \qquad 3.21$$

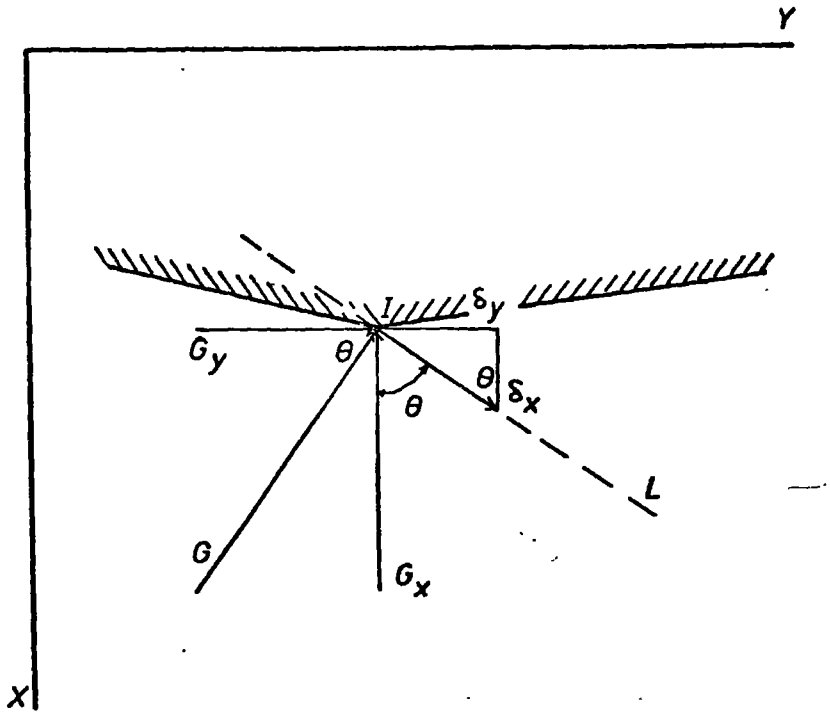

Fig. 3.4 Node, I, is forced to move at angle θ from the horizontal. The force causing the restriction, G, is applied normal to this direction and has components Gx and Gy.

Since G is unknown its components need to be eliminated. Substituting $G_x = G_y \tan\theta$ in 3.20, dividing by $\tan\theta$ and subtracting from 3.21 gives a new equation

$$\sum_{k=1}^{N} (M_{jk} - M_{ik}/\tan\theta)\, S_k = -b_i/\tan\theta + b_j \qquad 3.22$$

The constraint on I is imposed by replacing the two equations 3.20 and 3.21 in 3.17 by 3.19 and 3.22.

3.4 The integrated finite element system

The integration of the visco-elastic and heat flow analyses depends upon their interdependence. The mechanical system is generally considered as isothermal and the heat equations as isovolumetric. So during the mechanical solution heat is being added to the system and the change in temperature resulting from the subsequent thermal solution causes additional stresses.

The heat added to the system during the isothermal visco-elastic step is in two parts. The first is due to adiabatic compression or expansion of the rocks and the other the loss of mechanical energy by viscous flow.

The adiabatic heating in the i^{th} element is

$$H_i^a = T_i \alpha_i \Delta_i \delta P_i$$

where T_i is the mean temperature of the element

α_i is the thermal expansion coefficient

Δ_i is the area

and δP_i is the change in pressure.

The heat gained from the loss of mechanical energy by viscous flow H^V, is given by equation 3.10.

During the isovolumetric thermal solution (note we need to use C_v not C_p) the change in the initial stress for the next mechanical analysis is given by

$$\underset{\sim}{\Delta\sigma_i} = -\frac{E_i \alpha_i \delta T}{3(1-2\upsilon_i)} \begin{pmatrix} 1 \\ 1 \\ 1 \\ 0 \end{pmatrix}$$

where δT is the change in temperature

E_i is Young's modulus

α_i is the coefficient of thermal expansion

and υ_i is Poisson's ratio.

CHAPTER 4

STRESSES DUE TO PHASE CHANGES IN THE DESCENDING LITHOSPHERE

Bridgeman (1945) suggested that polymorphic transitions in the earth could cause earthquakes. This could be either by the catastrophic running of the transition and the associated volume change (Evison, 1967) or by the catastrophic release of stress by fracture after a critical stress has been built up slowly by gradual progress of a transition. Ringwood (1969b) suggested that the changes in phase as the lithosphere descends in a subduction zone may cause large stresses and be responsible for the intermediate and deep seismicity. There are two causes for such stresses. Firstly, since the slab is cooler, the phase changes occur at a different depth in the slab than in the surrounding asthenosphere and so the increased density across the transition causes an increase in the negative buoyancy (e.g. Toskoz et al., 1973). Secondly, the rock contracts as it changes phase producing local stresses.

Previously, the stresses associated with the sinking slab have been studied considering only the forces due to the negative buoyancy of the slab in the asthenosphere (e.g. Toskoz et al., 1973; Neugebauer and Breitmayer, 1975;

Sleep, 1975). These analyses started from an estimate of the temperature distribution and calculated the negative buoyancy as a function of depth and temperature. Viscous (Sleep, 1975) or visco-elastic (Tosköz et al., 1973; Neugebauer and Breitmayer, 1975) analyses were then performed to deduce the stresses associated with the process.

It is not clear in these analyses how the additional buoyancy due to the elevation of the phase boundaries are included, it being simply stated that the effect is approximately equivalent to multiplying the thermal contraction effect by 1.5 (Neugebauer and Breitmayer, 1975). The maximum stresses calculated from the analyses of the buoyancy effect are 0.5×10^8 N/m^2 (500 bar) and are aligned with one principal axis down the dip of the slab.

Recently Sung and Burns (1976) have suggested that the rate of the olivine-spinel transformation is slow in the cool interior of the slab so that the phase transition may be depressed rather than elevated. This depends on the temperature and hence the rate of subduction. If the transition is depressed (so that the centre of the slab contains metastable-olivine) then a positive buoyancy effect of similar magnitude to the negative buoyancy effect of a raised phase boundary would be exerted on the slab. When nucleation of the reaction does take place the reaction

is likely to run catastrophically. I assume, however, that equilibrium conditions are maintained throughout the model.

No account has yet been taken of any stresses due to the differential contraction at the phase boundaries. To gain an estimate of these effects an analysis of the stresses due to the lowering of a slab of mantle 100 km wide and 200 km long through the asthenosphere to intersect the garnet peridotite-spinel garnet phase boundary (fig.2.1) was performed.

The top of the slab was assumed to be initially at 100 km depth. The temperature of the outer edge of the model was assumed to be that of a reasonable oceanic geotherm (section 2.3). A linear decrease in temperature in the slab was assumed so that the axis of symmetry was 500^{o}C cooler than the outer edge (fig. 4.1). This lateral gradient is approximately that calculated in most thermal models of subduction zones (e.g. Toskoz et al., 1973). The initial densities were computed from equation 2.8 using these temperatures and the pressures expected at the appropriate depth in the mantle. The rheology of the slab was assumed to be either elastic or visco-elastic with elastic properties computed from Chapter 2.1.

The model was supported on its outside by the hydrostatic pressure of the asthenosphere. The bottom was lowered through the mantle at 4.0 cm/yr. with time steps of 10,000 yrs.

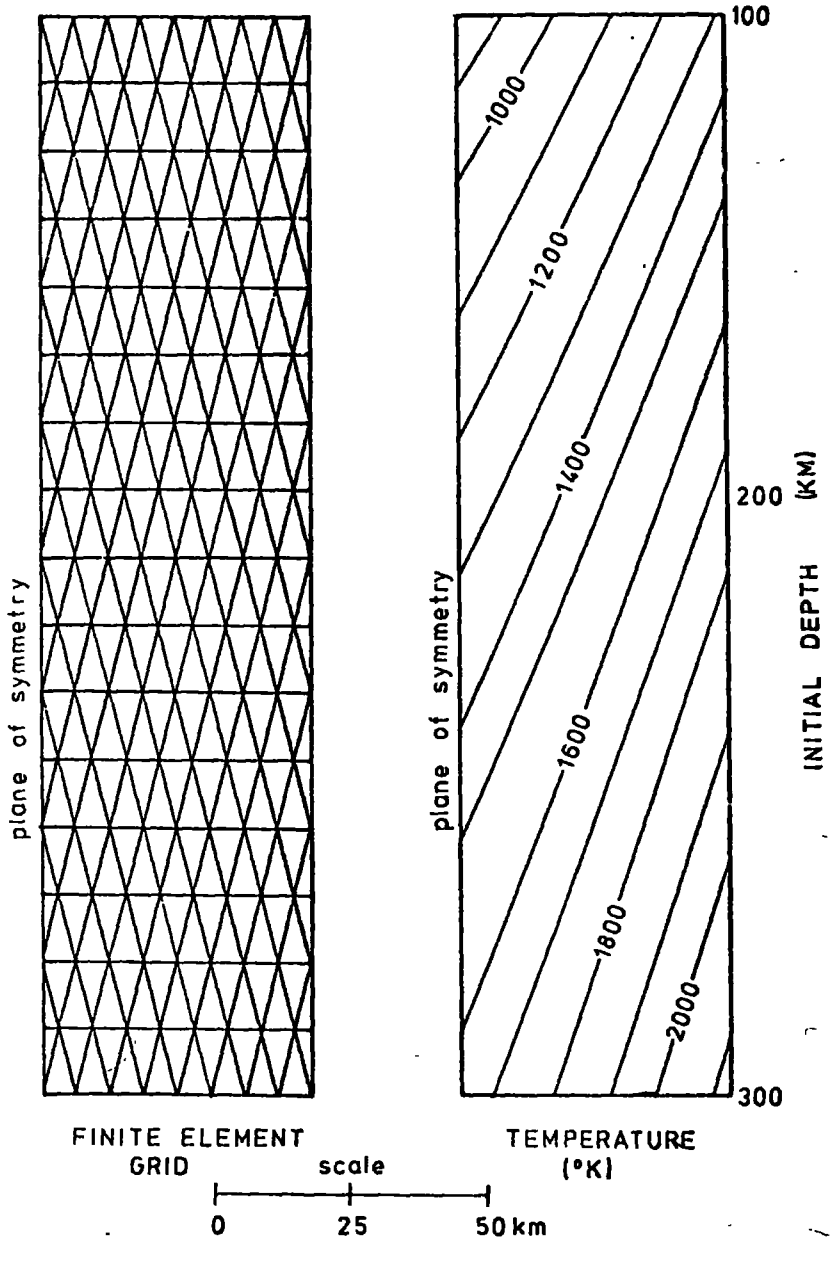

Fig. 4.1 Finite element net and temperature distribution of a model of part of a descending slab. The initial depth of the top is 100 km.

This boundary condition resulted in the additional body forces due to the model being more dense than the standard asthenosphere being supported by the base of the model thus producing compressional stresses near the bottom of the model. Since the model is symmetrical about the central vertical plane no movement of material was allowed through this plane and only half the slab was studied. Isothermal, elastic or visco-elastic finite element analyses were used, the nodes being progressively moved at each time step.

The incremental nature of the analyses was important for the elastic as well as the visco-elastic analyses since the elastic properties changed with pressure (section 2.1). The properties used for each time increment were determined from the conditions at the start of the step and assume mineralogical equilibrium.

4.1 Results

The stress distribution near the phase boundary for various models are shown in figs. 4.2, 4.3 and 4.4. The plotted stresses are the principal stresses in the model minus the hydrostatic pressure applied to the boundaries for the appropriate depth. Bars on the ends of the stresses indicate that they are tensional with respect to the ambient

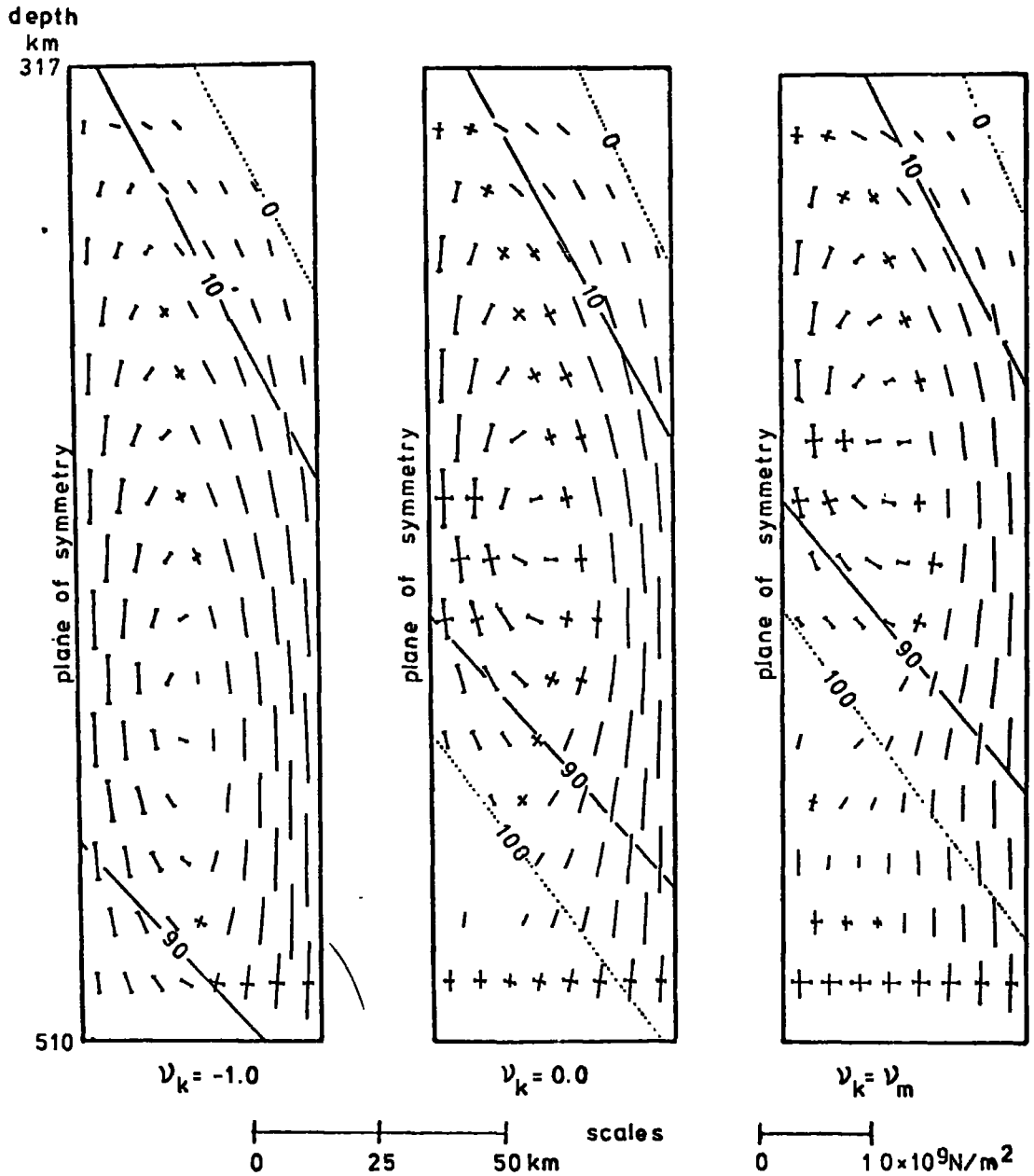

Fig. 4.2 Stress distribution calculated from an elastic analysis of the differential contraction at the garnet peridotite-spinel garnet phase boundary. The length of the lines represent the deviation of the principal stresses from the hydrostatic stress applied at the edges of the model. Stresses smaller than 1.0×10^6 N /m^2 are not plotted. The three models show the effect of varying ν_k. Contours of the percentage of spinel phase to olivine are also shown.

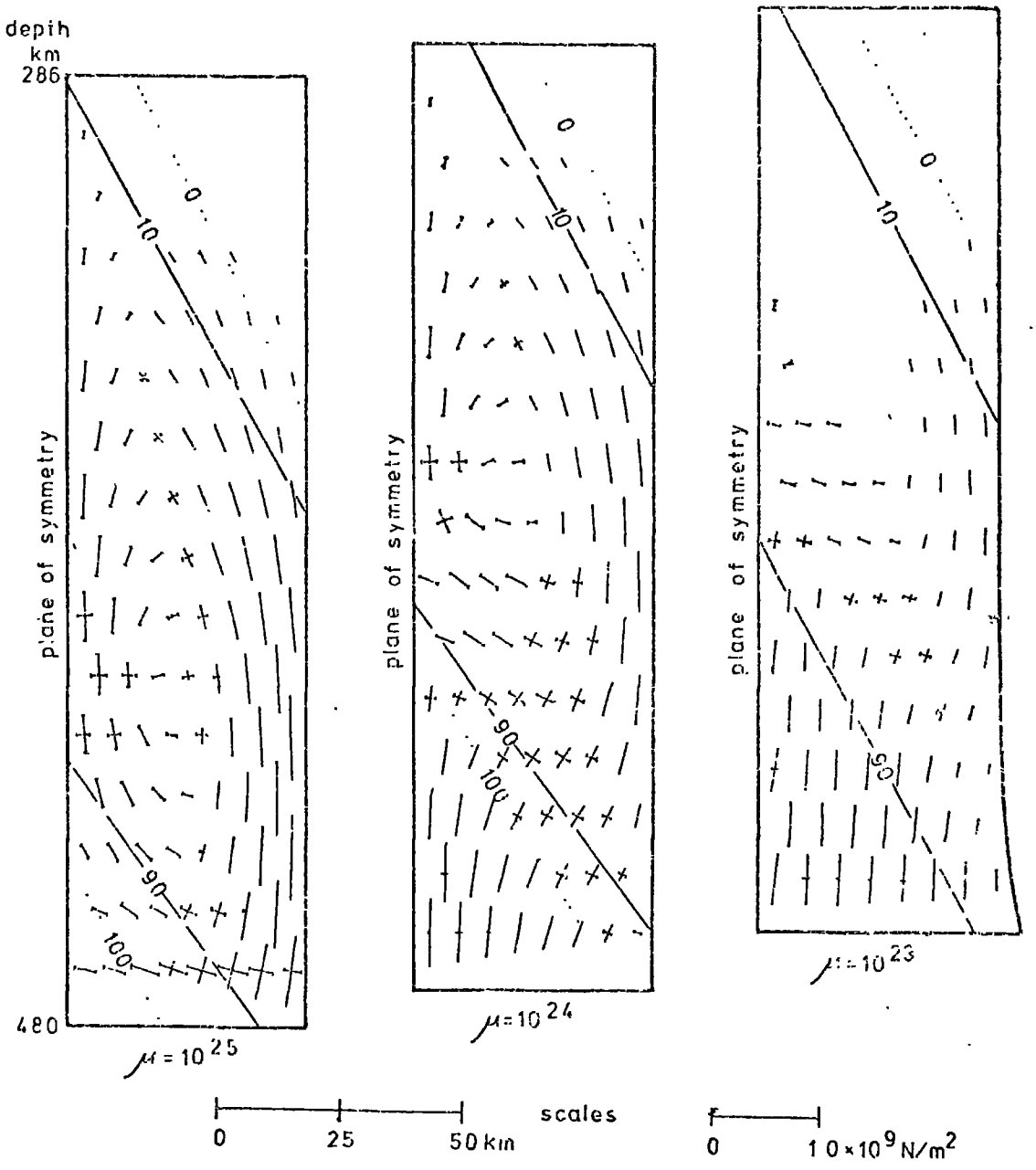

Fig. 4.3 Effect of viscosity on the stress distribution calculated from a visco-elastic analysis. $\nu_k = 0.0$ in all 3 models. Contours of the percentage of spinel phase to olivine are also shown.

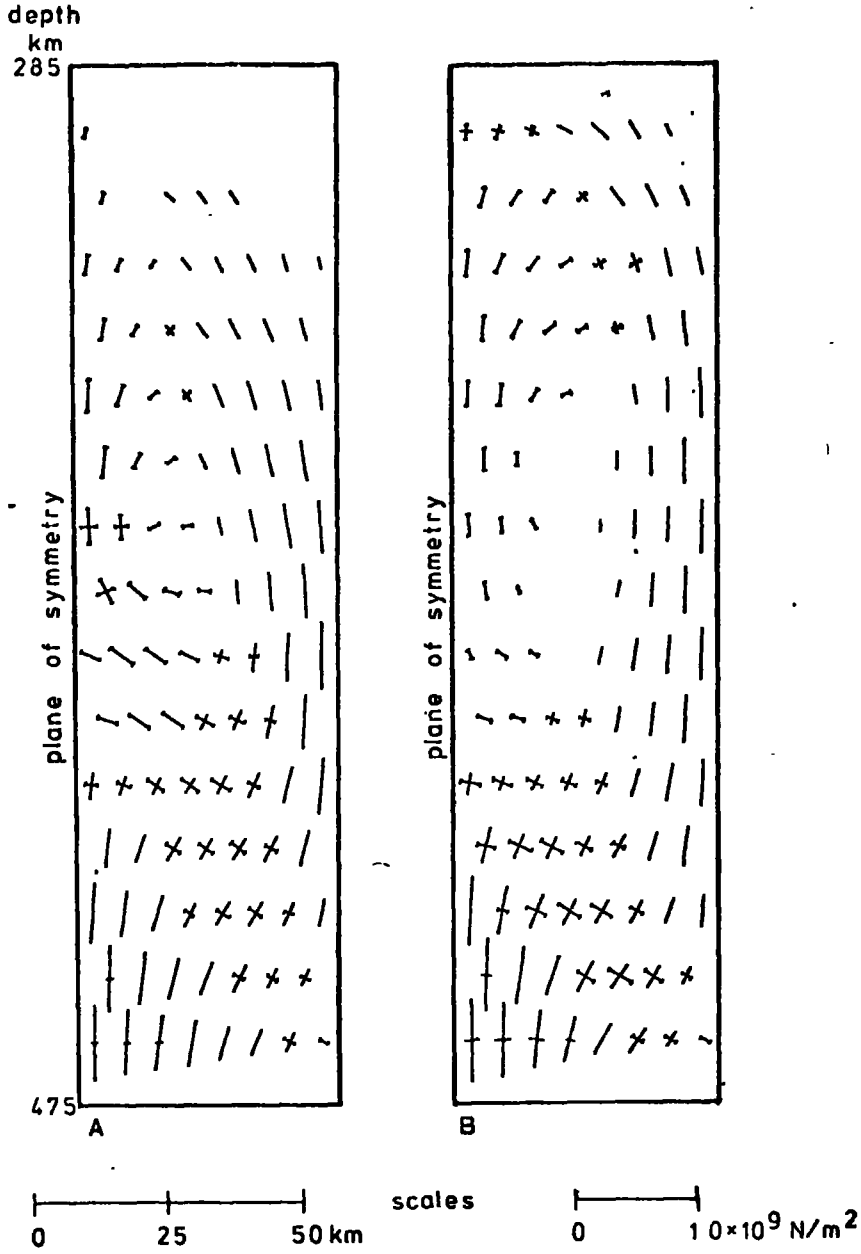

Fig. 4.4 The small effect on the stress distribution related to the choice of a linear (A) or non-linear (B) variation of the proportion of the phases in the transition zone ($\mu' = 1.0 \times 10^{24}$ Ns/m^2, $\nu_k = 0.0$).

hydrostatic pressure. The maximum stresses near the phase boundary in all the models are about 7 x 10^8 N/m^2 (7 kbar) and consequently about 15 times the maximum computed in models considering only the body forces due to the increased density in the slab (Sleep, 1975; Toskoz et al.,1973). In figs. 4.2 and 4.3 contours of the proportion of the olivine-spinel phase are also shown. The stresses caused by the phase change are sufficiently large to alter the depth range of the phase transition so that it is not the same in all models. Although the details of the stress distributions are different the overall pattern is the same with large vertical tensional stresses in the centre of the slab and compressional stresses at the edges. The horizontal components of the stresses are about equal to the hydrostatic stresses applied to the boundaries.

The physical properties used in the various models for figs. 4.2 to 4.4 were chosen so as to show the effect of changing the Poisson's ratio related to the phase change (ν_K), the viscosity (μ), and the assumption as to how the density varies across phase transition.

Elastic analyses were used for the first three models (fig. 4.2). The bulk modulus was determined from the equation of state but the Poisson's ratio corresponding to the phase change (ν_K in section 2.1) was given values of -1.0, 0.0 and the value which would be determined from the seismic velocities, ν_m (about 0.26). As ν_K increases the depth

range over which the phase change takes place decreases. The phase change is completed in the centre of the slab 80 km shallower for $\nu_K = \nu_m$ than $\nu_K = -1.0$. In all cases the steady state thickness of the transition zone (about 110 km) is extended to over 140 km by the stresses induced by the reduction in volume as the phase change proceeds. The maximum stress also decreases as ν_K increases. It is 8.22, 7.67 and 5.48 x 10^8 N/m^2 for ν_K = -1.0, 0.0 and ν_m respectively.

The effect of adding viscous relaxation to the stresses is shown in fig. 4.3. With uniform viscosities higher than 1.0 x 10^{25} Ns/m^2 the stresses are much the same as those for an elastic model (fig. 4.2b). With viscosities less than about 1.0 x 10^{23} the slab flowed outward at the bottom under its excess weight with respect to the warmer asthenospheric model used to compute the hydrostatic forces on its edges. At these viscosities the stresses caused by the phase change were nearly completely dissipated by creep and only those due to the excess density remained. The stresses for viscosities between these limits were intermediate, the tensional and excessively large compressional stresses decreasing with the viscosity.

Fig. 4.4 shows that the assumption as to how the density varies across the transition zone has only minor effects on the computed stresses. The proportion of each phase was

assumed to vary linearly with distance from the mean position of the phase boundary (equation 2.6) for fig. 4.4a and to vary non-linearly (equation 2.7) for fig. 4.4b. The stress patterns are nearly the same in both models.

4.2 Limitations of the model and conclusions

This model has several limitations on its applicability to the sinking slab in a subduction zone. These may be summarized as follows:

a) The slab as it sinks into the asthenosphere is not symmetrical but the temperature distribution is asymmetrical with high thermal gradients on the top side and more gentle ones on the lower side (e.g. Toskoz et al., 1973).

b) The sinking slab is seldom vertical. A test run on a sloping model, however, showed little difference in the stresses computed from that for a vertical slab. One of the principal stresses was still large and parallel to the edge of the slab. The assumption of symmetry, however, is further invalidated by the dip of the slab.

c) The width of the slab is assumed to be 100 km. This is probably too great so that the thermal gradients used are probably more applicable to the underside of the slab than the topside.

d) Uniform viscosity was used throughout the model. Since the viscosity has a large effect on the stresses (fig. 4.3) this is very important. The viscosity of the outside of the slab at the depths of the transition zone are probably less than 1.0×10^{23} Ns/m^2. The inside of the slab at 500°C lower temperature would have a viscosity greater than 1.0×10^{25} Ns/m^2. The shear stress dependence of the viscosity would also greatly affect the computed stresses.

e) I have assumed that mineralogical equilibrium is maintained. If Sung and Burns (1976) are correct in asserting that the phase change may not run in the centre of the slab because of the low temperature and high nucleation energy then the stress pattern will change different and the phase change will run catastrophically. Residual stresses will still be present in the vicinity of the phase transition because of the change in volume.

f) An isothermal analysis was used. The temperature rise in the slab as it descends over the range in which the model sank is about 250°C (Toksöz et al., 1973). This meant that the phase changes occurred too shallow in our models. More importantly the latent heat and the effect of the phase transition on the coefficient of thermal expansion (section 2.2.1) could modify the stresses.

g) No account has been made of possible failure and the subsequent stress release and deformation.

In spite of these limitations some things are clear from the models. It is certain that as the descending slab changes phase there is an increase in density and consequently a decrease in volume. This must a priori cause stresses in the surrounding rocks. The models show that these stresses are probably 10 to 15 times greater than those previously computed in the slab considering only its negative buoyancy in the asthenosphere. The stresses are relatively tensional in the cooler centre of the slab and compressional near the edges. They are approximately aligned to the edges of the slab.

The stresses are sufficiently large that they alter the equilibrium of the phases for a given depth and so if they are released the phase transition will run to change the density to that relevant to the new mean stress. If the initial release of stress was caused by failure and the resulting phase change ran catastrophically, then a volume change seismic radiation pattern would be superimposed upon the dislocation pattern. Evison (1967) presented some evidence that for large earthquakes (magnitude 8 and above) there may be such a radiation pattern. Randall and Knopoff (1970) indicate that the radiation pattern for deep earthquakes is compatible

with phase transformations and Gilbert and Dziewonski (1975) observed precursor volume changes for two deep focus earthquakes.

In our model we had the simple case of starting with an unstressed, uniform material all in one phase. If the starting conditions had straddled a phase boundary then some of the stresses induced due to the relative contraction of some of the initially unstressed rocks near the phase boundary would not have been dissipated as the material became of uniform phase. This could be very important where the starting material is not chemically homogeneous so that the phase transitions do not occur at the same depths. This is relevant to the crust-mantle boundary where the changes in density of adjacent parts of the crust and mantle will vary and cause large shearing stresses.

CHAPTER 5

BENDING THE OCEANIC LITHOSPHERE

The subduction of the oceanic lithosphere requires that it be bent from the earth's surface to dip at 30^{o} to 70^{o} into the asthenosphere (fig. 1.1). The surface expressions of this large deformation are the trench where the two plates abut and the outer rise. The bottom of the trench is typically 3.0 km below the normal oceanic depth (Hayes and Ewing, 1970). The sea floor slopes up from the trench at about 5^{o} onto the outer rise. This rise is about 700 m above the isostatic level of the ocean floor and extends to about 400 km from the trench (Le Pichon et al., 1973). There is a positive gravity anomaly over the rise which is consistent with the topography being simply due to flexure of the lithosphere (Watts and Talwani, 1974).

The deformation of the oceanic lithosphere in these regions has usually been modelled by comparing the surface topography to the deformation predicted for a semi-infinite uniform plate. The boundary conditions have been a load along the free edge and no displacements at infinite distances into the plate. The analyses have assumed the plate to be sandwiched between non-viscous ocean on top and asthenosphere beneath (Lliboutry, 1969; Walcott, 1970; Hanks, 1971; Watts and Talwani, 1974). The thin plate theory

used in these previous analyses assume that the plate is uniform, that the gradients of the deflections are small, and that the shearing stresses in the plane of the plate can be neglected (Hausner and Vreeland, 1966). The boundary conditions used assumes that there is no bending at the free-edge of the plate. These criteria are not strictly correct for this part of the lithosphere. The effective elasticity varies as a result of phase changes and the viscosity decreases with depth (Chapter 2). Although the lithosphere is about 75 to 100 km thick and the deflections studied are about 10 km, to model the shape of the topography adequately an "equivalent thickness" of 27 km (Watts and Talwani, 1974) to 50 km (Le Pichon et al., 1973) needs to be used. Even with such a thin "equivalent thickness", the stresses computed to exist in the model are sufficient to cause tensional failure in the crust (Le Pichon et al., 1973).

In this chapter I apply beam theory for composite beams to show the effect of the variable elasticity, fracture, and viscosity in reducing the flexural parameters for an 80 - 100 km thick beam to those estimated using the theory of thin beams.

5.1 Elastic bending of a uniform plate

Analytical solutions for the displacements of a thin

transversely loaded plate have been given by Hetenyi (1946), Walcott (1970) and Le Pichon et al., (1973).

Following the notation used by Le Pichon et al.,(1973) we define a rectangular coordinate system in which the origin is on the intersection of the free edge of the plate and the neutral fibre (fig. 5.1). The y axis is horizontal parallel to the free edge, the z axis points vertically downward and the x axis points along the undeformed neutral fibre and is positive in the plate as in fig. 5.1. If the plate is sandwiched between two fluids and the deformation is assumed to be cylindrical (uniform in the y direction), then the differential equation relating the vertical displacement of the neutral fibre, ω , and the distance from the free edge, x, is given by Le Pichon et al., (1973) as

$$D\frac{\partial^4\omega}{\partial x^4} + S\frac{\partial^2\omega}{\partial x^2} + k\omega = p \qquad 5.1$$

where D is the flexural rigidity

S is a horizontal force applied on the free edge

κ is $(\rho_m - \rho_w)g$

ρ_w, ρ_m are the density of the overlying (water) and underlying (asthenosphere) fluids

g is the gravitational acceleration

and p is a transversely applied external stress .

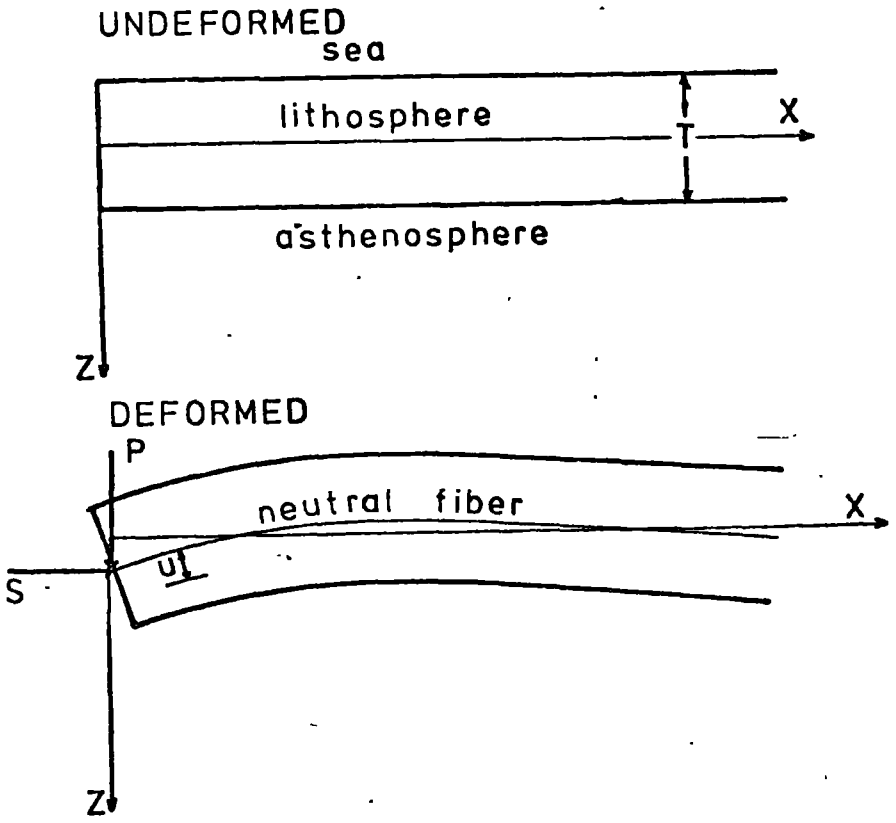

Fig. 5.1 Diagram of model for analysis of the bending of the lithosphere using the theory for thin plates. P and S are forces applied at the free end. The plate extends to infinity in the x direction.

For a uniform elastic plate, the flexural rigidity D is given by

$$D = \frac{E T^3}{12(1-\nu^2)}$$

where T is the thickness of the plate.

If we define variables ℓ and β such that

$$\ell = \sqrt[4]{D/k} = \alpha/\sqrt{2} ,$$

where α is the flexural parameter (Walcott, 1970), and

$$\cos 2\beta = S/2k\ell^2 ,$$

then the general solution of equation 5.1 is

$$\omega = A e^{-\frac{x}{\ell}\sin\beta} \cos\left(\frac{x}{\ell}\cos\beta + \varphi\right) + A' e^{\frac{x}{\ell}\sin\beta} \cos\left(\frac{x}{\ell}\cos\beta + \varphi'\right)$$

This is a damped harmonic wave. A, A', φ and φ' are constants determined by the boundary conditions.

If the vertical load, P, is applied only at x = 0 then the solution reduces to

$$\omega = A e^{-\frac{x}{\ell}\sin\beta} \cos\left(\frac{x}{\ell}\cos\beta + \varphi\right) \qquad 5.2$$

If in addition there is no horizontal force at x = 0, (S = 0)

$$\omega = A e^{-\frac{x}{\alpha}} \cos\frac{x}{\alpha} \qquad 5.3$$

(Le Pichon et al., 1973). Fig. 5.2 shows the variations of the topography according to equation 5.3 for A = 10.0 km

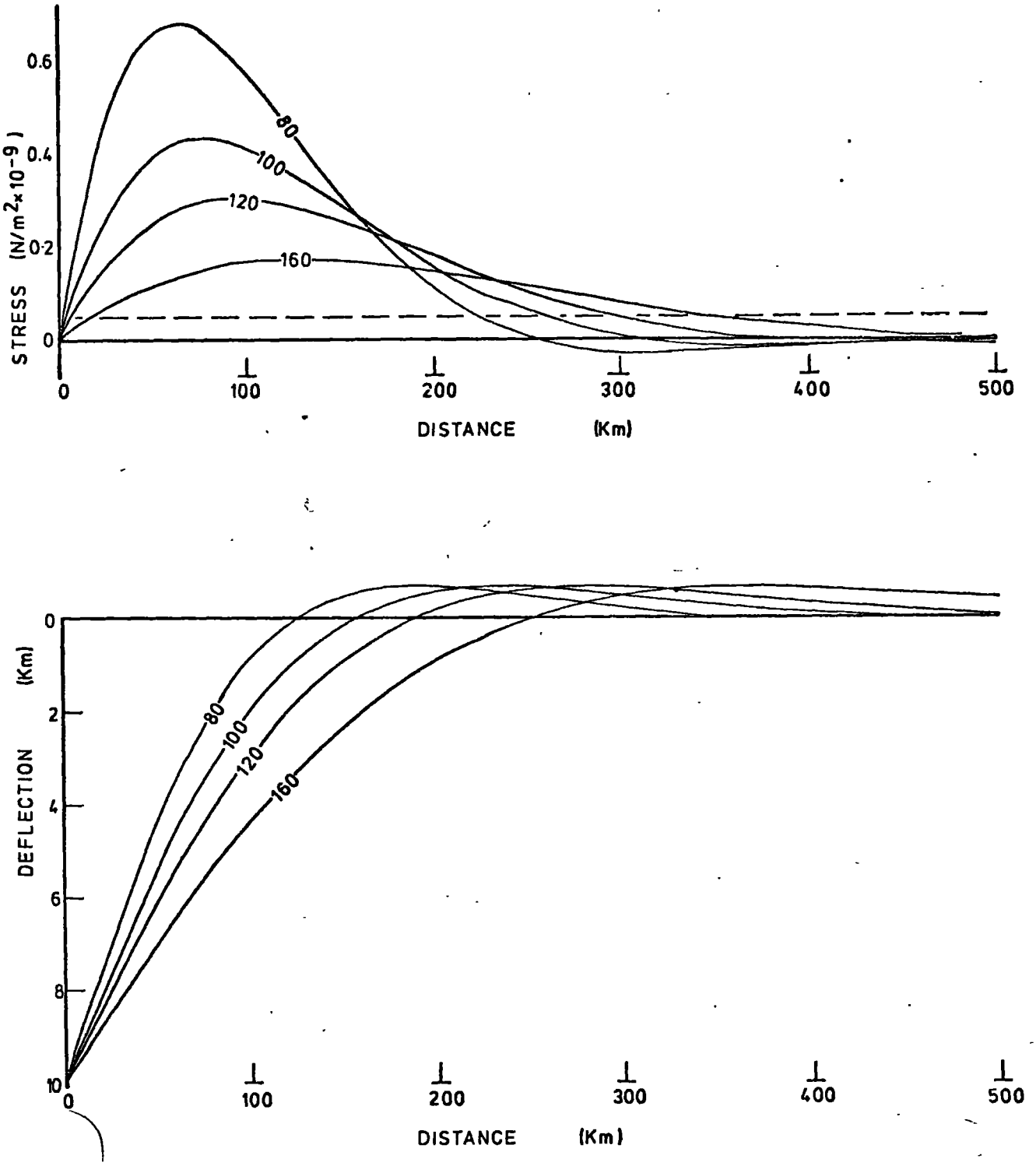

Fig. 5.2 The shape of the deformed plate for various flexural parameters and the stresses induced in the plate 13.5 km from the neutral fibre. If the tensile strength of the crust is 0.5 x 10^8 N/m^2 then failure would occur in the top of the crust at 220 to 350 km from the origin. This is near the top of the deflection for each flexural rigidity.

and various values of the flexural parameter, α .

The flexural rigidity, D, of the oceanic lithosphere has been estimated to be in the range 1.7 - 2.0 x 10^{23} N/m^2 by comparing the topography with computed curves of this type (Walcott, 1970; Hanks, 1971; Watts and Cochran, 1974; Watts et al., 1975). This is equivalent to a flexural parameter of 100-120 km and to an equivalent thickness of the lithosphere, T,

where $$T = \sqrt[4]{\frac{12(1-\nu^2)\,D}{E}}$$

of 27 to 50 km.

The stress due to the bending, σ_x , is given by

$$\sigma_x = -u E \frac{\partial^2 w}{\partial x^2}$$

where u is the distance from the centre of the plate (fig. 5.1). The stresses for u = 13.5 km for the various flexural parameters are also shown in fig. 5.2. These are computed using E = 1.0 x 10^{11} N/m^2 and are those which the theory would predict to occur at the surface of a 27 km thick lithosphere.

If the tensile strength of the oceanic crust is 0.5 x 10^8 N/m^2, then it will fracture near the top of the outer rise for all these models. This would then reduce the flexural rigidity and invalidate the analysis. The shape of the outer rise may be modelled by simple thin plate

theory but the bending stresses are strongly influenced by failure near the surface and creep near the base of the lithosphere. Variation of elastic properties within the lithosphere are also important.

5.2 Elastic bending of a transversely non-uniform plate

The differential equations relevant to the analysis of a transversely loaded beam in plane stress and to the cylindrical bending of thin plates (fig. 5.1) are

$$E I \frac{\partial^4 \omega}{\partial x^4} = q(x) \qquad 5.4$$

and

$$\frac{1}{1-\nu^2} E I' \frac{\partial^4 \omega}{\partial x^4} = q(x) \qquad 5.5$$

respectively (Hausner and Vreeland, 1966).

where

ω is the displacement in the z direction

q is the externally applied transverse stress

ν is Poisson's ratio

I is the second moment of the cross-section of the beam

I' is the second moment of unit length of the plate ($T^3/12$)

and T is the thickness of the plate.

These equations differ simply by a factor of $1/(1-\upsilon^2)$. The theory of the bending of beams may, therefore, be used to determine the parameters related to the cylindrical bending of the lithosphere even if E and υ vary with depth.

The variation of properties with depth can be accounted for by the methods used for composite beams. The width of the beam, b, (fig. 5.3) is transformed to b'

by $b' = \frac{E}{E'} b$ (Hausner and Vreeland, 1966).

where E is the Young's modulus at the given depth and E' an arbitrary value of Young's modulus for the transformed beam.

If I_z' is the second moment of the transformed cross-section the differential equation becomes

$$\frac{E' I_z'}{1-\upsilon^2} \frac{\partial^4 \omega}{\partial x^4} = q ,$$

the Poisson's ratio, υ , being assumed constant.

The bending stress in the plate is given by

$$\sigma_x = -u' E \frac{\partial^2 \omega}{\partial x^2}$$

where u' is the distance from the centre of gravity (y_0') of the section of the transformed section (fig. 5.3).

Thus, if the properties of the lithosphere vary only with depth, the results of previous analyses may be used with the flexural rigidity, D, given by

$$D = \frac{1}{1-\upsilon^2} E I_z' .$$

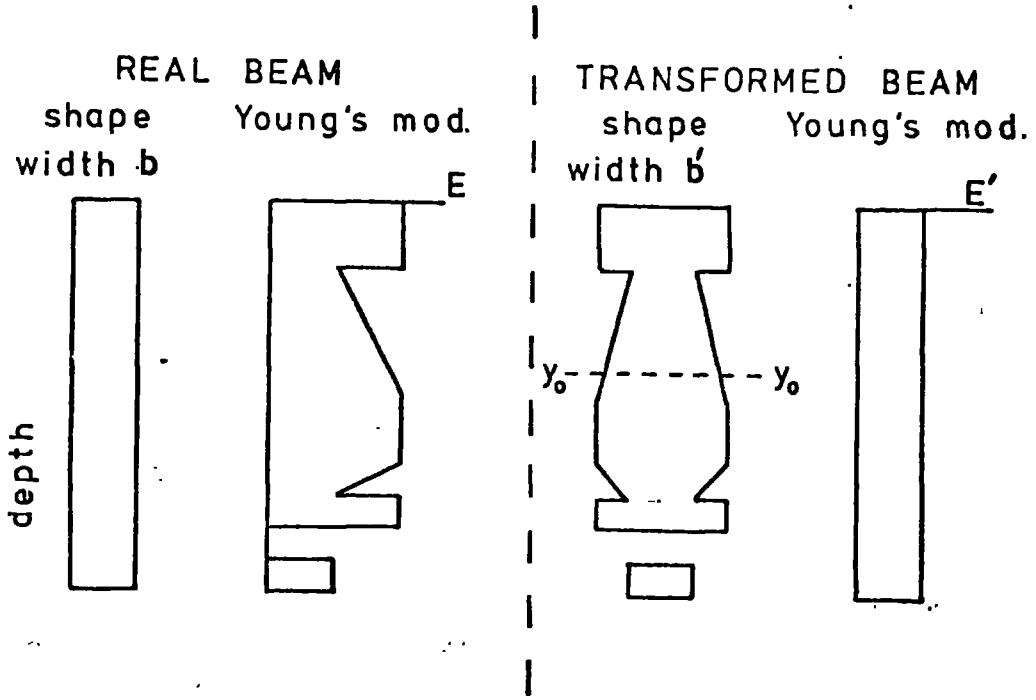

Fig. 5.3 Transformation of a beam of variable Young's modulus to an equivalent beam of variable cross-section. The neutral axis changes in the transformation.

Since this is an elastic analysis no allowance is made for creep in the lower lithosphere. This will reduce the "effective" flexural rigidity.

Using the elastic properties of the oceanic lithosphere determined in Chapter 2, the flexural rigidity was computed for various depths to the base of the lithosphere (fig. 5.4). These properties allow for the volume change as the stress changes in the phase transitions. This reduces the Young's modulus in these regions by an order of magnitude. The flexural rigidity for a uniform Young's modulus of 1.0×10^{11} N/m^2 is also shown for comparison.

Using equation 5.3, the maximum curvature $\frac{\partial^2 \omega}{\partial x^2}_{max}$ of the plate is given by

$$\frac{\partial^2 \omega}{\partial x^2}_{max} = \frac{2A}{\alpha^2} e^{-\frac{\pi}{\sqrt{2}}} \sin \frac{\pi}{\sqrt{2}} \qquad 5.6$$

This maximum curvature occurs 80-100 km from the origin but stresses much greater than the tensile strength of the crust and upper mantle occur near the top of the outer rise (fig. 5.2). The tensional fracturing of the rock dissipates the stress stored in it and also reduces its Young's modulus under tension. Hence the flexural parameter of the lithosphere should change as the depth of fracture increases with increasing curvature. The maximum curvature given by equation 5.6 was used to determine the maximum depth of the fracture assuming various thicknesses for the

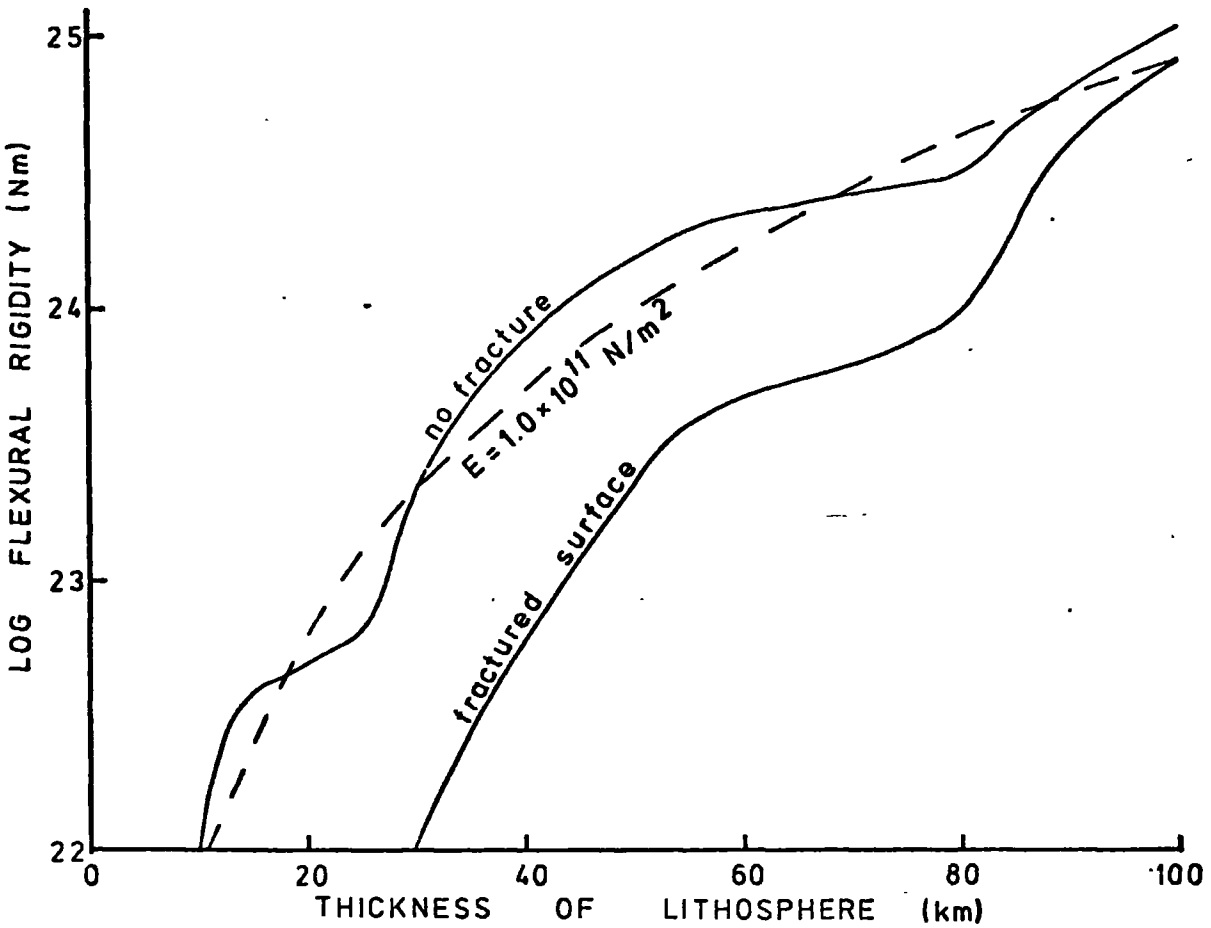

Fig. 5.4 Flexural rigidity as a function of various thicknesses of the lithosphere. The elastic parameters used are given in Chapter 2 and include decreasing the Young's modulus in the region of phase transitions. The flexural rigidity for a uniform Young's modulus of 1.0×10^{11} N/m^2 is shown for comparison. If the top of the lithosphere is fractured then the flexural rigidity is lowered.

lithosphere. The fractured portion was then assigned a zero Young's modulus and the apparent flexural rigidity (fig. 5.4), flexural parameter and depth to the centre of gravity of the transformed beam (fig. 5.5) were computed.

The maximum depth of fracture was 15 km and coincided with the top of the plagioclase-spinel phase transition. At this depth the effective Young's modulus and hence the computed stresses are reduced by an order of magnitude by the ability of the rock to change phase. The plagioclase-spinel phase transition stabilizes the depth of the fracture not only for various assumed thicknesses of the lithosphere but also for the curvature required for maximum fracture due to bending to occur.

The flexural parameter of 100-120 km estimated from the shape of the outer rise and the flexure around seamounts is equivalent to a lithospheric thickness of 65 to 85 km if the upper 15 km of the lithosphere is fractured. The substantial increase in flexural rigidity on increasing the thickness of the lithosphere from 80 to 100 km is due to the decrease in the amount of fracture and the bottom of the spinel-garnet transition being reached. However, at these depths the viscosity is decreasing and will effectively off-set the increase in flexural rigidity computed for an elastic model.

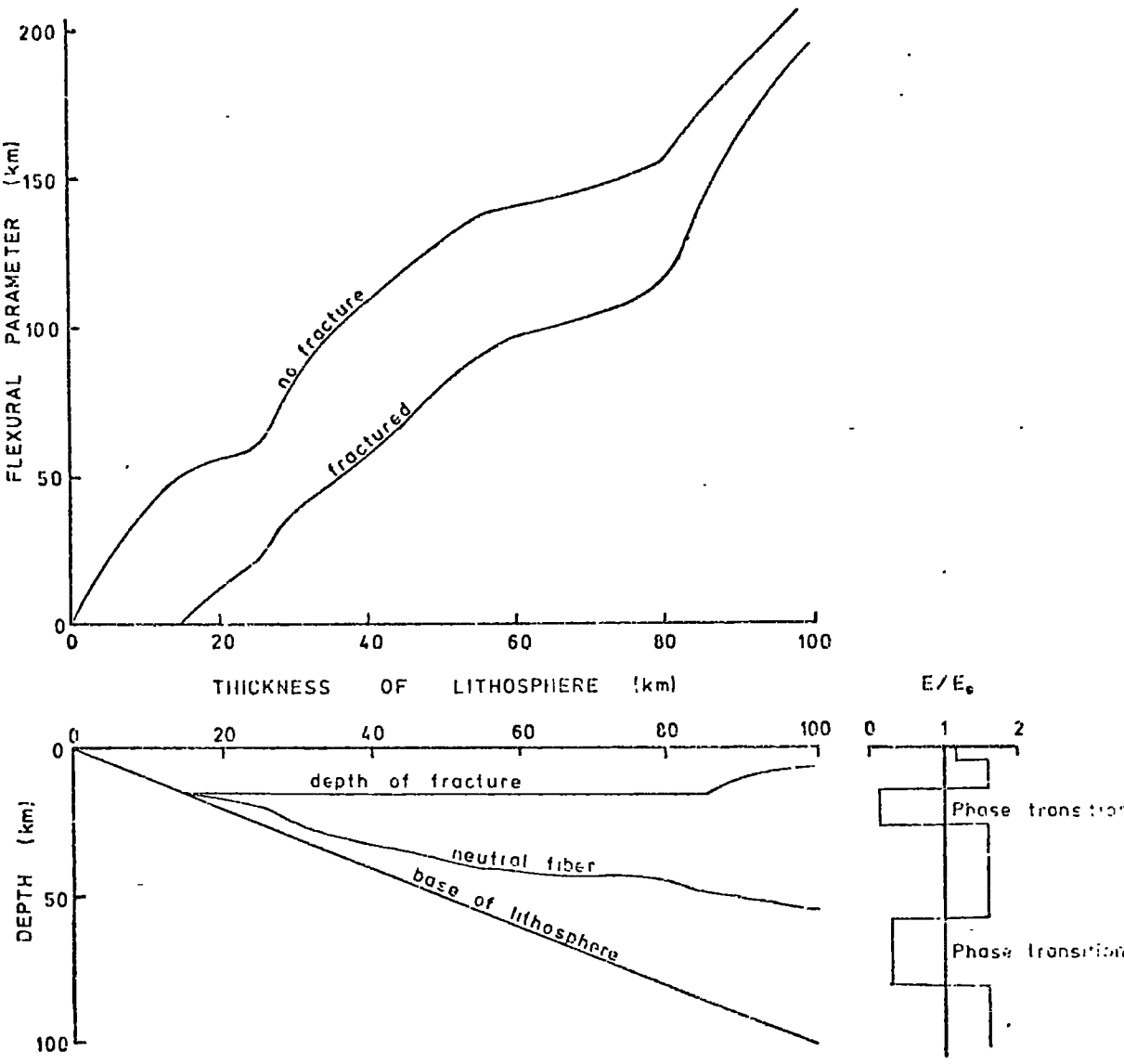

Fig. 5.5 Flexural parameter as a function of lithosphere thickness assuming the maximum curvature in fig. 5.2. The depth of fracture, neutral fibre and flexural parameter relative to the fractured lithosphere is also shown.

Failure of the top 15 km of the lithosphere may reduce the flexural parameter in the vicinity of subduction zones by 40 km but this can hardly be the case for the less extreme flexures calculated for oceanic islands (Walcott, 1970; Watts and Cochran, 1974; Watts et al., 1975). Viscous flow may be important to shallower depths in these regions because the times involved are much greater than the 5 M yr during which the lithosphere is in the region of the outer rise and trench (Walcott, 1970). These smaller flexures are caused by locally increasing the vertical load on the lithosphere so that transverse compression may be important if the stability of some of the phases are affected. This additional compressive effect is neglected in the theory. The mass of the sea-mount is assumed to cause a bending moment on the lithosphere and thus a flexure. The pressure is also increased below the sea-mount, however, and so compression takes place depending on the magnitude of the load and bulk modulus of the lithosphere. If phase changes can take place this compression may become significant so that the flexure of the sea-bed is increased and thus the estimate of flexural rigidity obtained from such studies is decreased.

5.3 Stress distribution for a given visco-elastic flow

It is possible to compute the flexure of a visco-elastic

plate in a similar manner to that of an elastic plate (e.g. Walcott, 1970). The behaviour of the oceanic lithosphere in the vicinity of a subduction zone, however, is different from that of a simply loaded plate in that the flexure moves along the lithosphere at the rate of subduction. The stress at any point (x_0 , u) in the plate is therefore dependent not only on the strain at that point but also on the strain at points outside it ($x \geq x_0$, u).

Iterative finite difference methods may be developed to allow for this progression of the flexure and stresses. These entail varying the effective flexural rigidity along the plate depending upon the current stress and strain in each cross-section. This, however, is far beyond the limits of the assumptions made in classical beam theory and the analysis is better carried out by finite element methods. Even so, it will be shown in the next chapter (section 6.4) that the results are very dependent upon the assumed boundary conditions. If the shape of the deformation is assumed then the stress distribution may be estimated along the plate to show the effect of creep and failure. This is only an order of magnitude calculation since the assumptions are recognised to be an over-simplification of the process.

It is assumed (1) that the strain is simply due to

the bending of the plate, (2) that if failure occurs the bending stress is reduced to zero and (3) that the stress distant from the trench is zero. The analysis is only approximate, the main errors arising from the neglect of the effect of failure on the adjacent rock and of slippage parallel to the plate similar to that which occurs when a pack of cards is bent.

Two different assumptions were made as to the effect of failure on Young's modulus. The first (Type 1) assumed that Young's modulus was unchanged by failure and the other (Type 2) that rock which had fractured could not sustain tension. Its Young's modulus in tension was set equal to zero.

The strain is assumed to be simply due to the bending of the plate so that the change in strain between two sections, $n-1$ and n, Δx apart (fig. 5.6) is given by

$$\Delta\epsilon(y) = (y - y_n^\circ)\,\omega_n'' - (y - y_{n-1}^\circ)\,\omega_{n-1}''$$

where ω'' is the curvature of the plate

y is the depth from the top of the plate

and y_0 is the depth of the neutral axis.

If the plate is moving around the flexure with a velocity $V_x = -\Delta x/\Delta T$ then the stress in section n is

$$\sigma_n(y) = E(y)\;\Delta\epsilon(y)\;\frac{\tau}{\Delta T}\left(1 - e^{-\frac{\Delta T}{\tau}}\right) + \sigma_{n-1}(y)\,e^{-\frac{\Delta T}{\tau}}$$

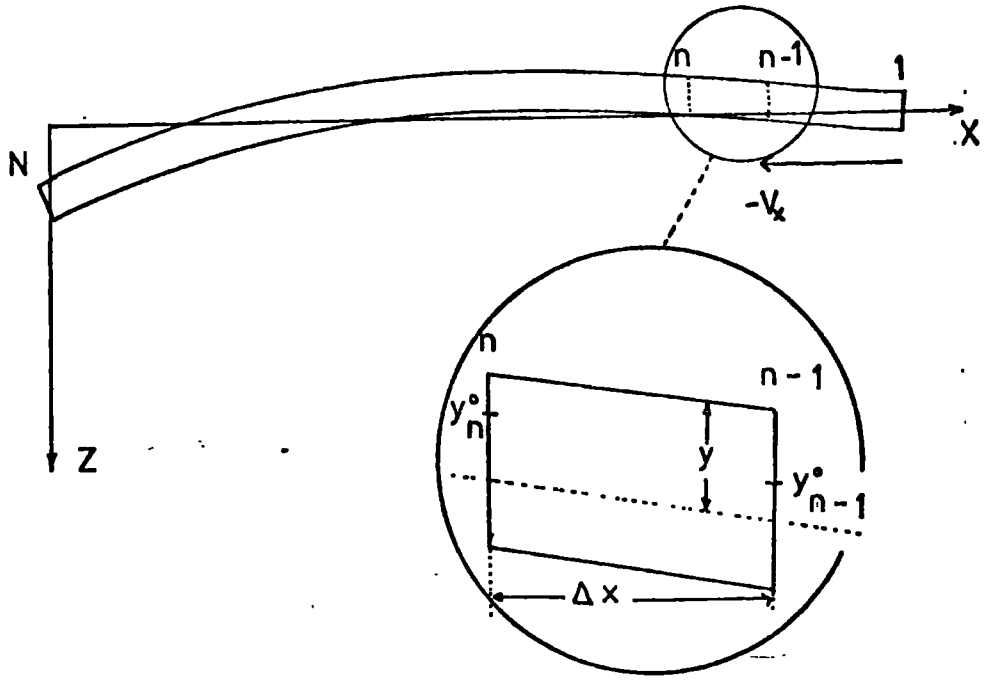

Fig. 5.6 Geometry for calculating the stress in a predetermined progression of a bend in a plate.

where E is the Young's modulus, $\tau = \mu/E$, and μ is the viscosity.

$\sigma'(y)$ may be specified for given discrete depths or fibres in the plate. This stress must be added to the hydrostatic pressure for depth, y, before applying the fracture criteria (section 2.1.6). The fracture criteria used assumed zero pore fluid pressure and so gave an upper limit to the stress required for fracture to occur. If fracture is computed to occur the stress is set equal to zero.

The location of the neutral fibre (y^o) for each section needs to be found by iteration. An effective Young's modulus, E*, is defined by

$$E^* = \sigma'/\epsilon$$

where σ' is the computed stress and ϵ is the strain computed from the curvature and the latest estimate of the position of the neutral fibre, y^o. E* is then used to compute a new transformed section as in section 5.2 and a new centre of gravity or neutral fibre.

The results of applying this analysis to a 100 km thick plate, with viscosity and Young's modulus dependent only upon depth is shown in fig. 5.7. The assumed deflections, w, were again given by equation 5.3 with A = 10 km and α = 100 km giving a typical shape for the outer rise (Le Pichon et al., 1973). The velocity was assumed to be

8 cm/yr. The distance interval (Δx) between sections was 5 km and the stresses and strains were calculated for depth intervals of 0.5 km through the plate. Zero stress was assumed at 500 km from the free edge of the plate.

In fig. 5.7 the stress distributions at various distances from the trench are shown for combinations of elastic and visco-elastic analyses with and without fracture. Compressional stresses are shaded and those above 2.5×10^9 N/m^2 (25 kbar) are not drawn.

In the elastic analysis with no fracture the stresses are dependent only upon the curvature, or relative strain, the distance from the neutral axis and the Young's modulus. The stresses are large and vary rapidly as the flexure is approached to above 25 kbar over most of the thickness of the lithosphere. At 0 km the curvature is zero and so the stresses are dissipated as the plate is re-straightened. In all sections the reduction of stress due to the lowering of Young's modulus by phase changes is evident.

If fracture occurs in the upper part of the plate the large tensions are reduced as the strain increases. Both methods of modelling failure were used. In type 1, if fracture occurred then the stress was set equal to zero but could immediately begin to increase again as the rock was further strained. In type 2,the fracture was assumed to also prevent the rock from sustaining tensional stresses.

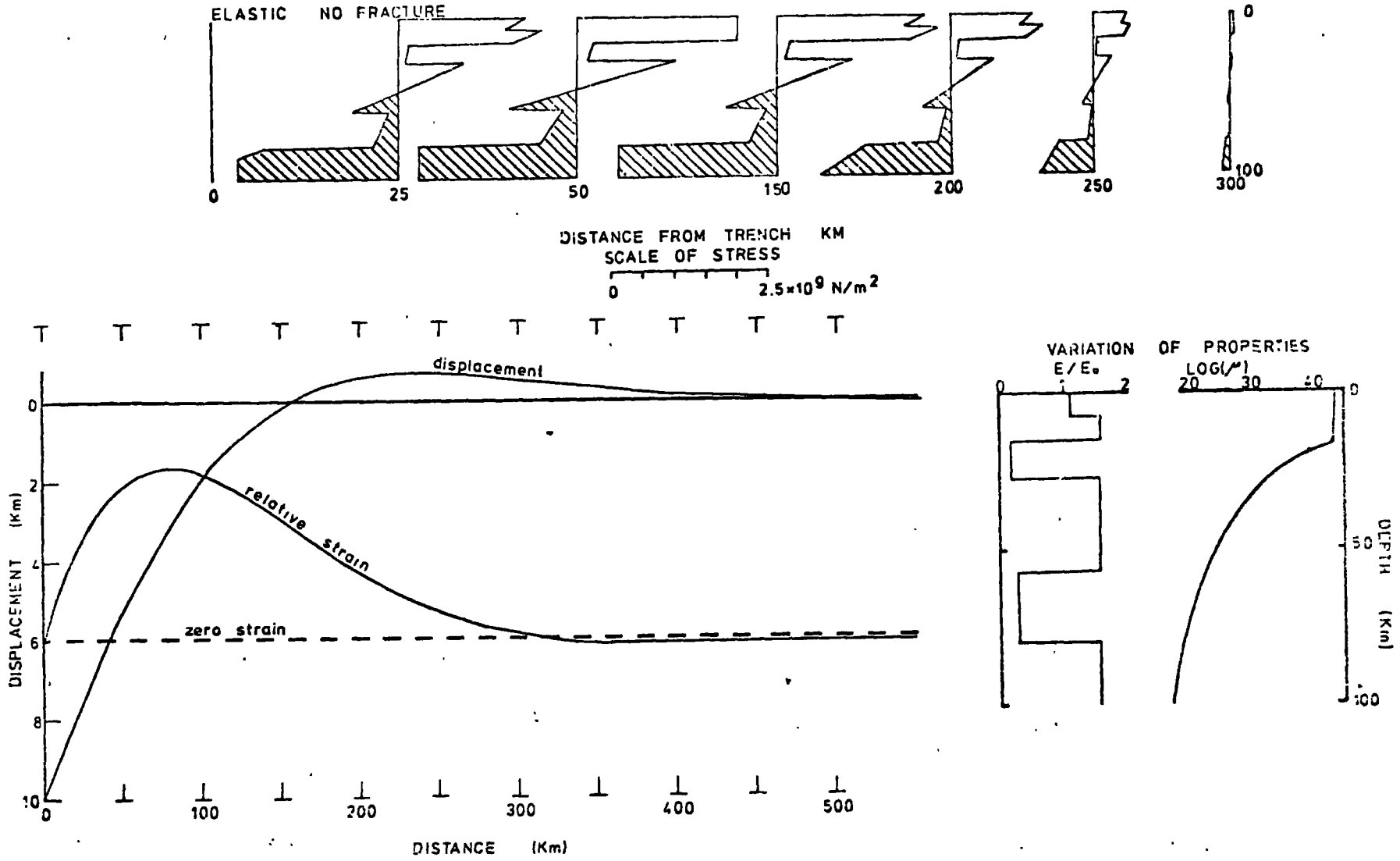

Fig. 5.7 Stress distribution due to bending in a plate moving around a predetermined curve. The plate is 100 km thick with Young's modulus and viscosity as shown. Two schemes were used to allow for fracture (see text). Compressive stresses are shaded and stresses greater than 2.5×10^9 N/m^2 not plotted. In the elastic model with type 2 fracture the plate was fractured throughout at 25 km from the trench and so the stresses at 0 km are probably in error.

As the overall strain decreases between 75 - 0 km compressional stresses are established in the top of the plate. The spiked nature of the stresses in the upper part of the plate for fracture type 1 are due to the gradual build up of stresses until they are suddenly relieved by fracture. At 25 km for fracture of type 2 the plate was fractured throughout so that the stresses at distance 0 km are probably in great error. The stresses in the lower part of the plate are reduced from the model with no fracture because the neutral fibre is lowered by the reduction of the stresses near the top of the plate.

The visco-elastic analysis with no fracture shows that the major effect of the creep is in the lower 40 km of the plate. No stresses are established below 60 km. The stresses in the top 60 km differ from those in the elastic-no fracture model because the neutral fibre is raised by the smallness of the effective Young's modulus in the lower part of the plate. The plate is effectively thinned by the creep.

The visco-elastic models with fracture shows how both stress relief mechanisms may complement each other to reduce the stresses throughout the plate. The largest stresses are at 0 and 25 km where the tensional stresses relieved by failure have been replaced by compressional stresses which need to be greater in magnitude for failure to occur.

It must be re-emphasised that this analysis is an over-simplification of the processes involved in the flexure in the vicinity of subduction zones but the effects shown are probably of the correct order of magnitude, though if the rocks contain significant amounts of fluids the stresses at which fracture will occur will be of much lower magnitude.

5.4 Conclusions

These models are all over-simplifications since it is recognised that thin plate theory cannot be applied to this tectonic process because the limitations assumed in the theory are not met. They do illustrate several points, and probably give results of the correct order of magnitude.

Phase transitions play an important role in the flexure of the lithosphere because they lower the effective Young's modulus. They alter the flexural rigidity of the lithosphere for any assumed thickness to about that of a uniform plate with Young's modulus of 1.0×10^{11} N/m^2. The Young's modulus of the mantle is about 1.5×10^{11} N/m^2. As far as thin plate theory can be applied to the outer rise and trench the flexural rigidity and flexural parameter are strongly affected by failure in the top of the lithosphere. If simple flexure was occurring in this region, the maximum depth at which failure would be induced by the bending

stresses would be 15 km. This corresponds to the top of the plagioclase-spinel phase transition.

The progression of the bend along the lithosphere as it is subducted has the effect of inducing opposite stresses as the plate is re-straightened, to any which have been dissipated by creep or failure. Hence, although the simple flexure theory would predict no residual stress once the lithosphere had completed passing around the bend, there is a large compressive stress near the base of the trench as a result of the previous tensional fracture between the outer rise and the trench.

The results of these calculations indicates that creep does effectively reduce the thickness of the lithosphere. The viscosities used may have been too low by as much as two orders of magnitude but this would have had little effect on the results. Only the mantle below the bottom of the spinel to garnet transition (80 km) needs to creep significantly to reduce the flexural parameters and stresses to those predicted here.

Although in the past, the theory of thin plates has been used to successfully model the shape of the outer rise, the significance of the model is obscure. The lithosphere does not act as a thin plate and the analysis is invalidated by the highly variable properties, fracture and creep. The stresses are not simply related to the curvature of the plate.

The large horizontal compressive stresses proposed for some subduction zones (Hanks, 1971; Watts and Talwani, 1974) could be a function of the analysis rather than the state of stress in the earth. The major assumption made in the previous analyses that has not yet been emphasised is that there is no moment acting on the free edge of the plate. Since the lithospheric plate continues down the subduction zone this assumption is unlikely to apply. The profiles which apparently require large horizontal compressive stresses could simply be ones in which the sinking slab is causing a larger bending moment at the assumed origin.

CHAPTER 6

FINITE ELEMENT ANALYSIS OF THE STRESSES IN THE SUBDUCTING PLATE

The two main difficulties in applying finite element analysis to the subducting plate are the reduction of the problem to one which can be solved with the computer resources available and the specification of the boundary conditions.

Previous applications of finite element analyses to this problem have treated the whole subduction zone and used rather coarse nets and predetermined temperature distributions to solve for the equilibrium stresses (Toksöz et al. 1973, Neugebaur and Breitmayer, 1975). The finite difference grid used by Sleep (1975) was also rather coarse (25 km^2 grid). All these analyses have shown that, although the stresses in the asthenosphere are small, the viscosity of the asthenosphere is important in providing support for the slab.

An attempt to analyse the whole region with a net fine enough to show the stresses due to the bending of the lithosphere and to phase changes, would result in the computer resources required making the problem unsolvable. In the previous chapter it was shown that the low viscosity below 60 km reduces the stresses by at least two orders of

magnitude for the bending of the lithosphere. It was therefore decided to try to model only the top 70 km of the lithosphere as it is subducted. It was planned to start with lithosphere in its equilibrium state and to progressively allow it to bend and sink into the asthenosphere. The boundary conditions are critical to the analysis and three separate sets of conditions have been used. Each model required several hours of computing time. None have been really successful but the computing requirements made it impossible to attempt further models. In spite of the limitations of these models, some interesting conclusions may be made about the stresses in the bending and descending lithosphere.

The physical properties used in the analyses were determined at the start of each time step from the expressions given in Chapter 2. Because of the assumption of zero pore fluid pressure the failure criteria in section 2.1.6 required that the ratio of the maximum to minimum principal stresses should be about 7:1 for failure to occur if all the cracks were closed. An additional failure criteria that the deviatoric stresses do not exceed 1.0×10^9 N/m^2 was also included. This is arbitrary but the reduced maximum differential stress may be considered as being due to the presence of pore fluids.

The viscosity of an element was reduced by a factor

of about 150 for each successive time step for which failure was estimated to occur. If the stress in an element which had previously failed was such that no further failure would occur the viscosity was increased by the same factor until it reached that computed from the creep laws. This gradual change in viscosity was necessary to reduce instabilities in the analyses due to large fluctuations in the viscosities and stresses.

Also to reduce the likelihood of instabilities in the solution, the viscosity was assumed to be greater than 5.0×10^{21} Ns/m^2 throughout the model. This is rather high compared to the values given for the asthenosphere but it gives a decay time for the stresses of about 30 yrs. The time steps used were between 50 and 12,500 yrs.

6.1 First Model

The first model began as a flat lying lithospheric plate 70 km thick with the end curved through 45° (fig. 6.1). The top of the model was assumed to be under 5 km of water. The top 7 km was assumed to be oceanic crust and the rest mantle with properties determined from Chapter 2. The initial temperature and pressure in the elements corresponded to the geotherm determined in section 2.3.

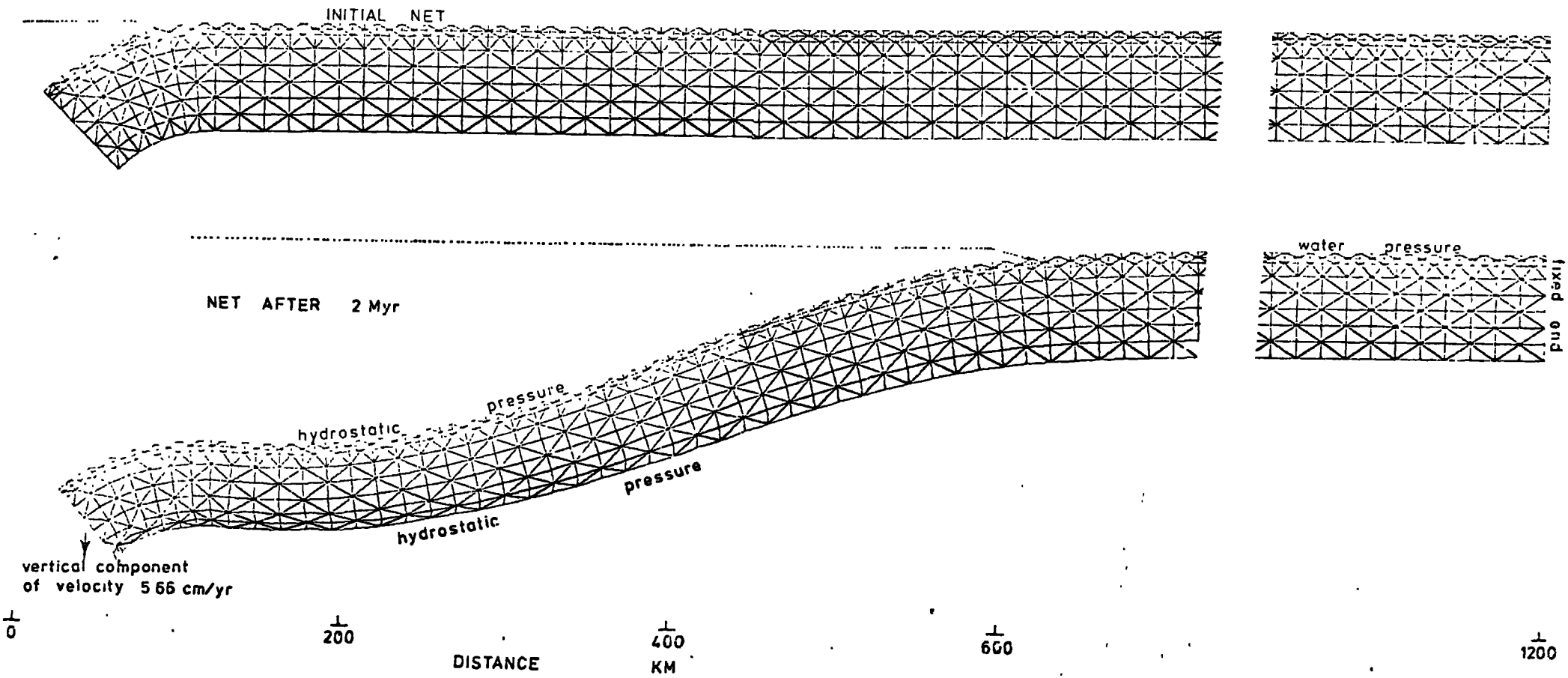

Fig. 6.1 Finite element net used for the first model of the subduction of the lithosphere. The initial net and the net after 2 M yr. subduction are shown. The top two rows of elements were given physical properties relevant to oceanic crust, the rest of the model was mantle.

6.1.1 Boundary conditions

The boundary conditions applied to the model (fig. 6.1) were:

(1) The base was subjected to hydrostatic stresses calculated for the normal oceanic lithosphere and asthenosphere (section 2.3).

(2) The end that was curved by 45^{o} from the vertical was forced to move downward with a vertical velocity component of 5.66 cm/yr corresponding to a subduction rate of 8 cm/yr for a dip of the descending slab of 45^{o}.

(3) As part of the top of the model became lower than 8 km, the hydrostatic pressure on it due to the sea was gradually increased so that it equalled the hydrostatic pressure of the normal oceanic section when the top became deeper than 11 km. That is the pressure, P, on the top of the model at depth X km was given by

$$P = f\,P_w + (1 - f)\,P_L$$

where P_w is the pressure due to the water $(1.00 \times 10^7 X)$

P_L is the pressure in the oceanic section

$$\text{and } f = \begin{cases} 1 & X \leqslant 8 \text{ km} \\ (11 - X)/3 & 8 < x < 11 \text{ km} \\ 0 & X > 11 \text{ km} \end{cases}$$

(4) The end of the lithosphere distant from the subduction zone was held on a vertical line. The displacements and velocities determined in the analysis were therefore relative to the oceanic plate.

The initial finite element net and boundary conditions and the net after 2 M yr. subduction are shown in Fig. 6.1.

The thermal boundary conditions were more difficult to ascribe. The sea-floor was held at $0^{o}C$. The heat flux which would normally be passing through the lower surface due to thermal conduction in a steady state oceanic environment was incorporated (section 2.3). There remained two major problems. Firstly, only part of the earth is being modelled and the thermal interaction between this part of the earth and its surroundings is important. Secondly, what should be done about the contentious shear strain heating on the upper surface of the lithosphere as it is subducted (Minear and Toksöz, 1970a and b; Griggs, 1972). The final choice built both these effects into a convenient though arbitrary addition to the heat flux across the top and bottom surfaces of the model deeper than 8 km. This heat flux was calculated according to the formula

$$q = k(T-To)/D$$

where k is an assumed thermal conductivity of 3.0 $J/ms^{o}C$, T is the temperature of the surfaces of the subducted slab, To is the

expected temperature at the same depth in the adjacent undisturbed mantle. (given by the conductive geotherm in Fig. 2.8) and D is an arbitrary distance over which it is assumed that the temperature gradient is constant. D was given a value of 3 km for the top surface and 30 km for the lower surface. The larger value for the lower surface was intended to compensate, in part, for the lithosphere below 70 km which is probably also subducted.

Using this formula had two advantages. The temperature in the descending lithospheric slab does not rise above that in the surrounding asthenosphere as it does in the model of Minear and Toksöz (1970). The shear zone is probably only about 3 km wide so the heating given by this arbitrary expression is probably of the right order of magnitude.

No heat flux was allowed across the ends of the model. The end being subducted was intended to represent a truncation of the subducted slab and the heat flow along the slab is much smaller than that across it (Griggs, 1972). This is different from the finite difference analyses of the thermal regimes of Minear and Toksöz (1970) and Toksöz et al. (1971, 1973) who considered the end of the slab to be in contact with the asthenosphere.

The heat sources incorporated in the model were, (1) the heat flux across the boundaries described above, (2)

adiabatic heating and (3) radiogenic heating. The latent heat was incorporated by appropriate modifications to the physical properties (section 2.2.3). Heating due to creep within the model was not incorporated in this first model.

6.1.2 The Analysis

The model was stepped through time with the nodes being shifted after each increment. The physical properties were calculated for each time step depending on the stress and temperature of the elements at the start of the step. Visco-elastic and thermal analyses were alternated. The changes in stress due to the temperature change during each iso-volumetric thermal analysis were added at the end of each step (section 3.4). The time-steps for this model varied from 50 to 5,000 yr.

6.1.3 Results

The results after 1 M yr and 2 M yr are shown in fig. 6.2. It can be seen that the choice of boundary conditions for the curved end of the model was unfortunate. The part of the model which was initially curved (Fig. 6.1) did not straighten but pulled the rest of the model down with an induced bending moment. The sag in the plate between

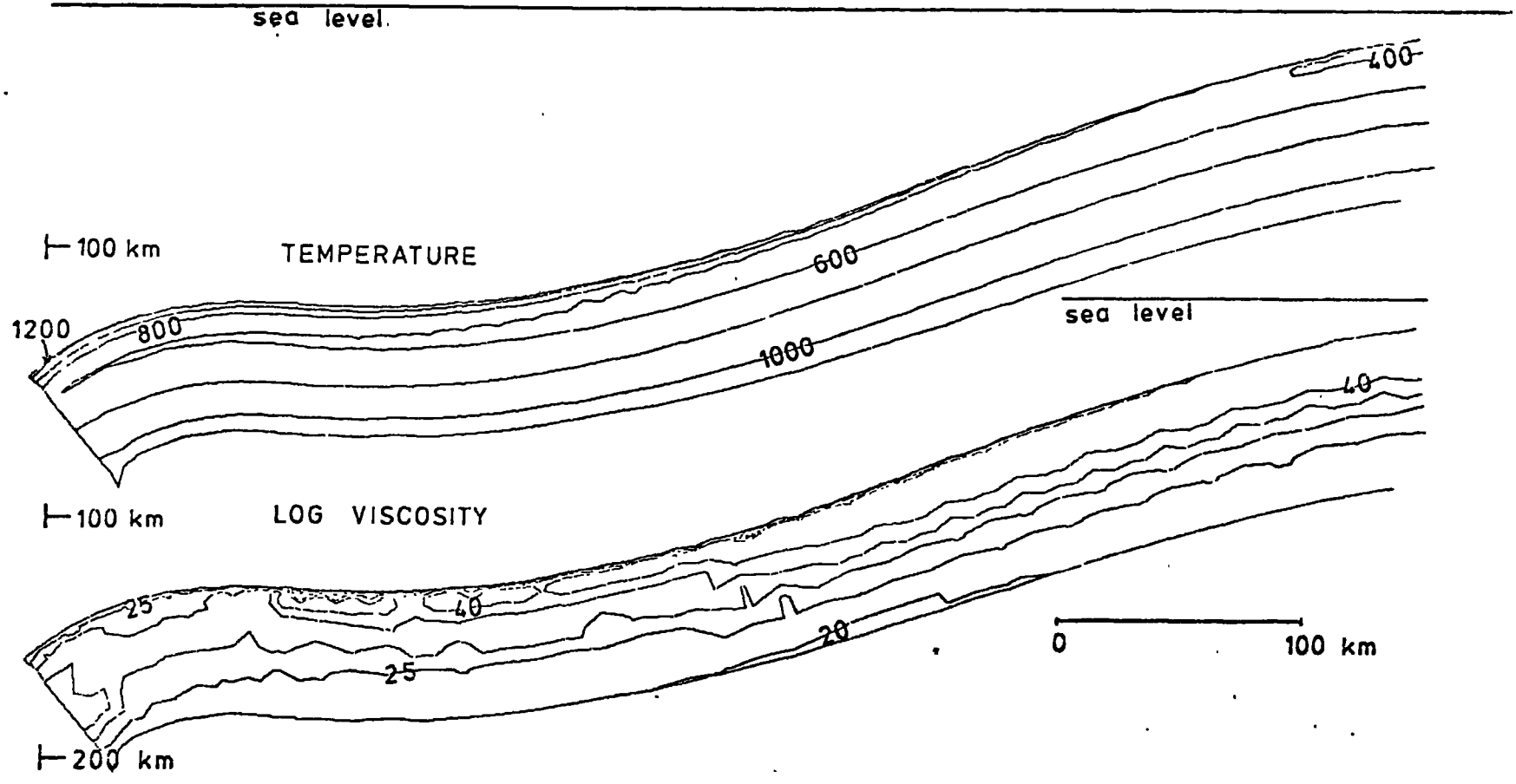

Fig. 6.2 Results of first model: Stresses, and areas of phase transition, after 1 M yr. and 2 M yr. subduction and the temperature and viscosity distribution after 2 M yr. The bend between ab was becoming more pronounced so the analysis was terminated. Note stresses due to this distortion of the subducted plate. The downward pull of the slab is transmitted to the un-subducted lithosphere.

a and b (Fig. 6.2) is caused by this bending moment and the low viscous resistance that the asthenosphere exerts on the sinking slab being neglected because of the hydrostatic stress boundary conditions.

In spite of these limitations the model is useful in illustrating some points. The model shows that (1) large stresses are induced in the slab wherever it is bent, (2) one of the principal stresses is nearly always parallel to the sides of the slab, and (3) down-dip tensional stresses may be transmitted into the lithosphere under the ocean basins but are concentrated at depths where spinel peridotite is the stable phase (30-50 km). In the surface layers (the plagioclase peridotite field and the oceanic crust), tensional stresses tend to be dissipated by failure and at depths corresponding to phase changes the bulk modulus is smaller thus reducing the stresses. In the vicinity of the trench and outer rise in this model the tensional stresses induced by the downward pull of the slab reduce the compressional stresses which would exist due to the flexure of the lithosphere. This again emphasises the danger of assuming simple flexure in this region (Chapter 5).

By the time the oceanic crust is subducted to about 100 km its temperature has increased to 500 to 600^{o}C (Fig. 6.2B). By the time it has reached 150 km its temperature is about 900^{o}C near the melting temperature of wet basalt (Fig. 2.7).

The viscosity which depends on the ratio of temperature and melting temperature is also reduced in the crust at these depths (Fig. 6.2B).

Because the sagging of the slab between a and b in Fig. 6.2 was becoming more pronounced as the analysis proceeded, this model was abandoned and a model with different boundary conditions attempted.

6.2 Second Model

The boundary conditions for the second model were similar to the first apart from three major changes. The model was initially flat without the initial curve of Fig. 6.1. The end of the lithosphere distant from the induced subduction was moved at a constant speed of 8 cm/yr towards the subduction zone (Fig. 6.3). The subduction process was induced into the model by forcing the lower corner node (a in Fig. 6.3) to move at 60^{o} to the horizontal. As other basal nodes passed the distance 0 km they were forced to move towards the previous basal node (Fig. 6.3). This criterion was introduced to minimize the sagging that occurred in the previous model. The rest of the base of the model was again supported by hydrostatic stresses.

The time steps for the model were 12,500 yrs which gave increments of 1 km to the end of the model being pushed.

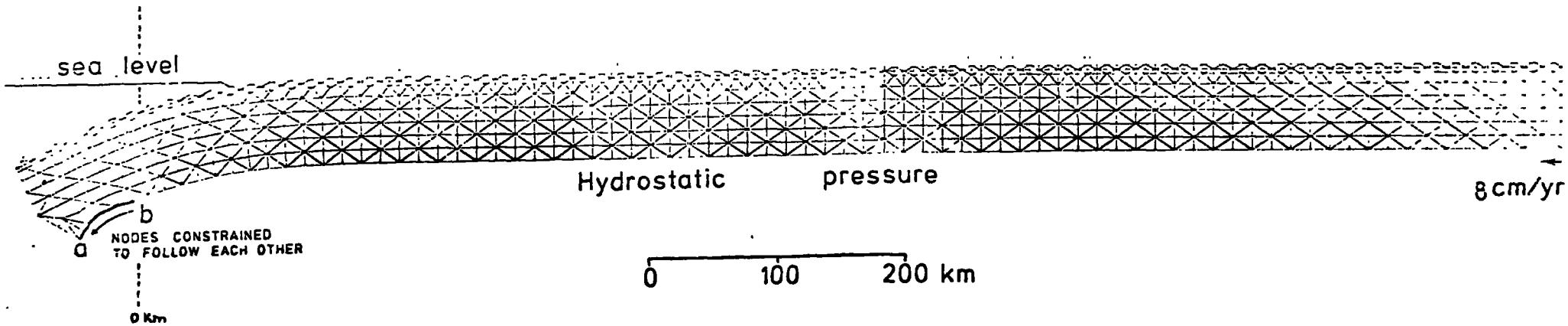

Fig. 6.3 Finite element net in second and third model after 1 M yr. subduction. The nodes between a and b were constrained to move towards the next adjacent one. Node a was forced to move at 60° to the horizontal.

This is a reasonable upper limit to the time step that could be taken without causing instabilities in the model.

The thermal analysis was similar to the first model but heating due to creep within the model was also incorporated.

The stresses in this model became more compressive as the analysis proceeded until after 2 M yr the stresses were large enough for a state of phase change, and correspondingly reduced bulk modulus, to exist throughout most of the model. There are two possible causes for this failure of the model. Both are again functions of the boundary condition.

The first is a result of the hydrostatic pressure applied to the end of the model being subducted. This pressure was assumed to be equal to that on the top and bottom of the lithosphere for the given depth. This was a reasonable choice at the time of the analysis because the stress in the descending slab was shown by Isacks and Molnar (1971) to have either the least or greatest principal stress aligned down-dip in the slab (Fig. 1.2). A neutral, no stress, condition appeared to be a reasonable first approximation. However, it is shown in Chapter 7 that the stress in the top of the slab must be tensional down-dip to maintain the observed gravity anomaly. The density inhomogeneities which give rise to the gravity anomaly

were incorporated in the model by applying the full lithospheric pressure only after the top of the slab had reached 11 km depth. Hence, there should have been a downward pull on the end of the lithosphere and an inconsistency was built into the boundary conditions.

The second possible cause for the failure of the model after 2 M yr was the application of the boundary condition in which some of the basal nodes were forced to follow each other down the subduction zone (Fig. 6.3). This was equivalent to applying pressure on the boundary. The horizontal component of this implied pressure was compressional towards the non-subducted lithosphere. This was not only effectively compressing the lithosphere but was also applying a bending moment to it.

The results of the analysis at 1 M yr and 2 M yr (Figs. 6.4 and 6.5) show that these effects were significant in inhibiting the subduction of the plate so that it became more dense rather than sink into the asthenosphere. The stress in the lithosphere outside the vicinity of the subduction zone gradually became more compressive. At 2 M yr the stresses had increased sufficiently so that phase change conditions, and hence a reduced bulk modulus, existed throughout most of the model.

Most of the displacement forced on the end distant from the subduction was dissipated by the compression of the non-

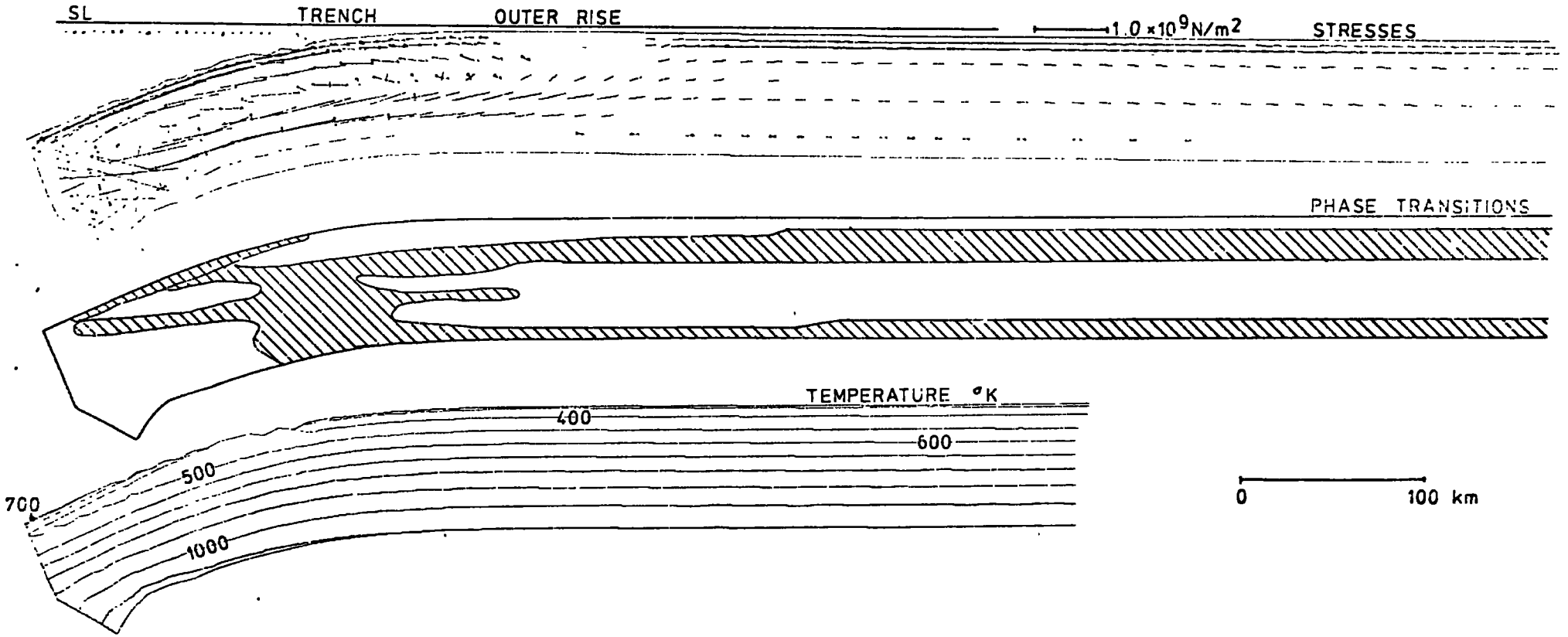

Fig. 6.4 Results of second model. Stresses, area of phase transition and temperatures at 1 M yr. The stresses near the end being subducted show the end being pulled towards the lower constrained boundary. Compressional stresses in the un-subducted lithosphere are about 1.0×10^8 N/m^2.

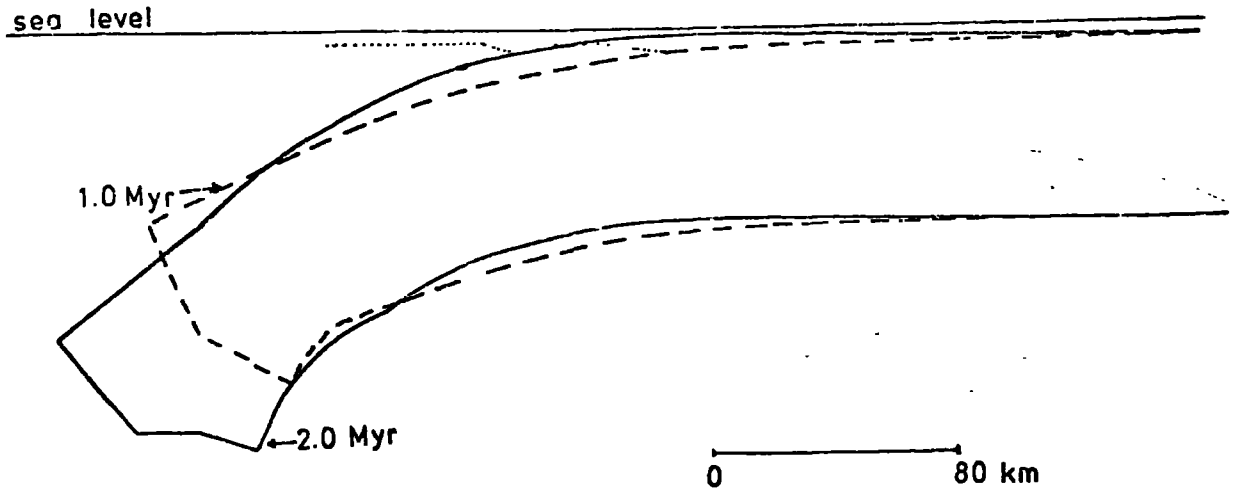

Fig. 6.5 Second model. The outline of the second model after 1 M yr. and 2 M yr. subduction. Although the end distant from that shown moved by 80 km this end only moved by about 25 km. The outer rise became more pronounced.

subducted plate. Between 1 M yr and 2 M yr although the end of the model distant from the subduction zone was forced to move 80 km the other end of the model only sank into the asthenosphere by an average of about 25 km (Fig. 6.5). The model was thus abandoned.

This model does emphasise two things. Firstly, the results are very dependent upon the boundary conditions used and simplifications may cause errors because some major effect may be ignored. Secondly, the pull of the lithospheric slab is important in controlling the subduction process.

6.3 Third Model

The conditions and net of the previous model at 1 M yr were used as the initial conditions for this model. Two changes were made in the analysis from 1 M yr to 2 M yr. The cooler convective geotherm (sections 2.3) was used and the hydrostatic pressure applied on the end of the model being subducted was reduced by 2.0×10^8 N/m^2. This is equivalent to applying a tensional pull of this magnitude to the end and is about the size of the stresses estimated to be in the upper part of the slab to maintain the gravity anomaly (Chapter 7).

This model again became unstable at 2 M yr. The reduced

pressure on the end had had the effect of reducing the stresses in the lithosphere but they were still significantly compressive.

At 2 M yr the restriction on the basal nodes which were being forced to follow each other (ab in Fig. 6.6) was lifted. Hydrostatic boundary conditions were then applied to all the base of the model. As a result of this the compressive stresses in the lithosphere were relaxed. Although there was variation of stress through the lithosphere the equilibrium equations and the hydrostatic boundary conditions now ensured that the mean stress in any section was about zero.

The effect of this relaxation on the shape of the model is shown in Fig. 6.6. The stress on the end of the model being subducted was further reduced to 4.0×10^8 N/m^2 below the ambient pressure and an elastic analysis performed starting from the previous conditions. The resulting shape of the sinking slab is also shown in Fig. 6.6.

The visco-elastic analysis was continued. The boundary conditions applied were now similar to model 1 (section 6.1) but instead of forcing the end to sink with a given vertical velocity the reduced pressure on the end of the model was used to induce the subduction process. The rest of the boundary was assumed to experience hydrostatic pressure calculated for an oceanic environment. The rate of descent

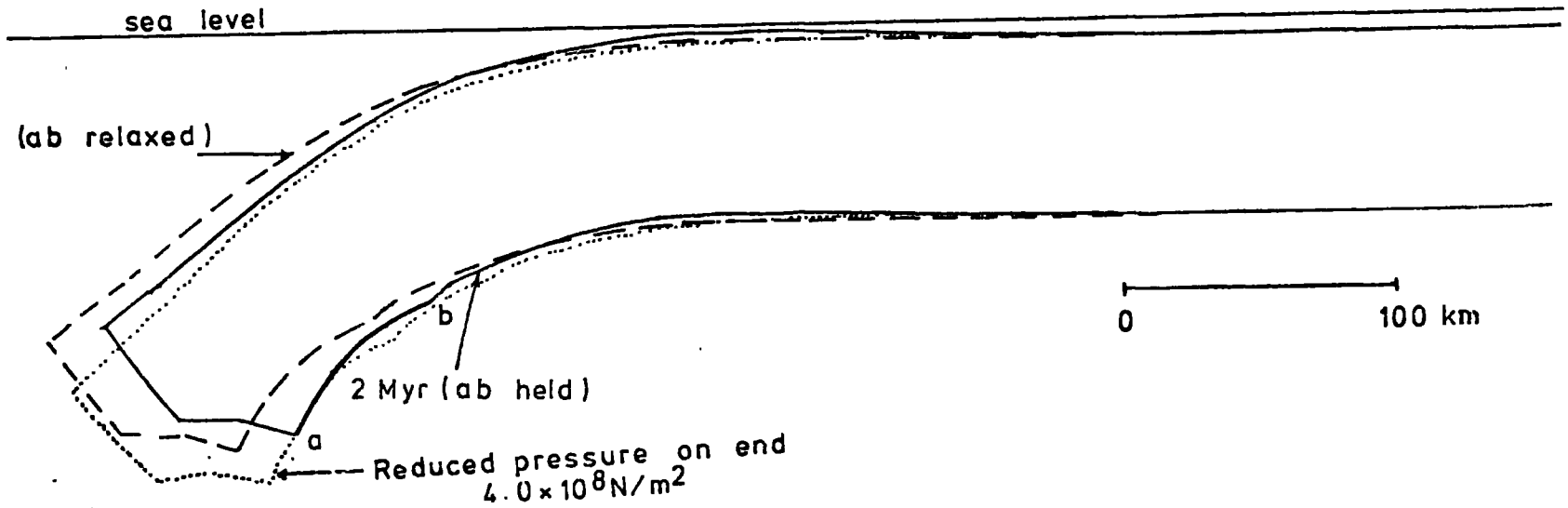

Fig. 6.6 Third model. The solid line shows the outline of the model at 2 M yr. The nodes between ab were forced to follow each other (solid line). Dashed line shows the elastic response to releasing this restriction while maintaining the 2×10^8 N/m^2 stress on the end. Dotted outline is the result of the elastic response of increasing the downward pull on the end of the lithosphere to 4.0×10^8 N/m^2.

of the subducted plate under these conditions was far too high (about 1 m/yr). Time steps of 1000 and 2500 years were used. The high rate of descent resulted in the viscous relaxations of stresses during descent not being fully incorporated. The temperatures in the centre of the slab were too low for a given depth because of the high thermal time constant for the problem.

The stresses, phase transition, temperature and viscosity distributions in the model when it reached to a depth of 240 km under these conditions is shown in Fig. 6.7.

The high rate of descent of the slab was probably caused by the lack of viscous drag on the model. Since the boundaries were assumed to be under hydrostatic pressure it was implied that they were held by a non-viscous fluid. Even the relatively low viscosity of the asthenosphere would have a marked effect on the dynamics of the plate (Neugebaur and Breitmeyer, 1975). Hence the model was insufficiently well specified for the analysis to continue.

The final conditions do emphasise some points. In this model the bending of the lithosphere occurs not only in the vicinity of the outer-rise but also down into the subducted part of the plate. Phase changes affect the stresses here by allowing some of the lithosphere to deform more readily than other parts. The stresses in the oceanic crust as it is transformed to eclogite are large and no consistent trends

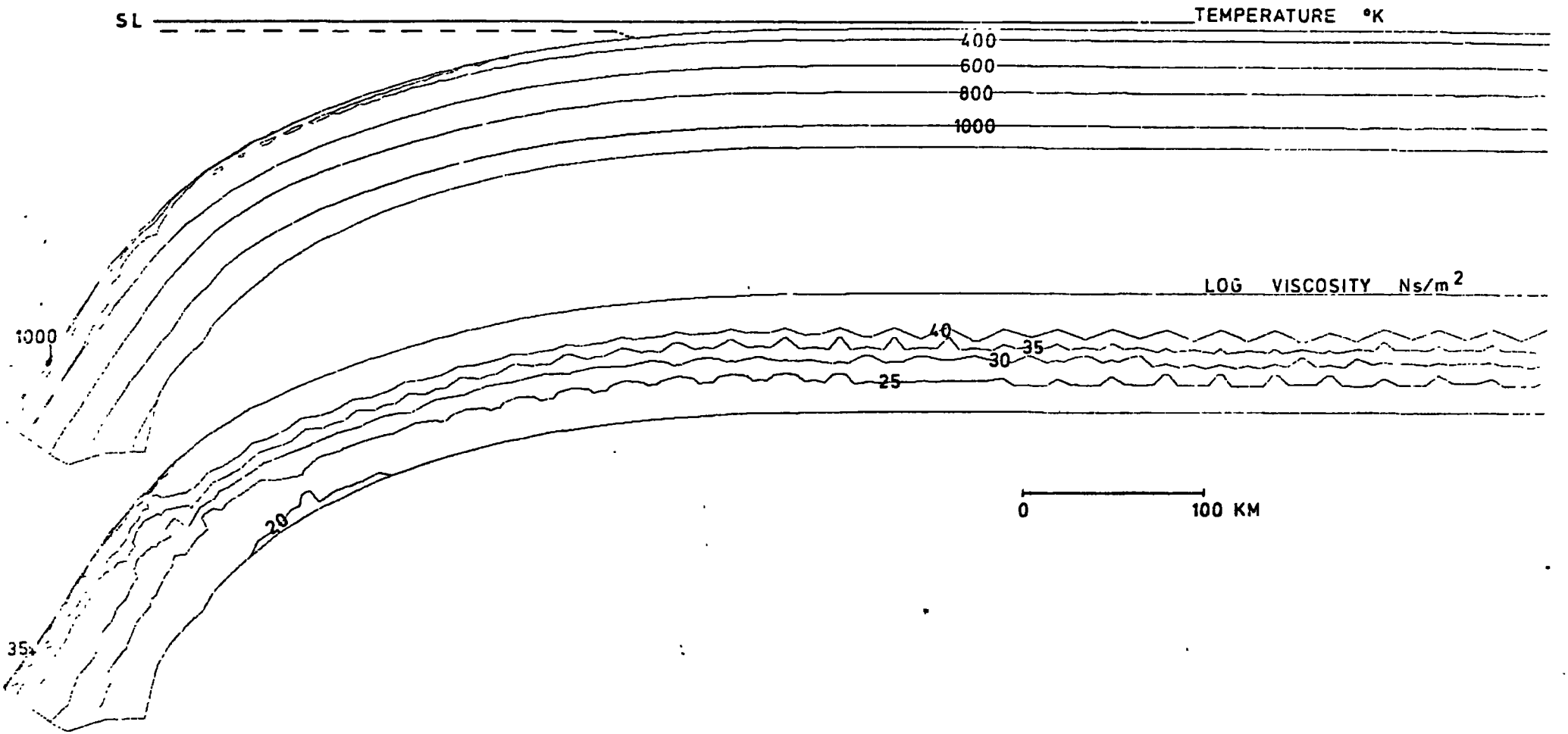

Fig. 6.7 Third model. Stresses, area of phase transition, temperature and viscosity of the third model at 2.1 M yr. The rate of subduction had been too large (about 1 m/yr) so the temperatures are too low and viscosities too great in the subducted slab. The stresses in the subducted crust are large and incoherent because of the inadequacy of the net in describing the gabbro-eclogite phase transition.

can be seen. Isolated elements changed phase and caused large local stresses which in turn indicated failure. This reduced the viscosity of the elements. The net is not fine enough to give the structure of this phase change and the apparently random stresses are probably a function of this net coarseness. The viscosities shown in fig. 6.7 are those computed before adjustment for fracture.

Because of the high rate of descent of the slab the temperatures are too low and viscosities too high. The lowering of the viscosity of the oceanic crust as it is heated is evident.

6.4 The shape of the outer rise

The flexural deformation of the lithosphere before it is subducted has been discussed in Chapter 5. The shape of the outer rise has been shown to vary between subduction zones but it is commonly about 300 km wide and 700 m high (Le Pichon et al., 1973; Watts and Talwani, 1974). Fig. 6.8 shows various shapes of the top of these three models for various times in their analysis. This may be compared with that used in Chapter 5 as a typical curve (equations 5.3 with A = 10 km and α = 100 kms).

As shown by Watts and Talwani (1974) horizontal compression in the lithosphere causes the flexure in the

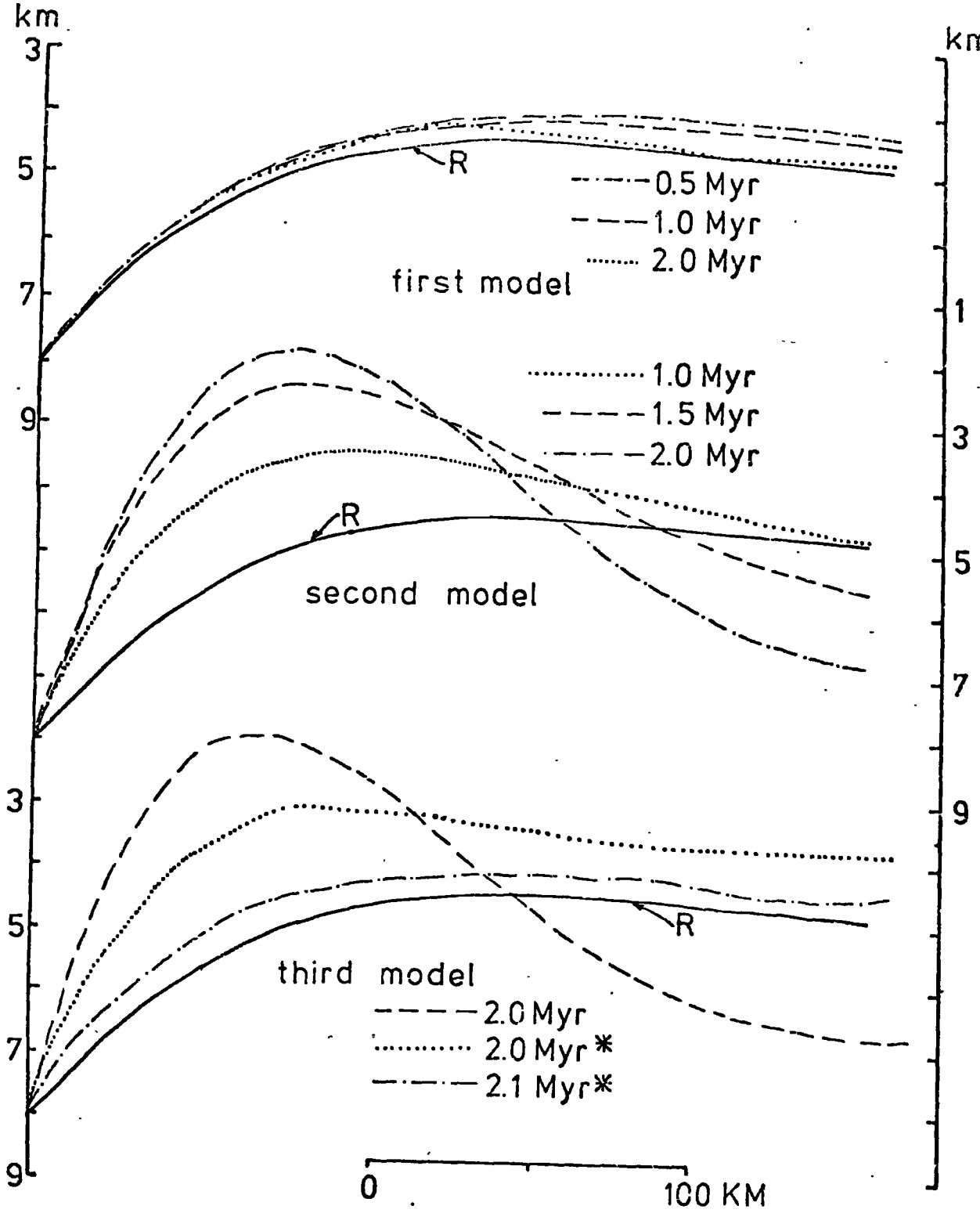

Fig. 6.8 Shape of outer-rise given for the various models. Reference curve R given by equation 5.3 and represents a typical observed topography (Le Pichon et al. 1973). The curves with boundary conditions which imply no net horizontal forces (first model and third model at 2.1 M yr*) are the only ones which approximate this shape. Curves marked with an asterisk in the third model are those for which the constraint on ab (fig. 6.6) is removed.

vicinity of the outer rise to become higher and of shorter wavelength. Only those models in which there is no horizontal constraint at the end being subducted (first model and third model at 2.1 M yr) approached the shape given by the above equation. The second model and third model at 2 M yr had flexures of 2-3 km, about three times that observed. The shape of the outer rise in a model is sensitive to the boundary conditions and together with the dynamics may provide a good check on future models as to how well the boundary conditions apply to the process.

In all the diagrams of stress in this chapter (Figs. 6.2, 6.4 and 6.7) the bending, shown by tension in the top and compression in the base of the slab, extends down the subduction zone and does not end at 10 km depth as assumed in the flexural analyses so there is a substantial bending moment on the slab, at this depth, which contributes to the flexure in the region of the outer rise.

Phase transitions do reduce the bending stresses in the vicinity of the outer rise but where the major bending takes place at 30-60 km down the subduction zone the stresses cause the area of phase change to increase. This results in the major bending occurring while the bulk modulus is reduced throughout the thickness of the lithosphere. The stresses are stabilized by the phase change.

6.5 Changes for Future Models

The choice of a finite element net and boundary conditions for a finite element visco-elastic and thermal model is difficult. It is not easy to see a priori what the effect of either one of these is until the analysis has begun or is near completion.

The effects of the choice of boundary conditions is illustrated in the three models presented here. At the time that the analyses were begun the boundary conditions seemed reasonable but as the analyses progressed the effects of the choice became evident. Eventually the dynamics and stresses were dominated by the arbitrary boundary conditions applied to the model.

Similarly the choice of the finite element net had its disadvantages. The oceanic crust was modelled by two rows of small elements (e.g. Fig. 6.1). These were 3-4 km thick. With time steps of 12,500 yrs for the visco-elastic analysis the end of the model distant from the induced subduction moved 1 km/time step and so instabilities were induced in the models. These instabilities were particularly noticed as the hydrostatic stress was applied to the top of the crust as it was subducted and as the crust changed phase from basalt-gabbro to eclogite. The effect of the oceanic crust on the stresses in the mantle seems small even in the

vicinity of the phase change but this may be due to the instabilities just described or to the inadequate description of a 7 km thick crust by the net. Hence the chosen net fell between the coarseness required for stability of the visco-elastic analysis and the fineness required to determine the detail of stress due to the junction of the crust and the mantle. This region should be studied in some detail since high stresses result from applying a uniform external pressure to a model with non-uniform properties.

These models have shown that the difficulty in allowing for the crust in modelling the subduction process as a whole makes its inclusion in the model unwarranted. By the time the crust has been subducted 50-100 km its viscosity has been reduced so that any stresses built up must decay rapidly.

The failure of the first and final models was due to the lack of viscous drag on the boundaries. This was predicted from the analyses of Toksöz et al. (1973) and Neugebaur and Breitmayer (1975) but the effect of the resistance must be greater than anticipated. Either a more extensive model with more constraint on the boundaries or a way of applying boundary conditions incorporating these resistive stresses needs to be developed for further models.

6.6 Conclusions and discussion

Finite element analysis of the visco-elastic flow and thermal regime in subduction zones has shown that the stresses

within the oceanic plate as it is subducted are mainly due to distortions and phase change. The gravitational body forces cause stresses of lower magnitude but they are more uniform and persistent in direction across the slab. The downward pull of the sinking slab can be transmitted to a horizontal tension in the oceanic lithosphere thus applying a force to contribute to the plate motions (e.g. fig. 6.2).

The oceanic crust is near its melting temperature at 100 - 150 km and so may rise to form the andesite volcanicity in the island arcs and contribute to the high heat flow. In these models it is assumed that the temperatures 3 km above the top of the descending slab are those in a uniform oceanic region. They may be maintained at this temperature by the upward movement of magma and shear strain heating in the shear zone. The heat supplied by shear strain in this region is probably minimal because of the low effective viscosity due to fracture and the probable high water content supplied from the oceanic crust which has failed in tension in the outer rise allowing water to percolate to depth.

The shape of the outer rise in the models varies depending on the boundary conditions. The largest causes for variation are compressive stresses in the oceanic lithosphere due to the boundary conditions and the bending moment imparted by the slab as it sinks into the asthenosphere. Increases in both of these cause an increase in the amplitude and

decrease in the width of the computed outer rise. The shape of the outer rise is probably one of the best checks on the applicability of the physical properties and boundary conditions used in modelling subduction zones.

Phase transitions play an important role in the bending of the lithosphere. The area of phase transition is extended by the bending stresses. Most of the bending occurs where the phase transitions extend nearly right through the lithosphere. This reduces the effective bulk modulus and flexural rigidity by an order of magnitude.

CHAPTER 7

STRESSES ASSOCIATED WITH THE NEGATIVE GRAVITY ANOMALY

One of the most consistent manifestations of subduction zones and island arcs is the large negative gravity anomaly (fig. 1.1). This is often associated with the inner-side of the trench but may be as much as 300 km in from the trench. Hatherton (1969) has shown that the negative isostatic anomalies are situated where the projection of the Benioff zone determined from intermediate depth earthquakes cuts the earth's surface.

The continuity of the negative isostatic anomalies along the subduction zones suggests that they are probably also persistent in time. This in turn implies that they must be maintained by tectonic forces, which are probably due to the geometry and the dynamics of the subduction process. They would otherwise decrease with time because of the isostatic restoring forces.

Gravity anomalies are a function of the density distribution within the earth. In the vicinity of subduction zones there are two major causes of positive gravity anomalies. Firstly, the positive anomaly over the outer rise can best be accounted for by flexure of the lithosphere (Watts and Talwani, 1974). Secondly, the lithospheric slab

as it sinks into the asthenosphere is cooler and hence more dense than its surroundings. This causes a broad positive gravity anomaly throughout the region of the subduction zone (Hatherton, 1969; Minear and Toksöz, 1970; Griggs, 1972; Watts and Talwani, 1974). The negative gravity anomaly considered here is superimposed on these positive anomalies so that only an approximate shape for it can be determined.

Two settings for the anomaly are studied. The first is in the North Island of New Zealand where the negative anomaly is over the continent and 250 to 300 km from the Hikurangi Trench (fig. 7.1). The second is a cross-section of the Tonga Trench where the free-air gravity anomaly is over the trench.

7.1 Negative gravity anomaly on a continent

Hatherton (1970) has given two interpretations of the negative anomaly over the North Island of New Zealand. One associates the mass deficiency with the shallow seismicity and the other associates it with a thickening of the continental crust. Fig. 7.1 gives a new interpretation of the gravity anomaly similar to the second of these but with the crustal thickening closely related to the top of the subducted plate. The continental and oceanic crust were

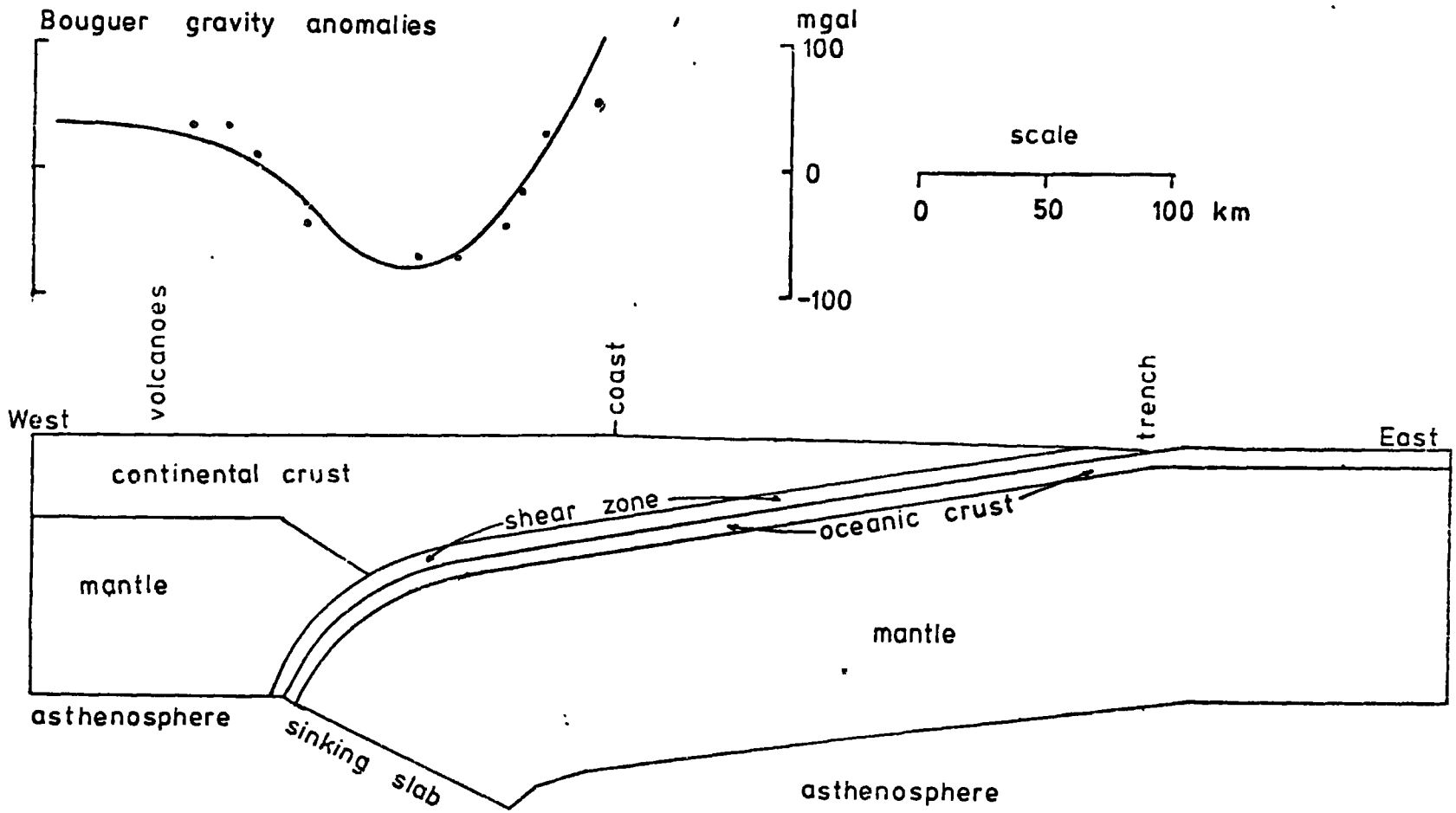

Fig. 7.1 Diagram of a section through the North Island, New Zealand showing the geological units used in the stress analysis. The Bouguer gravity anomalies taken from Reilly (1965) are modelled by a thickening of the continental crust. The shear zone joins the top of the Benioff zone of Hamilton and Gale (1968) and the Hikurangi Trench.

assumed to have densities of 2.7 and 2.9 Mg/m^3 respectively. The density of the mantle is assumed to be 3.3 Mg/m^3 for the gravity model. The upper surface of the subducted plate was estimated by joining the bottom of the trench to the top of the Benioff zone determined by Hamilton and Gale (1968). The base of the continental crust was chosen to be consistent with the gravity anomalies.

A finite element analysis of the stresses required to maintain these density inhomogeneities was performed. The properties used in the models were:-

	$\rho(Mg/m^3)$	$E(N/m^2)$	ν	$\mu(Ns/m^2)$
continental crust	2.7	0.5×10^{11}	0.25	0.5×10^{24}
oceanic crust	2.9	1.0×10^{11}	0.26	1.0×10^{30}
shear zone	2.7	0.5×10^{11}	0.25	0.5×10^{19}

The properties assigned to the mantle were determined from the expressions given in Chapter 2. The concentration of the relative motion between the two plates to the shear zone was modelled by the low viscosity in this region.

The finite element net used is shown in fig. 7.2. Initial stresses equal to the weight of overlying rock were applied and an elastic analysis performed. The relative motion between the plates was neglected. The boundary conditions for the elastic analysis assumed that the ends of the model were constrained to move only vertically. The part of the base of the model corresponding to the truncation

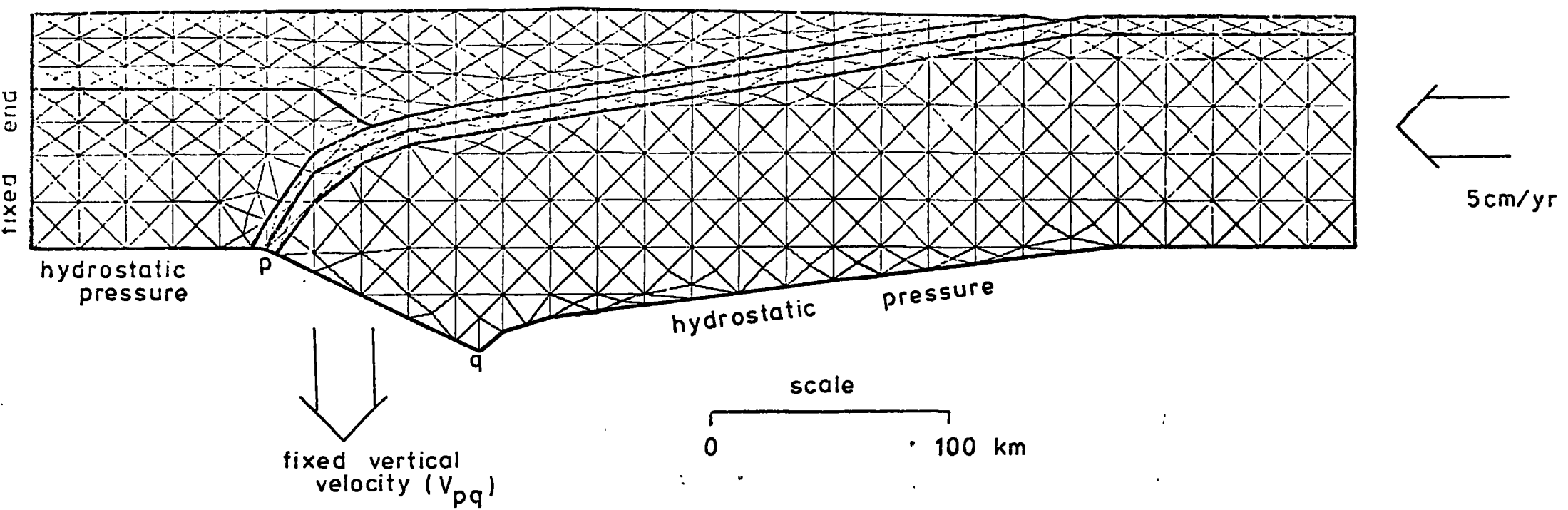

Fig. 7.2 Finite element net and boundary conditions used for studying the stresses in the vicinity of the North Island, New Zealand. The geological units are as shown in fig. 7.1.

of the subducted lithosphere (pq in fig. 7.2) was held at a fixed depth. The rest of the base was supported by a hydrostatic pressure equivalent to that expected under the oceanic plate.

The stress distribution due to an elastic analysis is shown in fig. 7.3. The stresses plotted in fig. 7.3A are the difference between the actual principal stresses and the hydrostatic stresses computed for the oceanic plate. Stresses less than 5.0×10^6 N/m^2 are not plotted. Nearly vertical tensional stresses are required in the descending slab to maintain the negative gravity anomaly. The stresses near the truncation of the descending slab (pq) are about 2.2×10^8 N/m^2. The tendency of the model to adjust isostatically is evident in the other stresses. The stresses in the under-riding plate are caused by a bending moment induced by the boundary condition on the end mn. (fig. 7.3). In the continental plate tensional stresses radiate out from the descending slab.

The state of stress in the continental crust is best considered in relation, not to stresses computed for the oceanic lithosphere, but to a hydrostatic stress distribution given by a uniform density of 2.7 Mg/m^3 (fig. 7.3B). Two different stress regimes are evident in the continental crust. Between the trench and the coast the stresses are horizontal and tensional with a maximum magnitude of about 1.0×10^8 N/m^2.

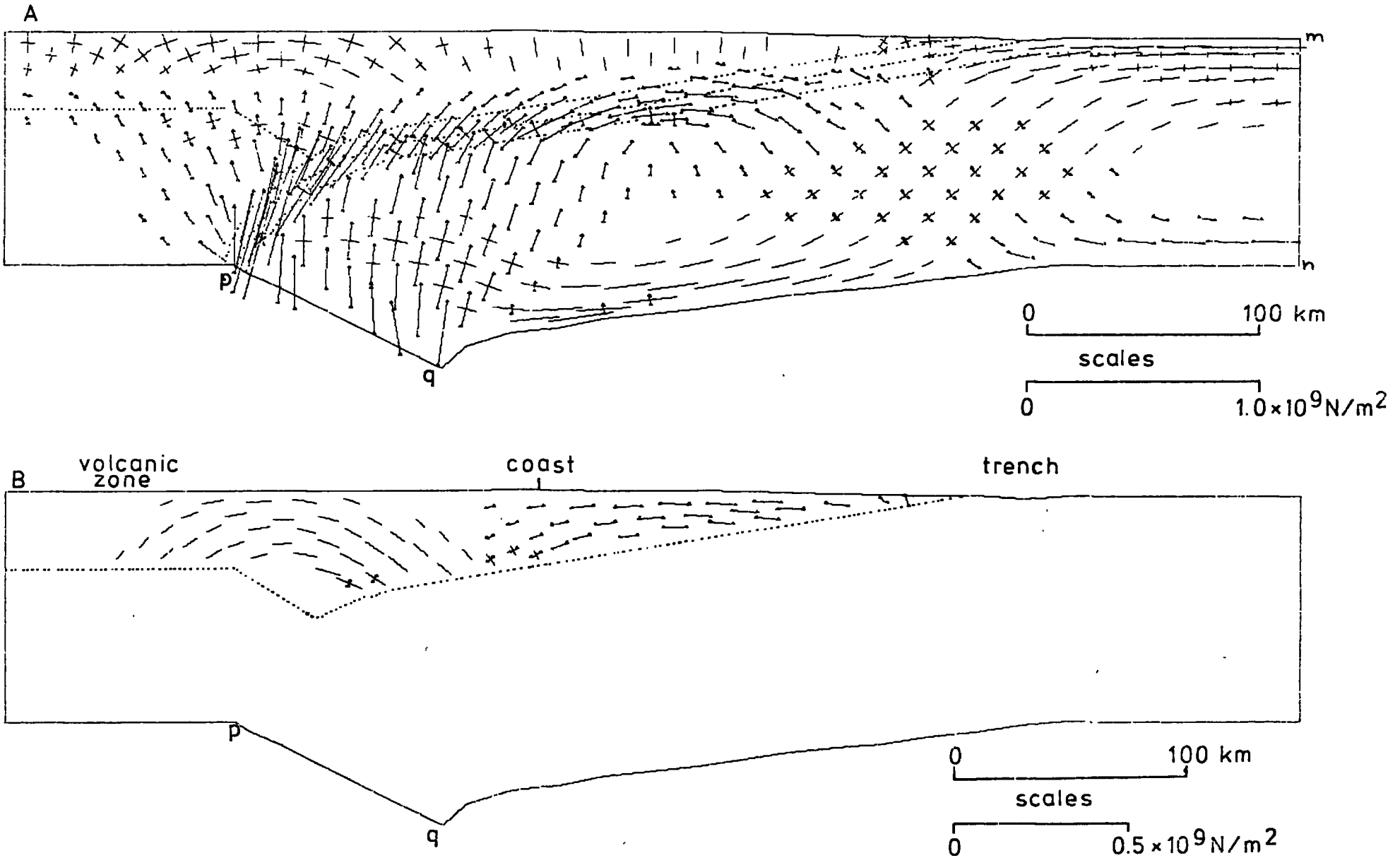
A
m
n
p
q
0
100 km
scales
0
1.0×10⁹N/m²
B
volcanic zone
coast
trench
p
q
0
100 km
scales
0
0.5×10⁹N/m²

In the vicinity of the gravity low the stresses in this elastic model are compressional with respect to the simple hydrostatic model and arch around the anomalously deep crust-mantle boundary.

A visco-elastic analysis with similar physical properties and boundary conditions was performed. This reduces the effect of the boundary conditions applied at the ends of the model. The time steps were 1000 yrs and the analysis was continued until the change in stress during one time step was less than 5.0×10^7 N/m^2 in all the elements. The resulting stress pattern is similar to that of the elastic model but the stresses in the continental crust were larger and horizontal (fig. 7.4). Those in the base of the lithosphere were much smaller because of the viscous relaxation.

These analyses suggest that the negative gravity anomaly is maintained by the tensional stresses in the descending slab and that as a result of the lateral density inhomogeneities horizontal tensions and compressions may be maintained within the lithosphere.

No account, however, has been taken of the motion of the plates. The ends of the model should be converging towards each other at a rate of about 5 cm/yr (Le Pichon et al., 1973). The vertical velocity of the part of the base of the model representing the truncation of the subducted slab

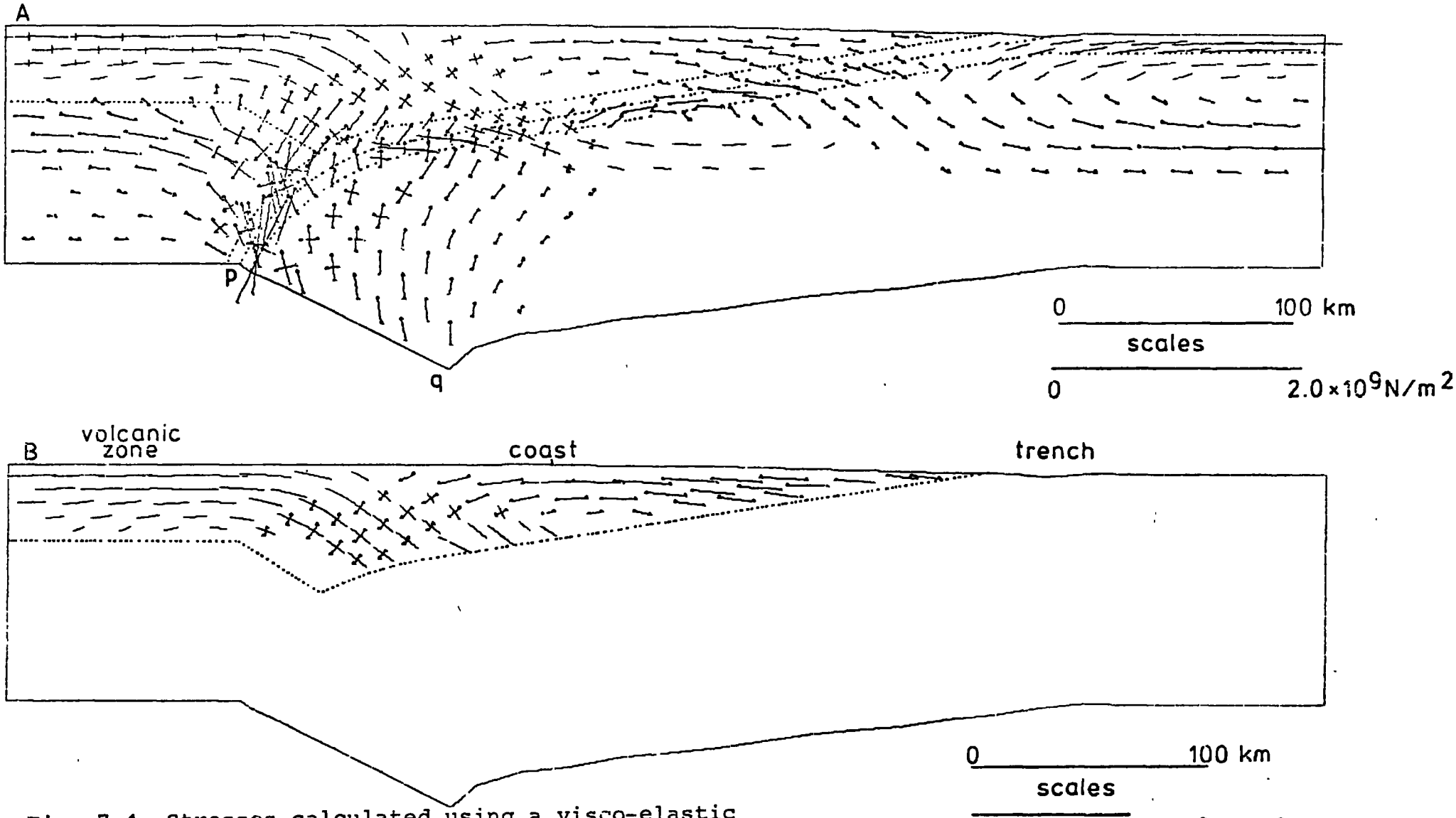

Fig. 7.4 Stresses calculated using a visco-elastic analysis of the model in Fig. 7.1. The ends are held stationary. Details as for fig. 7.3.

(pq in fig. 7.2) is not known. It is commonly assumed that the subducted plate is in steady state flow with respect to the overriding plate so that the shape of the boundary between the plates does not change and that the subducted plate simply follows itself around the bend. However, the Pacific Ocean is getting smaller and so the subduction zones on either side of it are approaching each other so this cannot be entirely correct.

Visco-elastic analyses were carried out with this part of the base of the model (pq in fig. 7.2) moving downward with vertical velocities, V_{pq} , of 2.5, 3.7 and 5.0 cm/yr. The stresses were adjusted between each time step but the nodes were not moved. Steady state conditions were not reached after 1 M yr. but the stress patterns were only changing slowly.

The stresses at 1.1 M yr. are shown in fig. 7.5. The largest stresses are in the subducted oceanic crust but this had been assigned a viscosity of 1.0×10^{30} Ns/m^2 and so was effectively acting as an elastic layer. Variations of V_{pq} have little effect on the computed stress pattern (fig. 7.5). Tensional stresses are present in the continental crust in the region of the volcanic zone and horizontal compressions near the surface between the negative gravity anomaly and the coast. These stresses are opposite to those computed in the previous models which neglected the relative motion of the plates.

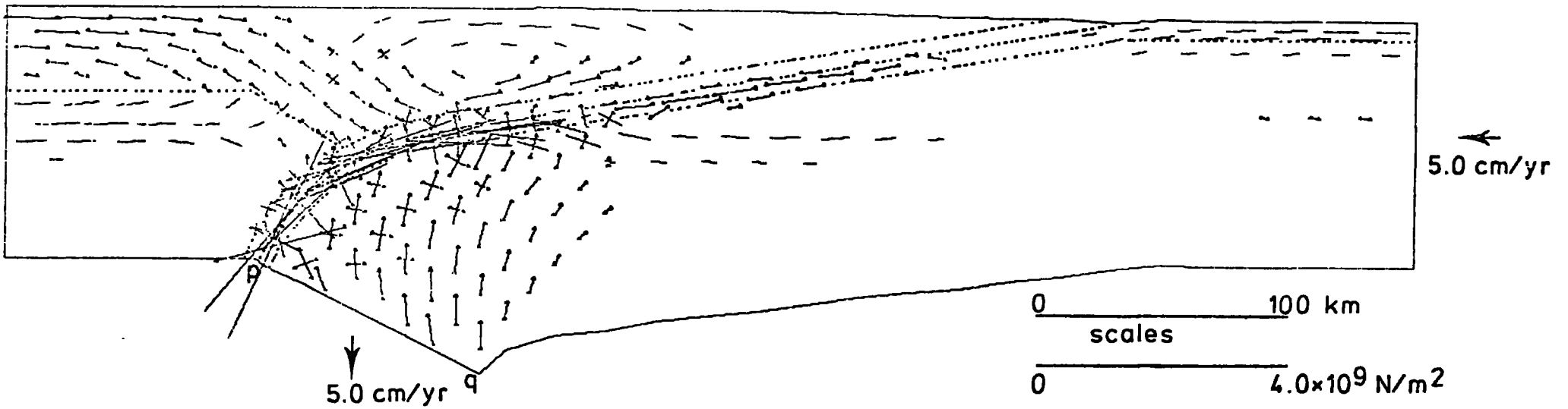

Fig. 7.5 Variation of stress as a function of the rate of descent of section pq of the base of the model. Stresses are relative to hydrostatic stress under the ocean. The rate of descent causes little variation in the stresses.

The stresses computed for the crustal rocks are so large that failure would have occurred. Moreover, in the volcanic region the temperatures are higher than normal and the viscosity of the rocks are probably quite low. The viscosity of the oceanic and continental crust were reduced to 0.5×10^{22} Ns/m^2. The shear zone viscosity was reduced to 0.5×10^{18} Ns/m^2. The upper limit of the viscosity of the mantle was reduced from 10^{43} Ns/m^2 to 5.0×10^{22} Ns/m^2 and steady state stresses re-computed. These were similar for values of V_{pl} of 2.5, 3.7 and 5.0 cm/yr. The stresses and flow pattern for V_{pl} = 3.7 cm/yr are shown in fig. 7.6. The stresses are all much smaller because of the reduced viscosities.

The stresses in the oceanic crust and shear zone near the thickened continental crust causing the negative gravity anomaly are hydrostatic (the principal stresses are equal) but at a lower stress level than that expected for a model in isostatic equilibrium. It is this area of low stress which is causing the horizontal tensions of about 0.5×10^9 N/m^2 in the mantle right across the model at a depth of 35 to 60 km. These stresses are effectively pulling the two plates together. These are present even for V_{pl} = 2.5 cm/yr for which one may have expected regional compression.

The tensions in the subducted plate below the gravity anomaly are directly related to the reduction in the body

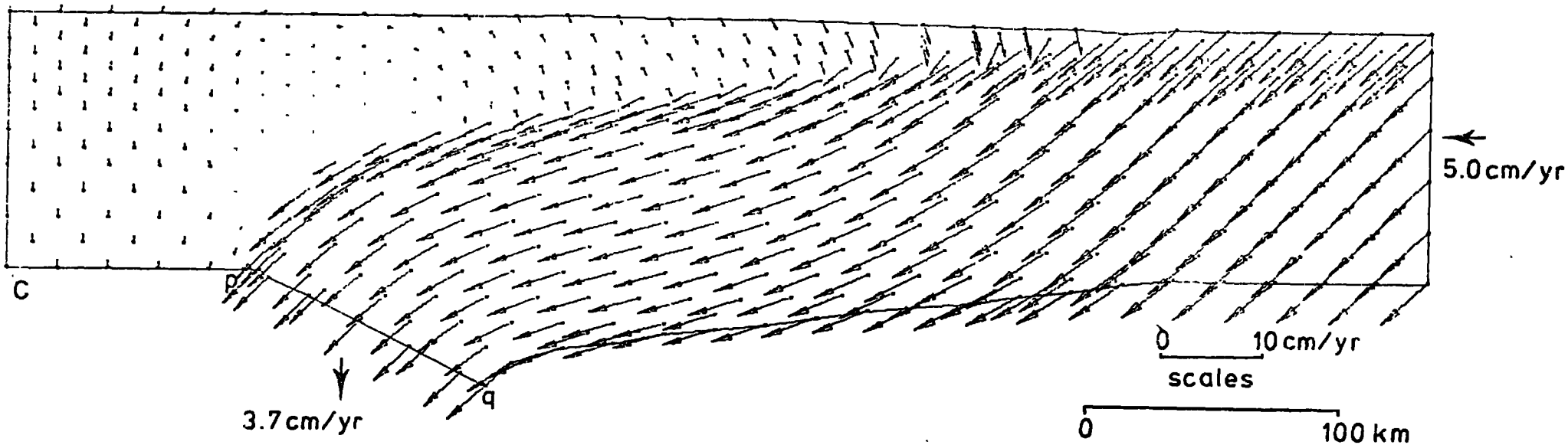

Fig. 7.6 Stresses in the lithosphere in the vicinity of the North Island, New Zealand computed by a visco-elastic analysis. The convergence rate is assumed to be 5 cm/yr and the descent velocity of pq 3.7 cm/yr. The top diagram (A) shows the stresses relative to the hydrostatic stress under the oceans. In (B) the stresses in the continental crust are shown relative to a uniform density of 2.7 Mg/m^3. Tensional stresses have bars on the ends. (C) shows the relative velocity of various parts of the model.

forces due to the increased thickness of the continental crust.

The flow of the continental crust, although an order of magnitude less than the subduction rate, does alter with V_{pq}. As V_{pq} decreases from 5 cm/yr to 2.5 cm/yr the rate of change in surface topography in the volcanic region changes from a downward velocity of about 0.5 cm/yr to an upward velocity of the same magnitude. These, however, are not reliable as the tensional stresses in the crust in the volcanic region are about 0.5×10^8 N/m^2 for all values of V_{pq} and so normal faulting would occur.

The stress pattern predicted here for the continental crust fits in well with the known tectonics of this region of New Zealand. The volcanic region is bounded by normal faults and the horizontal tensions would facilitate the upward movement of magma. The crustal stresses between the volcanic region and the coast are more complicated. Some horizontal compression is present. The Huiarau Range has a mean elevation of about 1.5 km and is a Mesozoic basement high (New Zealand Geological Survey, 1972). East of this range there is a substantial thickness of Tertiary sedimentary rocks. The computed stress pattern in the region between the Huiarau Range and the coast is suggestive of a downward flexure in the crust with compressional stresses near the surface and complementary tensional stresses in the base.

The tensional horizontal stresses between the coast and the trench correspond to an area in which normal faulting is common. HOutz et al.,(1967) also report some folding in this region. They show that the basement is irregular.

The continental plate in the model is being stretched at about 25% the convergence rate. About half this is due to extension of the crust off the coast and the rest to extension on the coastal side of the volcanic zone. Karig (1970a,b) has suggested that the Taupo Volcanic zone and its extension to the north, the Lau-Havre Trough, are extensional back arc features and this analysis would tend to confirm this.

7.2 Gravity anomaly over the trench

Talwani et al.,(1961) have interpreted gravity readings across the Tonga Trench in terms of the crustal structure of the trench and the Tonga Ridge. Their gravity profile is at about 22^{o}S latitude and lies nearly east-west across the centre of the Tonga Trench. Using seismic refraction sections previously determined by Raitt et al., (1955) they showed that the gravity readings are consistent with a crustal thickness of at least 20 km under the Tonga Ridge and about 6 km under the adjacent Pacific Ocean.

Griggs (1972) used the same data to show that the gravity

may be interpreted in terms of a dense sinking lithospheric slab, dipping at 45^{o} to 53^{o} from the trench under the Tonga Ridge, and the effect of the bathymetric low in the trench. These interpretations of the gravity data are not mutually exclusive. The model presented by Talwani et al., (1961) has a shape on the crust-mantle boundary consistent with both the subduction of the Pacific plate and approximate isostatic equilibrium between the ocean and the Tonga Ridge. Griggs took no account of the variation of elevation and crustal structure on either side of the trench; he used a symmetric model given by reflecting the oceanic side about the trench axis. Thus the upper parts of both models are in approximate isostatic equilibrium away from the immediate vicinity of the trench. Fig. 7.7 shows the model used in this study and the gravity anomalies calculated for it assuming densities of 2.8, 2.9 and 3.3 Mg/m^3 for the Tonga Ridge, oceanic crust and mantle respectively. These anomalies are of the same order as those which Griggs attributed to the trench. If we assume similar gravity effect of the sinking slab as Griggs did, then this model should be consistent with the total free-air gravity anomaly.

The finite element grid used is shown in Fig. 7.8. The sinking slab in this model dips at about 45^{o} - 50^{o} from the trench. This is the main difference between this model and the previous one in which the downward bend in the subducted

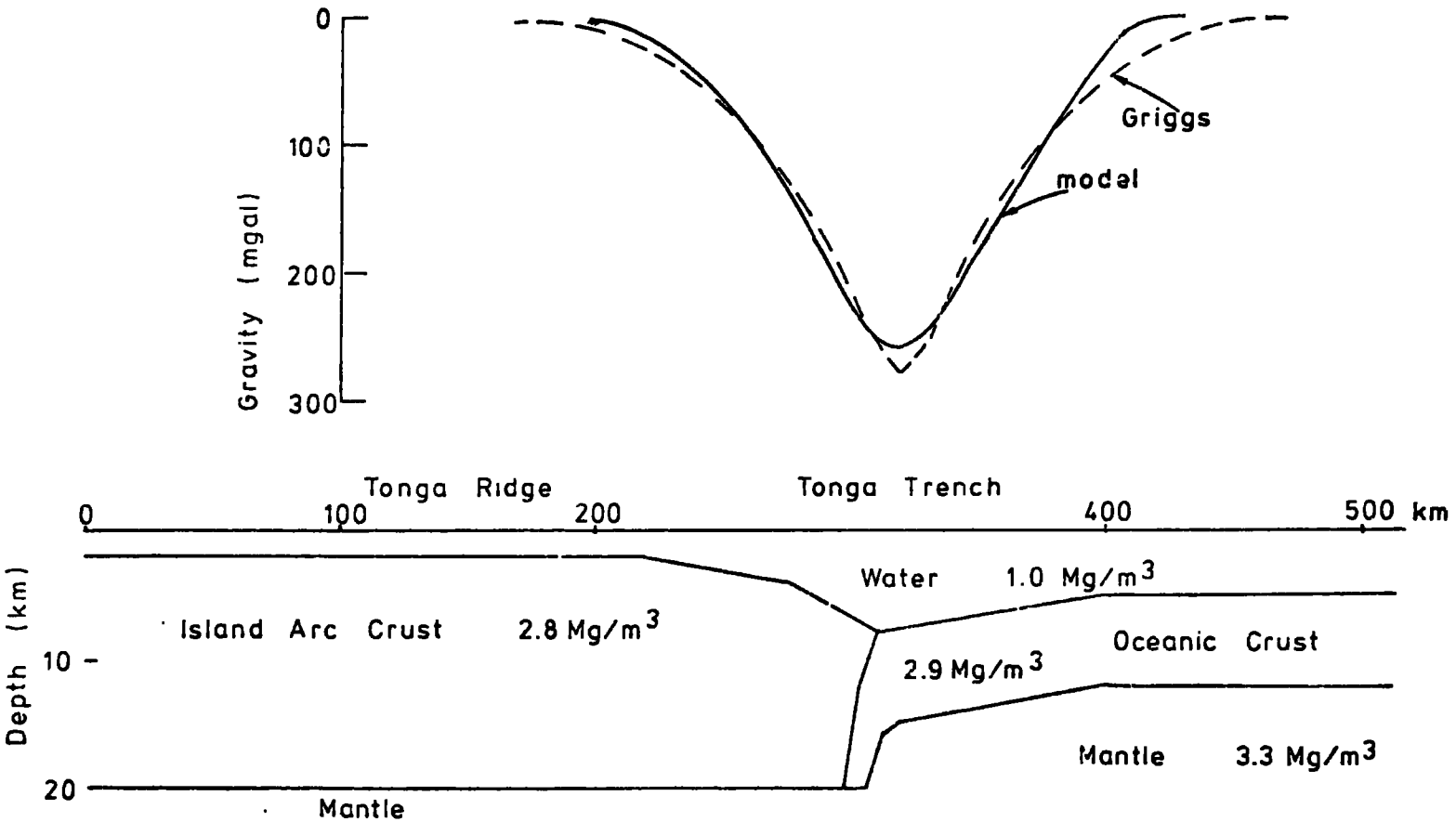

Fig. 7.7 Gravity model of the Tonga Ridge - Tonga Trench region. The gravity effect of the model is compared to that attributed to the topography by Griggs (1972).

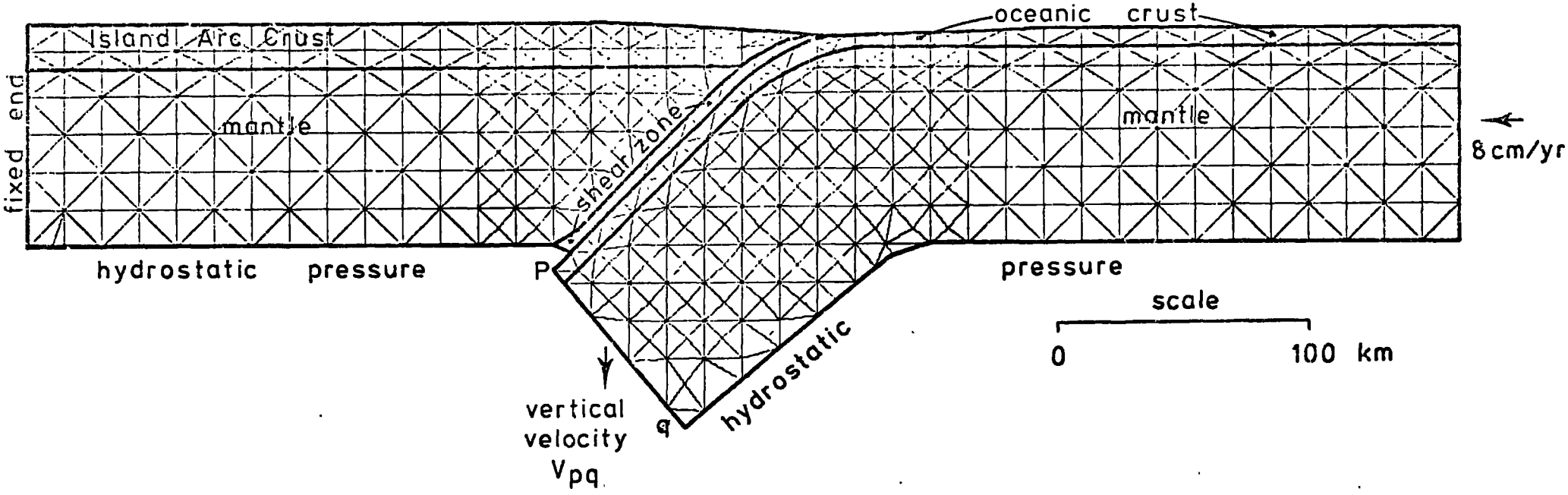

Fig. 7.8 Finite element net for elastic and visco-elastic analysis of the Tonga Region.

plate occurred about 250 km from the trench.

The properties of the mantle and oceanic crust were assumed to be those used in the previous model and the crust under the Tonga Ridge was assumed equivalent to the continental North Island of New Zealand for the purposes of ascribing physical properties. Its density, however, was increased to 2.8 Mg/m^3.

The results of elastic and visco-elastic analyses without accounting for the relative motions of the plates are shown in Fig. 7.9. The nodes on the base representing the truncation of the subduction zone were held at constant depth and the ends held vertical. As with the previous model the elastic analysis shows the strong influence of the boundary conditions on the ends. In both models, however, vertical tensions of about 2.5×10^8 N/m^2 are required in the top of the subducted lithosphere to maintain the density inhomogeneity causing the gravity anomaly. The lower viscosity at the base of the lithosphere reduces the stresses below 60 km outside the immediate vicinity of the subduction zone.

The visco-elastic analysis allowing for the relative motion between the plates was performed with time increments of 1000 yrs. The rate of convergence for the middle of the Tonga Trench is about 8 cm/yr (Le Pichon et al., 1973). A vertical velocity component of the part of the base of the

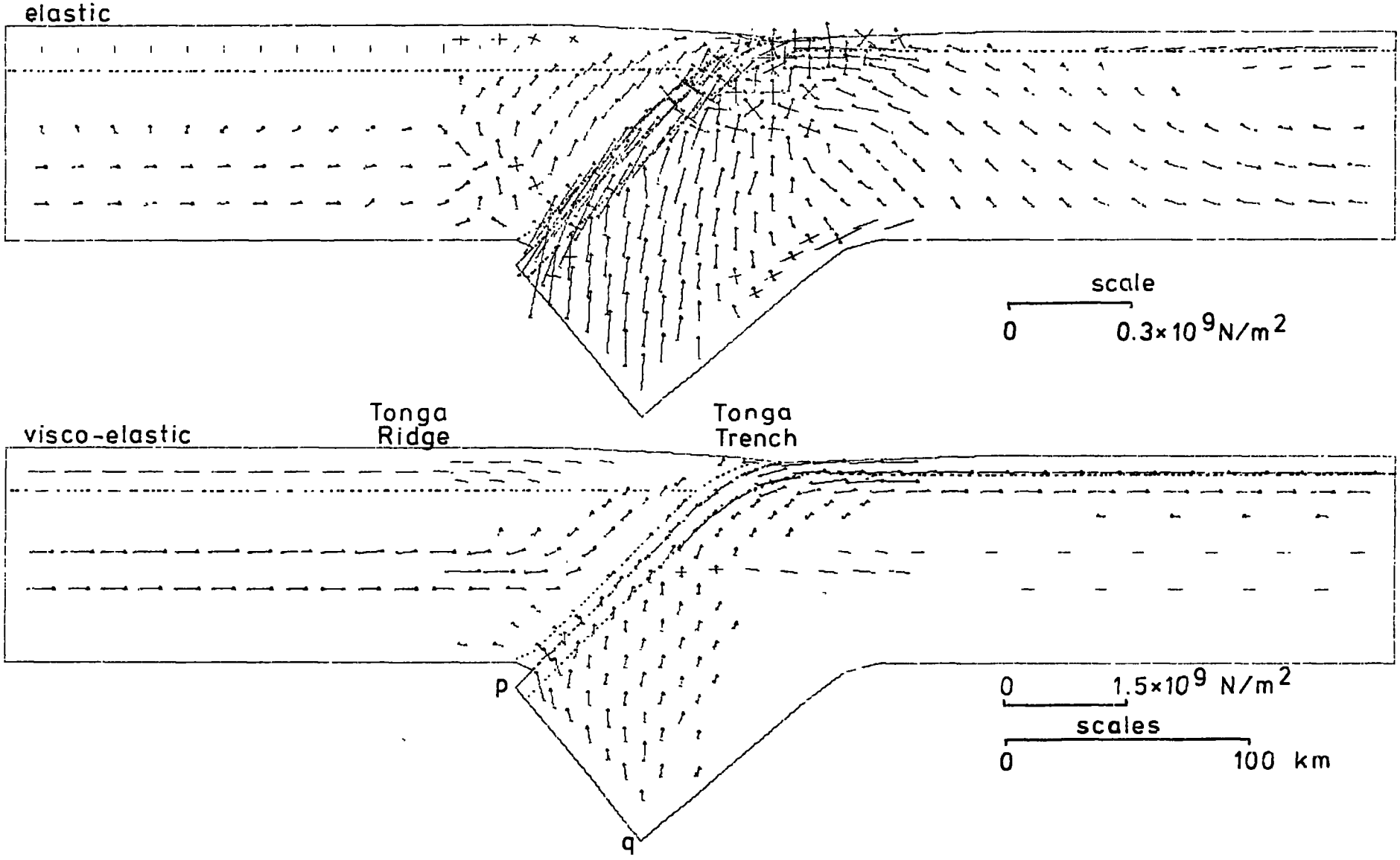
elastic
scale
0
0.3×10 9 N/m 2
visco-elastic
Tonga
Ridge
Tonga
Trench
p
q
0
1.5×10 9 N/m 2
scales
0
100 km

model representing the truncation of the subducted plate (V_{pq}) of 6.33 cm/yr was assumed giving a dip of the slab of about 50^{o}.

The viscosity of the crust was assumed to be 1.0×10^{25} Ns/m^2. This was also taken to be the upper limit for the viscosity of the mantle. A lower limit of the viscosity of the lithospheric mantle of 1.0×10^{21} Ns/m^2 and the viscosity of the shear zone of 1.0×10^{19} Ns/m^2 were also assumed. The temperature and viscosity distribution are shown in Fig. 7.10. The mantle viscosities were computed for a shear stress of 5.0×10^{7} N/m^2. The equilibrium stress pattern is shown in Fig. 7.11. The stresses plotted are the difference between the calculated stresses and the hydrostatic stress in the oceanic plate. The tensional downdip stresses are again evident but only in the mantle. The shear zone and subducted oceanic crust exhibit compressional downdip stresses as a result of the shearing between the two plates. The stresses in the immediate vicinity of the trench are large and incoherent as the topography and shearing have greater or lesser influence on the individual elements. Horizontal compressive stresses are calculated to extend right across the region at a depth of about 50 km. These are calculated to be about 8×10^{8} N/m^2 and would have a marked effect on the flexure of the outer-rise. Tensional stresses

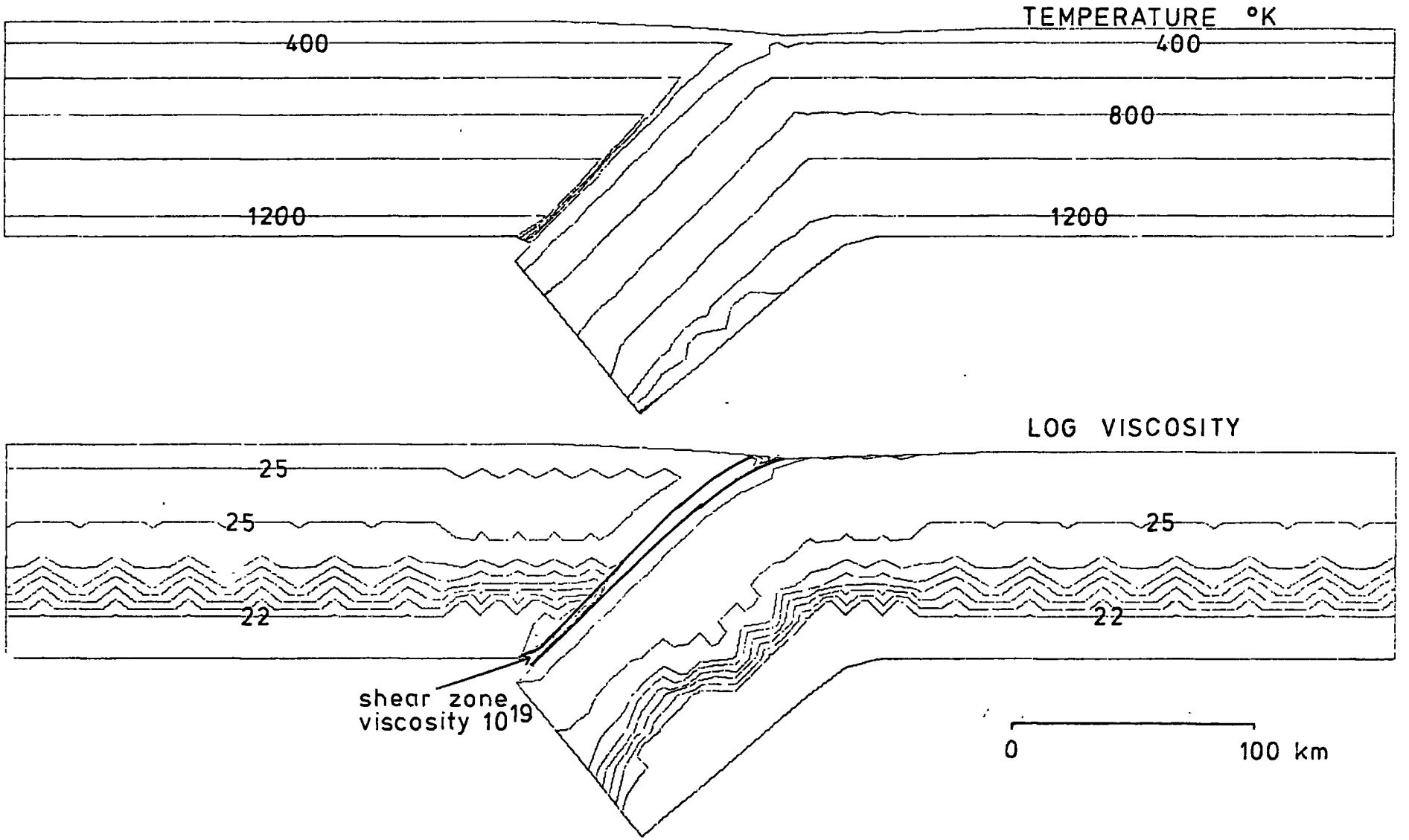
TEMPERATURE °K
400
400
800
1200
1200
LOG VISCOSITY
25
25
25
22
22
shear zone
viscosity 10^{19}
0
100 km

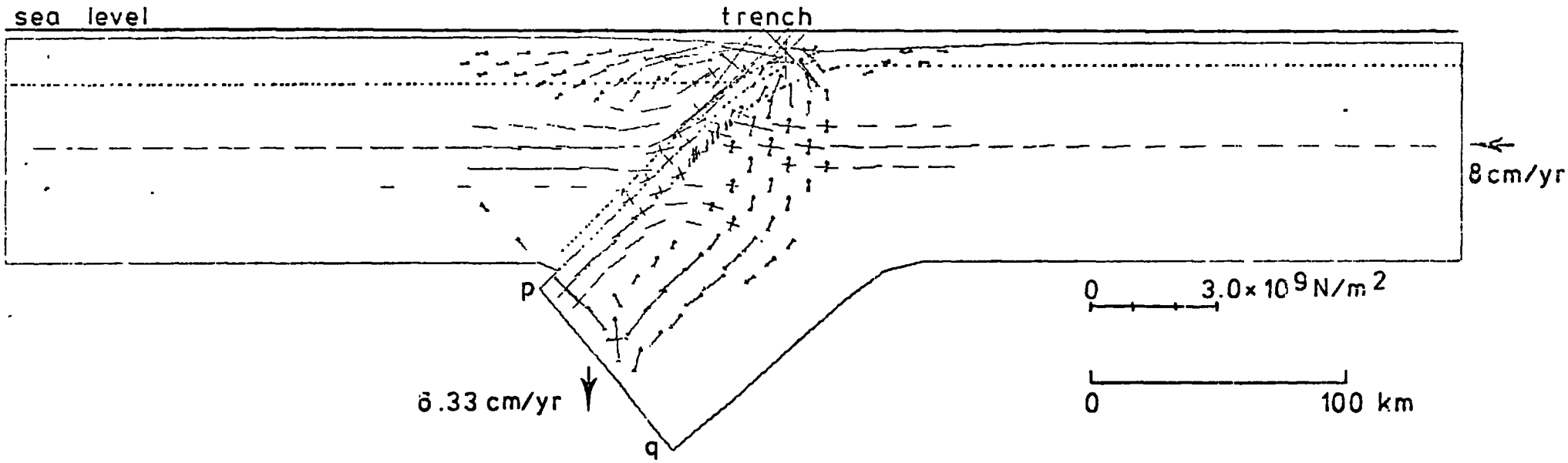

Fig.7.11 Results of visco-elastic analysis of the Tonga Region using the viscosity shown in fig. 7.11. The vertical velocity of pq is 6.33. Stresses are shown relative to hydrostatic stress in the oceanic lithosphere.

decreasing away from the trench shown in the region of the island arc would influence the back arc spreading in this region (Karig, 1970; Sclater et al., 1972).

7.3 Discussion and conclusions

The technique, used in this chapter, of adjusting the stresses and not moving the nodes in the finite element net has been used in the past (e.g. Tosköz et al., 1973; Neugebaur and Breitmayer, 1975). It has proved useful in visco-elastic analyses as it prevents the net from becoming too distorted. However, it can be seen from the stress distributions calculated in this chapter that the total distortional stresses are not determined by the scheme. The stresses due to the bending of the lithosphere are not evident in figs. 7.5, 7.6 or 7.11. The stresses calculated here are only those due to the density inhomogeneities and boundary constraints. Those due to the bending of the lithosphere must be superimposed upon them.

The large negative free air and isostatic gravity anomalies present in the vicinity of all subduction zones can only be maintained by vertical tensions of about 2.5×10^8 N/m^2 in the top of the sinking slab. These tensions are aligned approximately parallel to the slab and must result from the downward pull of the dense slab.

Earthquake mechanism studies suggest that if the subduction rate is high then the stresses being relieved by the earthquakes have the principal stress of greatest compression aligned down the dip of the Benioff zone. Isacks and Molnar (1969, 1971) and many others have suggested that this results from resistive forces on the base of the sinking slab being propagated up the slab to produce a down-dip compressional regime. This is also the conclusion reached from finite element analyses of the body forces in the region of subduction zones by Toskoz et al., (1973) who showed that their calculated stresses are consistent with the earthquake mechanisms if the parameters of their analyses are chosen correctly.

One of the regions studied in this chapter, the Tonga Trench, has a high subduction rate and compressional down-dip earthquake mechanisms (Isacks and Molnar, 1971) and yet it has been shown that tensional down-dip stresses are required to maintain the gravity anomalies. With a mean density contrast of 0.06 Mg/m^3, between the slab and the surrounding asthenosphere, estimated by Toskoz et al.,(1973), the downward stress of 2.5×10^8 N/m^2 is equivalent to the body forces of a slab about 400 km long if friction is ignored. The Benioff zone in the Tonga Trench region is much longer than this, about 700 km, but compressional down-dip earthquakes occur as shallow as 100 km (Isacks and

Molnar, 1971).

This again suggests that the earthquakes are not caused by the overall stress regime in the slab but by variations caused by differential volume changes between parts of the descending slab or distortion of the slab.

The effectiveness of the downdip tensions calculated here as driving mechanisms for plates depends largely on the variation of properties within the lithosphere and the depths at which the lateral density inhomogeneities exist. In the first set of models where the gravity anomaly was caused by the thickening of the continental crust the stresses distant from the subduction zone are tensional in the spinel peridotite stability field and compressional in and just below the oceanic crust. The tensional stresses are larger than the compressional stresses and the shallower stresses are more likely to be reduced by failure. In these regions the tensional stresses due to the density inhomogeneity may contribute to the dynamics of the plates.

CHAPTER 8

CONCLUSIONS AND DISCUSSION

Finite element analysis is useful in examining the stress and strain within parts of the earth during tectonic processes. The visco-elastic analysis developed in this thesis is particularly suited to these studies because variations in flow within the earth are generally slow so that long time steps may be taken without contravening the assumption of uniform creep within a time interval.

Phase changes and the stresses caused by them can be modelled adequately by developing an equation relating density to pressure and temperature. The differentials of this equation with respect to pressure and temperature give the bulk modulus and coefficient of thermal expansion respectively. These physical properties apply if mineralogical equilibrium is maintained. This is generally a valid assumption if temperatures are relatively high and water or another catalyst is present. This is the first known attempt to model phase changes in this way and to determine the stress pattern they cause.

The analyses presented here show three major effects in the stresses associated with subduction zones.

Firstly, it has been shown that phase changes in the descending slab cause large stresses as a result of the

relative contraction of part of the slab. The stresses so caused are an order of magnitude greater than any which are caused as a result of the body forces associated with the higher density of the slab with respect to the asthenosphere.

Secondly, the phase changes in the oceanic lithosphere reduce the flexural parameter from that calculated using elastic properties given by the compressibility of minerals. If fracture occurs this further reduces the flexural parameter but the analysis of the flexure becomes difficult and beyond the scope of simple beam theory. The stresses within the bent part of the lithosphere in the region of the trench and outer rise are reduced by viscous creep, and fracture. As the curvature is reduced and the plate re-straightened near the base of the trench the stresses previously relieved by these non-elastic processes are replaced by stresses of opposite sign so that residual stresses due to bending must be present after the beam is straightened. This is in contrast to the results of any simple analysis based on elastic beam theory. The stresses in areas of phase transition are an order of magnitude less than those expected for a uniform material because the ability of the rock to change phase effectively reduces its bulk modulus.

The flexure of the outer rise only accounts for a bend of about 5^{o}. A more difficult problem is the 30 - 60^{o} bend

when the top of the descending slab has reached 30 - 70 km. This study has shown that this bend may be enhanced by the stresses being stabilized by the extension of the areas of phase transition.

Thirdly, it has been shown that the maintenance of the negative gravity anomaly in the vicinity of the trench requires that the top of the sinking slab must be in tension. The down-dip tensional stresses required are $2 - 4 \times 10^8$ N/m^2 and correspond to the density inhomogeneity of a descending slab of about 400 km. This analysis applies to all subduction zones whatever the source mechanisms of the earthquakes.

It has been observed (e.g. Isacks and Molnar, 1971) that if the convergence rate is high then the earthquake source mechanisms indicate that the down-dip principal stress is compressional in the focal region (Fig. 1.2). Such earthquakes occur in the Tonga region at 100 km depth. Possible causes for compressional stresses in this region are distortional stresses and stresses due to phase change. The stresses due to the re-straightening of the lithosphere would be compressional near the top and tensional near the centre and base of the lithosphere. At fast convergence rates the top of the slab will remain cool and may fail by brittle fracture. For slow convergence rates the stress would be relieved by creep in a warmed upper part of the

descending slab. The gabbro or basalt-eclogite phase transition could also cause compressional stresses in the top of the mantle at depths of 50 - 120 km.

The contrast in earthquake mechanisms between regions of slow and high convergence is probably related to the variation of the thermal regime and hence the temperatures and depth that various phase transitions occur within the slab. The temperatures also play an important role in determining the viscosity in the slab and the dissipation of stress by creep.

It has been shown that the olivine-spinel transition causes tensional stresses in the centre of the slab and compressional stresses on the outside. If the subduction rate is slow the outer compressional stresses may be dissipated by creep whereas the inner tensional stresses are in the region of highest viscosity and strength and may be dissipated by brittle failure or accelerated creep (Griggs 1972). For higher subduction rates the outer parts of the subducted plate may be viscous enough for the stresses to build up until failure occurs.

Any distortion of the downgoing slab also causes large stresses approximately parallel to the sides of the slab. Such flexure of the Benioff zone has been demonstrated by Hamilton and Gale (1968) and Isacks and Molnar (1971).

The relative motions and density inhomogeneities in

areas of subduction zones result in stresses in the over-riding plate in the vicinity of the volcanic arc. Tensional stresses in this location will contribute to the ease of migration of the magma and to back arc extension.

Throughout this thesis the inhomogeneity of the composition of the mantle with depth has been ignored. It is difficult to see what the effect of the depleted dunite layer at the top of the mantle, for instance, may have on the stresses. The density changes at phase transitions and the compressibility of the various layers will differ causing local stresses as the slab is subducted.

The other assumption that has been made throughout this thesis is that of plane strain. No movement of material has been allowed into or out of a slab of unit thickness. With subduction zones in which the movement is commonly oblique to the structure this may have a profound effect on the stresses. The plane strain assumption, together with the neglect of the curvature of the earth, results in tensional stresses normal to the plane of the analysis as the rocks are subducted. The compression has to be anisotropic with zero strain normal to the model. This maximizes the strain in the plane of the model. An analysis in which the stress normal to the plane is the mean of the principal stresses may be more appropriate for the study of large movements in the earth even though it is physically less rigorous.

APPENDIX I

Numerical Techniques

In finite element visco-elastic analysis the main considerations in the programming of an electronic digital computer is the storage and time required to obtain the solution of a given problem. The main storage problems arise as the number of nodes increases since the array space required is about proportional to the square of the number of nodes. The time restrictions become critical as the number of nodes and the number of time steps required increase.

Apart from the standard finite element techniques some effort has been put into the reduction of these two factors so that bigger (more node) problems can be solved for longer term deformations.

Two aspects of the savings made will be discussed here and other less important considerations will become evident in the comments on the computer listings in appendix 2.

A1.1 Storage of the stiffness matrix

Each time step of the visco-elastic analysis requires the solution of equation 3.8 which may be re-written

$$[K]\,\underline{\delta} = -F(\sigma) \qquad \text{A1.1}$$

where $[K]$ is called the stiffness matrix. The total dimensions of $[K]$ are $2n \times 2n$ where n is the number of nodes but if the nodes are judiciously ordered the matrix becomes banded. It is symmetric. These facts have been used, in the past, to reduce the storage requirements of the stiffness matrix (e.g. Zienkiewiez, 1971). However, even for the best choice of the order of the nodes the band width of $[K]$ is above 20 for most realistic models and the band itself is sparsely populated. One common method of solution of the equations is to store half the band of the matrix and solve the equations by Cholesky decomposition. The use of this scheme requires that the stiffness matrix be stored in double precision on an I.B.M. computer. Large amounts of store are still required.

By solving the equation by the Seidal-Gauss iteration method it is sufficient to use single precision for the stiffness matrix and double precision for the $F(\sigma')$. Only the non-zero terms of the stiffness matrix need to be stored. The scheme finally adopted in the visco-elastic program is that at the start of the program indexing matrices are set up which give the position in the array AT. which will contain each possible element of $[K]$. The only elements of $[K]$ which can have a non-zero value are those for which both the row and column are connected by an element. The diagonal terms of $[K]$ are stored separately in array AND3 ,

Another advantage of this scheme is that the band width is no longer used so the nodes may be ordered in any convenient way. Alteration of the finite element net becomes trivial compared to when the band width is important when even a small alteration to the net usually requires re-numbering most of the nodes.

Storing only the non-zero terms in the matrix has another advantage in that the time in solving the equations by the Seidal-Gauss method is reduced. This arises from not needing to access and multiply the zero terms in the matrix. This approximately halved the time for a solution of the equations from that when half the band width of the matrix was stored.

A1.2 Solution of the equations

The equations represented by equation A1.1 are positive definite, symmetric, sparse and may be banded. There are several schemes for solving such equations but most of them require at least half the band width (together with the zeros within it) to be stored. Further, if the solution of one set of equations is likely to be similar to a previous set it is useful to use one solution as a first approximation to the next. Hence a Seidal-Gauss iteration scheme was chosen. The positive definite property of the equations is sufficient condition for the solution to converge but in initial tests the convergence was slow. An over relaxation

factor of 1.8 was found to improve the convergence rate. The solution was still approached slowly and monotonically. The introduction of a "jump" in the estimates of the solution after each twelve iterations seemed to give satisfactory convergence. The "jump" was applied if the last change in a variable was in the same direction as the total change during the previous six iterations. This "jump" could make the system divergent so it is progressively reduced each time it is used in a solution.

It is applied by changing the estimate of the variable by an amount proportional to the change in its value during the previous six iterations, i.e.

$$\delta_j^i = \delta_j^i + f(\delta_j^i - \delta_j^{i-6}) \qquad j = 1, N$$

where δ^i is the current estimate of the variable

δ^{i-6} is the estimate of the variable six iterations previously

and f is a factor which begins at 3 and is decreased each time it is used. The sum effect of the over relaxation factor and the "jump" reduced the number of iterations required for convergence by a factor of about three.

It was also found advantageous to work both up and down the matrices in solving the equations so as the i^{th}

estimate of δ_j is

$$\delta_j^i = \delta_j^{i-1} + 1.8\left(-F_j - \sum_{k=1}^{N} K_{jk}\delta_k\right)/K_{jj}$$

For each iteration we solve for j running from 1 to N and then N backwards to 1.

This technique is programmed in SUBROUTINE RSEID (page 173).

APPENDIX II

Computer Programs

A2.1 Introduction to structure of the programs

The finite element visco-elastic analysis of large models requires large computer resources so it is important to organise the structure of the programs so that the analyses may be continued if the computing is interrupted. It is also convenient to have the results in a form which can be used by further programs for X-Y plotter display. Because of this the computing was organised as a series of programs each performing various tasks. The general flow diagram is shown in fig. A2.1.

In general the results of one program are passed to the next by storing much of the COMMON COM1 in a permanent disc file. This is read and written to on route #8. The variables and arrays passed from program to program are

STRESS -	the stresses in each element
UV	the latest displacements of the nodes
X, Y	co-ordinates of the nodes
TOTIME	sum of time increments
DTIM	last time increment
HEATM	mechanical heat assigned to the nodes since the last thermal solution

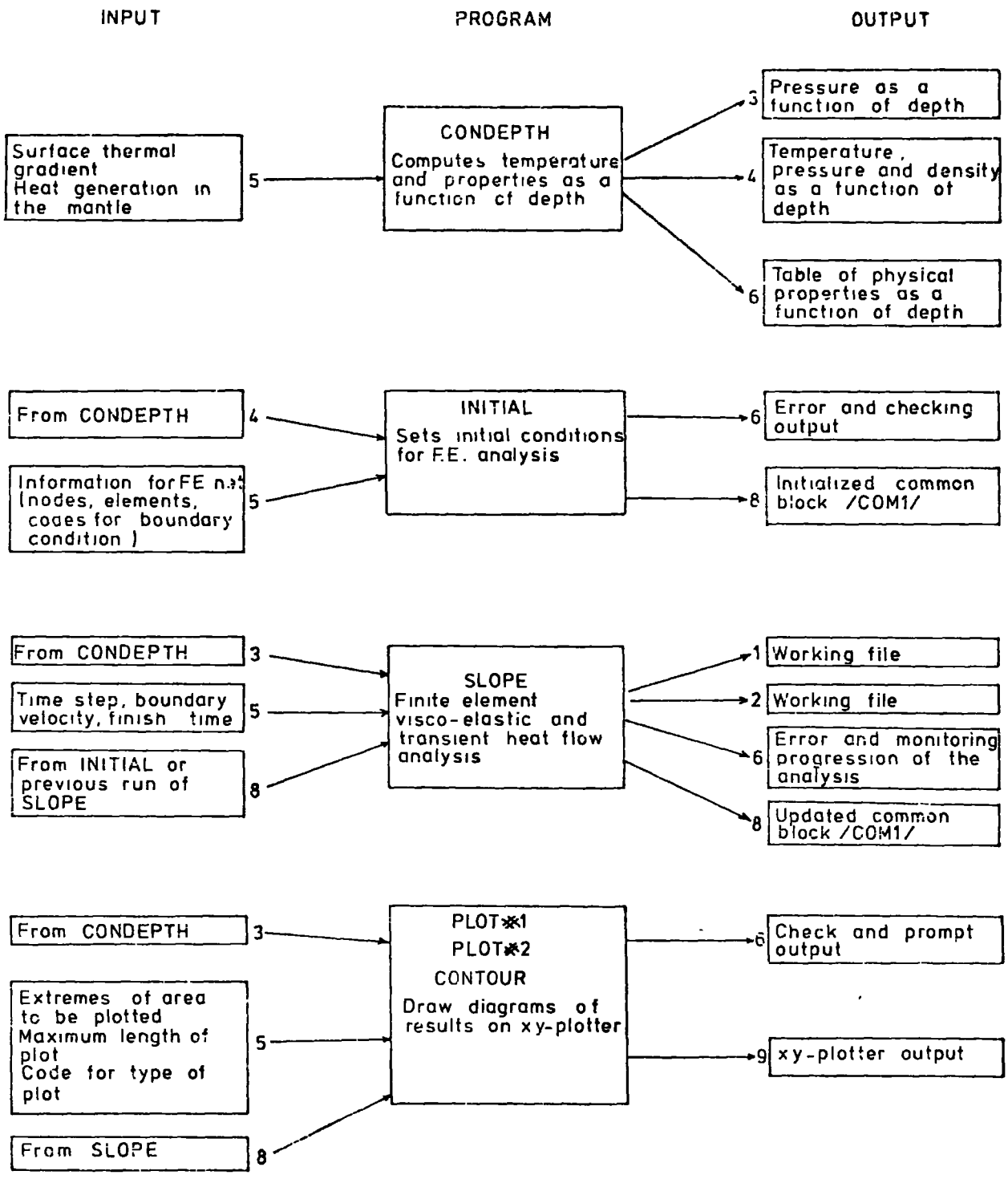
INPUT
PROGRAM
OUTPUT
Surface thermal gradient
Heat generation in the mantle
5
CONDEPTH
Computes temperature and properties as a function of depth
3
Pressure as a function of depth
4
Temperature, pressure and density as a function of depth
6
Table of physical properties as a function of depth
From CONDEPTH
4
Information for FE net (nodes, elements, codes for boundary condition)
5
INITIAL
Sets initial conditions for F.E. analysis
6
Error and checking output
8
Initialized common block /COM1/
From CONDEPTH
3
Time step, boundary velocity, finish time
5
From INITIAL or previous run of SLOPE
8
SLOPE
Finite element visco-elastic and transient heat flow analysis
1
Working file
2
Working file
6
Error and monitoring progression of the analysis
8
Updated common block /COM1/
From CONDEPTH
3
Extremes of area to be plotted
Maximum length of plot
Code for type of plot
5
From SLOPE
8
PLOT*1
PLOT*2
CONTOUR
Draw diagrams of results on xy-plotter
6
Check and prompt output
9
xy-plotter output

HTIM time since last thermal solution

FMASS gravitational body forces on nodes

TEMP temperature of nodes

BREAK code for failure of nodes - the viscosity is reduced depending on the magnitude of BREAK(I)

VD total distance moved by forced nodes

HEAT heat input which remains uniform during the analysis (radiogenic, normal heat flux)

II,JJ,MM nodes associated with each element

TP type of material for each element

normally TP = 1 mantle

TP = 2 oceanic crust

but others may be dictated according to variations of SUBROUTINE PROPS

TS nodes on the surface of the model specified in a clockwise order

NONODE number of nodes

NOEL number of elements

N2 22 x NONODE

IW total number of surface nodes

IW1-IW5 pointers for array TS specifying changes in the type of boundary conditions for SUBROUTINES SOLVE and TEMPGR

DY the velocity of part of the boundary.

Six programs are listed in this Appendix. The first, CONDEPTH, gives standard conditions in the oceanic basins (Chapter 2) and writes tables of the variation of density, pressure and temperature with depth for use in the other programs. INITIAL sets up the information listed above in COM1 and so initializes file #8 for the program SLOPE. Many variations of INITIAL may be made depending on the easiest way to specify one particular finite element grid. That presented was used for Model 2 of Chapter 6. The visco-elastic program SLOPE presented here was used in Chapter 6. It reads the initialized data from INITIAL or intermediate data written at the end of each time step and performs finite element visco-elastic and transient thermal analyses alternately. The other three programs are used to display the results in various forms on a X-Y plotter.

A2.2 PROGRAM CONDEPTH

This initial program calculates variation of properties and temperature of the oceanic basin as a function of depth. The program presented gives results for a conducting model and iterates to give the variation of temperature, pressure and density with depth for a given distribution of heat sources. The program can easily be changed to give these as a function of a given temperature distribution. The only input (route #5) is the surface heat flux (W/m^2) and

the assumed radiogenic heat sources at the top of the mantle and the base of the lithosphere. The variation between these is assumed linear. The heat sources in the oceanic crust and asthenosphere are assumed to be 1.6×10^{-10} W/kg and 0.11×10^{-10} W/kg respectively.

The line printer output (route ✻6) gives a tabulation of the variation of various properties with depth. Two files are output on routes ✻3 and ✻4. Route ✻3 contains pressure as a function of depth and route ✻4, pressure, density and temperature as a function of depth. All are tabulated at 0.5 km intervals.

```
C*************************************************************************
C    A PROGRAM TO CALCULATE THE VARIATION OF PROPERTIES WITH DEPTH       *
C    THIS PROGRAM ASSUMES STEADY STATE THERMAL CONDUCTION                *
C    THE RADIOGENIC HEAT SOURCES ARE ASSUMED TO BE :                     *
C    1.6E-10W/KG FOR THE OCEANIC CRUST  AND  0.11E-10W/KG FOR THE ASTHENOSPHERE
C    THE HEAT SOURCES IN THE MANTLE ARE ASSUMED TO VARY LINEARLY WITH DEPTH  *
C    THE UPPER AND LOWER VALUES AND THE SURFACE HEAT FLUX ARE READ IN    *
C*************************************************************************
      COMMON /NE/T(1600),DENS(1600),PRES(1600),EN,ANUN,TEXN,BETN,DENN,
     1 CV,CP,VP,VS,CONDN,TMN,VISN,X,SHEAR,MDT,MDPRES,I
      REAL  HT(1600),DTL(1600), MDT,SC(15),MDPRES
C********* X=DEPTH INTERVAL ,DEPTH=(I-1)*X ***********************************
      X=500.0
      AR=6370.0E+3
C*********** INPUT ROUTE # 5 ***************************************************
C'**** SHEAT=SURFACE HEAT FLUX (W/M**M) (CONDUCTIVITY ASSUMED TO BE 2.1 W/MC) ***
C********* ST1,ST2 RADIOGENIC HEAT SOURCES AT TOP AND BOTTOM OF LITHOSHERE *****
C********* THE VARIATION IS ASSUMED TO BE LINEAR ********************************
C ******** INITIALIZE TEMPERATURE AND PRESSURE ********************************
      DO 2 I=1,1600
      T(I)=300.
    2 PRES(I)=0.0
      READ(5,5)SHEAT
      WRITE(6,5) SHEAT
      G=SHEAT/2.1
      READ(5,5) ST1,ST2
      WRITE(6,7) ST1,ST2
    7 FORMAT(' HEAT AT TOP OF MANTLE  ',E14.5,/,' AT BOTTOM OF ',
     1 'LITHOSPHERE',E14.5)
    5 FORMAT(F10.5)
C****** MAXIMUM NUMBER OF ITERATIONS USUALLY IT ONLY REQUIRES ABOUT 10 *********
   21 DO 920 II=1,30
C****** SURFACE VALUES ***********************************************************
      IA=II
      T(1)=273.0
       PRES(1)=5000.0*9.8*1030.0
      DENS(1)=2800.0
      MDT=0.0
      MDPRES=0.0
      DN=0.0
      DDT=0.0
      CONDN=2.1
      DENN=DENS(1)
      GRADN=G
      HT(1)=GRADN*CONDN
      DO  900 IM=2,1600
      I=IM
C*************************************************************************
C GRADL GRADN ARE THE THERMAL GRADIENTS                                  **
C SQ HEAT SOURCES   OCEANIC CRUST 1.6E-10 W/KG                           **
C                   ASTHENOSPHERE 0.11E-10 W/KG                          **
C                   LITHOSPHERIC MANTLE LINEAR VARIATION FROM ST1 TO ST2 **
C HT HEAT FLUX AT I'TH DEPTH                                             **
C*************************************************************************
      DENL=DENN
      CONDL=CONDN
      GRADL=GRADN
      SQ=1.6E-10
      IF(I .GT. 14) SQ=0.11E-10
      IF(I .GT.14 .AND.I .LT. 200) SQ=ST2+(200.-I)/186.0*(ST1-ST2)
C******  GET PROPERTIES ************************************************
      IF(I .LE.14) CALL CCRUST
      IF(I .GT. 14) CALL MANTLE
      A=X/(AR-(I-1)*X)
      GRADN=(CONDL*GRADL-X*0.5*SQ*(1.0-A)*(DENN+DENL))/(CONDN*(1.0-2.0*A
     1 ))
      HT(I)=GRADN*CONDN
      T1=T(I-1)+0.5*X*(GRADN+GRADL)
      DT=T1-T(I)
  890 T(I)=T1
C******** TEST TO MAKE SURE ALL HEAT FLUX AT SURFACE NOT FORMED ABOVE I ********
  891 IF(T1 .LT. T(I-1)) GOTO 905
      MDT=AMAX1(ABS(DT),MDT)
  900 CONTINUE
  905 CONTINUE
C********** CHECK FOR CONVERGENCE ***************************************
      IF (MDT .LT. 0.1.AND. MDPRES.LT. 1.0E+4) GOTO  9
C******** LINEPRINTER OUTPUT OF VARIATION OF PROPERTIES WITH DEPTH **************
  920 CONTINUE
    9 CONTINUE
```

```
      WRITE(6,930) I4
  930 FORMAT(' CONVERGED AFTER ',I6,' ITERATIONS')
  494 SH=SHEAT/4.18E+4
      WRITE(6,490) SHEAT,SH
      WRITE(6,495) HT(I4)
  495 FORMAT(/,' HEAT INPUT AT BOTTOM= ',E14.4,' JOULES/METRE SQ')
  490 FORMAT(' HEAT LOST AT SURFACE ',E14.4,' JOULES/METRE SQUARE  OR ',
     1 E14.4,' CALS/SQ CM')
  450 FORMAT(1H1,//,' FIXED SURFACE TEMPERATURE =',F10.4,' DEGREES/METRE
     1 ',/,' HEAT SOURCE   JOULES/KILOGRAMME/SEC',/,' OCEANIC CRUST ',
     1 E14.4, /,' MANTLE MATERIAL ',E14.4)
      WRITE(6,470)
  470 FORMAT('  DEPTH TEMP DENSITY PRESSURE  YOUNGS  AND BULK MOD ',
     1 '  POISONS',
     1 'RAT THERMAL EXP CONDUCT  MELT TEMP CP CV   LOG VIS VP  VS  '
     2 ,'HT FLUX')
      IM=1
      DO 500 I=1,IM
      J=I
      IF(I .LE.14) CALL OCRUST
      IF(I .GT. 14) CALL MANTLE
      IF(MOD(I-1,10) .NE.0) GOTO 500
      DX=X*(J-1)*0.001
      VP=VP/1000.0
      VS=VS/1000.0
      DLVIS=ALOG10(VISN)
      WRITE(6,480) DX,T(J),DENS(J),PRES(J),EN,BETN,ANUN,TEXN,CONDN,TMN,
     1 CP,CV,DLVIS,VP,VS,HT(I)
  480 FORMAT(F6.1,2F7.1,3E10.3,F6.3,E10.3,F6.2,F8.2,2F6.1
     1 ,3F6.2,F10.4)
  500 CONTINUE
C******** FILES OUTPUT FOR INPUT TO OTHER PROGRAMS ****************************
C******** ROUTE #3 PRESSURE ONLY AS FUNCTION OF DEPTH ********* ****************
C******** ROUTE #4 TEMPERATURE,PRESSURE AND DENSITY AS FUNCTION OF DEPTH *******
      WRITE(4,600) T,PRES,DENS
      WRITE(3,600) PRES
  600 FORMAT(20A4)
 9999 STOP 2
      END



      SUBROUTINE OCRUST
C****** OCEANIC CRUST PROPERTIES ***************************************************
      COMMON /NE/T(1600),DENS(1600),PRES(1600),EN,ANUN,TEXN,BETN,DENN,
     1 CV,CP,VP,VS,CONDN,TMN,VISN,X,SHEAR,MDT,MDPRES,I
      REAL*8 BA,BB,BE,EA,EB,EC,ED,EE
      REAL  MDT,MDPRES
      DPRES=0.0
      IF(I .EQ.1) GOTO 10
      J=I-1
      PN=PRES(J)+(DENS(J)+DENS(I))*0.5*X*9.8
      DPRES=PN-PRES(I)
   10 PN=PRES(I)+DPRES
      MDPRES=AMAX1(ABS(DPRES),MDPRES)
      TEM=T(I)
      DTEM=TEM-300.0
      PRES(I)=PN
      BA=1.15E-11
      BB=-1.4E-5
      BE=8.0E-9
      EA=0.7645479424D-11
      EB=-0.4196515938D-4
      EC=-0.7063370539D-22
      ED=0.7717123599D-15
      EE=0.4788135955D-08
      EG=1.000+BA*PN+BB*DTEM+BE*DTEM*DTEM
      EE=1.000+EA*PN+EB*DTEM+EC*PN*PN+ED*PN*DTEM+EE*DTEM*DTEM
      EG=2900.0
      BE=3400.0
      AL1=BB+2.0*BE*DTEM
      AL2=EB+ED*PN+2*EE*DTEM
      BE1=BA
      BE2=EA+2*EC*PN+ED*DTEM
      D1=0.00059*(1500.0-2.3E-6*PN+DTEM)
      D2=0.002*(1080.0-DTEM+1.2E-7*PN)
      E1=AMAX1(0.0,AMIN1(0.5-D1,1.0))
      E2=AMAX1(0.0,AMIN1(0.5-D2,1.0))
      DEP1=0.00069*2.3E-6
      DET1=-0.00069
      DEP2=-0.002*1.2E-7
      DET2=0.002
      IF (E1*(1.0-E1) .GT. 0.0001) GOTO 600
```

```
      DFP1=0.0
      DFT1=0.0
  600 IF(F2*(1.0-F2) .GT. 0.0001) GOTO 700
      DFP2=0.0
      DFT2=0.0
  700 CONTINUE
      DF1=(RG*FG*(1.0-F1)+RE*FE*F1)
      DENN=DF1*(1.0-0.09*F2)
      BETN=(RG*(BF1*(1.0-F1)-FG*DFP1)+RE*(BE2*F1+FE*DFP1))*(1.0-0.09*F2
     1 )-DF1*0.09*DFP2
      BETN=BETN/DENN
      TEXN=(RG*(AL1*(1.0-F1)-FG*DFT1)+RE*(AL2*F1+FE*DFT1))*(1.0-0.09*F2
     1 )-DF1*0.09*DFT2
      TEXN=-TEXN/DENN
      VP=3.16*DENN-3000.0
      VS=1.63*DENN-1280.0
      R=(VP/VS)**2
      ANUN=(R-2.0)*0.5/(R-1.0)
      ANUN=AMIN1(0.495,ANUN)
      EN=3.0/BETN*(1.0-2.0*ANUN)
      A=1.288E-6*VP*DENN**0.667
      BS=2.1
      CONDN=AMAX1(A,BS)
      DENS(I)=DENN
      IF(TEM .GT. 500.0) CONDN=CONDN+2.3E-3*(TEM-500.0)
      TMN=1067.0+1.2E-7*PN
      IF (PN .LT. 3.0E+8) TMN=1315.0-8.5E-7*PN+5.0E-16*PN*PN
      SH=10.0E+5
      VISN=ALOG(1.5)+52.0*TMN/TEM-1.5*ALOG(SH)
      VISN=AMIN1(100.0,VISN)
      VISN=AMAX1(0.001,VISN)
      VISN=EXP(VISN)
      CP=988.56+0.20012*TEM-0.2503E+8/(TEM*TEM)
      CP=CP-(FE*FE-RG*FG)/(RE*FE*RG*FG)*(PN-1500.0/2.3E-6)*DFT1
     1 -0.09/(0.91*DF1)*(PN+1080.0/1.2E-7)*DFT2
      CV=CP-TEXN*TEXN*TEM/(DENN*BETN)
      RETURN
      END


      SUBROUTINE MANTLE
C********** CALCULATES  MANTLE  PROPERTIES **********************************
      COMMON /RE/T(1600),DENS(1600),PRES(1600),EN,ANUN,TEXN,BETN,DENN,
     1 CV,CP,VP,VS,CONDN,TMN,VISN,X,SHEAR,MDT,MDPRES,I
      REAL  MDT,MDPRES
      J=I-1
      PN=PRES(J)+(DENS(J)+DENS(I))*0.5*X*9.8
      DPRES=PN-PRES(I)
      MDPRES=AMAX1(ABS(DPRES),MDPRES)
      TEM=T(I)
      DTEM=TEM-273.0
      PRES(I)=PN
      RHO0=3240.0
      RHO1=80.0
      RHO2=60.0
      RHO3=3060.0
      RHO4=3170.0
      SA= 0.5407121747D-11
      SB=-0.2679282686D-04
      SC=-0.4187858999D-22
      SD= 0.3593745755D-15
      SE=0.1010133626D-08
      A= 0.7982656082D-11
      B=-0.2979325991D-04
      C=-0.1479570252D-21
      D= 0.8338005047D-15
      E=-0.3951057525D-08
      R= 0.3221268166D-32
      S=-0.3016923432D-25
      Y= 0.1610151893D-18
      Z= 0.6275833522D-12
      F=1.0+PN*(A+PN*(C+R*PN))+DTEM*(B+PN*(D+S*PN)+DTEM*(E+Y*PN+
     1 Z*DTEM))
      ALO=B+PN*(D+S*PN)+DTEM*(2.0*E+2*Y*PN+3.0*Z*DTEM)
      BEO=A+DTEM*(D+Y*DTEM)+PN*(2*C+3*D*PN+2*S*DTEM)
      SF=1.000+SA*PN+SB*DTEM+SC*PN*PN+SD*PN*DTEM+SE*DTEM*DTEM
      SALO=SB+SD*PN+2.000*SE*DTEM
      SBEO=SA+2.000*SC*PN+SD*DTEM
      D1=0.001*(1800+DTEM-300.0E-8*PN)
      D2=0.0025*(964+DTEM-80.3E-8*PN)
      D3=0.0011*(2401.0+DTEM-30.0E-8*PN)
      D4=0.0014*(1500+9.0E-8*PN-DTEM)
```

```
      D5=0.0313*(200.0-1.0E-8*PN)
      F1=AMAX1(0.0,AMIN1(0.5-D1,1.0))
      F2=AMAX1(0.0,AMIN1(0.5-D2,1.0))
      F3=AMAX1(0.0,AMIN1(0.5-D3,1.0))
      F4=AMAX1(0.0,AMIN1(0.5-D4,1.0))
      F5=AMAX1(0.0,AMIN1(0.5-D5,1.0))
      G3=1.0-F3
      DFP1=3.0E-9
      DFP2=80.3E-8*0.0025
      DFP3=0.0011*30.0E-8
      DFP4=-0.0014*9.0E-8
      DFP5=0.0313E-8
      DFT1=-0.001
      DFT2=-0.0025
      DFT3=-0.0011
      DFT4=0.0014
      IF(F1*(1.0-F1) .GT. 0.0001) GOTO 100
      DFP1=0.0
      DFT1=0.0
  100 IF (F2*(1.0-F2) .GT. 0.0001) GOTO 202
      DFP2=0.0
      DFT2=0.0
  202 IF(F3*(1.0-F3) .GT. 0.0001) GOTO 300
      DFP3=0.0
      DFT3=0.0
  300 IF(F4*(1.0-F4) .GT. 0.0001) GOTO 400
      DFP4=0.0
      DFT4=0.0
  400 IF (F5*(1.0-F5) .GT. 0.0001) GOTO 500
      DFP5=0.0
  500 CONTINUE
      E1=RHO0+RHO1*F1+RHO2*F2
      D1=E1*G3*F+RHO3*F3*SF
      DENN=D1*(1.0+0.08*F5)*(1.0-0.0225*F4)
      DENS(I)=DENN
      DE1=RHO1*DFP1+RHO2*DFP2
      DD1=DE1*G3*F-E1*DFP3*F+E1*G3*BFO+RHO3*DFP3*SF+RHO3*F3*SBE0
      BETN=DD1*(1.0+0.08*F5)*(1.0-0.0225*F4)+D1*(1-0.0225*F4)*0.08*DFP5
     1 -0.0225*D1*(1.0+0.08*F5)*DFP4
      BETN=BETN/DENN
      DE1=RHO1*DFT1+RHO2*DFT2
      DD1=DE1*G3*F-E1*DFT3*F+E1*G3*ALO+RHO3*DFT3*SF+RHO3*F3*SALO
      TEXN=DD1*(1+0.08*F5)*(1.0-0.0225*F4)-0.0225*D1*DFT4*(1.0+0.08*F5)
      TEXN=-TEXN/DENN
      CP=1033.84+0.19434*TEM-0.2419E+8/(TEM*TEM)
      R1=RHO1+RHO0
      R2=R1+RHO2
      R3=RHO3*SF
      R4=DENN/(1.0-0.0225*F4)
      RX=R4*0.5745
      CP=CP-DFT1*RHO1/(F*RHO0*F1)*(300.0E-8*PN-1527)/300.0E-8-DFT2*RHO2
     1 /(F*R1*R2)*(80.3E-8*PN-691.0)/80.3E-8-DFT3*(R3-R2*F)/(R3*R2*F)*
     1 (30.0E-8*PN-2127)/30.0E-8-DFT4*(RX-R4)/(RX*R4)*(1773+9.0E-8*PN)
     1 /9.0E-8
      CV=CP-TEM/BETN*TEXN*TEXN/DENN
      VP=-2206.0+3.16*DENN
      VS=1.63*DENN-880.0
      R=(VP/VS)**2
      ANUN=0.5*(R-2)/(R-1)
      EN=3.0/BETN*(1.0-2.0*ANUN)
      A=1.28E-6*VP*DENN**0.667
      C=1.0/(0.0741+5.01E-4*TEM)
      CONDN=AMAX1(A,C)
      IF (TEM.GT. 500.0) CONDN=CONDN+2.301E-3*(TEM-500.0)
      SH=10.0E+5
      IF (PN .LT. 3.0E+9) GOTO 10
      TMN=920.0+1.26E-7*PN
      VISN=ALOG(1.8E+13)+26.8*TMN/TEM-1.1*ALOG(SH)+4.909*F3
      GOTO 20
   10 TMN=1316.0+8.703E-8*PN-1.657E-17*PN*PN
      VISN=ALOG(2.1E+14)+40.0*TMN/TEM-2.0*ALOG(SH)
      IF(SH .GT. 1.0E+8)
     1 VISN=ALOG(1.1E+31)+40.0*TMN/TEM-4.0*ALOG(SH)
   20 CONTINUE
      VISN=EXP(AMIN1(100.0,AMAX1(10.0,VISN)))
      RETURN
      END
```

A2.3 PROGRAM INITIAL

The variables which are passed in file ✲8 between various programs need to be initialized. This is done in this program. The nodes and element specifications may be read in or generated or a combination of these can be used. The program listed reads in some of the nodes and elements and generates the rest by using the repetitive nature of the grid in the model. The initial stress, temperatures and densities are assigned by interpolation of the values passed from CONDEPTH route ✲4.

Some checking is done on the net to ensure that no elements have zero area (error in net specification). The total area is printed. The body forces due to the gravitational forces are entered in FMASS by the SUBROUTINE MASS.

If all checks are satisfactory the initialized values of data are passed through route ✲8 to further programs.

```
C*****************************************************************************
C     PROGRAM TO INTIALIZE A FINITE ELEMENT DATA                              *
C     THIS IS ONE EXAMPLE MANY VARIANTS MAY BE MADE DEPENDING ON THE EASIEST  *
C     WAY TO SPECIFY THE PROBLEM UNDER CONSIDERATION                          *
C*****************************************************************************
      COMMON /COM1/AREA,D(3,3),DB(3,6),AK(6,6),B(3,6),PHS(1980),
     1 DTEMP(990),SPROPS(6,1900),APP(1600),ST(3),
     2 STRESS(4,1900),UV(1980),X(990),Y(990),TOTIME,DTIM,HEATM(990),
     3 HTIM,EMASS(1980),TEMP(990),BREAK(1900),VD,HEAT(990),
     4 II(1900),JJ(1900),MM(1900),TP(1900),TS(260),
     5 NONODE,NOEL,N2,IW,IW1,IW2,IW3,IW4,IW5,DY,NO(6),FIRST,FRACT,NEW
      REAL*8 X,Y,PHS,STRESS,D,AK,DB,DTIM,AREA,ST,B,VD
      REAL*8 TOTIME,HTIM
      INTEGER*2 II,JJ,MM,CONSTR,TFIX,TP,TS
      LOGICAL FIRST,FRACT,NEW
      INTEGER*2 LEN
      DIMENSION OUTPUT(15968)
      REAL*8 OUTPUT
      EQUIVALENCE (OUTPUT(1),STRESS(1))
      REAL*8 SAREA
      DIMENSION IL(5),JL(5),ML(5)
      DIMENSION SPRES(1600),SDENS(1600),STEMP(1600)
      DIMENSION ITB(150)
      CALL TIME(0)
C*********** READ IN STANDARD CONDITIONS AT INTERVALS OF 500M ****************
      READ(4,4) STEMP,SPRES,SDENS
    4 FORMAT(20A4)
      HTIM=0.0
      IDUM=0
      FIRST=.TRUE.
C***********READ CO-ORDINATES OF FIRST 33 NODES ******************************
      READ(5,5)(X(I),Y(I),I=1,33)
C********READ IN NODES CORRESPONDING TO FIRST 42 ELEMENTS ********************
      READ(5,6)(II(I),JJ(I),MM(I),I=1,16)
      READ(5,6)(II(I),JJ(I),MM(I),I=17,42)
    5 FORMAT(16F5.0)
    6 FORMAT(1515)
C**********SET CODE FOR TYPE OF ROCK *****************************************
      DO 7 I=1,16
    7 TP(I)=2
      DO 8 I=17,42
    8 TP(I)=1
C********PROPAGATE NET TO 969 NODES AND 1680 ELEMENTS ***********************
      DO 9 I=34,969
      X(I)=X(I-24)
      Y(I)=Y(I-24)+30.0
    9 CONTINUE
      DO 110 I=43,1680
      II(I)=II(I-42)+24
      JJ(I)=JJ(I-42)+24
      MM(I)=MM(I-42)+24
      TP(I)=TP(I-42)
  110 CONTINUE
       NONODE=969
      N2=NONODE*2
      NOEL=1680
C************** CALCULATE WHICH NODES ARE ON BOUNDARIES AND ENTER IN TS ********
      DO 11 I=1,81
      TS(I)=969-(I-1)*12
   11 CONTINUE
      DO 12 I=1,8
      TS(I+81)=9-I
   12 CONTINUE
      DO 13 I=1,40
      J=(I-1)*24+9
      M=(I-1)*4+89
      TS(M+1)=J+1
      TS(M+2)=J+4
      TS(M+3)=J+13
      TS(M+4)=J+16
   13 CONTINUE
      DO 14 I=1,8
      TS(249+I)=NONODE-8+I
   14 CONTINUE
C*********** SET POINTERS FOR CORNERS OF NET IN ARRAY TS **********************
      IW1=81
      IW2=89
      IW4=249
      IW=257
C****** SET TEMPERATURE OF NODES AS FUNCTION OF DEPTH ************************
      DO 221 I=1,NONODE
      XS=X(I)*1000.0
      A=PX(XS,STEMP,AA)
```

```
      TEMP(I)=A
  221 CONTINUE
C********** CONVERT COORDINATES TO METERS AND INITIALIZE HEAT ARRAYS ******-
      DO 100 I=1,NONODE
      X(I)=X(I)*1000.0
      Y(I)=Y(I)*1000.0
      HEATM(I)=0.0
      HEAT(I)=0.0
  100 CONTINUE
C********* CHECK FOR COINCIDENT ELEMENTS(ANY REPEATED BY ACCIDENT) *************
      DO 90 I=1,NOEL
      UV(I)=(X(II(I))+X(JJ(I))+X(MM(I)))/3.0
      FMASS(I)=(Y(II(I))+Y(JJ(I))+Y(MM(I)))/3.0
   90 CONTINUE
      M=NOEL-1
      DO 95 I=1,M
      K=I+1
      DO 95 J=K,NOEL
      IF(ABS(UV(I)-UV(J)) .GT. 10.0) GOTO 95
      IF(ABS(FMASS(I)-FMASS(J)) .GT. 10.0) GOTO 95
      WRITE(6,96) I,J,II(I),JJ(I),MM(I),II(J),JJ(J),MM(J)
   96 FORMAT(' ELEMENTS THE SAME',/,8I6)
   95 CONTINUE
C********* INITIALIZE DISPLACEMENT ARRAY,TIMES ECT. ****************************
      DO 101 I=1,N2
      UV(I)=0.0
  101 CONTINUE
      TOTIME=0.0
      VD=0.0
      NEW=.TRUE.
      N2 =NONODE*2
  103 FORMAT(I4,F12.1)
      IW3=IW2
C***** INTERPOLATE FOR INTITIAL STRESS AND DENSITY FROM ARRAYS SPRES,SDENS *****
      DO 230 I=1,NOEL
      XS=(X(II(I))+X(JJ(I))+X(MM(I)))/3.0D0
      A=PX(XS,SPRES,AA)
      IF(XS .LT. 5000.0)A=XS*1030.0*9.8
      STRESS(1,I)=-A
      STRESS(2,I)=-A
      STRESS(3,I)=-A
      STRESS(4,I)=0.0
      A=PX(XS,SDENS,AA)
      BREAK(I)=A
  230 CONTINUE
      FIRST=.TRUE.
C******* CHECK ORDER OF II(I),JJ(I),MM(I) SO POSITIVE AREA ********************
C******** COMPUTE GRAVITATIONAL BODY FORCES ***********************************
      CALL MASS
C**** HEAT FLUX AT 70 KM IN CONDUCTION MODEL ADDED TO BASE IN ARRAY HEAT  ******
      DO 400 K=2,IW1
      I=TS(K-1)
      J=TS(K)
      YS=DABS(0.5*(Y(J)-Y(I))*0.0254)
      HEAT(I)=HEAT(I)+YS
      HEAT(J)=HEAT(J)+YS
  400 CONTINUE
C*** CALCULATE TOTAL AREA AS CHECK *****RADIOGENIC HEAT ADDED TO HEAT***********
      SAREA=0.0D0
      DO 300 K=1,NOEL
      KI=II(K)
      KJ=JJ(K)
      KM=MM(K)
      AREA=0.5*((X(KI)-X(KM))*(Y(KJ)-Y(KM))-(X(KJ)-X(KM))*(Y(KI)-Y(KM)))
      SAREA=SAREA+AREA
      XM=(X(KI)+X(KJ)+X(KM))/3.0-5000.0
      SQ=0.11E-10
      IF(XM .LT. 100.0E+3) SQ=0.6E-10
      IF (XM .LT. 7.0E+3) SQ=1.6E-10
      SH=AREA*SQ*BREAK(K)/3.0
      HEAT(KI)=HEAT(KI)+SH
      HEAT(KJ)=HEAT(KJ)+SH
      HEAT(KM)=HEAT(KM)+SH
  300 CONTINUE
      WRITE(6,199) SAREA
  199 FORMAT(' TOTAL AREA ',E20.15)
C******** SAVE RESULTS FOR RUNNING IN FINITE ELEMENT PROGRAM ******************
      LEN=32000
      CALL TIME(1,1)
      CALL WRITE(OUTPUT(1),LEN,1,1,8,66000)
      CALL WRITE(OUTPUT(400),LEN,1,1,8,66000)
      CALL WRITE(OUTPUT(800),LEN,1,1,8,66000)
      LEN=31744
```

```
      CALL WRITE(OUTPUT(12001),LEN,1,I,8,*6000)
      REWIND 8
      WRITE(6,10) IW4
   10 FORMAT(' WRITE COMPLETE IW4=',I6)
      CALL TIME(1,1)
      STOP
 6000 CONTINUE
      WRITE(6,6001)
 6001 FORMAT(' WRITE ERROR+++++++++++++++++++')
      STOP 22222
      END



      SUBROUTINE MASS
C****** CHECKS FOR ZERO AREA (MASS-SPECIFIED) ELEMENTS ************************
C***** CALCULATES GRAVITATIONAL BODY FORCES ***************************
      COMMON /COM1/AREA,DL(3,3),DR(3,6),AK(6,6),B(3,6),PHS(1980),
     1 DTEMP(990),SPROPS(6,1000),APR(1400),ST(3),
     2 STRESS(4,1900),UV(1980),X(990),Y(990),TOTIME,DTIM,HEATM(990),
     3 HTIM,EMASS(1980),TEMP(990),BREAK(1900),VD,HEAT(990),
     4 II(1900),JJ(1900),MM(1900),TP(1900),TS(260),
     5 NONODE,NOEL,N2,IW,IW1,IW2,IW3,IW4,IW5,GY,NO(6),FIRST,FRACT,NEW
      REAL*8 X,Y,RHS,STRESS,D,AK,DB,DTIM,AREA,ST,B,VD
      REAL*8 TOTIME,HTIM
      INTEGER*2 II,JJ,MM,CONSTR,TFIX,TP,TS
      LOGICAL FIRST,FRACT,NEW
      REAL*8 DAREA,DY1,DY2,DY3,DX1,DX2,DX3
      DO 10 I=1,N2
   10 EMASS(I)=0.0D0
   15 FRACT=.TRUE.
      DO 20 K=1,NOEL
   16 KI=II(K)
      KJ=JJ(K)
      KM=MM(K)
      AREA=(X(KI)-X(KM))*(Y(KJ)-Y(KM))-(X(KJ)-X(KM))*(Y(KI)-Y(KM))
      IF (AREA .GT. 0.0D0) GOTO 17
      IF (AREA .LT. 0.0D0) GOTO 13
      WRITE(6,12) K,KI,KJ,KM
   12 FORMAT(' AREA OF ELEMENT ',I6,' WITH NODES',3I6,' IS ZERO')
      FRACT=.FALSE.
      GOTO 20
   13 II(K)=KJ
      JJ(K)=KI
      GOTO 16
   17 CONTINUE
      AREA=AREA*0.5D0
      DEN=BREAK(K)*AREA*9.8/3.0D0
      EMASS(2*KI-1)=EMASS(2*KI-1)+DEN
      EMASS(2*KJ-1)=EMASS(2*KJ-1)+DEN
      EMASS(2*KM-1)=EMASS(2*KM-1)+DEN
   20 CONTINUE
C ********* STOPS PROGRAM IF ANY ZERO AREA ELEMENTS FOUND *****************
      IF (.NOT. FRACT) STOP 6
      RETURN
      END
```

A2.4 PROGRAM SLOPE

The visco-elastic heat flow program SLOPE was used for model 3 in section 6.3. The resources required for the solution required the analysis be made in several runs of the program, data being stored on route ※8 between each time step.

Route ※8 data and the pressure table (route ※3 from CONDEPTH) were read together with the time step, velocity of part of the boundary (DY) and time at which it was desired to stop the analysis for intermediate or final plotting.

The indexing for the array storage was performed at the start of the program and that for the visco-elastic analysis and heat flow analysis stored in temporary sequential files on routes ※14 and ※2 respectively. Visco-elastic and heat flow analyses were performed alternately and the results output to ※8 after each time step so that any interruption to the program caused the least possible recomputing.

Much of the computing was done in subroutines and is described by comments in the listings.

```
C*************************************************************************
C     PROGRAM TO PERFORM FINITE ELEMENT VISCO-ELASTIC ANALYSIS WITH TRANSIENT
C      THERMAL ANALYSES TO ALLOW FOR CHANGES IN TEMERATURE.
C*************************************************************************
      COMMON /SEIG/ IND(1980),JND(24000),ISP,ISDUM,AND3(1980),AT(24000)
      INTEGER*2 IND,JND
      COMMON /CCM1/AREA,D(3,3),DB(3,6),AK(6,6),B(3,6),RHS(1980),
     1 DTEMP(990),SPROPS(5,190),APR(1600),ST(3),
     2 STRESS(4,1900),UV(1980),X(990),Y(990),TOTIME,DTIM,HEATM(990),
     3 HTIM,EMASS(1980),TEMP(990),BREAK(1900),VD,HEAT(990),
     4 II(1900),JJ(1900),MM(1900),TP(1900),IS(260),
     5 NONODE,NOEL,N2,IW,IW1,IW2,IW3,IW4,IW5,DY,ND(6),FIRST,FPACT,NEW
      REAL*8 X,Y,RHS,STRESS,D,AK,DB,DTIM,AREA,ST,B,VD
      REAL*8 TOTIME,HTIM
      INTEGER*2 II,JJ,MM,CONSTR,TFIX,TP,TS
      LOGICAL FIRST,FPACT,NEW
      REAL*8 HA,G4,GB,GC,HB,GX,D1,D2,D3,S1,S2,S3,S4,DS1,DS2,DS3,
     1 DS4,SM
      REAL*8 OUTPUT(15968)
      EQUIVALENCE(OUTPUT(1),STRESS(1))
      INTEGER*2 LEN
      INTEGER*2 ITEMP(990),INDT(1980),JNDT(24000)
      EQUIVALENCE (ITEMP(1),SPROPS(1)),(INDT(1),AT(1)),
     1 (JNDT(1),INDT(1981)),(ISPT,JNDT(24001))
      CALL TIME(0)
C****** READ INITIAL OUTPUT FROM PROGRAM <INITIAL> OR ************************
C****** INTERMEDIATE OUTPUT FROM THIS PROGRAM FROM ROUTE#8*********************
      LEN=32000
      CALL READ(OUTPUT(1),LEN,1,I,8,66000)
      CALL READ(OUTPUT(4001),LEN,1,I,8,66000)
      CALL READ(OUTPUT(8001),LEN,1,I,8,66000)
      LEN=31744
      CALL READ(OUTPUT(12001),LEN,1,I,8,66000)
      REWIND 8
   15 FORMAT(F14.6)
C****** READ TIME STEP (YEARS) VELOCITY OF MOVING BOUNDARY (CM/YR) ************
      READ(5,15)TIMM,DY,FINTIM
      DTIM=3.155815D+7*TIMM
      DY=DY/3.155815D+7/100.0
      NW1=0
C****** READ PRESSURE AS FUNCTION OF DEPTH FROM PROGRAM <CONDEPTH>*************
C****** ROUTE#3 ***************************************************************
      READ(3,4) APR
    4 FORMAT(20A4)
      DO 220 I=1,NONODE
      DTEMP(I)=0.0
  220 CONTINUE
      A=TOTIME/3.155815E+7
      SG=DY*3.155815E+7
      WRITE(6,209) A,TIMM,SG
  209 FORMAT(' *********START TIME=',F14.2,'YEARS',/,
     1 ' INCREMENT ',F14.2,' YEARS',/' FORCED MOVEMENT ',F12.8,
     1 ' METRES/YEAR')
      NEW=.FALSE.
C****** SET UP INDEXING FILES FOR SOLVE AND TEMPGR ****************************
  401 ISP=0
      ISPT=0
      CALL TIME(1,1)
      DO 150 I=1,NONODE
  150 ITEMP(I)=0
      DO 160 I=1,NONODE
      DO 161 J=1,NOEL
      IF(II(J) .NE.I .AND.JJ(J).NE.I.AND.MM(J).NE.I)GOTO 161
      ITEMP(II(J))=1
      ITEMP(JJ(J))=1
      ITEMP(MM(J))=1
  161 CONTINUE
      ITEMP(I)=0
      ISP=ISP+1
      JND(ISP)=2*I
      DO 162 J=1,NONODE
      IF (ITEMP(J) .EQ.0 )GOTO 162
      ISP=ISP+1
      ISPT=ISPT+1
      JNDT(ISPT)=J
      JND(ISP)=2*J-1
      ISP=ISP+1
      JND(ISP)=2*J
      ITEMP(J)=0
  162 CONTINUE
      INDT(I)=ISPT
      IND(2*I-1)=ISP
      ISP=ISP+1
```

```
      JND(ISP)=2*I-1
      IP=2
      IF (I .GT.1)IP=IND(2*I-2)+2
      JP=ISP-IP+1
      MP=ISP-1
      DO 163 J=IP,MP
      JND(J+JP)=JND(J)
  163 CONTINUE
      ISP=MP+JP
      IND(2*I)=ISP
  160 CONTINUE
C****** NUMBER OF NON-ZERO TERMS FOR VISCOELASTIC AND THERMAL ***************
C************** EQUATIONS ***************************************************
      WRITE(6,170) ISP,ISPT
  170 FORMAT(' NUMBER OF POSSIBLE TERMS ',2I8)
C********STORE INDEX FOR THERMAL ANALYSIS IN FILE #1 ***************************
C********STORE INDEX FOR VISCO-ELASTIC ANALYSIS IN FILE #2 **********************
      LEN=32000
      CALL WRITE(IND(1),LEN,1,I,2,&6000)
      LEN=19964
      CALL WRITE(IND(16001),LEN,1,I,2,&6000)
      REWIND 2
      LEN=32000
      CALL WRITE(INDT(1),LEN,1,I,1,&6000)
      LEN=19964
      CALL WRITE(INDT(16001),LEN,1,I,1,&6000)
      REWIND 1
C****** RETURN TO 501 AT END OF EACH TIME STEP **********************************
  501 CONTINUE
      SG=0.0
C******* CLACULATE PROPERTIES FOR THIS TIME STEP *********************************
      CALL PROPS
C******** RECALL FILE #2 *********************************************************
      LEN=32000
      CALL READ(IND(1),LEN,1,I,2,&6000)
      LEN=19964
      CALL READ(IND(16001),LEN,1,I,2,&6000)
      REWIND 2
      NEW=.FALSE.
C********INITIALIZE RHS WITH GRAVITATIONAL BODY FORCES IN FMASS *****************
      DO 720 I=1,N2
  720 RHS(I)=FMASS(I)
C****** FORM AND SOLVE VISCO-ELASTIC EQUATIONS **********************************
      CALL SOLVE
      DSMAX=0.0
      HVM=0.0
C******** UPDATE STRESSES IN ELEMENTS ********************************************
      DO 800 K=1,NOEL
      E1=SPROPS(1,K)
      AN1=SPROPS(2,K)
      VIS=SPROPS(5,K)
      TEX=SPROPS(6,K)
      GA=E1*(1.0-AN1)/((1.0+AN1)*(1.0-2.0*AN1))
      GB=GA*AN1/(1.0-AN1)
      GC=0.5*(GA-GB)
      F=DTIM*GC/VIS
      GX=DEN2(F)
      I=II(K)
      J=JJ(K)
      M=MM(K)
      CALL FORMBT(B,X,Y,I,J,M,AREA)
      D1=B(1,1)*UV(2*I-1)+B(1,3)*UV(2*J-1)+B(1,5)*UV(2*M-1)
      D2=B(2,2)*UV(2*I)+B(2,4)*UV(2*J)+B(2,6)*UV(2*M)
      D3=B(2,2)*UV(2*I-1)+B(1,1)*UV(2*I)+B(2,4)*UV(2*J-1)
     1  +B(1,3)*UV(2*J)+B(2,6)*UV(2*M-1)+B(1,5)*UV(2*M)
      S1=STRESS(1,K)
      S2=STRESS(2,K)
      S3=STRESS(3,K)
      S4=STRESS(4,K)
      HA=GX*GA
      HB=GX*GB
      GX=F*GX/3.0
      STRESS(1,K)=S1-GX*(2.000*S1-S2-S3)+HA*D1+HB*D2
      STRESS(2,K)=S2-GX*(2.000*S2-S1-S3)+HB*D1+HA*D2
      STRESS(3,K)=S3-GX*(2.000*S3-S1-S2)+HB*(D1+D2)
      STRESS(4,K)=S4-3*GX*S4+0.5*D3*(HA-HB)
C***** CALCULATE ADIABETIC HEAT FOR EACH ELEMENT ***************************************
      DP=(STRESS(1,K)-S1+STRESS(2,K)-S2+STRESS(3,K)-S3)/3.0
      A=(TEMP(I)+TEMP(J)+TEMP(M))/3.0
      HTM=-A*DP*TEX*AREA
C****** FIND MAXIMUM CHAGE IN STRESS FOR MONITORING ***********************************
C****** VISCO-ELASTIC ANALYSIS ********************************************************
      SMAX=DABS(STRESS(1,K)-S1)+DABS(STRESS(2,K)-S2)+DABS(STRESS(3,K)-S
```

```
     1 3) +DABS(STRESS(4,K)-S4)
      IF(DSMAX .GT.SMAX) GOTO 790
      KS=K
      DSMAX=SMAX
      S1K=S1
      S2K=S2
      S3K=S3
      S4K=S4
      DPS=DP
      DXK=(X(I)+X(J)+X(M))/3.0
  790 CONTINUE
C******** CALCULATE VISCOUS HEATING ***********************************************
      U=DEN2(F)
      IF(F .GT. 0.01) V=1.0-2*U+DEN2(2.0*F)
      IF(F .LE. 0.01) V=F*F*(1.0/3.0-F*(0.25-F/20.01))
      TAU=VIS/GC
      Z1=DTIM/(6.0*VIS)*((S1-S2)**2+(S2-S3)**2+(S3-S1)**2+6*S4*S4)
      DS1=(2*S1-S2-S3)/TAU/3.0-(GA*D1+GB*D2)/DTIM
      DS2=(2*S2-S1-S3)/TAU/3.0-(GA*D2+GB*D1)/DTIM
      DS3=(2*S3-S1-S2)/TAU/3.0-(D1+D2)*GB/DTIM
      DS12=S4/TAU-GC*D3/DTIM
      Z2=-DTIM*(1-U)*(DS1*(2*S1-S2-S3)+DS2*(2*S2-S1-S3)+DS3*
     1 (2*S3-S1-S2)+6.0*DS12*S4)/(3.0*GC)
      Z3=TAU*DTIM/(6.0*GC)*V*((DS1-DS2)**2+(DS2-DS3)**2
     1 +(DS3-DS1)**2+6*DS12*DS12)
      HV=AREA*(Z1+Z2+Z3)
C******** TOTAL MECHANICAL HEAT INPUT TO ARRAY HEATM ***************************
      HTM=(HTM+HV)/3.0
      HEATM(I)=HEATM(I)+HTM
      HEATM(J)=HEATM(J)+HTM
      HEATM(M)=HEATM(M)+HTM
  800 CONTINUE
      WRITE(6,801)KS,DSMAX,STRESS(1,KS),S1K,STRESS(2,KS),S2K,
     1 STRESS(3,KS),S3K,STRESS(4,KS),S4K,TP(KS),DPS,SPROPS(5,KS),
     2 BREAK(KS),DXK
  801 FORMAT(' STRESS CHANGE',I6,E14.5,/' NEW         OLD'/,4(2E14.5,/),
     1 I6,4F14.5)
      NEW=.FALSE.
C******** INCREMENT TIME AND MOVE NODES ********************************************
      TOTIME=TOTIME+DTIM
      DO 511 I=1,NCNODE
      X(I)=X(I)+UV(2*I-1)
  511 Y(I)=Y(I)+UV(2*I)
      HTIM=HTIM+DTIM
C******* ADD ADDITIONAL HEAT FLUX TO UPPER SURFACE *****************************
C****** SEE SECTION 6.1 FOR EXPLANATION ***************************************
      IT=0
      A=30.0E+3
      IN=1
      JN=IW1-1
  510 DO 512 I=IN,JN
      J=TS(I)
      K=TS(I+1)
      R=DTIM*DSQRT((X(J)-X(K))**2+(Y(J)-Y(K))**2)
      H1=3.0*(ENTEMP(X(J))-TEMP(J))/A
      H2=3.0*(ENTEMP(X(K))-TEMP(K))/A
      HEATM(J)=HEATM(J)+R*(H1/3.0+H2/6.0)
      HEATM(K)=HEATM(K)+R*(H1/6.0+H2/3.0)
  512 CONTINUE
      IF(IT .EQ.1) GOTO 513
      IT=1
      IN=IW2
      JN=IW3-1
      A=3.0E+3
      GOTO 510
  513 CONTINUE
C******* THERMAL SOLUTION *****************************************************
      CALL TEMPGR
      CALL TIME(1,1)
  514 A=TOTIME/3.155815E+7
      NW1=NW1+1
      VD=VD+DTIM*DY
      WRITE(6,615)NW1,A,VD
  615 FORMAT(' ITER',I4,' AT ',F12.4,' YEARS', ' SUBDUCTION EXTENDS  ',
     1 'TO ',F14.6,' METRES')
C****** STORE RESULTS AT END OF THIS TIME STEP IN FILE #8 *********************
      LEN=32000
      CALL WRITE(OUTPUT(1),LEN,1,I,8,66000)
      CALL WRITE(OUTPUT(4001),LEN,1,I,8,66000)
      CALL WRITE(OUTPUT(8001),LEN,1,I,8,66000)
      LEN=31744
      CALL WRITE(OUTPUT(12001),LEN,1,I,8,66000)
      REWIND 8
```

```
C***** TEST FOR END OF RUN ***************************************************
      IF(A .GT. FINTIM) STOP 20
C***** RETURN FOR NEXT TIME STEP *********************************************
      GOTO 501
 6000 CONTINUE
      WRITE(6,6001)
 6001 FORMAT(' READ WRITE ERROR+++++++++')
      STOP 2222
      END



      SUBROUTINE PROPS
      COMMON /COM1/AREA,D(3,3),DB(3,6),AK(6,6),P(3,6),RHS(1980),
     1 DTEMP(990),SPROPS(6,1900),APP(1600),ST(3),
     2 STRESS(4,1900),DV(1980),X(990),Y(990),TOTIME,DTIM,HEATM(990),
     3 HTIM,EMESS(1980),TEMP(990),BREAK(1900),VD,HEAT(990),
     4 II(1900),JJ(1900),MM(1900),TP(1900),TS(260),
     5 NCNODE,NCEL,N2,IW,IW1,IW2,IW3,IW4,IW5,DY,NO(6),FIRST,FRACT,NEW
      REAL*8 X,Y,RHS,STRESS,D,AK,DB,DTIM,AREA,ST,B,VD
      REAL*8 TOTIME,HTIM
      INTEGER*2 II,JJ,MM,CONSTR,TFIX,TP,TS
      LOGICAL FIRST,FRACT,NEW
      REAL*8 DPN
      REAL*8 B1,B2,B3,B4,B5
      REAL*8 A1,A2,A3,A4,A5,A6,A7,A8,A9
      REAL*8 PA,BB,BE,EA,EB,EC,ED,EE,S1,S2,S3
C****** CONSTANTS FOR OCEANIC CRUST ******************************************
      DATA PA,BB,BE,EA,EB,EC,ED,EE/1.15D-11,-1.40-5,-8.00-9,
     1  0.7695494240-11,-0.4196515938D-4,-0.70633705390-22,
     1  0.7717,235990-15,0.47881359550-8/
      DATA RHO0,RHO1,RHO2,RHO3/3240.0,80.0,60.0,3660.0/
      DATA RG,RF/2900.0,3400.0/
C****** CONSTANTS FOR MANTLE *************************************************
      DATA A1,A2,A3,A4,A5,A6,A7,A8,A9/+0.7982656C8D-11,
     1 -0.2979329991D-04,-0.1479570252D-21,+0.9338005087D-15,
     1 -0.3951057525D-C8,+0.2221268166D-32,-0.3016923432D-25,
     1 +0.1610151893D-18,+0.6275833522D-12/
      DATA B1,B2,B3,B4,B5/+0.5407121747D-11,-0.2679282686D-04,
     1 -0.4187858999D-22,+0.3593745755D-15,0.1010133626D-08/
      DO 2000 I=1,NOEL
      DPN=-(STRESS(1,I)+STRESS(2,I)+STRESS(3,I))/3.DO
      TEM=(TEMP(II(I))+TEMP(JJ(I))+TEMP(MM(I)))/3.0
      DTEM=TEM-300.0
      S1=DSQRT(0.25DC*(STRESS(1,I)-STRESS(2,I))**2+STRESS(4,I)**2)
      S2=(STRESS(1,I)+STRESS(2,I))/2.0DO
      S3=STRESS(3,I)
C******* MAXIMUM SHEAR STRESS FOR CALCULATION OF VISCOSITY *************
      SH=(DMAX1(S1+S2,S2-S1,S3)-DMIN1(S1+S2,S2-S1,S3))/2.0DO
      SMIN=-DPN-SH
      SMAX=-DPN+SH
C******* TEST FOR FRACTURE ****************************************************
      T=0.5E+8
      IF (SH .LT. 10.0E+8) GOTO 111
      FAIL=1.0
      GOTO 444
  111   IF(3.0*SMAX+SMIN .LT. 0.01 GOTO 222
      FAIL=SMAX/T-1.0
      GOTO 444
  222 IF (SMAX .LT. -4.19*T)GOTO 333
      FAIL=((SMAX-SMIN)/T)**2+8.0*(SMIN+SMAX)/T
      GOTO 444
  333 CONTINUE
      FAIL=(2.356*SMAX-0.356*SMIN)/T-0.02
  444 CONTINUE
      PN=DPN
      PN=AMAX1(1000.0,PN)
      SH=AMAX1(100.0,SH)
C******** TP(I)=1 MANTLE          TP(I)=2 OCEANIC CRUST ***********************
      IF (TP(I) .EQ. 2) GOTO 200
C ******* MANTLE MATERIAL PROPERTIES********
      E=1.0+PN*(A1+PN*(A3+A6*PN))+DTEM*(A2+PN*(A4+A7*PN)+DTEM*(A5+
     1 A8*PN+A9*DTEM))
      AL0=A2+PN*(A4+A7*PN)+DTEM*(2.0*A5+2*A8*PN+3.0*A9*DTEM)
      BE0=A1+DTEM*(A4+A8*DTEM)+PN*(2*A3+3*A6*PN+2*A7*DTEM)
      SF=1.0D0+B1*PN+B2*DTEM+B3*PN*PN+B4*PN*DTEM+B5*DTEM*DTEM
      SAL0=B2+B4*PN+2.0D0*B5*DTEM
      SBE0=B1+2.0D0*B3*PN+B4*DTEM
      D1=0.001*(1000+DTEM-300.0E-8*PN)
      D2=0.0025*(964+DTEM-80.3E-8*PN)
      D3=0.0011*(2401.0+DTEM-30.0E-8*PN)
      D4=0.0014*(1500+9.0E-8*PN-DTEM)
      D5=0.0313*(200.0-1.0E-8*PN)
```

```
      F1=AMAX1(0.0,AMIN1(0.5-D1,1.0))
      F2=AMAX1(0.0,AMIN1(0.5-D2,1.0))
      F3=AMAX1(0.0,AMIN1(0.5-D3,1.0))
      F4=AMAX1(0.0,AMIN1(0.5-D4,1.0))
      F5=AMAX1(0.0,AMIN1(0.5-D5,1.0))
      G3=1.0-F3
      DFP1=3.0E-9
      DFP2=80.3E-8*0.0025
      DFP3=0.0011*30.0E-8
      DFP4=-0.0014*9.0E-8
      DFP5=0.0313E-8
      DFT1=-0.001
      DFT2=-0.0025
      DFT3=-0.0011
      DFT4=0.0014
C***** TEST FOR PHASE TRANSITIONS ***************************************
      IF(F1*(1.0-F1) .GT. 0.0001) GOTO 100
      DFP1=0.0
      DFT1=0.0
  100 IF (F2*(1.0-F2) .GT. 0.0001) GOTO 202
      DFP2=0.0
      DFT2=0.0
  202 IF(F3*(1.0-F3) .GT. 0.0001) GOTO 300
      DFP3=0.0
      DFT3=0.0
  300 IF(F4*(1.0-F4) .GT. 0.0001) GOTO 400
      DFP4=0.0
      DFT4=0.0
  400 IF (F5*(1.0-F5) .GT. 0.0001) GOTO 500
      DFP5=0.0
  500 CONTINUE
      E1=RHO0*RHO1*F1+RHO2*F2
      D1=E1*G3*F+RHO3*F3*SF
      DENN=C1*(1.0+0.08*F5)*(1.0-0.09*F4)
      DE1=RHO1*DFP1+RHO2*DFP2
      DD1=DE1*G3*F-E1*DFP3*F+E1*G3*BE0+RHO3*DFP3*SF+RHO3*F3*SBE0
      BETN=DD1*(1.0+0.08*F5)*(1.0-0.09*F4)+D1*(1-0.09*F4)*0.08*DFP5
     1 -0.09*D1*(1.0+0.08*F5)*DFP4
      BETN=BETN/DENN
      DE1=RHO1*DFT1+RHO2*DFT2
      DD1=DE1*G3*F-E1*DFT3*F+E1*G3*ALO+RHO3*DFT3*SF+RHO3*F3*SALO
      TEXN=DD1*(1+0.08*F5)*(1.0-0.09*F4)-0.09*D1*DFT4*(1.0+0.08*F5)
      TEXN=-TEXN/DENN
      CP=1033.84+0.19434*TEM-0.2419E+8/(TEM*TEM)
      R1=RHO1+RHO0
      R2=R1+RHO2
      R3=RHO3*SF
      R4=DENN/(1.0-0.09*F4)
      RX=R4*0.91
      CP=CP-DFT1*RHO1/(F*RHO0*R1)*(300.0E-8*PN-1527)/300.0E-8-DFT2*RHO2
     1 /(F*R1*R2)*(80.3E-8*PN-691.0)/80.3E-8-DFT3*(R3-R2*F)/(R3*R2*F)*
     1 (30.0E-8*PN-2127)/30.0E-8-DFT4*(RX-R4)/(PX*R4)*(1773+9.0E-8*PN)
     1 /9.0E-8
      VP=-2206.0+3.16*DENN
      VS=1.63*DENN-880.0
      IF (PN .LT. 3.0E+9) GOTO 10
      TMN=920.0+1.26E-7*PN
      VISN=ALOG(1.8E+13)+26.8*TMN/TEM-1.1*ALOG(SH)+6.909*F3
      GOTO 20
   10 TMN=1316.0+8.703E-8*PN-1.657E-17*PN*PN
      VISN=ALOG(2.1E+14)+40.0*TMN/TEM-2.0*ALOG(SH)
      IF(SH .GT. 1.0E+8)
     1 VISN=ALOG(1.1E+31)+40.0*TMN/TEM-4.0*ALOG(SH)
   20 CONTINUE
      BS=1.0/(0.0741+5.01E-4*TEM)
      GOTO 1000
  200 CONTINUE
C*********OCEANIC CRUST MATERIAL PROPERTIES********
      EQ=1.000+EA*PN+EB*DTEM+BE*DTEM*DTEM
      EE=1.000+EA*PN+EB*DTEM+EC*PN*PN+ED*PN*DTEM+EE*DTEM*DTEM
      AL1=BB+2.0*BE*DTEM
      AL2=EB+ED*PN+2*EE*DTEM
      BE1=BA
      BE2=EA+2*EC*PN+ED*DTEM
      D1=0.00069*(1500.0-2.3E-6*PN+DTEM)
      D2=0.002*(1080.0-DTEM+1.2E-7*PN)
      F1=AMAX1(0.0,AMIN1(0.5-D1,1.0))
      F2=AMAX1(0.0,AMIN1(0.5-D2,1.0))
      DFP1=0.00069*2.3E-6
      DFT1=-0.00069
      DFP2=-0.002*1.2E-7
      DFT2=0.002
C******** TEST FOR PHASE TRANSITIONS ***************************************
```

```
      IF (F1*(1.0-F1) .GT. 0.0001) GOTO 600
      DFP1=0.0
      DFT1=0.0
  600 IF(F2*(1.0-F2) .GT. 0.0001) GOTO 700
      DFP2=0.0
      DFT2=0.0
  700 CONTINUE
      DE1=(RG*FG*(1.0-F1)+RE*FE*F1)
      DENN=DE1*(1.0-0.09*F2)
      BETN=(RG*(BE1*(1.0-F1)-FG*DFP1)+RE*(BE2*F1+FE*DFP1))*(1.0-0.09*F2
     1 )-DE1*0.09*DFP2
      BETN=BETN/DENN
      TEXN=(RG*(AL1*(1.0-F1)-FG*DFT1)+RE*(AL2*F1+FE*DFT1))*(1.0-0.09*F2
     1 )-DE1*0.09*DFT2
      TEXN=-TEXN/DENN
      VP=3.16*DENN-3000.0
      VS=1.63*DENN-1280.0
      TMN=1067.0+1.2E-7*PN
      IF (PN .LT. 3.0E+8) TMN=1315.0-8.5E-7*PN+5.0E-16*PN*PN
      VISN=ALOG(1.5)+53.0*TMN/TEM-1.5*ALOG(SH)
      CP=988.56+0.2002*TEM-0.2503E+8/(TEM*TEM)
      CP=CP-(RE*FE-RG*FG)/(RE*FE*RG*FG)*(PN-1500.0/2.3E-6)*DFT1
     1 -0.09/(0.91*DE1)*(PN+1000.0/1.2E-7)*DFT2
      BS=2.1
 1000 CONTINUE
C*******COMMON PROPERTIES********
      VISN=AMIN1(100.0,VISN)
      VISN=AMAX1(50.0,VISN)
      IF(DTIM .LT. 3.1E+7) GOTO 1102
      IF(FAIL .LT. 0.0) GOTO 1101
      BREAK(I)=BREAK(I)+2
 1101 CONTINUE
      IF(BREAK(I) .GT.0) BREAK(I)=BREAK(I)-1
 1102 CONTINUE
      A=1.288E-6*VP*DENN**0.667
      COND=AMAX1(BS,A)
      IF (TEM .GT. 500.0) COND=COND+2.301E-3*(TEM-500.0)
      R=(VP/VS)**2
      ANU1=0.5*(R-2)/(R-1)
      E1=3.0*(1.0-2.0*ANU1)/BETN
      CV=CP-TEM*TEXN*TEXN/(DENN*BETN)
      VISN=(50.0*BREAK(I)+(10.0-BREAK(I))*VISN)/10.0
      VISN=AMAX1(50.0,AMIN1(100.0,VISN))
      VIS=EXP(VISN)
 1001 SPROPS(1,I)=E1
      SPROPS(2,I)=ANU1
      SPROPS(3,I)=COND
      SPROPS(4,I)=CV*DENN
C*****************************************************************************
C*****************************************************************************
C   REMOVE THE COMMENTS FROM THE START OF THES STATEMENTS FOR USING THIS
C   SUBROUTINE IN THE PLOTTING PROGRAMS
C
C       TEST=(F1*(F1-1)+F2*(F2-1)+F3*(F3-1)+F4*(F4-1))*100.0
C       IF(TP(I) .NE. 1)TEST=(F1*(F1-1)+F2*(F2-1))*100.0
C       SPROPS(3,I)=TEST
C       SPROPS(4,I)=DENN
C
C*****************************************************************************
C*****************************************************************************
      SPROPS(5,I)=VIS
      SPROPS(6,I)=TEXN
 2000 CONTINUE
      RETURN
      END
```

```
      SUBROUTINE RSEID(UV1,N)
C******* SOLVES N EQUATIONS BY SEIDAL-GAUSS ITERATIONS **********************
C******* ANSWERS IN UV1 ***************************************************
      DIMENSION UV1(1)
      COMMON /SEID/IND(1980),JND(24000),ISP,ISCUM,AND3(1980),AT(24000)
      INTEGER *2 IND,JND
      COMMON /COM1/AREA,D(3,3),DB(3,6),AK(6,6),B(3,6),RHS(1980),
     1 DTEMP(990),SPROPS(6,1900),APR(1600),ST(3),
     2 STRESS(4,1900),UV(1980),X(990),Y(990),TOTIME,DTIM,HEATM(990),
     3 HTIM,EMASS(1980),TEMP(990),BREAK(1900),VD,HEAT(990),
     4 II(1900),JJ(1900),MM(1900),TP(1900),TS(260),
     5 NONODE,NOEL,N2,IW,IW1,IW2,IW3,IW4,IW5,DY,NO(6),FIRST,FRACT,NEW
      REAL*8 X,Y,RHS,STRESS,D,AK,DB,DTIM,AREA,ST,B,VD
      REAL*8 TOTIME,HTIM
      INTEGER*2 II,JJ,MM,CONSTR,TFIX,TP,TS
      LOGICAL FIRST,FRACT,NEW
C *******ARRAYS FOR ADDITIONAL OVER-RELAXATION ********************************
      REAL*4 Z(1980),U2(1980)
      REAL*8 F1,SUM,DDD,BB,FSMALL,FD,A
      LOGICAL CHAN
      ISM=0
      F1=3.0D0
      ITER=0
      DO 10 I=1,N
   10 U2(I)=UV1(I)
  102 KP=0
      DO 440 I=1,N
  120 SUM=0.000
      JP=KP+1
      KP=IND(I)
      DO 820 IP=JP,KP
  820 SUM=SUM+AT(IP)*UV1(JND(IP))
      BB=(RHS(I)-SUM)/AND3(I)
      Z(I)=BB-UV1(I)
      UV1(I)=1.8D0*BB-0.8D0*UV1(I)
  440 CONTINUE
      JP=IND(N)+1
      DO 540 J=1,N
      I=N+1-J
      SUM=0.0D0
      KP=JP-1
      JP=1
      IF(I .GT.1)JP=IND(I-1)+1
      DO 520 IP=JP,KP
  520 SUM=SUM+AT(IP)*UV1(JND(IP))
      BB=(RHS(I)-SUM)/AND3(I)
      Z(I)=Z(I)+BB-UV1(I)
      UV1(I)=1.8D0*BB-0.8D0*UV1(I)
  540 CONTINUE
      ITER=ITER+1
      IF (MOD(ITER,6) .NE. 0) GOTO 102
      FSMALL =0.0D0
C********** CONVERGENCE TESTS ***********************************************
      DO 610 I=1,N
      FD=0.0D0
      BB=ABS(UV1(I))
      DDD=ABS(Z(I))
      IF (DDD .LT. 0.05) GOTO 610
      IF(BB .LT. 0.05) GOTO 610
      FD=DDD/BB
      IF (FD .LT. FSMALL) GOTO 610
      FSMALL=FD
      ISM=I
  610 CONTINUE
      IF (ITER .GT. 4000) GOTO 410
      IF (FSMALL .LT. 1.0E-4) GOTO 411
      CHAN=(MOD(ITER,12) .EQ.0)
C******* ADDITIONAL RELAXATION AFTER 12 ITERATIONS ***************************
      DO 1820 I=1,N
      A=UV1(I)-U2(I)
      U2(I)=UV1(I)
      IF (CHAN) GOTO 1820
      IF (A*Z(I) .GT. 1.0D-6) UV1(I)=UV1(I)+A*F1
 1820 CONTINUE
      IF (.NOT. CHAN) GOTO 102
      F1=(F1-1.0)/1.05+1.0
      GOTO 102
  411 WRITE(6,401) ITER
  401 FORMAT(17H CONVERGED AFTER  ,I6,12H ITERATIONS  )
      GOTO 500
  410 WRITE(6,402) ITER,FSMALL,UV1(ISM),ISM
  402 FORMAT(' NOT CONVERGED',I6,2E12.4,I6,F12.4,2(I6,2F12.4))
  500 SD=0.0
```

```
C********* OUTPUT TO MONITOR RUNNING OF VISCO-ELASTIC SOLUTION ***************
      DO 510 I=1,N
      IF(ABS(UV1(I)) .LT. SG) GOTO 510
      JT=I
      SG=ABS(UV1(I))
  510 CONTINUE
      WRITE(6,521) JT,UV1(JT)
  521 FORMAT(' MAXIMUM CHANGE FOR VARIABLE ',I8,E12.4)
      RETURN
      END



      FUNCTION VISD(K)
C******FORMS ARRAY DEPENDENT ON PROPERTIES FOR VISCO-ELASTIC ANALYSIS **********
C****** AND MODIFIES RHS OF EQUATIONS FOR INITIAL STRESS AND PROPERTIES*********
C****** OF ELEMENTS ***************************************************
      COMMON /COM1/AREA,D(3,3),DP(3,3),AK(6,6),B(3,6),RHS(1980),
     1 DTEMP(990),SPROPS(5,1900),APP(1600),ST(3),
     2 STRESS(4,1900),UV(1980),X(990),Y(990),TOTIME,DTIM,HEATM(990),
     3 HTIM,EMASS(1980),TEMP(990),BREAK(1900),VD,HEAT(990),
     4 II(1900),JJ(1900),MM(1900),TP(1900),TS(260),
     5 NONODE,NOEL,N2,IW,IW1,IW2,IW3,IW4,IW5,DY,NO(6),FIRST,FRACT,NEW
      REAL*8 X,Y,RHS,STRESS,D,AK,DB,DTIM,AREA,ST,B,VD
      REAL*8 TOTIME,HTIM
      INTEGER*2 II,JJ,MM,CONSTR,TFIX,TP,TS
      LOGICAL FIRST,FRACT,NEW
      REAL*8 GA,GB,GC,SX,SY,SZ,SXY,FA,FB,F,GX,GZ,HA,
     1 S1,S2,S3,HGS3
      REAL*8 B1,B2,B3,B4,B5,B6
C******* INCREASE SPEED BY USEING SIMPLE VARIABLES NOT ARRAY ELEMENTS **********
      EQUIVALENCE (B1,B(1,1)),(B2,B(1,3)),(B3,B(1,5)),
     1 (B4,B(2,2)),(B5,B(2,4)),(B6,B(2,6))
      E1=SPROPS(1,K)
      ANU1=SPROPS(2,K)
      VIS=SPROPS(5,K)
      I=II(K)
      J=JJ(K)
      M=MM(K)
C******* FORM VISCO-ELASTIC PROPERTY MATRIX ***************************@
      GA=E1*(1.0-ANU1)/((1.0+ANU1)*(1.0-2.0*ANU1))
      GB=GA*ANU1/(1.0-ANU1)
      GC=0.5*E1/(1.0+ANU1)
      F=DTIM*GC/VIS
      GZ=2.0*DEN(F)
      D(1,1)=GA*GZ
      D(2,2)=GA*GZ
      D(1,2)=GB*GZ
      D(2,1)=GB*GZ
      D(3,3)=GC*GZ
      CALL FORMBT(B,X,Y,I,J,M,AREA)
C********** MODIFY RHS FOR INITIAL STRESS AND VISCOSITY ***********************
      SX=STRESS(1,K)*AREA
      SY=STRESS(2,K)*AREA
      SZ=STRESS(3,K)*AREA
      SXY=STRESS(4,K)*AREA
      F=GZ*0.500*F
      S1=SX-F*(2*SX-SY-SZ)/3.0
      S2=SY-F*(2*SY-SX-SZ)/3.0
      HGS3=SXY*(1.0-F)
      RHS(2*I-1)=RHS(2*I-1)-(B1*S1+B4*HGS3)
      RHS(2*I)=RHS(2*I)-(B4*S2+HGS3*B1)
      RHS(2*J-1)=RHS(2*J-1)-(B2*S1+HGS3*B5)
      RHS(2*J)=RHS(2*J)-(B5*S2+HGS3*B2)
      RHS(2*M-1)=RHS(2*M-1)-(B3*S1+HGS3*B6)
      RHS(2*M)=RHS(2*M)-(B6*S2+HGS3*B3)
      VISD=SG
      RETURN
      END
```

```
      SUBROUTINE FORMBT(B,X,Y,I,J,K,AREA)
C******** FORM B MATRIX WHICH MAPS DISPLACEMENTS INTO STRAINS ***********************
      DIMENSION B(3,6),X(1),Y(1)
      REAL*8 B,AREA,X,Y,X1,X2,X3,Y1,Y2,Y3
    2 X1 =X(I)
      X2 =X(J)
      X3= X(K)
      Y1= Y(I)
      Y2= Y(J)
      Y3= Y(K)
      AREA=(X1 -X3)*(Y2-Y3)-(X2-X3)*(Y1-Y3)
   30 B(1,1)=(Y2-Y3)/AREA
      B(1,3)=(Y3-Y1)/AREA
      B(1,5)=(Y1-Y2)/AREA
      B(2,2)=(X3-X2)/AREA
      B(2,4)=(X1-X3)/AREA
      B(2,6)=(X2-X1)/AREA
      B(3,1)=B(2,2)
      B(3,2)=B(1,1)
      B(3,3)=B(2,4)
      B(3,4)=B(1,3)
      B(3,5)=B(2,6)
      B(3,6)=B(1,5)
      B(1,2)=0
      B(1,4)=0
      B(1,6)=0
      B(2,1)=0
      B(2,3)=0
      B(2,5)=0
      AREA=AREA/2.000
      RETURN
      END


      SUBROUTINE TEMPGR
C********** THERMAL SOLUTION ***************************************************
      COMMON /COM1/AREA,D(3,3),DB(3,6),AK(6,6),P(3,6),RHS(1980),
     1 DTEMP(990),SPROPS(6,1900),APR(1600),ST(3),
     2 STRESS(4,1900),UV(1980),X(990),Y(990),TOTIME,DTIM,HEATM(990),
     3 HTIM,EMASS(1980),TEMP(990),BREAK(1900),VD,HEAT(990),
     4 II(1900),JJ(1900),MM(1900),TP(1900),TS(260),
     5 NONODE,NOEL,N2,IW,IW1,IW2,IW3,IW4,IW5,DY,ND(6),FIRST,FRACT,NEW
      REAL*8 X,Y,RHS,STRESS,D,AK,DB,DTIM,AREA,ST,B,VD
      REAL*8 TOTIME,HTIM
      INTEGER*2 II,JJ,MM,CONSTR,TFIX,TP,TS
      LOGICAL FIRST,FRACT,NEW
      COMMON /SFIC/IND(1980),JND(24000),ISP,ISDUM,AND3(1980),AT(24000)
      INTEGER*2 IND,JND
      INTEGER*2 LEN
C****** RESTORE INDEX INFORMATION FOR THERMAL ANALYSIS FROM FILE #1 ************
      LEN=32000
      CALL READ(IND(1),LEN,1,I,1,&6000)
      LEN=19964
      CALL READ(IND(16001),LEN,1,I,1,&6000)
      REWIND 1
C****** INITIALIZE ARRAYS ********************************************************
      DO 171 I=1,ISP
      AT(I)=0.0
  171 CONTINUE
      IF(HTIM.EQ. 0) HTIM=1.0
C********* RHS= HEAT INPUT/UNIT TIME ***********************************************
      DO 10 I=1,NONODE
      RHS(I)=2.0*(HEAT(I)+HEATM(I)/HTIM)
      AND3(I)=0.0
   10 CONTINUE
C******** FORM THE THERMAL EQUATIONS ***********************************************
      DO 100 K=1,NOEL
      IP=II(K)
      JP=JJ(K)
      MP=MM(K)
      COND=SPROPS(3,K)
C********** CV=SPECIFIC HEAT /UNIT VOLUME ***************************************
      CV=SPROPS(4,K)
      BI=Y(JP)-Y(MP)
      BJ=Y(MP)-Y(IP)
      BM=Y(IP)-Y(JP)
      CI=X(MP)-X(JP)
      CJ=X(IP)-X(MP)
      CM=X(JP)-X(IP)
      AREA=0.5*(BI*CJ-BJ*CI)
      F=0.25*COND/AREA
      CO=2.0*AREA*CV/(HTIM*6.0)
```

```
      COD=0.5*CD
      FII=F*(BI*BI+CI*CI)
      FIJ=F*(BI*BJ+CI*CJ)
      FIM=F*(BI*BM+CI*CM)
      FJJ=F*(BJ*BJ+CJ*CJ)
      FJM=F*(BI*BM+CJ*CM)
      FMM=F*(BM*BM+CM*CM)
      TI=TEMP(IP)*FII+TEMP(JP)*FIJ+TEMP(MP)*FIM
      TJ=TEMP(IP)*FIJ+TEMP(JP)*FJJ+TEMP(MP)*FJM
      TM=TEMP(IP)*FIM+TEMP(JP)*FJM+TEMP(MP)*FMM
      RHS(IP)=RHS(IP)-2.0*TI
      RHS(JP)=RHS(JP)-2.0*TJ
      RHS(MP)=RHS(MP)-2.0*TM
      AND3(IP)=AND3(IP)+FII+COD
      AND3(JP)=AND3(JP)+FJJ+COD
      AND3(MP)=AND3(MP)+FMM+COD
      KI=1
      IF(IP .GT.1)KI=IND(IP-1)+1
      KL=IND(IP)
      DO 200 I=KI,KL
      IF(JND(I) .EQ. JP) AT(I)=AT(I)+FIJ+COD
      IF(JND(I) .EQ. MP) AT(I)=AT(I)+FIM+COD
  200 CONTINUE
      KI=1
      IF(JP .GT.1)KI=IND(JP-1)+1
      KL=IND(JP)
      DO 210 I=KI,KL
      IF(JND(I) .EQ. IP) AT(I)=AT(I)+FIJ+COD
      IF(JND(I) .EQ. MP) AT(I)=AT(I)+FJM+COD
  210 CONTINUE
      KI=1
      IF(MP .GT.1)KI=IND(MP-1)+1
      KL=IND(MP)
      DO 220 I=KI,KL
      IF(JND(I) .EQ.IP) AT(I)=AT(I)+FIM+COD
      IF(JND(I) .EQ.JP) AT(I)=AT(I)+FJM+COD
  220 CONTINUE
  100 CONTINUE
C******** FIXED TEMPERATURE ALONG SEA-BED ***************************************
      DO 230 JN=IW3,IW4
      I=TS(JN)
      KI=1
      IF(I .GT.1) KI=IND(I-1)+1
      KL=IND(I)
      DO 240 L=KI,KL
      AT(L)=0.0
  240 CONTINUE
      RHS(I)=0.0
      AND3(I)=1.0
  230 CONTINUE
C******* SOLVE EQATIONS *********************************************************
      CALL RSFID(DTEMP,NCNODE)
      HTIM=0.0
C******* CALCULATE AND APPLY THERMAL STRESSES ************************************
      DO 11 I=1,NOEL
      DTMEAN=(DTEMP(II(I))+DTEMP(JJ(I))+DTEMP(VM(I)))/3.0
      E1=SPROPS(1,I)
      ANU1=SPROPS(2,I)
      TEX=SPROPS(6,I)
      DSTR=E1*TEX*DTMEAN/(1.0-2.0*ANU1)/3.0
      STRESS(1,I)=STRESS(1,I)-DSTR
      STRESS(2,I)=STRESS(2,I)-DSTR
      STRESS(3,I)=STRESS(3,I)-DSTR
   11 CONTINUE
C****** REINITIALIZE MECANICAL HEAT SOURCES AND INCREMENT TEMPERATURES
      DO 500 I=1,NCNODE
      HEATM(I)=0.0
  500 TEMP(I)=TEMP(I)+DTEMP(I)
      RETURN
 6000 STOP 68
      END
```

```
      SUBROUTINE SOLVE
C******* SET UP AND SOLVE VISCO-ELASTIC EQUATIONS **************************
      COMMON /SEED/IND(1980),JND(24000),ISP,ISDUM,AND3(1980),AT(24000)
      INTEGER*2 IND,JND
      COMMON /COM1/AREA,D(3,3),DB(3,6),AK(6,6),B(3,6),RHS(1980),
     1 DTEMP(990),SPPOPS(6,1900),APP(1600),ST(3),
     2 STRESS(4,1900),DV(1980),X(990),Y(990),TOTIME,DTIM,HEATM(990),
     3 HTIM,EMASS(1980),TEMP(990),AREAM(1900),VD,HEAT(990),
     4 II(1900),JJ(1900),MM(1900),TP(1900),TS(260),
     5 NONODE,NOEL,N2,IW,IW1,IW2,IW3,IW4,IW5,DY,NO(6),FIRST,FRACT,NEW
      REAL*8 X,Y,RHS,STRESS,C,AK,CH,DTIM,AREA,ST,B,VD
      REAL*8 TOTIME,HTIM
      INTEGER*2 II,JJ,MM,CONSTR,TFIX,TP,TS
      LOGICAL FIRST,FRACT,NEW
      REAL*8 P1,P2,PN,XS,YS,DELD,E,PX
 7000 CONTINUE
      J=IND(N2)
C******* ZEROIZE ARRAYS ***************************************************
      DO 10 I=1,J
      AT(I)=0.0
   10 CONTINUE
      DO 20 I=1,N2
      AND3(I)=0.0
   20 CONTINUE
      D(1,3)=0.0D0
      D(2,3)=0.0D0
      D(3,1)=0.0D0
      D(3,2)=0.0D0
      DO 100 K=1,NOEL
      IP=II(K)
      JP=JJ(K)
      MP=MM(K)
      SG=VISD(K)
      DO 350 IIP=1,3
      DO 350 JJP=1,6
      DB(IIP,JJP)=D(IIP,1)*B(1,JJP)+D(IIP,2)*B(2,JJP)+D(IIP,3)*B(3,JJP)
  350 CONTINUE
      DO 351 IIP=1,6
      DO 351 JJP=1,IIP
      AK(IIP,JJP)=AREA*(B(1,IIP)*DB(1,JJP)+B(2,IIP)*DB(2,JJP)+
     1 B(3,IIP)*DB(3,JJP))
      AK(JJP,IIP)=AK(IIP,JJP)
  351 CONTINUE
      NO(1)=2*IP-1
      NO(2)=2*IP
      NO(3)=2*JP-1
      NO(4)=2*JP
      NO(5)=2*MP-1
      NO(6)=2*MP
      DO 400 IIK=1,6
      KT=NO(IIK)
      KI=1
      IF(KT .NE.1)KI=IND(KT-1)+1
      KL=IND(KT)
      DO 410 JJK=1,6
      IF(JJK .EQ.IIK) GOTO 410
      JK=NO(JJK)
      DO 420 LLK=KI,KL
      MK=LLK
      IF(JND(LLK) .EQ.JK)GOTO 421
  420 CONTINUE
      WRITE(6,999) K,KT,KI,KL,MK,JK
  999 FORMAT(' NOT FOUND ',6I6)
  421 AT(MK)=AT(MK)+AK(IIK,JJK)
  410 CONTINUE
      AND3(KT)=AND3(KT)+AK(IIK,IIK)
  400 CONTINUE
  100 CONTINUE
C******* APPLY BOUNDARY CONDITIONS ****************************************
C********* PUT ON HYDROSTATIC PRESSURE ***********************************
      IT=0
      ITB=1
      ITL=IW3-1
  690 DO 700 I=ITB,ITL
      J=TS(I)
      K=TS(I+1)
      YS=Y(K)-Y(J)
      XS=X(K)-X(J)
C******* P1,P2 PRESSURE AT DEPTHS OF J,K NODES ****************************
      P1=PX(X(J),APP,DELD)
      P2=PX(X(K),APP,E)
C****** REDUCE PRESSURE ON END OF MODEL ***********************************
      IF(J .LT. IW1 .OR. K .GT. IW2) GOTO 691
```

```
      P1=P1-4.0E+8
      P2=P2-4.0E+8
  691 CONTINUE
      DFLD=DMAX1(DFLD,F)
      PN=P1/3.0+P2/6.0
      RHS(2*J-1)=RHS(2*J-1)+YS*PN
      RHS(2*J)=RHS(2*J)-XS*PN
      PN=P1/6.0+P2/3.0
      RHS(2*K-1)=RHS(2*K-1)+YS*PN
      RHS(2*K)=RHS(2*K)-XS*PN
      F=DFLD*YS/3.0
      NO(1)=2*J-1
      NO(2)=2*J
      NO(3)=2*K-1
      NO(4)=2*K
      AK(1,1)=F
      AK(1,2)=-DFLD*XS/6.0
      AK(1,3)=F/2
      AK(1,4)=(2*P1+P2)/6.0
      AK(2,1)=AK(1,2)
      AK(2,2)=0.0
      AK(2,3)=-(P1+2.0*P2)/6.0
      AK(2,4)=0.0
      AK(3,1)=AK(1,3)
      AK(3,2)=AK(2,3)
      AK(3,3)=F
      AK(3,4)=-DFLD*XS/6.0
      AK(4,1)=AK(1,4)
      AK(4,2)=AK(2,4)
      AK(4,3)=AK(3,4)
      AK(4,4)=0.0
      DO 710 IIK=1,4
      KT=NO(IIK)
      KI=1
      IF(KT .GT.1)KI=IND(KT-1)+1
      KL=IND(KT)
      DO 720 JJK=1,4
      IF(JJK.EQ.IIK .OR. AK(IIK,JJK) .EQ.0.0) GOTO 720
      JK=NO(JJK)
      DO 730 LLK=KI,KL
      MK=LLK
      IF(JND(LLK).EQ.JK)GOTO 731
  730 CONTINUE
  731 AT(MK)=AT(MK)-AK(IIK,JJK)
  720 CONTINUE
      AND3(KT)=AND3(KT)-AK(IIK,IIK)
  710 CONTINUE
  700 CONTINUE
  750 CONTINUE
C******* HYDROSTATIC PRESSURE ON ENDS AND BASE NOW ENTERED ***********************
C******* PUT ON HYDROSTAIC  PRESSURE OF SEA ***********************************
      ITL=IW4-1
      A=1030.0*9.8
      FIRST=.TRUE.
      DO 760 I=IW3,ITL
      J=TS(I)
      K=TS(I+1)
      P1=X(J)*A
      P2=X(K)*A
      IF(X(J) .LT. 8000.0 .OR. .NOT. FIRST) FIRST=.FALSE.
      IF(.NOT. FIRST) GOTO 751
C******* INCREASE PRESSURE AS SURFACE NODES SINK FROM 8KM TO 11KM **************
      F=(11000.0-X(J))/3000.0
      F=DMAX1(0.000,DMIN1(1.000,F))
      P1=F*P1+(1.0-F)*PX(X(J),APR,DFLD)
      F=(11000.0-X(K))/3000.0
      F=DMAX1(0.000,DMIN1(1.000,F))
      P2=F*P2+(1.0-F)*PX(X(K),APR,DFLD)
  751 CONTINUE
      IF (X(J) .LT. 0.0) P1=0.0
      IF(X(K) .LT. 0.0) P2=0.0
      XS=X(J)-X(K)
      YS=Y(K)-Y(J)
      PN=P1/3.0+P2/6.0
      RHS(2*J-1)=RHS(2*J-1)+PN*YS
      RHS(2*J)=RHS(2*J)+PN*XS
      PN=P1/6.0+P2/3.0
      RHS(2*K-1)=RHS(2*K-1)+PN*YS
      RHS(2*K)=RHS(2*K)+PN*XS
  760 CONTINUE
      J=TS(IW3+1)
      IF(X(J) .GT. 11000.0) IW3=IW3+1
      DO 3600 I=1,IW1
```

```
      J=TS(I)
      K=TS(I+1)
      IF (Y(J) .GE. -1.0) GOTO 3000
C****** FORCE NODES ON BASE WITH Y<0.0 TO FOLLOW EACH OTHER **********
C****** DOWN SUBDUCTION ZONE ***************************************
C****** CORNER FORCED TO MOVE WITH DIP OF 70 DEGREES ****************
      TANTH=-(X(J)-X(K))/(Y(J)-Y(K))
      IF (I .EQ. IW1) TANTH=DSQRT(3.000)
      IF(TANTH .LT. 1.0) GOTO 2900
      IP=IND(2*J-2)+1
      IK=IP+1
      IL=IND(2*J-1)
      JP=IL+1
      JL=IND(2*J)
      JK=IL+2
      DO 3100 IK=IK,IL
      AT(IK)=AT(IK)-AT(JK)/TANTH
      AT(JK)=0.0
      JK=JK+1
 3100 CONTINUE
      AT(IP)=AT(IP)-AND3(2*J)/TANTH
      AND3(2*J-1)=AND3(2*J-1)-AT(JP)/TANTH
      AT(JP)=1.0/TANTH
      AND3(2*J)=1.0
      RHS(2*J-1)=RHS(2*J-1)-RHS(2*J)/TANTH
      RHS(2*J)=0.0
      GOTO 3000
 2900 JP=IND(2*J-2)+1
      JK=JP+1
      JL=IND(2*J-1)
      IP=JL+1
      IK=IP+1
      IL=IND(2*J)
      DO 3101 IK=IK,IL
      AT(IP)=AT(IK)- AT(JK)*TANTH
      AT(JK)=0.0
      JK=JK+1
 3101 CONTINUE
      AT(IP)=AT(IP)-AND3(2*J-1)*TANTH
      AND3(2*J)=AND3(2*J)-AT(JP)*TANTH
      AT(JP)=TANTH
      AND3(2*J-1)=1.0
      RHS(2*J)=RHS(2*J)-RHS(2*J-1)*TANTH
      RHS(2*J-1)=0.0
 3000 CONTINUE
C***** FORCE END TO MOVE WITH HORIZONTAL VELOCITY OF DY M/YR **********
      DO 800 JN=IW4,IW
      I=TS(JN)
      N=2*I
      AND3(N)=1.0
      RHS(N)=-DY*DTIM/3.155158E+7
      KI=IND(N-1)+1
      KL=IND(N)
      DO 805 J=KI,KL
      AT(J)=0.0
  805 CONTINUE
  800 CONTINUE
      CALL RSEID(UV,N2)
      RETURN
      END
```

```
      FUNCTION FNTEMP(HA)
C***** CALCULATES NORMAL THERMAL GRADIENT ***************************************
      REAL*8 HA
      X=HA/1000.0
      IF(X .GT. 100.0)  GOTO 10
C******** CONDUCTIVE GEOTHERM ***********************************************
      FNTEMP=176.94+X*(19.895-X*(0.12896-X*(0.56553E-3-X*(0.14517E-5
     1 -X*(0.21222E-8-X*(0.16426E-11-X*0.52222E-15))))))
      RETURN
C****** CONVECTIVE GEOTHERM ************************************************
   10 FNTEMP=1150.0+1.4*X
      RETURN
      END



      DOUBLE PRECISION FUNCTION DEN(X)
      IMPLICIT REAL*8 (A-H,O-Z)
C******* EVALUATE (1/X-1/X**2*(1-EXP(-X))) ******************************
C ********** CARE NEEDS TO BE TAKEN FOR SMALL VALUES OF X*********************
      IF (X .GT. 0.00001) GOTO 20
      DEN=0.500*(1.000-X/3.000*(1.000-X/4.000*(1.000-X/5.000*(1.000
     1 -X/6.000*(1.000-X/7.000)))))
      RETURN
   20 DEN=1.000/X-(1.000-1.000/X*(1.000-DEXP(-X)))
      RETURN
      END



      DOUBLE PRECISION FUNCTION DEN2(X)
      IMPLICIT REAL*8(A-H,O-Z)
C******** EVALUATE (1-EXP(-X))/X ***************************************
C******* CARE NEEDS TO BE TAKEN FOR SMALL VALUES OF X ***********************
      IF(X .GT. 0.00001) GOTO 30
      DEN2=(1.000-X/2.000*(1.000-X/3.000*(1.000-X/4.000*(1.000
     1 -X/5.000*(1.000-X/6.000*(1.000-X/7.000))))))
      RETURN
   30 DEN2=(1.000-DEXP(-X))/X
      RETURN
      END



      DOUBLE PRECISION  FUNCTION PX(X,AP,DP)
C****** INTERPOLATE PRESSURE AND PRESSURE GRADIENT (DP) FOR ****************
C******* DEPTH X FROM VALUES IN ARRAY AP *************************************
      REAL*8 X,DP,XS,DX
      DIMENSION AP(1)
      XS=X/1000.0-5.0
      NX=XS*2.0
      DX=NX*0.5
      NX=NX+1
      IF(XS .LT.0.0) GOTO 80
      PX=(AP(NX)*(0.5-XS+DX)+AP(NX+1)*(XS-DX))*2.0
      DP=(AP(NX+1)-AP(NX))/500.0
      RETURN
   80 DP=1030.0*9.8
      PX=X*DP
      RETURN
      END
```

A2.5 PROGRAM PLOT*1

This program reads the data stored in file *8 and plots various parameters of the elements on a X-Y plotter.

The input is

Route *8 output from SLOPE

Route *3 pressure variation with depth (CONDEPTH)

Route *5 Y and X boundaries of the plot in km.
and a code as to what is to be plotted.

The Y and X extremes of the plot are read one per line followed by the maximum length of the plot (pmx) in F12.4 format.

The two codes IPLOT and K are read in 2I2 format. Valid values of IPLOT and the variable or symbol plotted at the centre of each element are

1 number of element

2 spare

3 cross at centre of element

4 only the finite element net

5 principal stresses

6 lines of likely failure

7 principal stresses - standard pressure

8 flow lines (at nodes)

9 log viscosity

10 break (state of failure of element)

11 phase transition function

if k = 0 the finite element net is also drawn.

This program also used SUBROUTINES PROPS (with the marked comments removed) and PX from PROGRAM SOLVE (Pages 170 and 178).

```
C*********=*********=*********=*********=*********=*********=*********=**
C********** PROGRAM TO PLOT NUMBERS AND SYMBOLS AT THE CENTER OF EACH ELEMENT **
C********** IN A SPECIFIED PART OF A GRID ***********************************
C*********=*********=*********=*********=*********=*********=*********=**
      COMMON /COM1/AREA,DI(3,3),DB(3,6),AK(6,6),P(3,6),RHS(1980),
     1 DTEMP(990),SPROPS(6,1900),APR(1600),S1(3),
     2 STRESS(4,1900),NV(1990),X(990),Y(990),TOTIME,DTIM,HEATN(990),
     3 HTIM,EMASS(1980),TEMP(990),BREAK(1900),VC,HEAT(990),
     4 II(1900),JJ(1900),MM(1900),TP(1900),TS(260),
     5 NONODE,NOEL,N2,IW,IW1,IW2,IW3,IW4,IW5,DY,NO(6),FIRST,FRACT,NEW
      REAL*6 X,Y,RHS,STRESS,D,AK,DB,DTIM,AREA,ST,B,VD
      REAL*8 TOTIME,HTIM
      INTEGER*2 II,JJ,MM,CONSTR,TFIX,TP,TS
      LOGICAL FIRST,FRACT,NEW
      REAL*8 OUTPUT(15968)
      EQUIVALENCE(OUTPUT(1),STRESS(1))
      LOGICAL NET,NOTFIR
      INTEGER *2 LVIS(1900)
      DIMENSION AAPR(1900),XX(2),YY(2),IYM(1900)
      INTEGER TYPE(10)
      REAL*8 TOT
      CALL PLTXMX(50.0)
C****** INPUT RESULTS OF FINITE ELEMENT PROGRAM ON ROUTE #8 ******************
      LEN=32000
      CALL READ(OUTPUT(1),LEN,1,I,8,&6000)
      CALL READ(OUTPUT(4001),LEN,1,I,8,&6000)
      CALL READ(OUTPUT(8001),LEN,1,I,8,&6000)
      LEN=31744
      CALL READ(OUTPUT(12001),LEN,1,I,8,&6000)
      REWIND 8
      TOT=TOTIME/3.155815E+7
C**** INPUT VARIATION OF PRESSURE WITH DEPTH ********************************
      READ(3,4)APR
    4 FORMAT(20A4)
C******** FIND EXTREMES OF NET ***********************************************
      YMIN=Y(1)
      YMAX=Y(1)
      XMIN=X(1)
      XMAX=X(1)
      DO 52 I=1,NONODE
      X1=X(I)
      Y1=Y(I)
      XMAX=AMAX1(X1,XMAX)
      XMIN=AMIN1(X1,XMIN)
      YMAX=AMAX1(Y1,YMAX)
      YMIN=AMIN1(Y1,YMIN)
   52 CONTINUE
      YMIN=YMIN/1000.0
      YMAX=YMAX/1000.0
      XMIN=XMIN/1000.0
      XMAX=XMAX/1000.0
C********* PRINT EXTREMES OF NET IN KM *****************************************
      WRITE(6,51) YMIN,YMAX,XMIN,XMAX
   51 FORMAT(' Y AND X EXTREMES',4F12.2)
C****** READ LIMITS OF REQUIRED PLOT IN KM AND MAXIMUM LENTH OF PLOT ***********
C***** IN INCHES  THE HEIGHT OF PLOT IS ASSUMED TO BE 9 INCHES ****************
      READ(5,15) YMIN,YMAX,XMIN,XMAX,PMX
   15 FORMAT(F12.4)
      YMIN=YMIN*1000.0
      YMAX=YMAX*1000.0
      XMAX=XMAX*1000.0
      XMIN=XMIN*1000.0
C********** CALCULATE SCALING FACTORS ***************************************
      XSCALE=9.0/(XMAX-XMIN)
      XMAXA=XMAX+0.5/XSCALE
      YSCALE=PMX/(YMAX-YMIN)
      IF(YSCALE .GT.XSCALE)YSCALE=XSCALE
      YMINA=YMIN-3.0/YSCALE
      IP=0
C****** SCALE CO-ORDINATES TO INCHES ON PLOT **********************************
      DO 300 I=1,NONODE
      X(I)=(XMAXA-X(I))*XSCALE
      Y(I)=(Y(I)-YMINA)*YSCALE
  300 CONTINUE
      XMAX=(XMAXA-XMIN)*XSCALE
      YMAX=(YMAX-YMINA)*YSCALE
      YMIN=(YMIN-YMINA)*YSCALE
```

```
      YMIN=0.5
  310 FORMAT(2I2)
C********** READ PLOT CODE AND K (FORMAT(2I2)) ***************************
C******* K=0 THE FINITE ELEMENT NET IS NOT DRAWN THIS IS MOST COMMON VALUE *****
C******* PLOT CODE AS FOLLOWS                                                **
C******* 1  NUMBER OF ELEMENT                                                **
C******* 2  SPARE                                                            **
C******* 3  CROSS AT CENTER OF ELEMENT (USED FOR CHECKING NET SPECIFICATION)  **
C******* 4  NET ONLY                                                         **
C******* 5  PRINCIPAL STRESSES                                               **
C******* 6  LINES OF LIKELY FAILURE                                          **
C******* 7  PRINCIPAL STRESSES - HYDROSTATIC PRESSURE                        **
C******* 8  FLOW LINES AS ARROWS AT EACH NODE                                **
C******* 9  LOG VISCOSTY AS NUMBER                                           **
C******* 10 BREAK (A NUMBER INDICATING HOW OFTEN THE ELEMENT HAS FAILED)     **
C******* 11 PHASE BOUNDARIES                                                 **
C******* 12 DENSITY                                                          **
C*****************************************************************************
      READ(5,310) IPLOT,K
      NET=K .EQ.0
C****** LABEL THE PLOT ********************************************************
      CALL PSYMB(1.5,0.1,-0.15,' TIME = ',90.0,8)
      CALL PENWRP(1.5,2.0,-0.15,TOT,90.0,'E8.8 *',0.0)
      GOTO(910,920,930,940,950,960,970,980,990,995,996,997),IPLOT
      WRITE(6,900) IPLOT
  900 FORMAT(' ERROR IN IPLOT =',I8)
      STOP
  910 CALL PSYMB(1.0,0.1,-0.15,' NUMBER OF ELEMENTS',90.0,19)
      GOTO 1000
  920 CALL PSYMB(1.0,0.0,-0.15,'   SPARE            ',90.0,19)
      GOTO 1000
  930 CALL PSYMB(1.0,0.0,-0.15,' CROSS AT CENTER OF ELEMENT ',90.0,28)
      GOTO 1000
  940 CALL PSYMB(1.0,0.0,-0.15,'  NET ONLY',90.0,10)
      GOTO 1000
  950 CALL PSYMB(1.0,0.0,-0.15,' PRINCIPAL STRESSES',90.0,19)
      GOTO 1000
  960 CALL PSYMB(1.0,0.0,-0.15,' LINES OF LIKELY FAILURE',90.0,24)
      GOTO 1000
  970 CALL PSYMB(1.0,0.0,-0.15,' PRINCIPAL STRESSES - STANDARD STATE'
     1 ,90.0,36)
      GOTO 1000
  980 CALL PSYMB(1.0,0.1,-0.15,' FLOW LINES ',90.0,12)
      GOTO 1000
  990 CALL PSYMB(1.0,5.0,-0.15,' LOG VISCOSITY IN ELEMENTS ',90.0,27)
      GOTO 1000
  995 CALL PSYMB(1.0,5.0,-0.15,' BREAKS ',90.0,8)
      GOTO 1000
  996 CALL PSYMB(1.0,5.0,-0.15,' PHASE BOUNDARIES ',90.0,18)
      GOTO 1000
  997 CALL PSYMB(1.0,5.0,-0.15,'   DENSITY ',90.0,11)
 1000 CONTINUE
C******* DRAW BOUNDARY OF THE MODEL ********************************************
      IWM=IW-1
      DO 50 JN=1,IWM
      KN=JN
      IF(Y(TS(JN)) .LT. YMAX)GOTO 60
   50 CONTINUE
   60 DO 70 JN=KN,IWM
      KN=JN
      IF(X(TS(JN)).LT. XMAX)GOTO 80
   70 CONTINUE
   80 CONTINUE
      DO 100 JN=KN,IWM
      I=TS(JN)
      J=TS(JN+1)
      IF(Y(I).GT. YMAX)GOTO 100
      IF(Y(I) .LT. YMIN) GOTO 100
      IF(X(I) .LT. XMIN)GOTO 100
      IF(X(I) .GT. XMAX) GOTO 100
      IF(Y(J) .GT. YMAX) GOTO 100
      IF(Y(J) .LT. YMIN) GOTO100
      IF(X(J) .LT. XMIN)GOTO 100
      IF(Y(J) .GT. XMAX)GOTO 100
      CALL PENUP(Y(I),X(I))
      CALL PENDN(Y(J),X(J))
  100 CONTINUE
      IF (IPLOT .GT.4)GOTO 150
      CALL PELEM(IPLOT,TP,YMAX,YMIN,XMAX,XMIN,NET,SCALE)
      CALL PLTEND
      STOP
  150 CONTINUE
      IF (IPLOT .EQ.8) GOTO 1500
```

```
      NTF(1)=0
      NTF(2)=0
      NTF(3)=0
C******** CALCULATE PROPERTIES, DENSITY,PHASE TRANSITIONS ECT. **********=*******
      CALL PROPS
      IF (IPLOT .EQ.10) GOTO 1600
      DO 200 I=1,NOEL
      VIS=SPROPS(5,I)
      LVIS(I)=ALOG10(VIS)
      IF(IPLOT .EQ. 10) LVIS(I)=BREAK(I)
      IF(IPLOT .EQ.11)LVIS(I)=SPROPS(3,I)
      IF (LVIS(I) .GE.99)LVIS(I)=1500
      IF (IPLOT .GT. 9) GOTO 200
      YM=DMIN1(Y(II(I)),Y(JJ(I)),Y(MM(I)))
      IF (YM .GT. YMAX) GOTO 200
      IF (DMIN1(Y(II(I)),Y(JJ(I)),Y(MM(I))) .LT. YMIN)GOTO 200
      IF (DMAX1(X(II(I)),X(JJ(I)),X(MM(I))).GT. XMAX)GOTO 200
      IF(DMIN1(X(II(I)),X(JJ(I)),X(MM(I))).LT. XMIN)GOTO 200
      STR=0.5E+8
C******** CALCULATE LIKELY HOOD OF FAILURE AND THE ANGLE **********************
      FMASS(I)=FAIL(I,IP,BETA,B1,FRACT,STR)
      SH=DSQRT((STRESS(1,I)-STRESS(2,I))**2*0.25+STRESS(4,I)**2)
      SD=(STRESS(1,I)+STRESS(2,I))/2.0
C*****************************************************************************
C     CHANGE ARRAY STRESS SO THAT:                                            **
C     STRESS(1,M)=MAXIMUN PRINCIPAL STRESS
C     STRESS(2,M)=MINIMUM PRINCIPAL STRESS
C     STRESS(3,M)=ANLE BETWEEN MINIMUM PRINCIPAL STRESS AND X AXIS
C     STRESS(4,M)=ANLE BETWEEN MINIMUM STRESS AND FRACTURE DIRECTION
C     FMASS(M)=A NUMBER WHOSE SIZE DEPENDS ON THE LIKELY HOOD OF FAILURE
C*****************************************************************************
      STRESS(1,I)=SH+SD
      STRESS(2,I)=SD-SH
      STRESS(3,I)=BETA
      STRESS(4,I)=B1
      TP(I)=IP
      NTF(IP)=NTF(IP)+1
      IYM(I)=-1
      IF (FRACT) IYM(I)=8
      FMASS(I)=ATAN(0.01*FMASS(I))*0.5/ATAN(1.0)+1.0
  200 CONTINUE
      IF (IPLOT .LT. 9) GOTO 201
      IP=2
C******  PLOT NUMBERS AT CENTER OF ELEMENTS ************************************
      CALL PELEM(IP,LVIS,YMAX,YMIN,XMAX,XMIN,NET,0.1)
      CALL PLTEND
      STOP 11
  201 CONTINUE
      WRITE(6,740) (I,NTF(I),I=1,3)
  740 FORMAT(' TYPE OF INCIPIENT FAILURE',/,' TYPE     NO OF ELEMENTS'
     1 ,/,(2I8))
      IF (IPLOT .EQ. 9) STOP
 1210 S1=0.0
      S2=0.0
      DO 1220 I=1,NOEL
      YM=DMIN1(Y(II(I)),Y(JJ(I)),Y(MM(I)))
      IF(YM .GT. YMAX) GOTO 1220
      IF (DMIN1(Y(II(I)),Y(JJ(I)),Y(MM(I))) .LT. YMIN)GOTO 1220
      IF (DMAX1(X(II(I)),X(JJ(I)),X(MM(I))).GT. XMAX)GOTO 1220
      IF(DMIN1(X(II(I)),X(JJ(I)),X(MM(I))).LT. XMIN)GOTO 1220
      IF (IPLOT .NE. 7) GOTO 215
C******* FIND STANDARD PRESSURE FOR THE DEPTH OF EACH ELEMENT AND ADD TO *******
C******* THE PRINCIPAL STRESSES ***************************************************
      XM=(X(II(I))+X(JJ(I))+X(MM(I)))/(3.0*XSCALE)
      XM=XMAXA-XM
      A=PX(XM,APR,DUM)
      IF(XM .LT.5000.0)A=1000.0*9.8*XM
      STRESS(1,I)=STRESS(1,I)+A
      STRESS(2,I)=STRESS(2,I)+A
C******* FIND MAXIMUM SIZE OF VARIABLE TO BE PLOTTED ****************************
  215 A=DMAX1(DABS(STRESS(1,I)),DABS(STRESS(2,I)))
      S1=AMAX1(S1,A)
      S2=AMAX1(S2,FMASS(I))
 1220 CONTINUE
C******  WRITE MAXIMUM SIZE OF VARIABLES AND COMPUTE SCALE OF SYMBOLS SO *******
C*****  THE BIGGEST IS 0.5 INCHES ***************************************************
      WRITE(6,1230) S1,S2
 1230 FORMAT(' RANGE OF VALUES OF STRESS IS ',1PD12.4,' AND OF '
     1, 'FAILURE ',1PD12.4)
      S1=0.5/S1
      S2=0.5/S2
      IF (IPLOT .EQ. 6) S1=S2
      TOT=1.0/S1
```

```
      CALL PSYMB(2.0,0.1,-0.15,' SCALE OF SYMBOLS ',90.0,18)
      CALL PSYMB(2.0,5.0,-0.15,'  UNIT/INCH    ',90.0,14)
      CALL PENMBR(2.0,2.5,-0.15,TOT,90.0,' E2.4 *',0.0)
      CALL PELEM(IPLOT,TP,YMAX,YMIN,XMAX,XMIN,NET,S1)
      CALL PLTEND
      STOP
 1500 CONTINUE
C******* PLOT FLOW VECTORS AS ARROWS SHOWING VELOCITIES OF EACH NODE ***********
      R=0.0
       DO 1510 I=1,NONODE
       IF(Y(I) .GT. YMAX) GOTO 1510
       IF(Y(I) .LT. YMIN) GOTO 1510
       IF(X(I) .LT. XMIN)GOTO 1510
      IF(X(I) .GT. XMAX) GOTO 1510
      A=SQRT(UV(2*I)**2+UV(2*I-1)**2)
      R=AMAX1(A,R)
 1510 CONTINUE
C******  LARGEST ARROW 0.5 INCHES ***********************************************
      IF (DTIM .LT. 0.0001)DTIM=0.0001
      S1=0.5/R
      TOT=S1*DTIM/3.155815E+7
      TOT=1.0/TOT
      CALL PSYMB(2.0,0.1,-0.15,' VELOCITY GIVEN BY ',90.0,19)
      CALL PENMBR(2.0,2.5,-0.15,TOT,90.0,'E2.4 *',0.0)
      CALL PSYMB(2.0,4.5,-0.15,' (METRES/YEAR)/INCH ',90.0,20)
      DO 1520 I=1,NONODE
      IF (Y(I) .GT. YMAX) GOTO 1520
      IF(Y(I) .LT. YMIN) GOTO 1520
      IF(X(I) .LT. XMIN) GOTO 1520
      IF(X(I) .GT. XMAX)GOTO 1520
      YY(1)=Y(I)
      XX(1)=X(I)
      CALL PSYMB(YY(1),XX(1),-0.02,0,0.0,-1)
      YY(2)=YY(1)+UV(2*I)*S1
      XX(2)=XX(1)-UV(2*I-1)*S1
      R=S1*SQRT(UV(2*I)**2+UV(2*I-1)**2)
      IF (R .LT. 0.03) GOTO 1520
      R=R/3.0
      CALL PARROW(YY,XX,2,1,R,0,0.0)
 1520 CONTINUE
      CALL PLTEND
      STOP
 1600 CONTINUE
C******** PLOT DENSITY ***************************************************
      DO 1610 I=1,NOEL
      TP(I)=SPROPS(4,I)/10.0+0.5
 1610 CONTINUE
      CALL PELEM(IPLOT,TP,YMAX,YMIN,XMAX,XMIN,NET,SCALE)
      CALL PLTEND
      STOP
 6000 WRITE(6,6100)
 6100 FORMAT(' READ ERROR')
      END
```

```
      SUBROUTINE PELEM(ICODE,LL,YMAX,YMIN,XMAX,XMIN,NET,SCALE)
C*****************************************************************************
C
C     SUBROUTINE TO PLOT NUMBERS OR SYMBOLS AT THE CENTER OF EACH ELEMENT
C      IN A GIVEN AREA OF A FINITE ELEMENT GRID
C
C*****************************************************************************
      INTEGER*2 LL(1)
      LOGICAL NET,ALL
      COMMON /COM1/AREA,D(3,3),DB(3,6),AK(6,6),F(3,6),PHS(1980),
     1 DTEMP(990),SPROPS(6,1900),APR(1600),ST(3),
     2 STRESS(4,1900),UV(1980),X(990),Y(990),TOTIME,DTIM,HEATM(990),
     3 HTIM,EMASS(1980),TEMP(990),BREAK(1900),VD,HEAT(990),
     4 II(1900),JJ(1900),MM(1900),TP(1900),TS(260),
     5 NLNODE,NOEL,N2,IW,IW1,IW2,IW3,IW4,IW5,DY,NO(6),FIRST,FRACT,NEW
      REAL*8 X,Y,PHS,STRESS,D,AK,DP,DTIM,AREA,ST,B,VD
      REAL*8 TOTIME,HTIM
      INTEGER*2 II,JJ,MM,CONSTR,TFIX,TP,TS
      LOGICAL FIRST,FRACT,NEW
      DO 300  M=1,NOEL
      I=II(M)
      J=JJ(M)
      K=MM(M)
      IF (DMAX1(Y(I),Y(J),Y(K)) .GT. YMAX) GOTO 300
      IF (DMIN1(Y(I),Y(J),Y(K)) .LT. YMIN) GOTO 300
      IF(DMAX1(X(I),X(J),X(K)) .GT. XMAX) GOTO 300
      IF (DMIN1(X(I),X(J),X(K)) .LT. XMIN) GOTO 300
      XK=X(K)
      XI=X(I)
      XJ=X(J)
      YK=Y(K)
      YI=Y(I)
      YJ=Y(J)
      XMEAN=(XI+XJ+XK)/3.0
      YMEAN=(YI+YJ+YK)/3.0
      IF (.NOT. NET) GOTO 611
      CALL PENUP(YI,XI)
      CALL PENDN(YJ,XJ)
  402 CALL PENDN(YK,XK)
      CALL PENDN(YI,XI)
  611 GOTO(601,613,614,615,616,617,618),ICODE
      WRITE(6,550) ICODE
  550 FORMAT(' ERROR IN ICODE=',I10,' PERMISSIBLE RANGE 1 TO 7')
      STOP
  613 YMEAN=YMEAN-0.1
      NBV=LL(M)
      IF(NBV .EQ.0)GOTO 300
      IF(NBV .GT. 999 ) GOTO 614
      CALL PENMBR(YMEAN,XMEAN,-0.05,NBV,0.0,'I3 *',0.0)
      GOTO 300
  614 CONTINUE
      CALL PSYMB(YMEAN,XMEAN,0.1,3,0.0,-1)
      GOTO 300
  601 CONTINUE
      YMEAN=YMEAN-0.2
      NBV=M
      CALL PENMBR(YMEAN,XMEAN,-0.08,NBV,0.0,'I5 *',0.0)
      GOTO 300
  615 CONTINUE
C*****************************************************************************
C *****PLOT SYMBOL  DEPENDING ON LL(I) AT CENTER OF ELEMENTS*****************
      NBV=LL(M)
      IF (NBV .LT.0) GOTO 300
      CALL PSYMB(YMEAN,XMEAN,0.1,NBV,0.0,-1)
      GOTO 300
C STRESS HAS BEEN CHANGED  SO THAT.......
C
C     STRESS(1,M)=MAXIMUM STRESS
C      STRESS(2,M)=MINIMUM STRESS
C      STRESS(3,M)= ANGLE BETWEEN X AXIS AND MINIMUM STRESS
C      STRESS(4,M)= ANGLE BETWEEN MINIMUM STRESS AND THE EXPECTED FRACTURE
C
C      LL(M)= TYPE OF FRACTURE
C      EMASS(M)= LIKELY HOOD OF FRACTURE
C
C*****************************************************************************
  616 CONTINUE
  618 CONTINUE
C *******PLOT PRINCIPAL STRESSES ***********************************************
      CS=STRESS(3,M)-1.5708
      SN=SIN(CS)
      CS=COS(CS)
      R=STRESS(1,M)/2.0*SCALE
```

```
      P=STRESS(2,M)/2.0*SCALE
      X1=XMEAN-R*CS
      X2=XMEAN+P*SN
      X3=XMEAN+R*CS
      X4=XMEAN-P*SN
      Y1=YMEAN+R*SN
      Y2=YMEAN+P*CS
      Y3=YMEAN-R*SN
      Y4=YMEAN-P*CS
      IF(ABS(R) .LT. 0.025) GOTO 501
      IF(STRESS(3,M) .GT. 0.0) GOTO 502
      CALL PENUP(Y1,X1)
      CALL PENDN(Y3,X3)
      GOTO 501
  502 CALL PSYMB(Y1,X1,0.03,2,0.0,-1)
      CALL PSYMB(Y3,X3,0.03,2,0.0,-2)
  501 IF (ABS(P) .LT. 0.05) GOTO 300
      IF(STRESS(2,M) .GT. 0.0) GOTO 503
      CALL PENUP(Y2,X2)
      CALL PENDN(Y4,X4)
      GOTO 300
  503 CALL PSYMB(Y2,X2,0.03,2,0.0,-1)
      CALL PSYMB(Y4,X4,0.03,2,0.0,-2)
      GOTO 300
  617 CONTINUE
C ****PLOT LINES OF LIKELY FAILURE ***********************************************
      R=FMASS(M)*SCALE*0.5
      B1=STRESS(3,M)-STRESS(4,M)
      CS=COS(B1)
      SN=SIN(B1)
      X1=XMEAN-R*CS
      Y1=YMEAN+R*SN
      X3=XMEAN+R*CS
      Y3=YMEAN-R*SN
      B1=STRESS(3,M)+STRESS(4,M)
      CS=COS(B1)
      SN=SIN(B1)
      X2=XMEAN-R*CS
      Y2=YMEAN+R*SN
      X4=XMEAN+R*CS
      Y4=YMEAN-R*SN
      CALL PENUP(Y1,X1)
      CALL PENDN(Y3,X3)
      CALL PENUP(Y2,X2)
      CALL PENDN(Y4,X4)
      GOTO 300
  300 CONTINUE
      RETURN
      END



      FUNCTION FAIL(I,ITP,ANG,B1,YZ,T)
C ****** CALCULATE FAILURE CRITERIA AND ANGLE OF FAILURE ***********************
      REAL*8 SX,SY,SXY,SH,SD,SZ,SMAX,SMIN
      LOGICAL YZ
      COMMON /COM1/AREA,D(3,3),DB(3,6),AK(6,6),B(3,6),PHS(1980),
     1 DTEMP(990),SPROPS(6,1900),APR(1600),ST(3),
     2 STRESS(4,1900),UV(1980),X(990),Y(990),TOTIME,DTIM,HEATM(990),
     3 HTIM,FMASS(1980),TEMP(990),PPEAK(1900),VD,HEAT(990),
     4 II(1900),JJ(1900),MM(1900),TP(1900),TS(260),
     5 NONODE,NOEL,N2,IW,IW1,IW2,IW3,IW4,IW5,DY,NO(6),FIRST,FRACT,NEW
      REAL*8 X,Y,RHS,STRESS,D,AK,DB,DTIM,AREA,ST,B,VD
      REAL*8 TOTIME,HTIM
      INTEGER*2 II,JJ,MM,CONSTR,TFIX,TP,TS
      LOGICAL FIRST,FRACT,NEW
      COMMON/PRO/E1,ANU1,DEN,COND,SO,CV,VIS,TEX,BETA,SG
      SX=STRESS(1,I)
      SY=STRESS(2,I)
      SZ=STRESS(3,I)
      SXY=STRESS(4,I)
      SH=DSQRT((SX-SY)**2*0.25+SXY*SXY)
      SD=(SX+SY)/2.0
      SMIN=DMIN1(SD-SH,SZ)
      SMAX=DMAX1(SD+SH,SZ)
      ANG=0.5*DATAN2(2.000*SXY,SX-SY)+1.5708
      B1=0.0
      YZ=(SZ .EQ. SMIN .OR. SZ .EQ. SMAX)
      IF((3.0*SMAX+SMIN) .LT. 0.0) GOTO 20
C***** PURE TENSIONAL FAILURE ***************************************************
      A=SMAX/T
      FAIL=15.0*A*(A-1)
      ITP=1
```

```
      RETURN
   20 IF(SMAX .LT. -4.19*T) GOTO 30
C******** OPEN CRACK FAILURE **********************************************
      SD=DSQRT(4.0*SD*SD-SH*SH)
      IF (SD .LT. 1.0 .AND. SH .LT.1.0) SD=1.0
      P1=0.5*DATAN2(SD,SH)
      FAIL=((SMAX-SMIN)/T)**2+8.0*(SMIN+SMAX)/T
      ITP=2
      RETURN
   30 A1=SMIN/T
C******** CLOSED CRACK FAILURE **********************************************
      A=(4.19+A1)**2+8.0*(A1-4.19)
      A=ABS(4/(2.356*4.19+0.356*A1+0.02))
      C=(4.19*T/SMAX)**2
      A=((A-1)*C+1)
      FAIL=((2.356*SMAX-0.356*SMIN)/T-0.02)*A
      B1=0.5*ATAN(0.91/44)
      ITP=3
      RETURN
      END
```

A2.6 PROGRAM PLOT#2

This program is similar to PROGRAM PLOT# 1 but the stresses, viscosity etc. are smoothed to give mean values at the nodes. This is important in finite element analysis where there is much bending of the grid since this tends to distort the stresses but the mean is a much nearer approximation to the correct solution. The input is the same as PLOT # 1 but IPLOT can only take the values of 5,6,7,8,9,10,11. K is not read and the net not drawn.

This program also uses SUBROUTINES PROPS and PX. (pages 170 and 178).

```
C*********************************************************************
C****** PROGRAM PLOT#2 TO PLOT RESULTS OF FINITE ELEMENT PROGRAM *******
C****** THIS PROGRAM SMOOTHS THE RESULTS AND PLOTS STRESSES ECT. AT THE NODES **
C*********************************************************************
      COMMON /COM1/AREA,D(4,3),DM(3,6),AK(6,6),B(3,6),PHS(1280),
     1 DTEMP(990),SPROPS(6,1900),APR(1600),ST(3),
     2 STRESS(4,1900),UV(1980),X(990),Y(990),TOTIME,DTIM,HEATM(990),
     3 HTIM,EMASS(1980),TEMP(990),DENS(1900),VD,HEAT(990),
     4 II(1900),JJ(1900),MM(1900),TP(1900),TS(260),
     5 NONODE,NOEL,N2,IW,IW1,IW2,IW3,IW4,IW5,DY,NO(6),FIRST,FRACT,NEW
      REAL*8 X,Y,PHS,STRESS,D,AK,DB,DTIM,AREA,ST,B,VD
      REAL*8 TOTIME,HTIM
      INTEGER*2 II,JJ,MM,CONSTR,TFIX,TP,TS
      LOGICAL FIRST,FRACT,NEW
      REAL*8 OUTPUT(15968)
      REAL*8 UMX(990),UMN(990),USH(990)
      REAL*8 SX,S,SW,SY,SZ,SH
      EQUIVALENCE(OUTPUT(1),STRESS(1))
      LOGICAL NET,NOTFIR
      INTEGER *2 LVIS(1900)
      DIMENSION AAPR(1900),XX(2),YY(2),IYM(1900)
      INTEGER *2 IYM,NTF(3)
      INTEGER TYPE(10)
      REAL*8 TOT
      CALL PLTXMX(100.0)
      SG=0.0
C***** READ PRESSURE DEPTH TABLE ***************************************
      READ(3,4) APR
    3 FORMAT(F12.5)
    4 FORMAT(20A4)
C***** READ RESULTS OF FINITE ELEMENT ANALYSIS *************************
      LEN=32000
      CALL READ(OUTPUT(1),LEN,1,I,8,66000)
      CALL READ(OUTPUT(4001),LEN,1,I,8,66000)
      CALL READ(OUTPUT(8001),LEN,1,I,8,66000)
      LEN=31744
      CALL READ(OUTPUT(12001),LEN,1,I,8,66000)
      REWIND 8
      TOT=TOTIME/3.155815E+7
C**** FIND EXTREMES OF NET ********************************************
      YMIN=Y(1)
      YMAX=Y(1)
      XMIN=X(1)
      XMAX=X(1)
      DO 50 I=1,NONODE
      X1=X(I)
      Y1=Y(I)
      XMAX=AMAX1(X1,XMAX)
      XMIN=AMIN1(X1,XMIN)
      YMAX=AMAX1(Y1,YMAX)
      YMIN=AMIN1(Y1,YMIN)
   50 CONTINUE
      YMIN=YMIN/1000.0
      YMAX=YMAX/1000.0
      XMIN=XMIN/1000.0
      XMAX=XMAX/1000.0
C***** WRITE EXTREMES OF THE NET (KM) **********************************
      WRITE(6,51) YMIN,YMAX,XMIN,XMAX
   51 FORMAT(' Y AND X EXTREMES',4F12.2)
C**** READ THE AREA OF THE NET WHICH IS TO BE PLOTTED (KM) AND THE LENGTH ******
C**** OF THE PLOT (PMX) IN INCHES *************************************
      READ(5,15) YMIN,YMAX,XMIN,XMAX,PMX
   15 FORMAT(F12.4)
      YMIN=YMIN*1000.0
      YMAX=YMAX*1000.0
      XMAX=XMAX*1000.0
      XMIN=XMIN*1000.0
C***** COMPUTE SCALING FACTORS *****************************************
      XSCALE=6.0/(XMAX-XMIN)
      XMAXA=XMAX+0.5/XSCALE
      YSCALE=PMX/(YMAX-YMIN)
      IF(YSCALE .GT.XSCALE)YSCALE=XSCALE
      YMINA=YMIN-3.0/YSCALE
      IP=0
      DO 300 I=1,NONODE
      X(I)=(XMAXA-X(I))*XSCALE
      Y(I)=(Y(I)-YMINA)*YSCALE
  300 CONTINUE
      XMAX=(XMAXA-XMIN)*XSCALE
      YMAX=(YMAX-YMINA)*YSCALE
      YMIN=(YMIN-YMINA)*YSCALE
      XMIN=0.5
  310 FORMAT(I5)
```

```
C*****************************************************************************
C READ PLOT TYPE (FORMAT(I5))                                                 ***
C        5 PRINCIPAL STRESSES                                                 ***
C        7 PRINCIPAL STRESSES-STANDARD PRESSURE                               ***
C        8 FLOW LINES                                                         ***
C        9 VISCOSITY                                                          ***
C       10 DENSITY                                                            ***
C       11 PHASE TRANSITIONS                                                  ***
C*****************************************************************************
      READ(5,310) IPLOT
      CALL PSYMB(1.5,0.1,-0.15,' TIME = ',90.0,8)
      CALL PENNB(1.5,2.0,-0.15,TOT,90.0,'F8.8 ',0.0)
      GOTO(910,920,930,940,950,960,970,980,990,995,996,997),IPLOT
      WRITE(6,900) IPLOT
  900 FORMAT(' ERROR IN IPLOT =',I8)
      STOP
  910 CONTINUE
  920 CONTINUE
  930 CONTINUE
  940 CONTINUE
  960 CONTINUE
      WRITE(6,961) IPLOT
  961 FORMAT(' THIS VALUE OF IPLOT NOT VALID FOR THIS VERSION',I6)
      STOP
  950 CALL PSYMB(1.0,0.0,-0.15,' PRINCIPAL STRESSES',90.0,19)
      GOTO 1000
  970 CALL PSYMB(1.0,0.0,-0.15,' PRINCIPAL STRESSES - STANDARD STATE'
     1 ,90.0,36)
      GOTO 1000
  980 CALL PSYMB(1.0,0.1,-0.15,' FLOW LINES ',90.0,12)
      GOTO 1000
  990 CALL PSYMB(1.0,5.0,-0.15,' LOG VISCOSITY IN ELEMENTS ',90.0,27)
      GOTO 1000
  995 CALL PSYMB(1.0,5.0,-0.15,' DENSITY/10.0 ',90.0,14)
      GOTO 1000
  996 CALL PSYMB(1.0,0.1,-0.15,' PHASE BOUNDARIES ',90.0,17)
 1000 CONTINUE
C******** DRAW OUTLINE OF THE MODEL BY FOLLOWING AROUND NODES IN TS ***********
      IWM=IW-1
      DO 50 JN=1,IWM
      KN=JN
      IF(Y(TS(JN)) .LT. YMAX)GOTO 60
   50 CONTINUE
   60 DO 70 JN=KN,IWM
      KN=JN
      IF(X(TS(JN)).LT. XMAX)GOTO 80
   70 CONTINUE
   80 CONTINUE
      DO 100 JN=KN,IWM
      I=TS(JN)
      J=TS(JN+1)
      IF(Y(I).GT. YMAX)GOTO 100
      IF(Y(I) .LT. YMIN) GOTO 100
      IF(X(I) .LT. XMIN)GOTO 100
      IF(X(I) .GT. XMAX) GOTO 100
      IF(Y(J) .GT. YMAX) GOTO 100
      IF(Y(J) .LT. YMIN) GOTO100
      IF(X(J) .LT. XMIN)GOTO 100
      IF(X(J) .GT. XMAX)GOTO 100
      CALL PENUP(Y(I),X(I))
      CALL PENDN(Y(J),X(J))
  100 CONTINUE
      IF (IPLOT .EQ.8) GOTO 1500
      NTF(1)=0
      NTF(2)=0
      NTF(3)=0
C****** GET THE PROPERTIES (REMEMBER TO REMOVE COMMENT C'S FROM ***************
C****** SUBROUTINE PROPS ***************************************************
      CALL PROPS
C************ SMOOTH DATA FROM ELEMENTS TO NODES ******************************
      DO 700 I=1,NONODE
      IF (Y(I) .GT. YMAX) GOTO 700
      IF(Y(I) .LT. YMIN) GOTO 700
      IF(X(I) .LT. XMIN)GOTO 700
      IF(X(I) .GT. XMAX) GOTO 700
      SVIS=0.0
      SX=0.0
      S=0.0
      SW=0.0
      SP=0.0
      SD=0.0
      SY=0.0
      SZ=0.0
```

```
      DO 680 J=1,NCEL
      KI=II(J)
      KJ=JJ(J)
      KK=MM(J)
      IF (KI .NE. I .AND. KJ .NE. I .AND. KK .NE. I) GOTO 660
      XM=(X(KI)+X(KJ)+X(KK))/3.0-X(I)
      YM=(Y(KI)+Y(KJ)+Y(KK))/3.0-Y(I)
      X1=X(KI)-X(I)
      X2=X(KJ)-X(I)
      X3=X(KK)-X(I)
      Y1=Y(KI)-Y(I)
      Y2=Y(KJ)-Y(I)
      Y3=Y(KK)-Y(I)
      XT=X1*(Y2-Y3)+X2*(Y3-Y1)+X3*(Y1-Y2)
      YT=Y1*(Y2+Y3)+Y2*Y3+X1*(X2+X3)+X2*X3
      W=ABS(ATAN2(XT,YT))/SQRT(XM*XM+YM*YM)
      SX=SX+W*STRESS(1,J)
      SY=SY+W*STRESS(2,J)
      VIS=SPROPS(5,J)
      SZ=SZ+W*STRESS(3,J)
      S=S+W*STRESS(4,J)
      SVIS=SVIS+W*VIS
      SW=SW+W
      SP=SP+W*SPROPS(3,J)
      SD=SD+W*SPROPS(4,J)
  680 CONTINUE
      IF(SW .EQ.0.0) GOTO 700
      SX=SX/SW
      SY=SY/SW
      SZ=SZ/SW+1.0E-4
      SZ=S/SW+1.0E-4
      SH=DSQRT((SX-SY)**2*0.25D0+SZ*SZ)
      USH(I)=SH
      UMX(I)=(SX+SY)*0.5+SH
      UMN(I)=(SX+SY)*0.5-SH
      USH(I)=0.5*DATAN2(2.0*SZ,SX-SY)+1.5708
      IF (IPLOT .EQ.9) LVIS(I)=0.5+DLOG(SVIS/SW)
      IF (IPLOT .EQ. 12) LVIS(I)=0.5+SH*1.0E-6
      IF (IPLOT .EQ. 11) LVIS(I)=0.5+SP/SW
      IF (IPLOT .EQ. 10) LVIS(I)=0.5+SD/SW-3000.0
  700  CONTINUE
      DO 200 I=1,NONODE
      STRESS(1,I)=UMX(I)
      STRESS(2,I)=UMN(I)
      STRESS(3,I)=USH(I)
  200 CONTINUE
C*****  WRITE NUMBERS ..... IF SYMBOLS GOTO 201 ***************************
      IF (IPLOT .LT.9 ) GOTO 201
      DO 2222 I=1,IW
      J=TS(I)
      LVIS(J)=-1000.0
 2222 CONTINUE
      IP=2
      CALL PNODE(IP,LVIS,YMAX,YMIN,XMAX,XMIN,NET,0.1)
      CALL PLTEND
      STOP 10
  201 CONTINUE
 1210 S1=0.0
      S2=0.0
      DO 1220 I=1,NONODE
      YM=Y(I)
      IF(YM .GT. YMAX) GOTO 1220
      IF(Y(I) .LT. YMIN) GOTO 1220
      IF(X(I) .GT. XMAX) GOTO 1220
      IF(X(I) .LT. XMIN) GOTO 1220
      IF (IPLOT .NE. 7) GOTO 1220
C******** ADD STANDARD PRESSURE IF IPLOT=7 ***************************
      XM=X(I)/XSCALE
      XM=XMAXA-XM
      A=PX(XM,APR,DP)
      STRESS(1,I)=STRESS(1,I)+A
      STRESS(2,I)=STRESS(2,I)+A
 1220 CONTINUE
C******* REMOVE BOUNDARY NODES FROM THE PLOT ***************************
      DO 1222 I=1,IW
      J=TS(I)
      STRESS(1,J)=0.0
      STRESS(2,J)=0.0
      STRESS(3,J)=0.0
 1222 CONTINUE
      DO 1221 I=1,NONODE
      IF (Y(I) .LT. YMIN)GOTO 1221
      IF(Y(I) .GT. YMAX)GOTO 1221
```

```
      IF(X(I) .LT. XMIN)GOTO 1221
      IF(X(I) .GT. XMAX) GOTO 1221
  215 A=CMAX1(CABS(STRESS(1,I)),CABS(STRESS(2,I)))
      S1=AMAX1(S1,A)
 1221 CONTINUE
      WRITE(6,1230) S1
 1230 FORMAT(' RANGE OF VALUES OF STRESS IS ',1PD12.4)
      S1=1.0/S1
      TOT=1.0/S1
C****** PRINT SCALE OF SYMBOLS ON PLOT HEADING ********************************
      CALL PSYMB(2.0,0.1,-0.15,' SCALE OF SYMBOLS ',90.0,18)
      CALL PSYMB(2.0,5.0,-0.15,'  UNITS/INCH  ',90.0,14)
      CALL PENMBR(2.0,2.5,-0.15,TOT,90.0,' E2.4 *',0.0)
C ******** PLOT STRESSES ********************************************************
      CALL PNODE(IPLOT,TP,YMAX,YMIN,XMAX,XMIN,NET,S1)
      CALL PLTEND
      STOP
 1500 CONTINUE
C****** PLOT FLOW LINES AT NODES ***********************************************
      P=0.0
       DO 1510 I=1,NONODE
       IF(Y(I) .GT. YMAX) GOTO 1510
       IF(Y(I) .LT. YMIN) GOTO 1510
       IF(X(I) .LT. XMIN)GOTO 1510
      IF(X(I) .GT. XMAX) GOTO 1510
      A=SQRT(UV(2*I)**2+UV(2*I-1)**2)
      R=AMAX1(A,R)
 1510 CONTINUE
      IF (DTIM .LT. 0.0001) DTIM=0.0001
      S1=0.5/R
      TOT=S1*DTIM/3.155815E+7
      TOT=1.0/TOT
      CALL PSYMB(2.0,0.1,-0.15,' VELOCITY GIVEN BY ',90.0,19)
      CALL PENMBR(2.0,2.5,-0.15,TOT,90.0,'E2.4 *',0.0)
      CALL PSYMB(2.0,4.5,-0.15,' (METRES/YEAR)/INCH ',90.0,20)
      DO 1520 I=1,NONODE
      IF (Y(I) .GT. YMAX) GOTO 1520
      IF(Y(I) .LT. YMIN) GOTO 1520
      IF(X(I) .LT. XMIN) GOTO 1520
      IF(X(I) .GT. XMAX)GOTO 1520
      YY(1)=Y(I)
      XX(1)=X(I)
      CALL PSYMB(YY(1),XX(1),-0.02,0,0.0,-1)
      YY(2)=YY(1)+UV(2*I)*S1
      XX(2)=XX(1)-UV(2*I-1)*S1
      R=S1*SQRT(UV(2*I)**2+UV(2*I-1)**2)
      IF (R .LT. 0.03) GOTO 1520
      R=R/3.0
      CALL PARROW(YY,XX,2,1,P,0,0.0)
 1520 CONTINUE
      CALL PLTEND
      STOP
 6000 WRITE(6,6100)
 6100 FORMAT(' READ ERROR')
      END
```

```
      SUBROUTINE PNODS(ICODE,LL,YMAX,YMIN,XMAX,XMIN,NET,SCALE)
C*****************************************************************************
C***** PLOTS DATA AND SMOOTHED DATA AT THE NODES OF A FINITE ELEMENT NET /******
C***** THIS SUBROUTINE IS SIMILAR TO PELEM IN PLOT#1 BUT SYMBOLS ARE PLOTTED ***
C***** AT THE NODES AND NOT AT THE CENTER OF THE ELEMENTS ********************
C*****************************************************************************
      INTEGER*2 LL(1)
      LOGICAL NET,ALL
      COMMON /CCM1/AREA,D(3,3),DB(3,6),AK(6,6),B(3,6),RHS(1980),
     1 DTEMP(990),SPROPS(6,1900),PR(1600),ST(3),
     2 STRESS(4,1900),UV(1980),X(990),Y(990),TOTIME,DTIM,HEAT(990),
     3 HTIM,EMASS(1980),TEMP(990),DENS(1900),VC,HEAT(990),
     4 II(1900),JJ(1900),MM(1900),TP(1900),TS(260),
     5 NONODE,NOEL,N2,IW,IW1,IW2,IW3,IW4,IW5,DY,NO(6),FIRST,FRACT,NEW
      REAL*8 X,Y,RHS,STRESS,D,AK,DB,DTIM,AREA,ST,B,VC
      REAL*8 TOTIME,HTIM
      INTEGER*2 II,JJ,MM,CONSTR,TFIX,TP,TS
      LOGICAL FIRST,FRACT,NEW
C*****************************************************************************
C  STRESS HAS BEEN CHANGED  SO THAT.......                                     *
C                                                                              *
C       STRESS(1,M)=MAXIMUM STRESS                                             *
C        STRESS(2,M)=MINIMUM STRESS                                            *
C        STRESS(3,M)= ANGLE BETWEEN X AXIS AND MINIMUM STRESS                  *
C        STRESS(4,M)= ANGLE BETWEEN MINIMUM STRESS AND THE EXPECTED FRACTURE   *
C                                                                              *
C        LL(M)= TYPE OF FRACTURE                                               *
C        EMASS(M)= LIKELIHOOD OF FRACTURE                                      *
C*****************************************************************************
      DO 300  M=1,NONODE
      IF (Y(M) .GT. YMAX) GOTO 300
      IF (Y(M) .LT. YMIN) GOTO 300
      IF(X(M) .GT. XMAX) GOTO 300
      IF (X(M) .LT. XMIN) GOTO 300
      XMEAN=X(M)
      YMEAN=Y(M)
      IF (.NOT. NET) GOTO 611
      CALL PENUP(YI,XI)
      CALL PENDN(YJ,XJ)
  402 CALL PENDN(YK,XK)
      CALL PENDN(YI,XI)
  611 GOTO(601,613,614,615,616,617,618),ICODE
      WRITE(6,550) ICODE
  550 FORMAT(' ERROR IN ICODE=',I10,' PERMISSIBLE RANGE 1 TO 7')
      STOP
  613 YMEAN=YMEAN-0.2
      NBV=LL(M)
      IF(NBV .LT.-999.0) GOTO 300
      IF(NBV .GT. 999) GOTO 614
      CALL PENMBR(YMEAN,XMEAN,-0.1,NBV,0.0,'I3 *',0.0)
      GOTO 300
  614 CONTINUE
      CALL PSYMB(YMEAN,XMEAN,0.1,3,0.0,-1)
      GOTO 300
  601 CONTINUE
      YMEAN=YMEAN-0.2
      NBV=M
      CALL PENMBR(YMEAN,XMEAN,-0.08,NBV,0.0,'I5 *',0.0)
  615 CONTINUE
C ******PLOT SYMBOL  DEPENDING ON LL(M) AT CENTER OF ELEMENTS********
      NBV=LL(M)
      IF (NBV .LE.0) GOTO 300
      CALL PSYMB(YMEAN,XMEAN,0.1,NBV,0.0,-1)
      GOTO 300
  616 CONTINUE
  618 CONTINUE
C ********PLOT PRINCIPAL STRESSES ***************************************
      CS=STRESS(3,M)-1.5708
      SN=SIN(CS)
      CS=COS(CS)
      P=STRESS(1,M)/2.0*SCALE
      P=STRESS(2,M)/2.0*SCALE
      X1=XMEAN-P*CS
      X2=XMEAN+P*SN
      X3=XMEAN+P*CS
      X4=XMEAN-P*SN
      Y1=YMEAN+P*SN
      Y2=YMEAN+P*CS
      Y3=YMEAN-P*SN
      Y4=YMEAN-P*CS
      IF(ABS(P) .LT. 0.025) GOTO 501
      IF(STRESS(1,M) .GT. 0.0) GOTO 502
      CALL PENUP(Y1,X1)
```

```
      CALL PENDN(Y3,X3)
      GOTO 501
  502 CALL PSYMB(Y1,X1,0.03,2,0.0,-1)
      CALL PSYMB(Y3,X3,0.03,2,0.0,-2)
  501 IF (ABS(P) .LT. 0.05) GOTO 300
      IF(STRESS(2,M) .GT. 0.0) GOTO 503
      CALL PENUP(Y2,X2)
      CALL PENDN(Y4,X4)
      GOTO 300
  503 CALL PSYMB(Y2,X2,0.03,2,0.0,-1)
      CALL PSYMB(Y4,X4,0.03,2,0.0,-2)
      GOTO 300
  617 CONTINUE
C ****PLOT LINES OF LIKELY FAILURE ***************************************
      R=EMASS(M)*SCALE*0.5
      P1=STRESS(3,M)-STRESS(4,M)
      CS=COS(B1)
      SN=SIN(B1)
      X1=XMEAN-P*CS
      Y1=YMEAN+P*SN
      X3=XMEAN+R*CS
      Y3=YMEAN-R*SN
      B1=STRESS(3,M)+STRESS(4,M)
      CS=COS(B1)
      SN=SIN(B1)
      X2=XMEAN-R*CS
      Y2=YMEAN+R*SN
      X4=XMEAN+R*CS
      Y4=YMEAN-R*SN
      CALL PENUP(Y1,X1)
      CALL PENDN(Y3,X3)
      CALL PENUP(Y2,X2)
      CALL PENDN(Y4,X4)
      GOTO 300
  300 CONTINUE
      RETURN
      END
```

A2.7 PROGRAM CONTOUR

This program draws contour maps of the variation of various variables over the finite element net. The extremes of the plot are read in as for PLOT ※ 1 but the codes are read as IPLOT and IFIRST (2I2).

Valid values of IPLOT are

1 Maximum and minimum stresses (not generally used)

2 Log viscosity

3 Shear stresses

4 Temperature

5 Failure criteria

6 Density

The first run should have IFIRST = 0 thereafter IFIRST = 1.

The program returns for further codes after the completion of the contour drawing. The program is stopped by entering a letter for IPLOT.

```
C*****************************************************************************
C  A PROGRAM TO CONTOUR FINITE ELEMENT RESULTS ON THE X-Y PLOTTER              *
C  INPUT FROM THE FE PROGRAM IS THROUGH CHANNEL #8                            **
C  INPUT OF VARIATION OF PRESSURE WITH DEPTH ON CHANNEL #3                    **
C  CONTROL DATA THROUGH CHANNEL #5                                            **
C*****************************************************************************
      DIMENSION UDENS(990),USH(990),UMN(990),UMX(990),UVIS(990)
      COMMON /COM1/AREA,D(3,3),DH(3,6),AK(6,6),B(3,6),PHS(1980),
     1 DTEMP(990),SPROPS(6,1900),APR(1600),ST(3),
     2 STRESS(4,1900),UV(1980),X(990),Y(990),TOTIME,DTIM,HEATM(990),
     3 HTIM,EMASS(1980),TEMP(990),PREAR(1900),VD,HEAT(990),
     4 II(1900),JJ(1900),MM(1900),TP(1900),TS(260),
     5 NCNODE,NCEL,N2,IW,IW1,IW2,IW3,IW4,IW5,DY,NG(6),FIRST,FRACT,NEW
      REAL*8 X,Y,PHS,STRESS,D,AK,DB,DTIM,AREA,ST,B,VD
      REAL*8 TOTIME,HTIM
      INTEGER*2 II,JJ,MM,CONSTR,TFIX,TP,TS
      LOGICAL FIRST,FRACT,NEW
      REAL*8 OUTPUT(15968)
      EQUIVALENCE(OUTPUT(1),STRESS(1))
      LOGICAL NET,NOTFIR
      INTEGER *2 LVIS(1900)
      DIMENSION AAPR(1900),XX(2),YY(2),IYM(1900)
      INTEGER *2 IYM,NTF(3)
      REAL*8 TOT
      CALL PLTXMX(50.0)
C***** READ RESULTS OF FINITE ELEMENT PROGRAM ***********************************
      LEN=32000
      CALL READ(OUTPUT(1),LEN,1,I,8,66000)
      CALL READ(OUTPUT(4001),LEN,1,I,8,66000)
      CALL READ(OUTPUT(8001),LEN,1,I,8,66000)
      LEN=31744
      CALL READ(OUTPUT(12001),LEN,1,I,8,66000)
      REWIND 8
      TOT=TOTIME/3.155815E+7
C******  READ PRESSURE DEPTH TABLE ************************************************
      READ(3,4)APR
    4 FORMAT(20A4)
C****** FIND EXTREMES OF FINITE ELEMENT NET ***************************************
      YMIN=Y(1)
      YMAX=Y(1)
      XMIN=X(1)
      XMAX=X(1)
      DO 52 I=1,NCNODE
      X1=X(I)
      Y1=Y(I)
      XMAX=AMAX1(X1,XMAX)
      XMIN=AMIN1(X1,XMIN)
      YMAX=AMAX1(Y1,YMAX)
      YMIN=AMIN1(Y1,YMIN)
   52 CONTINUE
      YMIN=YMIN/1000.0
      YMAX=YMAX/1000.0
      XMIN=XMIN/1000.0
      XMAX=XMAX/1000.0
C****** WRITE EXTREMES OF NET (KM) ************************************************
      WRITE(6,51) YMIN,YMAX,XMIN,XMAX
   51 FORMAT(' Y AND X EXTREMES',4F12.2)
C***** READ PLOT LIMITS (KM) AND MAXIMUM LENGTH OF PLOT (INCHES) ****************
      READ(5,15) YMIN,YMAX,XMIN,XMAX,PMX
   15 FORMAT(F12.4)
      YMIN=YMIN*1000.0
      YMAX=YMAX*1000.0
      XMAX=XMAX*1000.0
      XMIN=XMIN*1000.0
C****** CALCULATE THE SCALES  ****************************************************
      XSCALE=9.0/(XMAX-XMIN)
      XMAXA=XMAX+0.5/XSCALE
      YSCALE=PMX/(YMAX-YMIN)
      IF(YSCALE .GT.XSCALE)YSCALE=XSCALE
      YMINA=YMIN-3.0/YSCALE
      IP=0
C***** SCALE X AND Y TO INCHES ON PLOT ********************************************
      DO 300 I=1,NONODE
      X(I)=(XMAXA-X(I))*XSCALE
      Y(I)=(Y(I)-YMINA)*YSCALE
  300 CONTINUE
      XMAX=(XMAXA-XMIN)*XSCALE
      YMAX=(YMAX-YMINA)*YSCALE
      YMIN=(YMIN-YMINA)*YSCALE
      XMIN=0.5
```

```
C*****************************************************************************
C                                                                             **
C   RETURNS HERE AFTER EACH PLOT TO END PROGRAM TYPE INVALID IPLOT (E.G. AAA)  *
C VALUES OF IPLOT                                                             **
C                1 MAXIMUM AND MINIMUM STRESSES (NOT OFTEN USED)              **
C                2 LOG VISCOSITY                                              **
C                3 SHEAR STRESS                                               **
C                4 TEMPERATURE                                                **
C                5 FAILURE CRITERIA                                           **
C                6 DENSITY                                                    **
C                                                                             **
C    IFIRST = 0 FOR FIRST CONTOUR MAP (OTHER THAN TEMPERATURE)                **
C *****************************************************************************
  309 READ(5,310) IPLOT,IFIRST
  310 FORMAT(3I2)
      GOTO (911,920,930,940,950,960),IPLOT
      WRITE(6,901) IPLOT
  901 FORMAT(' ERROR IN IPLOT =',I10)
      GOTO 309
  911 CALL PSYMB(1.0,0.1,-0.15,' MAXIMUM AND MINIMUM STRESSES',90.0,29)
      GOTO 1000
  920 CALL PSYMB(1.0,0.1,-0.15,' LOG VISCOSITIES ',90.0,17)
      GOTO 1000
  930 CALL PSYMB(1.0,0.1,-0.15,' SHEAR STRESSES',90.0,15)
      GOTO 1000
  940 CALL PSYMB(1.0,0.1,-0.15,' TEMPERATURES',90.0,13)
      GOTO 1000
  950 CALL PSYMB(1.0,0.1,-0.15,' FAILURE CRITERIA',90.0,17)
      GOTO 1000
  960 CALL PSYMB(1.0,0.1,-0.15,' DENSITY',90.0,8)
 1000 CONTINUE
      CALL PSYMB(1.5,0.1,-0.15,' TIME=',90.0,6)
      CALL PENMBR(1.5,1.5,-0.15,TOT,90.0,' FR.8 **',0.0)
C******* DRAW BOUNDARY OF MODEL ***************************************************
      IWM=IW-1
      DO 50 JN=1,IWM
      KN=JN
      IF(Y(TS(JN)) .LT. YMAX)GOTO 60
   50 CONTINUE
   60 DO 70 JN=KN,IWM
      KN=JN
      IF(X(TS(JN)).LT. XMAX)GOTO 80
   70 CONTINUE
   80 CONTINUE
      DO 100 JN=KN,IWM
      I=TS(JN)
      J=TS(JN+1)
      IF(Y(I).GT. YMAX)GOTO 100
      IF(Y(I) .LT. YMIN) GOTO 100
      IF(X(I) .LT. XMIN)GOTO 100
      IF(X(I) .GT. XMAX) GOTO 100
      IF(Y(J) .GT. YMAX) GOTO 100
      IF(Y(J) .LT. YMIN) GOTO100
      IF(X(J) .LT. XMIN)GOTO 100
      IF(X(J) .GT. XMAX)GOTO 100
      CALL PENUP(Y(I),X(I))
      CALL PENDN(Y(J),X(J))
  100 CONTINUE
      IF(IPLOT .EQ.4) GOTO 860
      IXX=1
C******* IF PROPERTIES AND SMOOTHIN ALREADY DONE JUMP TO 750 ********************
      IF(IFIPST .NE.0) GOTO 750
      DO 20 I=1,NCNODE
      USH(I)=-1.0E+60
      UMX(I)=-1.0E+60
      UMN(I)=-1.0E+60
      UVIS(I)=-1.0E+60
      UDENS(I)=-1.0E+60
   20 CONTINUE
C******  CALCULATE PROPERTIES ***************************************************
      CALL PROPS
      DO 700 I=1,NCNODE
C******* SMOOTH DATA FROM ELEMENTS TO THE NODES ***********************************
      IF (Y(I) .GT. YMAX) GOTO 700
      IF(Y(I) .LT. YMIN) GOTO 700
      IF(X(I) .LT. XMIN)GOTO 700
      IF(X(I) .GT. XMAX) GOTO 700
      SVIS=0.0
      SX=0.0
      S=0.0
      SW=0.0
      SP=0.0
      SD=0.0
```

```
      SY=0.0
      SZ=0.0
      DO 680 J=1,NOEL
      KI=II(J)
      KJ=JJ(J)
      KK=MM(J)
      IF (KI .NE. I .AND. KJ .NE. I .AND. KK .NE. I) GOTO 680
      XM=(X(KI)+X(KJ)+X(KK))/3.0-X(I)
      YM=(Y(KI)+Y(KJ)+Y(KK))/3.0-Y(I)
      X1=X(KI)-X(I)
      X2=X(KJ)-X(I)
      X3=X(KK)-X(I)
      Y1=Y(KI)-Y(I)
      Y2=Y(KJ)-Y(I)
      Y3=Y(KK)-Y(I)
      XT=X1*(Y2-Y3)+X2*(Y3-Y1)+X3*(Y1-Y2)
      YT=Y1*(X2+X3)+Y2*X3+X1*(X2+X3)+X2*X3
      W=ABS(ATAN2(XT,YT))/SQRT(XM*XM+YM*YM)
      SX=SX+W*STRESS(1,J)
      SY=SY+W*STRESS(2,J)
      VIS=SPROPS(5,J)
      SZ=SZ+W*STRESS(3,J)
      S=S+W*STRESS(4,J)
      SVIS=SVIS+W*VIS
      SW=SW+W
      SP=SP+W*SPROPS(3,J)
      SD=SD+W*BREAK(J)
  680 CONTINUE
      IF(SW .EQ.0.0) GOTO 700
      SX=SX/SW
      SY=SY/SW
      SZ=SZ/SW+1.0E-4
      SZ=S/SW+1.0E-4
      SH=DSQRT((SX-SY)**2*0.25D0+SZ*SZ)
      USH(I)=SH
      UMX(I)=(SX+SY)*0.5+SH
      UMN(I)=(SX+SY)*0.5-SH
      UVIS(I)=ALOG10(SVIS/SW)
      UDENS(I)=SD/SW
  700 CONTINUE
  750 CONTINUE
C******** CHOOSE WHAT IS TO BE CONTOURED ***************************************
  760 GOTO(910,500,800,860,851,855),IPLOT
      GOTO 900
C******** PLOT MAXIMUM AND MINIMUM STRESS CONTOURS (NOT MUCH USE) **************
  910 AMA=-1.0E+60
      AMI=-AMA
      BMA=AMA
      BMI=AMI
      DO 400 I=1,NONODE
      IF(Y(I) .GT. YMAX .OR. UMX(I) .LT. -1.0E+30) GOTO 400
      IF (Y(I) .LT. YMIN) GOTO 400
      IF (X(I) .GT. XMAX)GOTO 400
      IF(X(I) .LT. XMIN) GOTO 400
      AMA=AMAX1(AMA,UMX(I))
      AMI=AMIN1(AMI,UMX(I))
      BMA=AMAX1(BMA,UMN(I))
      BMI=AMIN1(BMI,UMN(I))
  400 CONTINUE
      DG=AMAX1(AMA-AMI,BMA-BMI)
      NC=25
      IC=ALOG10(DG/NC)
      CI=10.0**IC
      WRITE(6,410) AMA,AMI,BMA,BMI,CI,TOT,ITY
  410 FORMAT(' MAXIMUM STRESS IN RANGE',E14.6,' TO ',E14.6,/,
     1 ' MINIMUM STRESS IN RANGE OF ',E14.6,' TO ' ,E14.6,/,
     2 ' CONTOUR INTERVAL IS ',E14.6
     3 ,/,' AT TIME=',F12.3,' YEARS  ZONE ',I6)
      A1=AMAX1(0.1E-50,ABS(AMA))
      A2=AMAX1(0.1E-50,ABS(AMI))
      A3=AMAX1(0.1E-50,ABS(BMA))
      A4=AMAX1(0.1E-50,ABS(BMI))
      L1=ALOG10(A1)
      L2=ALOG10(A2)
      L3=ALOG10(A3)
      L4=ALOG10(A4)
      LV=MAXO(L1,L2,L3,L4)
      ALV=10.0**LV
      WRITE(6,711) ALV
  711 FORMAT(' STRESSES PLOTTED',/,'POINTS LABELLED G(I)/',E10.4)
      IP=1
      CALL CONTOR(X,Y,NOEL,NONODE,II,JJ,MM,UMX,CI,ALV,IP,YMAX,YMIN,
     1 XMAX,XMIN)
```

```
      IP=-1
      CALL CONTOP(X-Y,NOEL,NONODE,II,JJ,MM,UMN,CI,ALV,IP,YMAX,YMIN,
     1 XMAX,XMIN)
      GOTO 710
  500 CONTINUE
C******  DRAW CONTOURS OF VISCOSITY ***************************************
      WRITE(6,600) TOT
  600 FORMAT(' DRAW CONTOURS OF LOG VISCOSITY'
     1 ,' AT TIME ',F13.3,' YEARS  ')
      CALL DRAWC(UVIS,NONODE,NOEL,II,JJ,MM,X,Y,YMAX,YMIN,XMAX,XMIN,IXX)
      GOTO 710
  800 CONTINUE
C******* DRAW CONTOURS OF SHEAR STRESS ***********************************
      WRITE(6,850) TOT
  850 FORMAT(' DRAW SHEAR STRESS CONTOURS AT TIME =',F12.3,
     1 ' YEARS  ')
      CALL DRAWC(USH,NONODE,NOEL,II,JJ,MM,X,Y,YMAX,YMIN,XMAX,XMIN,IXX)
      GOTO 710
  851 CONTINUE
C******* CONTOUR LIKELYHOOD OF FAILURE ***********************************
      DO 852 I=1,NONODE
      IF (USH(I) .LT. -1.0E+30) GOTO 852
      SZ=(UMX(I)+UMN(I))/2.0
      USH(I)=FAIL2(I,IP,ANG,B1,BY,STR(ITY),UMX(I),UMN(I),SZ,0.0)
  852 CONTINUE
      WRITE(6,854)TOT
  854 FORMAT(' DRAW CONTOURS OF THE LIKELYHOOD OF FAILURE',
     1 '  TIME= ',F13.3,' YEARS')
      CALL DRAWC(USH,NONODE,NOEL,II,JJ,MM,X,Y,YMAX,YMIN,XMAX,XMIN,IXX)
      GOTO 710
  855 CONTINUE
C******** DRAW CONTOURS OF DENSITY ***************************************
      WRITE(6,856) TOT
  856 FORMAT(' DRAW CONTOURS OF DENSITY AT TIME',F13.3,' YEARS')
      CALL DRAWC(UDENS,NONODE,NOEL,II,JJ,MM,X,Y,YMAX,YMIN,XMAX,XMIN,IXX)
      GOTO 710
  860 CONTINUE
C PLOT TEMPERATURES
C****** PLOT TEMPERATURE CONTOURS ***************************************
      WRITE(6,870)TOT
  870 FORMAT(' DRAW CONTOURS OF TEMPERATURES TIME =',F13.3,' YEARS')
      CALL DRAWC(TEMP,NONODE,NOEL,II,JJ,MM,X,Y,YMAX,YMIN,XMAX,XMIN,1)
  710 CONTINUE
      CALL PLTEND
      GOTO 309
  900 CONTINUE
      WRITE(6,910)
  810 FORMAT(' NO PLOT WHAT DID YOU RUN THIS FOR')
      GOTO 309
 6000 WRITE(6,6100)
 6100 FORMAT(' READ ERROR')
      END
```

```
      SUBROUTINE DRAWC(UVIS,NONODE,NOEL,II,JJ,MM,X,Y,YMAX,YMIN,XMAX,
     1 XMIN,NZ)
C******* SETS UP ARRAYS AND SCALING FOR CONTOUR DRAWING OF VARIABLE IN UVIS*****
      DIMENSION UVIS(1),II(1),JJ(1),MM(1),X(1),Y(1)
      REAL*8 X,Y,DD
       INTEGER*2 II,JJ,MM
      GMAX=-1.0E+60
      GMIN=-GMAX
      LNO=0
      DO 600 I=1,NONODE
C***** FIND EXTEMES OF VARIABLE ************************************************
      IF (Y(I) .GT. YMAX .OR. UVIS(I) .LT. -1.0E+30) GOTO 600
      IF(Y(I) .LT. YMIN)GOTO 600
      IF(X(I) .GT. XMAX )GOTO 600
      IF(X(I) .LT. XMIN) GOTO 600
      GMAX=AMAX1(GMAX,UVIS(I))
      GMIN=AMIN1(GMIN,UVIS(I))
      LNO=LNO+1
  600 CONTINUE
      IF (LNO .GT. 0) GOTO 620
      WRITE(6,670)
  670 FORMAT(' ZONE NOT REPRESENTED IN AREA')
      RETURN
  680 CONTINUE
      DG=GMAX-GMIN
      NC=10
      IF (ABS(DG) .GT. 1.0E-30) GOTO 700
      WRITE(6,690) GMIN,DG,GMAX
  690 FORMAT(' VARIABLE IS CONSTANT IN THE FIELD DG=',3E12.4)
      RETURN
  700 CONTINUE
C******* FIND 'NICE' CONTOUR INTERVAL ***************************************
      IC=ALOG10(DG/NC)
      CI=10.0**IC
      NC=DG/CI
C****** DEEP THIS CONTOUR INTERVAL.... REPLY C TO ACCEPT OR ALTERNATIVE *******
C******  CONTOUR INTERVAL YOU WISH TO BE USED ********************************
      WRITE(6,705) NC,CI
      READ(5,706) CCI
      IF (CCI .GT.0.0) CI=CCI
  705 FORMAT(I6,' CONTURS WITH INTERVAL OF ',E14.2,/,' ENTER DIFFERENT '
     1 ' INTERVAL OR 0')
  706 FORMAT(F12.2)
      GMAX=AMAX1(0.1E-50,ABS(GMAX))
      GMIN=AMAX1(0.1E-50,ABS(GMIN))
      LV=ALOG10(GMAX)
      L=ALOG10(GMIN)
      LV=MAXO(L,LV)
      ALV=10.0**LV
C****** CALCULATE SCALING TO LABEL SOME OF THE NODES WITH VALUES OF        *****
C***** THE FUNCTION ......... THE CONTOURS ARE NOT LABELLED ******************
      WRITE(6,650) ALV
  650 FORMAT(/,' POINTS LABELLED WITH G(I)/',E10.4)
      DC=1.0+1.5*NZ
C******  HEAD THE PLOT ********************************************************
      CALL PSYMB(DC,0.1,-0.15,' CONTOUR INTERVAL',90.0,17)
      DD=CI
      CALL PENNBR(DC,2.5,-0.15,DD,90.0,'E1.4 *',0.0)
      DC=DC+0.5
      CALL PSYMB(DC,0.1,-0.15,' MAXIMUM                    MINIMUM  ',
     1 90.0,36)
      DD=GMAX
      CALL PENNBR(DC,1.5,-0.15,DD,90.0,'E1.4 *',0.0)
      DD=GMIN
      CALL PENNBR(DC,4.5,-0.15,DD,90.0,'E1.4 *',0.0)
      IP=NZ-1
C********* DRAW CONTOURS ********************************************************
      CALL CONTOR(X,Y,NOEL,NONODE,II,JJ,MM,UVIS,CI,ALV,IP,YMAX,YMIN,
     1 XMAX,XMIN)
      RETURN
      END
```

```
      SUBROUTINE CONTOR(X,Y,NOEL,NCNODE,II,JJ,MM,G,CI,LV,IP,YMAX,YMIN,
     1 XMAX,XMIN)
C***** DRAWS CONTOURS OF G WITH CONTOUR INTERVAL CI OVER FIELD SPECIFIED  *****
C***** BY YMAX,YMIN,XMAX,XMIN **********************************************
      DIMENSION X(1),Y(1),II(1),JJ(1),MM(1),G(1),CX(101,2),CY(101,2)
      REAL*8 X,Y,DG
      INTEGER *2 II,JJ,MM
      REAL LV
      LOGICAL*1 DONE(990)
      LOGICAL FOUND
      ADD=CI
      DO 1 I =1,NCNODE
      IF(Y(I) .GT. YMAX .OR. G(I) .LT. -1.0E+30)GOTO 1
      IF(Y(I) .LT. YMIN)GOTO 1
      IF(X(I) .LT. XMIN)GOTO 1
      IF(X(I) .GT. XMAX) GOTO 1
      DONE(I)=.FALSE.
      ADD=AMIN1(ADD,G(I))
    1 CONTINUE
      IA=-ADD/CI
      ADD=CI*(IA+1)
      DO 1000 IQ=1,NOEL
      I=II(IQ)
      J=JJ(IQ)
      M=MM(IQ)
      YM=DMAX1(Y(I),Y(J),Y(M))
      GM=AMIN1(G(I),G(J),G(M))
      IF(YM .GT. YMAX .OR. GM .LT. -1.0E+30) GOTO 1000
      IF(DMIN1(Y(I),Y(J),Y(M)) .LT. YMIN)GOTO 1000
      IF(DMAX1(X(I),X(J),X(M)) .GT. XMAX)GOTO 1000
      IF(DMIN1(X(I),X(J),X(M)) .LT. XMIN)GOTO 1000
      IC=(G(I)+ADD)/CI
      JC=(G(J)+ADD)/CI
      MC=(G(M)+ADD)/CI
      MAXC=MAXO(IC,JC,MC)
      MINC=MINO(IC,JC,MC)+1
      NC=MAXC-MINC+1
      IF(NC .LT.1) GOTO 150
      IF(NC .GT. 100) NC=100
      FOUND=.FALSE.
      IF(IC .EQ.JC) GOTO 20
      KX=MAXO(IC,JC)
      MI=MINO(IC,JC)+1
      JK=2
      IF(KX .NE. MAXC .OR. MI .NE. MINC) GOTO 5
      JK=1
      FOUND=.TRUE.
    5 IF( MI .GT. KX) GOTO 20
      DO 10 IM=MI,KX
      CG=IM*CI-ADD
      L=IM-MINC+1
      IF (L .GT.100) GOTO 10
      F=(CG-G(J))/(G(I)-G(J))
      CX(L,JK)=X(J)+F*(X(I)-X(J))
      CY(L,JK)=Y(J)+F*(Y(I)-Y(J))
   10 CONTINUE
   20 IF(JC .EQ.MC) GOTO 40
      KX=MAXO(JC,MC)
      MI=MINO(JC,MC)+1
      JK=2
      IF (KX.NE.MAXC .OR. MI .NE.MINC .OR.FOUND)GOTO 25
      JK=1
      FOUND=.TRUE.
   25 IF(MI .GT.KX) GOTO 40
      DO 30 IM=MI,KX
      CG=IM*CI-ADD
      L=IM-MINC+1
      IF(L .GT. 100) GOTO 30
      F=(CG-G(M))/(G(J)-G(M))
      CX(L,JK)=X(M)+F*(Y(J)-X(M))
      CY(L,JK)=Y(M)+F*(Y(J)-Y(M))
   30 CONTINUE
   40 IF(MC .EQ.IC)GOTO 60
      KX=MAXO(MC,IC)
      MI=MINO(MC,IC)+1
      JK=1
      IF (FOUND) JK=2
      IF(MI .GT. KX) GOTO 60
      DO 50 IM=MI,KX
      CG=IM*CI-ADD
      L=IM-MINC+1
      IF(L .GT. 100) GOTO 50
      F=(CG-G(I))/(G(M)-G(I))
```

```
      CX(L,JK)=X(I)+F*(X(M)-X(I))
      CY(L,JK)=Y(I)+F*(Y(M)-Y(I))
   50 CONTINUE
   60 CONTINUE
      JK=1
      DO 100 IK=1,NC
      CALL PENUP(CY(IK,JK),CX(IK,JK))
      JK=3-JK
      CALL PENDN(CY(IK,JK),CX(IK,JK))
  100 CONTINUE
  150 CONTINUE
C*************************************************************************
C                                                                        **
C THESE STATEMENTS WITH COMMENT 'C' LABEL SOME OF THE NODES WITH THE     **
C VALUES OF THE FUNCTION.......... CONTOURS ARE NOT LABELLED            **
C*************************************************************************
C 150 IF (DONE(I)) GOTO 210
C     XX=X(I)+IP*0.1
C     YY=Y(I)-0.2
C     DG=G(I)/LV
C     IF (MOD(I,5) .EQ.0)
C    1CALL PENMBR(YY,XX,-0.05,DG,0.0,'F5.2 *',0.0)
C     DONE(I)=.TRUE.
C 210 IF (DONE(J)) GOTO 220
C     XX=X(J)+IP*0.1
C     YY=Y(J)-0.2
C     DG=G(J)/LV
C     IF (MOD(J,5) .EQ.0)
C    1 CALL PENMBR(YY,XX,-0.05,DG,0.0,'F5.2 *',0.0)
C     DONE(J)=.TRUE.
C 220 IF (DONE(M)) GOTO 230
C     XX=X(M)+IP*0.1
C     YY=Y(M)-0.2
C     DG=G(M)/LV
C     IF (MOD(M,5) .EQ.0)
C    1 CALL PENMBR(YY,XX,-0.05,DG,0.0,'F5.2 *',0.0)
C     DONE(M)=.TRUE.
C 230 CONTINUE
 1000 CONTINUE
      RETURN
      END


      FUNCTION FAIL2(I,ITP,ANG,B1,YZ-T,SX,SY,SZ,SXY)
C****** CALCULATES FAILURE CRITERIA ***************************************
      REAL*8 SX,SY,SXY,SH,SD,SZ,SMAX,SMIN
      LOGICAL YZ
      COMMON /COM1/AREA,D(3,3),DB(3,6),AK(6,6),B(3,6),PHS(1980),
     1 DTEMP(990),SPROPS(6,1900),ADS(1600),ST(3),
     2 STRESS(4,1900),IDV(1980),X(990),Y(990),TOTIME,DTIM,HEATM(990),
     3 HTIM,EMASS(1980),TEMP(990),BREAK(1900),VD,HEAT(990),
     4 II(1900),JJ(1900),MM(1900),TP(1900),TS(260),
     5 NONODE,NOEL,N2,IW,IW1,IW2,IW3,IW4,DY,NO(6),FIRST,FRACT,NEW
      REAL*8 X,Y,PHS,STRESS,D,AK,DB,DTIM,AREA,ST,B,VD
      REAL*8 TOTIME,HTIM
      INTEGER*2 II,JJ,MM,CONSTR,TFIX,TP,TS
      LOGICAL FIRST,FRACT,NEW
      COMMON/PRO/E1,ANU1,DEN,COND,SC,CV,VIS,TEX,BETA,SG
      SH=DSQRT((SX-SY)**2+0.25*SXY*SXY)
      SD=(SX+SY)/2.0
      SMIN=DMIN1(SD-SH,SZ)
      SMAX=DMAX1(SD+SH,SZ)
      ANG=0.5*DATAN2(2.0D0*SXY,SX-SY)+1.5708
      B1=0.0
      YZ=(SZ .EQ. SMIN .OR. SZ .EQ. SMAX)
      IF((3.0*SMAX+SMIN) .LT. 0.0) GOTO 20
      A=SMAX/T
      FAIL2=16.0*A*(A-1)
      ITP=1
      RETURN
   20 IF(SMAX .LT. -4.19*T) GOTO 30
      SD=DSQRT(4.0*SD*SD-SH*SH)
      IF (SD .LT. 1.0 .AND.SH .LT.1.0) SD=1.0
      B1=0.5*DATAN2(SD,SH)
      FAIL2=((SMAX-SMIN)/T)**2+8.0*(SMIN*SMAX)/T
      ITP=2
      RETURN
   30 A1=SMIN/T
      A=(4.19+A1)**2+8.0*(A1-4.19)
      A=ABS(A/(2.356*4.19+0.356*A1+0.02))
      C=(4.19*T/SMAX)**2
      A=((A-1)*C+1)
```

```
FAIL2=((2.35*SMAX-0.35*SMIN)/T-0.021*A
RL=0.5*ATAN(0.01744)
ITP=3
RETURN
END
```

REFERENCES

Abe, K. (1972). Lithospheric normal faulting beneath the Aleutian trench, Phys. Earth Planet. Int., 5, 190-198.

Ahrens, T.J. (1973). Petrological properties of the upper 670 km of the earth's mantle, Phys. Earth Planet. Int., 7, 167-186.

Ahrens, T.J. (1975). Equations of state of the earth, Rev. of Geophys. and Space Phys.,13, 335-339.

Anderson, D.J. (1967). Phase changes in the Upper Mantle, Science N.Y. 157, 1165-1173.

Anderson, O.L. (1972). Shock wave determination of the shear velocity at high pressure, Phys. Earth Planet. Int., 6, 136-

Ave' Lallemant, H.G. and Carter, N.L. (1970). Syntectonic recrystallization of olivine and modes of flow in the upper mantle, Bull. geol. Soc. Am., 81, 2203-2220.

Barth, T.F.W. (1952). Theoretical Petrology, Wiley and Sons N.Y., 387 pp.

Benioff, H. (1955). Seismic evidence for crustal structure and tectonic activity, In : Poldervaart (Ed.), Crust of the Earth (a Symposium). Geol. Soc. Am. Spec. Papers, 62, 67-74.

Birch, F. (1952). Elasticity and constitution of the Earth's interior, J. geophys Res., 57, 227-286.

Birch, F. (1961a). The velocity of compressional waves in rocks to 10 kilobars, part 2, J. geophys Res., 66, 2199-2224.

Birch, F. (1961b). Composition of the Earth's mantle, Geophys. J. R. astr. Soc., 4, 295-311.

Bott, M.H.P. and Dean, D.S. (1972), Stress systems at young continental margins, Nature (Phys. Sci.) Lond., 235, 23-25.

Brace, W.F. (1961). Dependence of fracture strength on grain size, Bull. Miner. Inds. Str. Penn. Univ., 76, 99-103.

Bridgman, P.W. (1945). Polymorphic transitions and geological phenomena, Am. J. Sci., 243A., 90-97.

Bridwell, R.J. (1964). Non-linear in-plane bending of a plane stress-strain finite element model, J. geophys. Res., 79, 1674-1678.

Bridwell, R.J. and Swolfs, H.S., (1974). Stability analysis of an experimentally deformed single layer of Indiana limestone using finite element analysis, J. geophys. Res., 79, 1679-1686.

Bullen, K.E. (1963). An introduction to the theory of seismology, Third edition, Cambridge University Press, London and New York, 381 pp.

Cann, J.R. (1974). A model of oceanic crustal structure developed, Geophys. J. R. astr. Soc., 39, 169-187.

Carpenter, W.C. (1972). Visco-elastic stress analysis, Int. J. Num. Meth. in Eng., 4, 357-366.

Carter, N.L. (1975). High temperature flow of rocks, Rev. of Geophys. Space Phys., 13, 344-349.

Carter, N.L. and Ave' Lallemant, H.G. (1970). High temperature flow of dunite and peridotite, Bull. geol. Soc. Am., 81, 2181-2202.

Christensen, N.I. (1968). Chemical changes associated with upper mantle structure, Tectonophysics, 6, 331-342.

Christoffel, D.A. and Calhaem, I. (1973). Upper mantle viscosity determined from Stokes Law, Nature, Lond., 243, 51-52.

Chung, D.H. (1971). Elasticity and equations of state of olivines in the Mg_2SiO_4 - Fe_2SiO_4 system, Geophys. J. R. astr. Soc., 25, 511-538.

Chung, D.H. (1972). Equation of state of olivine transformed spinels, Earth & planet. Sci. Lett., 14, 348-356.

Chung, D.H., Wang, H., and Simmons, G. (1970). On the calculation of the seismic parameter ϕ at high pressure and high temperature, J. geophys. Res., 75, 5113-5120.

Clark, S.P.(editor)(1966). Handbook of physical constants, Revised edition, Mem. geol. Soc. Am., 97, 587pp.

Clark, S.P. and Ringwood, A.E. (1964). Density distribution and constitution of the mantle, Rev. geophys., 2, 35-88.

Cohen, L.H., Ito, K. and Kennedy, G.C. (1967). Melting and phase relations in an anhydrous basalt to 40 kilobars, Am. Jour. Sci., 265, 475-518.

Daniel, J.W. and Moore, R.E. (1970). Computation and theory in ordinary differential equations, W.H. Freeman, San Francisco, 172 pp.

Davies, D. and McKenzie, D.P. (1969). Seismic travel-time residuals and plates, Geophys. J. R. astr. Soc., 18, 51-63.

Davis, B.T.C. and England, J.L. (1964). The melting of forsterite up to 50 kbar, J. geophys. Res., 69, 1113-1116.

Edmond, O. and Murrell, S.A.F. (1973). Experimental confirmation of three-dimensional theory of fracture for rock at pressures up to 7 kb and its relation to the physical mechanism of earthquakes, Tectonophysics, 16, 71-81.

Elssasser, W.M. (1971). Sea-floor spreading as thermal convection, J. geophys. Res., 76, 1101-1112.

Evison, F.F. (1967). On the occurrence of volume change at the earthquake source, Bull seism. Soc. Am., 57, 9-25.

Ewing, M., Houtz, R. and Ewing, J. (1969). South Pacific sediment distribution, J. geophys. Res., 74, 2477-2493.

Fedotov, S.A. (1968). On deep structure, properties of the upper mantle, and volcanism of the Kurile-Kamchatka Island Arc according to seismic data. In: L. Knopoff, C.L. Drake and P.J. Hart (Editors), The Crust and Upper Mantle of the Pacific Area, Am. Geophys. Union, Washington D.C., 131-139.

Fitch, T.J. (1970). Earthquake mechanisms and island arc tectonics in the Indonesian-Philippine region, Bull. seism. Soc. Am., 60, 565-591.

Forsyth, D. and Uyeda, S. (1975). On the relative importance of the driving forces of plate motion, Geophys. J. R. astr. Soc., 43, 163-200.

Gilbert, F. and Dziewonski, A.M. (1975). An application of normal mode theory to the retrieval of structural parameters and source mechanisms for seismic spectra, Phil. Trans. Roy. Soc., A278, 187-269.

Green, D.H. (1973). Experimental melting studies on a model upper mantle composition at high pressure under water-saturated and water-undersaturated conditions, Earth & planet. Sci. Letts., 19, 37-53.

Green, D.H. and Ringwood, A.E. (1963). Mineral assemblages in a model mantle composition, J. geophys. Res., 68, 937-945.

Green, D.H. and Ringwood, A.E. (1967). An experimental investigation of the gabbro to eclogite transformation and its petrological applications, Geochim. et cosmochim. Acta, 31, 767-833.

Green, D.H. and Ringwood, A.E. (1970). Mineralogy of peridotitic compositions under upper mantle conditions, Phys. Earth Planet. Interiors, 3, 359-371.

Griggs, D.T. (1972). The sinking lithosphere and the focal mechanism of deep earthquakes, in Nature of the solid earth, pp.361-384, edited by E.C. Robertson, McGraw-Hill, New York.

Gutenburg, B. and Richter, C.F. (1954). Seismicity of the Earth and associated phenomena, second edition, Princeton University Press, Princeton, New Jersey, 310 pp.

Hamilton, R.M. and Gale, A.W. (1968). Seismicity and structure of North Island, New Zealand, J. geophys. Res., 73, 3859-3876.

Hamilton, R.M. and Gale, A.W. (1969). Thickness of the mantle seismic zone beneath the North Island of New Zealand, J. geophys. Res., 74, 1608-1613.

Hanks, T.C. (1971). The Kuril trench - Hokkaido rise system: large shallow earthquakes and simple models of deformation, Geophys. J. R. astr. Soc., 23, 173-189.

Hanks, T.C. and Whitcomb, J.H. (1971). Comments on paper by J.W. Minear and M. Nafi Toksöz, 'Thermal regime of a downgoing slab and new global tectonics', J. geophys. Res., 76, 613-616.

Harper, J.F. (1975). On the driving forces of plate tectonics, Geophys. J. R. astr. Soc., 40, 465-474.

Harris, P.G., Hutchinson, R. and Paul, D.K. (1972). Plutonic xenoliths and their relation to the upper mantle, Phil. Trans. Roy. Soc., A271, 313-323.

Hasebe, K., Kujii, N. and Uyeda, S. (1970). Thermal processes under island arcs, Tectonophysics, 10, 335-355.

Haskell, N.A. (1935). The motion of a viscous fluid under a surface load, Physics, 6, 265-269.

Haskell, N.A. (1937). The viscosity of the asthenosphere, Am. Jour. Sci., 33, 22-28.

Hatherton, T. (1969). Gravity and seismicity of assymetric active regions, Nature, Lond., 221, 353-355.

Hatherton, T. (1970). Upper mantle inhomogeneity beneath New Zealand : Surface manifestations, J. geophys. Res., 75, 269-284.

Hayes, D.E. and Ewing, M. (1970). Pacific boundary structure: in The Sea Ideas and observations in progress in the study of the seas, 4(2), pp.29-72,edited by A.W. Maxwell, Wiley-Interscience, New York.

Hetényi, M. (1946). Beams on elastic foundation, The University of Michigan Press, Ann Arbor, Michigan.

Housner, G.W. and Vreeland, T. (1966) The analysis of stress and deformation Macmillian, N.Y., pp434,

Houtz, R., Ewing, J., Ewing, M. and Lonardi, A.G. (1967). Seismic reflexion profiles of the New Zealand Plateau, J. geophys. Res., 72, 4713-4729.

Isacks, B., and Molnar, P. (1969). Mantle earthquake mechanisms and the sinking of the lithosphere, Nature, Lond., 223, 1121-1124.

Isacks, B., and Molnar, P. (1971). Distribution of stresses in the descending lithosphere from a global survey of focal mechanism solutions of mantle earthquakes, Rev. Geophys. Space. Phys., 9, 103-174.

Isacks, B., Oliver, J. and Sykes, L.R. (1968). Seismology and the new global tectonics, J. geophys. Res., 73, 5855-5899.

Ito, K. and Kennedy, G.C. (1967). Melting and phase relations in a natural peridotite to 40 kilobars, Am. Jour. Sci., 265, 519-538.

Jaeger, J.C. and Cook, N.G.W. (1969). Fundamentals of rock mechanics. Chapman and Hall, London, pp.515.

Julian, B.R. and Anderson, D.L. (1968). Travel times, apparent velocities and amplitudes of body waves, Bull. Seism. Soc. Am., 58, 339-366.

Karig, D.E. (1970). Ridges and basins of the Tonga-Kermadec island arc system, J. geophys. Res., 75, 239-254.

Karig, D.E. and Sharman, G.F. (1975). Subduction and accretion in trenches, Bull. geol. Soc. Am., 86, 377-389.

Kelley, K.K. (1960). Contributions to the data on theoretical metallurgy XIII. High temperature heat content, heat capacity and entropy data for the elements and inorganic compounds, Bulletin 585 U.S. Bureau of Mines U.S. Govt. Print. Office, Washington D.C.

Kirby, S.H. and Raleigh, C.B. (1973). Mechanisms of high temperature solid state flow in minerals and ceramics and their bearing on creep behaviour of the mantle, Tectonophysics, 19, 165-194.

Knopoff, L. (1964). The convection current hypothesis, Rev. Geophys., 2, 89-122.

Kohlstedt, D.L. and Goetze, C. (1974). Low stress high temperature creep in olivine single crystals, J. geophys. Res., 79, 2045-2051.

Kushiro, I., Syono, Y. and Akomoto, S. (1968). Melting of a peridotite nodule at high pressures and high water pressures, J. geophys. Res., 73, 6023-6029.

Le Pichon, X. (1968). Sea-floor spreading and continental drift, J. geophys. Res., 73, 3661-3697.

Le Pichon, X., Francheteau, J. and Bonnin, J. (1973). Plate Tectonics, Elsevier, Amsterdam, pp.300.

Lee, E.H., Radok, T.R.M. and Woodward, W.B. (1959). Stress analysis for linear visco-elastic materials, Trans. of the Soc. of Rheology, 3, 41-59.

Lee, T.C. and Henyey, T.L. (1974). Heat flow refraction across dissimilar media, Geophys. J. R. astr. Soc., 39, 319-333.

Linde, A.T. and Sacks,I.S. (1972). Dimensions, energy and stress release for South American deep earthquakes, J. geophys.Res., 77, 1439-1451.

Liu Lin-Gun,(1975). High pressure disproportionation of Co_2SiO_4 spinel and implications for Mg_2SiO_4 spinel, Earth & planet. Sci. Lett., 25, 286-290.

Ludwig, W.J., Ewing, J.I., Ewing, M., Murauchi, J., Den, N., Asano, S., Hotta, H., Hayakawa, M., Asanuma, T., Ichikiwa, K. and Noguchi, I. (1966). Sediments and structure of the Japan Trench, J. geophys. Res., 71, 2121-2137.

Luyendyk, B.P. (1971). Comments on Paper by J.W. Minear and M.N. Toksöz, "Thermal regime of a downgoing slab and new global tectonics", J. geophys. Res., 76, 605-606.

McConnell, R.K. (1968). Viscosity of the earth's mantle. in Proc. Conf. History of the Earth's crust 1966, edited by, R.A. Phinney, Princeton University Press, Princeton, New Jersey.

McClintock, F.A. and Walsh, J.B. (1962). Friction of Griffith cracks under pressure, Proc. U.S. Natn. Congr. appl. Mech., 4, vol.2, 1015-1021, Am. Soc. of Mech. Eng., New York.

MacDonald, G.J.F. (1965). Geophysical deductions from observations of heat flow. In Terrestrial Heat Flow pp.191-210, edited by Lee, W.H.K., Geophys. Monogr. No.8, American Geophysical Union, Washington, D.C.

McKenzie, D.P. (1969). Speculations on the consequences and causes of plate motions, Geophys. J. R. astr. Soc., 18, 1-32.

McKenzie, D.P. (1970). Temperature and potential temperature beneath island arcs, Tectonophysics, 10, 357-366.

McKenzie, D.P. (1971). Comments on paper by J.W. Minear and M.N. Toksöz,"Thermal regime of a downgoing slab and new global tectonics", J. geophys. Res., 76, 607-609.

McKenzie, D.P. and Parker, R.L. (1967). The north Pacific: an example of tectonics on a sphere, Nature, Lond., 216, 1276-1280.

McKenzie, D.P., and Sclater, J.G. (1968). Heat flow inside island arcs of the northwestern Pacific, J. geophys. Res., 73, 3137-3179.

Minear, J.W. and Toksöz, M.N. (1970a). Thermal regimes of a downgoing slab and new global tectonics, J. geophys. Res., 75, 1397-1419.

Minear, J.W. and Toksöz, M.N. (1970b). Thermal regime of a downgoing slab, Tectonophysics, 10, 367-390.

Minear, J.W. and Toksöz, M.N. (1971a). Reply to Hanks and Whitcomb (1971), J. geophys. Res., 76, 610-612.

Minear, J.W. and Toksöz, M.N. (1971b). Reply to McKenzie (1971), J. geophys. Res., 76, 617-626.

Morgan, W.J. (1968). Rises, trenches, great faults and crustal blocks, J. geophys. Res., 73, 1959-1982.

Morgan, W.J. (1972). Plate motions and deep mantle convection. In. Hess Volume - Geol. Soc. Am. Mem. 132, 7-22.

Murrell, S.A.F. (1964). Theory of propagation of elliptical cracks under various conditions of plane strain or plane stress Part I and Part II, Brit. J. appl. Phys., 15, 1195-1223.

Murrell, S.A.F. (1965). The effect of triaxial stress systems on the strength of rocks at atmospheric temperatures, Geophys. J.R. astr. Soc., 10, 231-281.

Murrell, S.A.F. and Chakravarty, S. (1973). Some new rheological experiments on igneous rocks at temperatures up to 1120°C, Geophys. J. R. astr. Soc., 34, 211-250.

Neugebauer,H.J. and Breitmayer, G. (1975). Dominant creep mechanism and the descending lithosphere, Geophys. J. R. astr. Soc., 43, 873-895.

New Zealand Geological Survey (1972) North Island (1st Ed.) Geological map of New Zealand 1:1000000 Department of Scientific and Industrial Research, Wellington, New Zealand.

Oliver, J. and Isacks, B. (1967). Deep earthquake zones, anomalous structures in the upper mantle, and the lithosphere, J. geophys. Res., 72, 4259-5275.

Raitt, R.W., Fisher, R.L. and Mason, R.G. (1955). Tonga Trench, Geol. Soc. Am. Spec. Paper, 62, 237-254.

Raleigh, C.B. and Kirby, S.H. (1970). Creep in the upper mantle. In. Fiftieth anniversary Symposium : Mineralogy and Petrology of the Upper Mantle, Sulfides, Mineralogy and Geochemistry of Non-marine Evaporites. Special Paper No.3. pp. 113-121 edited by Morgan, B.A. Mineralogical Society of America.

Randall, M.J. and Knopoff, L. (1970). The mechanism at the focus of deep earthquakes, J. geophys. Res., 75, 4965-4976.

Reilly, W.I. (1965). Gravity map of New Zealand 1: 4,000,000 Bouguer Anomalies Department of Scientific and Industrial Research, Wellington, New Zealand.

Ricci, J.E. (1951). The phase rule and heterogeneous equilibrium D. Van Nostrand, New York pp505.

Ringwood, A.E. (1962a). A model for the upper mantle 1, J. geophys. Res., 67, 857-866.

Ringwood, A.E. (1962b). A model for the upper mantle 2, J. geophys. Res., 67, 4473-4477.

Ringwood, A.E. (1966a). The chemical composition and origin of the earth. In: Advances in Earth Sciences, pp 287- edited by Hurley, P.M., M.I.T. Press, Cambridge, Mass.

Ringwood, A.E. (1966b). Mineralogy of the mantle. In: Advances in Earth Sciences, pp 357- , edited by Hurley, P.M., M.I.T. Press, Cambridge, Mass.

Ringwood, A.E. (1969a). Composition of the crust and upper mantle. In: The earth's crust and upper mantle pp 1-17, edited by Hart, P.J., Geophys. Monogr. No.13, American Geophysical Union, Washington, D.C.

Ringwood, A.E. (1969b). Phase transformations in the mantle, Earth & planet. Sci. Lett., 5, 401-412.

Ringwood, A.E. (1972). Phase transformations and mantle dynamics, Earth & planet. Sci. Lett., 14, 233-241.

Ringwood, A.E. and Green, D.H. (1966). An experimental investigation of the gabbro-eclogite transformation and some geophysical implications, Tectonophysics, 3, 383-427.

Schaltz, J.F. and Simmons, G. (1972). Thermal conductivity of earth materials at high temperatures, J. geophys. Res., 77, 6966-6983.

Sclater, J.G. and Francheteau, J. (1970). The implication of terrestrial heat flow observations on current tectonic and geochemical models of the crust and upper mantle of the earth, Geophys. J.R. astr. Soc., 20, 509-542.

Sclater, J.G., Hawkins, J.W., Mammerickx, J. and Chase, C.G. (1972). Crustal extension between the Tonga and Lau ridges; Petrologic and geophysical evidence, Geol. Soc. Am. Bull., 83, 505-518.

Service, K.G. and Douglas, A. (1973). Boundaries and fractures in finite element models of geological structures, Geophys. J. R. astr. Soc., 32, 1-14.

Shor, G.G., Menard, W.W. and Raitt, R.W. (1971). Structure of the Pacific basin. In: The Sea, 4, pp 3-27, edited by Maxwell, A.E., Wiley-interscience, New York.

Skinner, B.J. (1966). Thermal expansion. In: Handbook of physical constants, revised edition, pp.75-96, edited by Clark, S.P., Memoir 397, Geological Society of America, New York.

Sleep, N.H. (1975). Stress and flow beneath Island Arcs, Geophys. J.R. astr. Soc., 42, 827-857.

Smith, A.T. and Toksöz, M.N. (1972). Stress distribution beneath Island Arcs, Geophys. J. R. astr. Soc., 29, 289-318.

Stauder, W. (1968). Tensional character of earthquake foci beneath the Aleutian Trench with relation to sea-floor spreading, J. geophys. Res., 73, 7693-7701.

Stauder, W. (1973). Mechanism and spatial distribution of Chilean earthquakes with relation to subduction of the oceanic plate, J. geophys. Res., 78, 5033-5061.

Stauder, W. (1975). Subduction of the Nazca Plate under Peru as evidenced by focal mechanisms and by seismicity, J. geophys. Res., 80, 1053-1064.

Stephansson, O. and Berner, H. (1971). The finite element method in tectonic processes, Phys. Earth planet Interiors, 4, 301-321.

Stocker, R.L. and Ashby, M.F. (1973). On the rheology of the upper mantle, Reviews of Geophys. Space Phys.,11, 391-426.

Sung, C.M. and Burns, R.G. (1976). Kinetics of high-pressure phase transformations: implications to the evolution of the olivine-spinel transition in the downgoing lithosphere and its consequences on the dynamics of the mantle, Tectonophysics, 31, 1-32.

Sykes, L.R. (1966). The seismicity and deep structure of island arcs, J. geophys. Res., 71, 2981-3006.

Sykes, L.R. (1971). Aftershock zones of great earthquakes, seismicity gaps and earthquake prediction for Alaska and the Aleutians, J. geophys. Res., 76, 8021-8041.

Talwani, M., Worzel, J.L. and Ewing, M. (1961). Gravity anomalies and crustal section across the Tonga Trench, J. geophys. Res., 66, 1265-1278.

Toksöz, M.N., Chinnery, M.A. and Anderson, D.L. (1966). Inhomogeneities in the Earth's mantle, Geophys. J. R. astr. Soc., 13, 31-59.

Toksöz, M.N., Minear, J.W. and Julian, B.R. (1971). Temperature field and geophysical effects on a downgoing slab, J. geophys. Res., 76, 1113-1138.

Toksöz, M.N., Sleep, N.H. and Smith, A.T. (1973). Evolution of the downgoing lithosphere and the mechanism of deep focus earthquakes, Geophys. J. R. astr. Soc., 35, 285-310.

Turcotte, D.L. and Oxburgh, E.R. (1969). Convection in a mantle with variable physical properties, J. geophys. Res., 74, 1458-1474.

Turcotte, D.L. and Schubert, G. (1971). Structure of the olivine-spinel phase boundary in the descending lithosphere, J. geophys. Res., 76, 7980-7987.

Uffen, R.J. (1952). A method of estimating the melting point gradient in the Earth's mantle, Trans. Am. geophys. Un., 33, 893-896.

Uyeda, S. and Vacquier, V. (1968). Geothermal and geomagnetic data in and around the island arc of Japan. In. The crust and Upper Mantle of the Pacific Area pp. 349-366, edited by Knopoff, L., Drake, C. and Hart, P., Geophys. Monogr. No.12, American Geophysical Union, Washington, D.C.

Vine, F.J. and Matthews, D.H. (1963). Magnetic anomalies over oceanic ridges, Nature, Lond., 199, 947-949.

Walcott, R.I. (1970). Flexural rigidity, thickness and viscosity of the lithosphere, J. geophys. Res., 75, 3491-3954.

Watts, A.B. and Cochran, J.R. (1974). Gravity anomalies and flexure of the lithosphere along the Hawaiian-Emperor seamount chain, Geophys. J. R. astr. Soc., 38, 119-141.

Watts, A.B., Cochran, J.R. and Selzer, G. (1975). Gravity anomalies and flexure of the lithosphere: A three-dimensional study of the Great Meteor Seamount, Northeast Atlantic, J. geophys. Res., 80, 1391-1398.

Watts, A.B. and Talwani, M. (1974). Gravity anomalies seaward of deep-sea trenches and their tectonic implications, Geophys. J. R. astr. Soc., 36, 57-90.

Weertman, J. (1970). The creep strength of the Earth's mantle, Reviews of geophys. Space phys. 8, 145-168.

Wilson, T. (1965). A new class of faults and their bearing on continental drift, Nature, Lond., 207, 343-347.

Wyllie, P.J. (1971). The Dynamic Earth: Textbook in geosciences John Wiley & Sons, New York. pp415.

Wyss, M. (1970). Stress estimates for South American shallow and deep earthquakes, J. geophys.Res., 75, 1529-1544.

Yoder, H.S. and Tilley, C.E. (1962). Origin of basalt magmas: an experimental study of natural and synthetic rock systems, J. Petrology, 3, 342-532.

Zienkiewicz, O.C. (1971). The finite element method in engineering science. McGraw-Hill, London, pp521.